

# **Investigations of primary active transporters expressed in *Xenopus laevis* oocytes**

**Wilson Disease Protein, a P-type ATPase  
and  
Proteorhodopsin, a light driven proton pump**

Dissertation  
zur Erlangung des Doktorgrades  
der Naturwissenschaften

Vorgelegt beim Fachbereich  
Chemische und pharmazeutische Wissenschaften  
der Johann Wolfgang Goethe-Universität  
in Frankfurt am Main

von  
**Éva Lórinzi**  
aus Bukarest

**Frankfurt am Main  
2006**

Vom Fachbereich Chemische und pharmazeutische Wissenschaften der  
Johann Wolfgang Goethe-Universität als Dissertation Angenommen

Dekan: Prof. Harald Schwalbe

Gutacher: Prof. Ernst Bamberg

Prof. Clemens Glaubitz

Datum der Disputation: 29.08.2006

# Contents

|   |           |
|---|-----------|
| Foreword  | 7         |
| <i>On the importance of transmembrane proteins for cell homeostasis</i>   | 7         |
| <b>WILSON DISEASE PROTEIN</b>   | <b>9</b>  |
| <b>1. Introduction</b>  | <b>11</b> |
| 1.1. <i>History</i>   | 14        |
| 1.2 <i>Physiological importance of Cu<sup>+</sup>-ATPases</i>   | 15        |
| 1.2.1 <i>Wilson Disease Protein (WNDP)</i>  | 15        |
| 1.2.2 <i>Menkes Disease Protein (MNKP)</i>  | 15        |
| 1.3 <i>Structure of WNDP</i>  | 16        |
| 1.4 <i>Functional properties of WNDP</i>  | 19        |
| 1.5 <i>The copper-dependent localisation of WNDP and MNKP</i>   | 21        |
| 1.6 <i>Molecular mechanism of copper-dependent trafficking</i>  | 23        |
| 1.7 <i>Disease mutations that affect the function of WNDP and MNKP</i>  | 26        |
| 1.8 <i>The aim of the work</i>  | 28        |
| <b>2. Results</b>   | <b>29</b> |
| 2.1 <i>Topological model of WNDP</i>  | 29        |
| 2.2 <i>Expression of the full length WNDP in oocytes</i>  | 30        |
| 2.3 <i>Localisation of WNDP at the cell surface using immunoluminescence</i>  | 31        |
| 2.4 <i>Immunogold labelling of the surface expressed WNDP</i>   | 33        |
| 2.5 <i>Functional characterisation of the HA-tagged WNDP</i>  | 34        |
| <b>3. Discussion</b>  | <b>39</b> |
| 3.1 <i>WNDP is expressed in <i>Xenopus laevis</i> oocytes</i>   | 40        |
| 3.2 <i>The chemiluminescence experiments confirm the suggested topology of WNDP</i>                                     | 40        |
| 3.3 <i>The effects of sequence modifications on the surface expression of WNDP in oocytes</i>                           | 41        |
| 3.3.1 <i>The N-terminal copper binding domains are not necessary for plasma membrane localisation</i>                   | 41        |
| 3.3.2 <i>The triple-Leu motif might be involved in the retrieval of WNDP from the cell surface</i>                      | 42        |
| 3.3.3 <i>Mutations supposed to impair catalytic activity of WNDP not always affect its plasma membrane localisation</i> | 43        |
| <b>4. Conclusions</b>   | <b>45</b> |
| <b>PROTEORHODOPSIN</b>  | <b>46</b> |
| <b>1. Introduction</b>  | <b>48</b> |
| <i>Retinylidene proteins</i>  | 48        |
| 1.1 <i>Bacteriorhodopsin</i>  | 48        |
| 1.1.1 <i>Photocycle, spectral characteristics, structure and photocurrents: a summary</i>                               | 49        |
| 1.1.2 <i>Probing the photocycle of BR with blue light</i>   | 53        |
| 1.2 <i>Proteorhodopsin</i>  | 54        |
| 1.2.1 <i>Structure</i>  | 55        |
| 1.2.2 <i>Photocycle and spectral characteristics</i>  | 57        |
| 1.2.3 <i>Photocurrents of Proteorhodopsin</i>   | 60        |

|   |            |
|---|------------|
| 1.2.4 Proteorhodopsin variants  | 62         |
| 2.3 <i>The aim of the work</i>  | 64         |
| <b>2. Results</b>   | <b>65</b>  |
| 2.1 <i>Action spectrum of PR wild-type</i>  | 65         |
| 2.2 <i>Voltage dependence of the proton transport in the presence or absence of pH gradients</i>  | 66         |
| 2.2.1 <i>In the presence of a pH gradient (asymmetrical pH conditions)</i>  | 66         |
| 2.2.2 <i>In the absence of a pH gradient (symmetrical pH conditions)</i>  | 68         |
| 2.3 <i>Investigating the effects of the applied electric field</i>  | 69         |
| 2.4 <i>The effect of azide on photocurrents of PR wt</i>  | 79         |
| 2.5 <i>Light intensity dependence of PR wt</i>  | 80         |
| 2.6 <i>Mutants of proteorhodopsin</i>   | 80         |
| 2.6.1 <i>Mutations of the proton donor E108</i>   | 82         |
| 2.6.2 <i>Mutations of the proton acceptor D97</i>   | 88         |
| 2.6.3 <i>L105Q, the spectral tuning switch</i>  | 94         |
| 2.7 <i>Localisation of bacteriorhodopsin (BR) and proteorhodopsin (PR) at the surface of the oocyte membrane, investigated by chemiluminescence</i> | 95         |
| 2.7.1 <i>Functional assessment of HA-tagged retinylidene proteins</i>   | 97         |
| <b>3. Discussion</b>  | <b>99</b>  |
| 3.1 <i>Action spectrum of PR wild-type</i>  | 99         |
| 3.2 <i>Regulation of H<sup>+</sup> translocation by pH and transmembrane potential in PR wt</i>   | 100        |
| 3.3 <i>The photocycles of PR and BR probed by potential changes and laser flash experiments</i>   | 101        |
| 3.4 <i>Light intensity dependence of PR wild-type</i>   | 106        |
| 3.5 <i>Mutants of proteorhodopsin</i>   | 106        |
| 3.5.1 <i>Mutations of the proton donor E108</i>   | 107        |
| 3.5.2 <i>Mutations of the proton acceptor D97</i>   | 109        |
| 3.5.3 <i>L105Q, the spectral tuning switch</i>  | 113        |
| 3.6 <i>The effect of azide on the photocurrents of proteorhodopsin</i>  | 114        |
| 3.7 <i>Inward pumping by proteorhodopsin</i>  | 118        |
| 3.8 <i>Localisation of bacteriorhodopsin (BR) and proteorhodopsin (PR) at the surface of the oocyte membrane, investigated by chemiluminescence</i> | 123        |
| 3.8.1 <i>Whether the HA-tag interferes with the function of an HA-tagged retinal H<sup>+</sup> pump depends on its position</i>                     | 124        |
| <b>4. Conclusions</b>   | <b>125</b> |
| <b>Materials and Methods</b>  | <b>127</b> |
| <b>On the use of <i>Xenopus laevis</i> oocytes for the heterologous expression of membrane proteins</b>   | <b>128</b> |
| <b>1. Molecular biology</b>   | <b>129</b> |
| 1.1 <i>cDNA constructs and cRNA synthesis</i>   | 129        |
| Wilson Disease Protein (WNDP)   | 129        |
| Proteorhodopsin (PR) and Bacteriorhodopsin (BR)   | 129        |
| 1.2 <i>Heterologous expression in <i>Xenopus laevis</i> oocytes</i>   | 130        |
| <b>2. Surface detection using chemiluminescence (WNDP HA-constructs, PR- and BR-NT-HA)</b>  | <b>130</b> |
| <b>3. Western Blot (WNDP-, PR-, BR- HA-constructs)</b>  | <b>131</b> |

|  |            |
|--|------------|
| <b>4. Electron microscopy (WNDP constructs)</b>                                  | <b>132</b> |
| <i>4.1 Postembedding immunogold labelling</i>                                    | <i>132</i> |
| <i>4.2 Freeze-fracture replica labelling</i>                                     | <i>133</i> |
| <b>5. Expression of WNDP constructs in Sf9 cells</b>                             | <b>134</b> |
| <b>6. Electrophysiology: two-electrode voltage clamp (PR- and BR constructs)</b> | <b>135</b> |
| <b>Zusammenfassung</b>   | <b>138</b> |
| <b>Bibliography</b>  | <b>144</b> |
| <b>Acknowledgements</b>  | <b>156</b> |
| <b>Glossary</b>  | <b>157</b> |
| <b>Curriculum Vitae</b>  | <b>159</b> |



# Foreword

## On the importance of transmembrane proteins for cell homeostasis

Cell membranes are vital for the life of the cell, and further on for the organisation of tissues, organs and proper function of an organism. Inside eukaryotic cells they confer specificity to the membranous organelles (nucleus, endoplasmatic reticulum, Golgi apparatus, mitochondria, chloroplasts, vacuoles). The *fluid mosaic model* of cell membranes proposed by J. Singer and G. Nicolson (1972) is still valid today. In this model membranes are built up by phospholipids with peripheral and integral proteins (Singer and Nicolson, 1972). The authors also recognised that the latter protein group is of crucial importance for the structural integrity of membranes. Since the publication of this model, a tremendous amount of information has been learned about the variety, structure and function of integral (or transmembrane) proteins. They confer functional specificity to the different types of membranes and contribute to communication between cells.

Transport proteins are a subgroup of transmembrane proteins which have a great importance in the cell homeostasis by facilitating the passage of ions and molecules, for which the lipid bilayer has a low permeability; by building up electro- and or chemical gradients across membranes necessary for cell energetics. Transport proteins can be divided into two major groups: **channels** (transport their substrate in the direction of its electrochemical gradient and interact only weakly with it) and **carriers** or **transporters** (most of which transport their substrate against its concentration gradient and undergo a series of conformational changes to transfer the bound substrate across the membrane = ‘active transport’) (based on *The Molecular Biology of the Cell*). Transmembrane ion gradients, necessary for excitability, energy storage and volume regulation are built up by two broad classes of active transport systems. Primary active transport utilises a primary energy source, such as light, redox energy or energy derived from ATP hydrolysis. In secondary active transport, the uphill movement of an ion species or solute molecule is coupled to the downhill movement of another ion species (Adam *et al.*, 1995; Bröer and Wagner, 2003; Läuger, 1991).

The present work wishes to contribute with information on two members of the primary active transporter group, which differ both in structure and function: **Wilson Disease Protein** which uses the energy released by ATP hydrolysis to transport copper across cell membranes, and **Proteorhodopsin**, which uses the energy of light to build up a proton gradient across the bacterial cell membrane.





# **Wilson Disease Protein**

**The effect of sequence variations on the plasma membrane localisation  
in *Xenopus laevis* oocytes**



## 1. Introduction

Copper (Cu) is an essential trace metal found in all living organisms. As a transition metal, it has partially filled *d* orbitals and has more than one stable valence state, the oxidized  $\text{Cu}^{2+}$  and the reduced  $\text{Cu}^+$ , being able to mediate electron transfer by valence-shuttle mechanism (Malmström and Leckner, 1998; Tapiero *et al.*, 2003). It is required for cell survival and serves as an important cofactor in redox chemistry for proteins required for growth and development, e.g. cytochrome-*c* oxidase (necessary for respiration), superoxide dismutase (protects against free radical damage), lysyl oxidase (required for collagen and elastase cross-linking), and dopamine- $\beta$ -monoxygenase (role in neurotransmission). Moreover, Cu is essential for efficient iron (Fe) uptake and mobilization in mammals (Cox and Moore, 2002; Tapiero *et al.*, 2003). The concentration of free Cu is very low, estimated in the order of  $10^{-18}$  –  $10^{-13}$  M in yeast cells and human plasma, respectively. When exceeding cellular needs,  $\text{Cu}^{2+}$  can be cytotoxic by participating in reactions that result in highly reactive oxygen species, which are responsible for lipid peroxidation in membranes, direct oxidation of proteins and cleavage of DNA and RNA molecules. In addition to this, Cu ions may displace other metal cofactors (like Zn) from their natural ligands [reviewed in Tapiero *et al.* (2003)]. For this reason, cellular Cu ions are bound to different metalloproteins like glutathion, metallothioneins and chaperones, and mechanisms of copper homeostasis are critical for survival of organisms and highly conserved throughout living species (Cox and Moore, 2002). (For a complete review of copper homeostasis and related disorders, see (Cox and Moore, 2002; Malmström and Leckner, 1998; Mercer, 2001; Puig and Thiele, 2002; Tapiero *et al.*, 2003))

Two typical ATPases, ATP7A (Menkes Disease Protein or MNKP) and ATP7B (Wilson Disease Protein, or WNDP) play an important role in maintaining the balance of copper. Both belong to the group of  $\text{P}_1$ -type heavy-metal transporting ion pumps (Palmgren and Axelsen, 1998) which share homology with various metal transporting ATPases identified in all kingdoms of life (Argüello, 2003) – see **figures 1.1** and **1.2**. ATP7A is expressed in most tissues except the liver and plays a role in dietary copper uptake through the epithelial cells of the intestine, whereas ATP7B is highly expressed in the liver, but also found in the brain, kidneys, placenta and the heart [reviewed in (Lutsenko and Petris, 2002; Tsivkovskii *et al.*, 2004)].

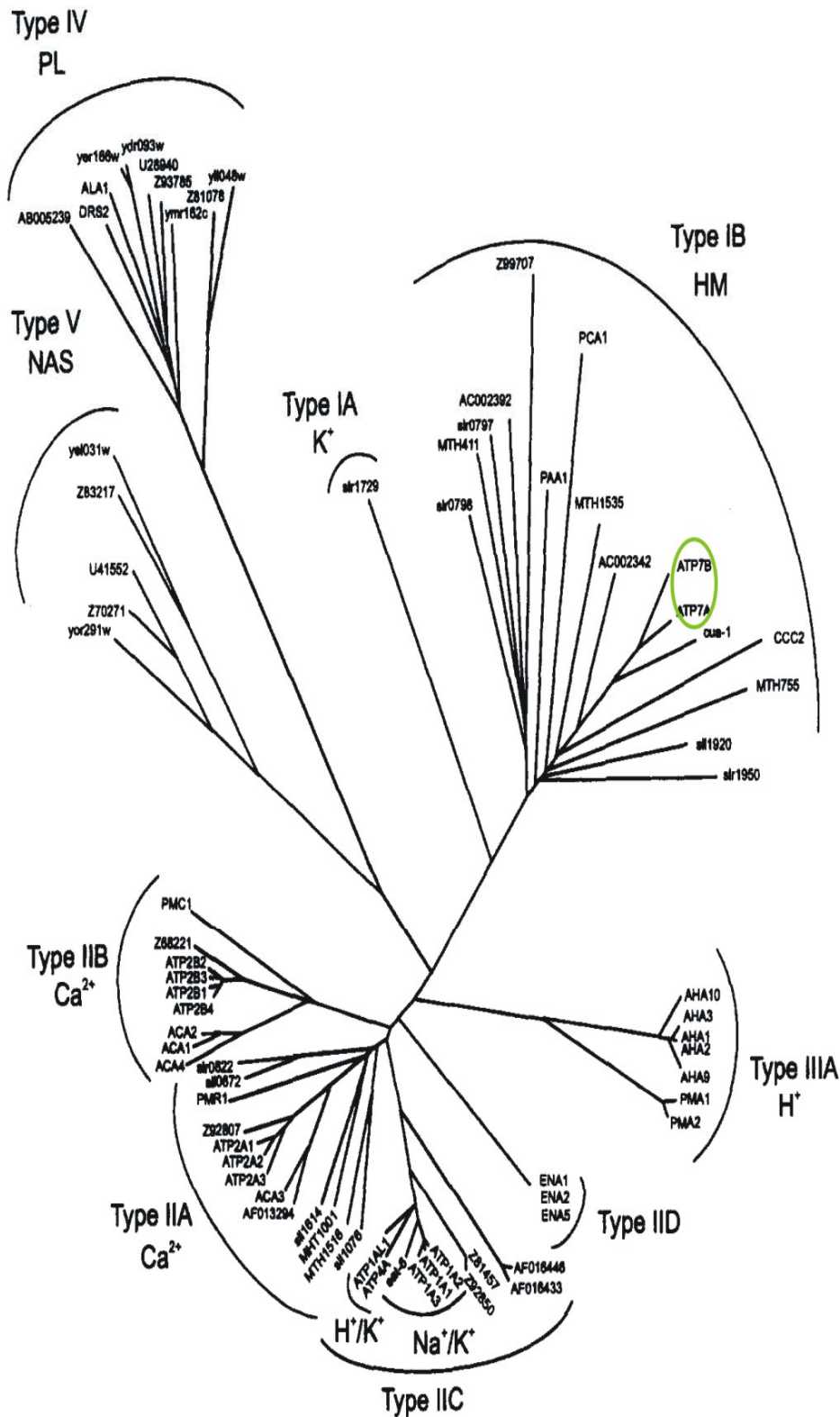


**Figure 1.1 Phylogenetic tree of P-type ATPases**

Human copper-transporting ATPases highlighted with green.

Abbreviations: HM, heavy metals; NAS, no assigned specificity; PL, phospholipids.

From Palmgren, M.G. and Axelsen, K.B., (1998) *Biochimica et Biophysica Acta*, **1365**, 37-45.

Since their identification, there are more structural and functional data available from ATP7A than ATP7B. A brief introduction of MNKP is important for understanding how specific residues or motifs of WNDP were chosen for mutagenesis, using information already available on MNKP.

```

WNDP      1 mpeqerqitaregasrkilsklslptraewepamkksfafdnvgyegglldglgppssqvattstvrilgmtcqcscvksiedri
MNKP      1 -----mdpsmgvnsvtisvegmtcncscwtieqqi

WNDP     81 snlkgiismkvsleqdsatvkvypsvvclqqvchqigdmgeasi-----
MNKP     31 gkvnvgvhhikvsleeknatiiydpkltqtpktlqeaiddmgfdavlnhpdplpvltdtflftvtasltlpwdhiqstllkt

WNDP    126 -----aegkaaswpsrslp-aeavvklrvegmtcqcscvssie
MNKP    111 kgvtdikiyppqkrtvavtiipsivnanqikelvpelsldtgtlekksagedhsmagagevvlkmkvegmtchscvstie

WNDP    163 gkvrklqgvrvkvslsnqeaivityqpyliqpeldlrhvdmgfeaaikskvaplslgpidierlqstnprkplssangn
MNKP    191 gkigklqgvqrikvslndqeativypplisveemkkqieamgfafvkkqpkylklgaidverlkntrpvks--segsqg

WNDP    243 fnnsetlghqgshvvtlqlridgmhckscvlnieenigllgvqsiqvslenktaqvkydpsectspvalqraiealppgn
MNKP    269 rpsytndstatfi-----idgmhckscvsniestlsalqyvssivvslenrsaivkynassvtpeslrkaieavspgl

WNDP    323 fkvsldpdaegsgtdhrsssshspspprnqv-ggtcsttliiaiegmtcascvhsiegmisqlegvqqisvslaegtatv
MNKP    343 yrvsitsevests---nspssslqkiplnvsvspltqetvinicgmtcncscvqsiegviskkpgvksirvslansgtv

WNDP    402 lynpsvispeelraaiedmgfeasvsvscstnplgnhsagnsmvqtdtgdtpsvgevaphtgrlpanhapdilakspqs
MNKP    420 eydplltspetlrgaiedmgfdatl---sdtnepl-----vviaqpssemplltstnefytkgmtpvqdkkeegk

WNDP    482 travapgkcfliqiegmtcascvsniernlqkeagvlsvlvalmagkaeikydpviegpleiaqfiqdlgfgeaavmedyag
MNKP    486 nss----keyiqvtgmtcascvsniernlrreegiysilvalmagkaevrynypaviappmiaefirelfgfatvienade

WNDP    562 sdgnieltitgmtcascvhnieskltrtngityasvalatskalvkfdpeiigprdiikiieeigfhaslaqrnphahl
MNKP    562 gdgvlelvrgmtcascvhnieslktkrgilycsvalatnkahikydppeiigprdiiehtieslgfeaslkkdrssashl

WNDP    642 dhkmeikqwkksflcslvfgipvmalmiym-----lipsnep-----hqsmlvdhniipglsilnlfifilct
MNKP    642 dhkreirgwrslvslffcipvmglmiymmvmdghhfatlhhnqmskeeminlhssmflerqilpglsvmnlisflfcv

WNDP    705 fvqllggwyfyvqaykslrhrsanmdvllvlatiayvyslvilvavaekaerspvtffdtppmlfvfialgrwleha
MNKP    722 pvqffggwyfyiqaykalkhktanmdvllvlattiafaysliillvamyarakvnpitffdtppmlfvfialgrwleha

WNDP    785 ksktsealaklmslqateatvvtlgednliireeqvpmelvrqgdvkvvpggkfpvdgkvlegntmadeslitgeampv
MNKP    802 kgktsealakilslqateatvltltdsdnillseeqvdelvrqgdvkvvpggkfpvdgrviegmsmvdeslitgeampv

WNDP    865 tkkpgstviarsinahgsvlkathvgntdtlaqivklveeaqmskapiqqladrfsgyfvpiiimstltlvwvwigf
MNKP    882 akkpgstviagsinqngsllicathvgadttlsqivklveeaqtskapiqqfadklsqyfvpfivfvsiatllvwvwigf

WNDP    945 idfgvvqkyfnpnkhisqteviirfafqtsitvclciacpcslglatptavmvgtgvaagngilikgkplmahkikt
MNKP    962 lnfeivetyfpgynrsisrtetiirfafqasitvclciacpcslglatptavmvgtgvaagngilikggeplemahkvkv

WNDP   1025 mfktdctithgvprvmrlllgdvatlprkvlavvgtaeassehplgvavtkyckeeigtetlgyctdfqavpgcgigc
MNKP   1042 vfktdctithgtpvvngvkvlttesnrishhilaivgtaesrsehgtaiktyckqeldtetlgtcidfqvvpvcgigc

WNDP   1105 kvsnvegilahserpls-----apashlneagslpaekdavnqtf-----vllignrewlrrngltissdvsd
MNKP   1122 kvtniegllhknwniednnknaslvqidasnqssstssmiidaqisnalnaqqykvllignrewmirnglvinnvdnd

WNDP   1168 amtthemkgqtailvaidgvlcgmiaiadavkgeaalavhtlqsmgvdvvlitgdnrktaraiatqvginkvfaevlpsh
MNKP   1202 fmteherkgrtavlvavddelcgliaiadvkpeaelaihiiksmglevlvltgdnrsktarsiasvgvitkvfaevlpsh

WNDP   1248 kvakvqelqngkqkvamvgdgvnospalagadmvgvaigtgtdvaieaadvvlirndlldvvasihlskrtvrririnvl
MNKP   1282 kvakvqelqngkqkvamvgdgvnospalamanvgiaigtgtdvaieaadvvlirndlldvvasidlsrktvkririnvf

WNDP   1328 aliynlvqipiaagvfmpigivlqpwmgsaamaassvsvlsslqlkcykkpdleryeaqahgmkpltasqsvshigm
MNKP   1362 aliynlvqipiaagvfmpigivlqpwmgsaamaassvsvlsslflklyrkptyesyelparsiqgkspseisvhvgid

WNDP   1408 drwrdspratpvdqvsyvsqvsllslltsdkpsrhaaaddgdkslllmg--rdeeqyi
MNKP   1442 dtsrnspkllldrivnysrasinsllsdrkslnsvvtsep-dkhslllvgdfreddtal

```

**Figure 1.2** Alignment of the aminoacid sequences of WNDP (PDB entry # P35670) and MNKP (PDB entry # NP 000043) The overall sequence identity of the two copper transporting ATPases (CTAs) is more than 54%. Identical residues are highlighted with blue. The orange squares depict the 6 putative metal binding sites in the N-terminal domain and the CPC motif within the 6<sup>th</sup> transmembrane domain involved the binding of Cu<sup>+</sup> during catalytic transport, the black squares the conserved sequences present in P<sub>2</sub>-type ATPases and the purple square the leucine residues involved in regulating endocytosis of the protein –see description in ‘Structure of WNDP’ below. Alignment accomplished with Clone Manager 5.

### 1.1. History

In 1912, the British neurologist Samuel A. K. Wilson (Wilson, 1912) reported on seven patients with a familial form of a primary neurological disorder associated with liver cirrhosis, which he referred to as progressive lenticular degeneration. In the same year, Fleischer described patients with a combination of corneal pigmentation, neuropsychiatric symptoms and liver cirrhosis. All these symptoms are related to the disorder recognised as Wilson Disease (WD) with an incidence of 1:30 000, where copper accumulates in various tissues, especially in the liver and brain. In 1960, Bearn demonstrated the autosomal recessive nature of WNDP and in 1985 Frydman *et al.* established a linkage of WD to the esterase D locus on chromosome 13q14.3 (Langner and Denk, 2004). In 1993 the WD gene (*ATP7B*) was cloned and shown that it encodes a 1465 amino acid long new member of the cation-transporting P-type ATPase family, ATP7B.

Menkes Disease (MNK) was first described in 1962 (Menkes *et al.*, 1962) as an X-linked recessive disorder characterised by early retardation in growth, peculiar hair, and focal cerebral and cerebellar degeneration. Other symptoms observed in the following years were, among others, spastic dementia, seizures, defective hair (Bray, 1965); kinky hair, retarded growth, decline in mental development, changes in the metaphyses of the long bones and tortuosity of cerebral arteries, patchy abnormality of systemic arteries with stenosis (Danks and Cartwright, 1973). The first indication that Menkes disease is a copper related disorder came from Danks *et al* (1972) who presented evidence of impaired copper absorption that can lead to connective tissue changes. Later Menkes *et al* (1988) listed 6 cuproenzymes, 5 of which may account for features in the disorder (see later). A series of genetic linkage studies refined the MNK locus to Xq12-q13 and finally the candidate gene was cloned by three independent groups in 1993: Chelly *et al*, Mercer *et al.* and Vulpe *et al*, where the latter succeeded in obtaining a complete set of clones corresponding to an 8.5 kb transcript (*ATP7A*) that encodes a 1500 amino acid protein (ATP7A or MNKP) with a strong homology to P-type ATPases.

## 1.2 Physiological importance of Cu<sup>+</sup>-ATPases

### 1.2.1 Wilson Disease Protein (W NDP)

W NDP has two important functions in cell physiology: to deliver copper to the secretory pathway for incorporation into copper-dependent enzymes and to facilitate export of copper from the cell. Which of these functions is carried out at any given moment, appears to depend on the intracellular concentration of copper. Consistent with these requirements, W NDP is primarily found in the Trans Golgi Network (or TGN) under low copper conditions but redistributes to a vesicular compartment when the intracellular copper concentration increases (Schaefer *et al.*, 1999). Malfunction of W NDP results in Wilson's disease, characterised by copper accumulation in a number of tissues, particularly in the liver, kidneys and brain, damaging the DNA, mitochondria, causing inactivation of a series of copper-dependent enzymes (ceruloplasmin, cytochrome-*c* oxidase, dopamine- $\beta$ -monooxygenase, lysyl oxidase, peptidylglycine- $\alpha$ -monooxygenase, superoxid dimutase and tyrosinase) and lipid peroxidation. Besides various degrees of liver pathology, patients with Wilson disease may present neurological and psychiatric problems [reviewed in (Cox and Moore, 2002; Lutsenko *et al.*, 2002; Mercer, 2001; Tapiero *et al.*, 2003)]. Borjigin and coworkers (1999) identified a pineal night-specific ATPase (PINA), a splice variant of ATP7B with copper transporting activity, selectively expressed at night, with a yet unrecognised rhythmic physiological function in the pineal gland. It is not clear, if PINA has any contribution to the pathogenesis of Wilson's disease, but there are no circadian defects reported in WD yet. Lutsenko and Cooper (1998) found two forms of W NDP, a 160 kDa form in the TGN and a 140 kDa form in the mitochondria of HepG2 cells, human skeletal muscle and heart cells suggesting that W NDP may play an important role in the copper dependent processes taking place in this organelle.

### 1.2.2 Menkes Disease Protein (MNKP)

MNKP, the other Cu<sup>+</sup>-ATPase identified as being important for copper homeostasis, presents a 54% sequence identity with W NDP. The clinical difference between Menkes and Wilson's patients is probably due to the difference in their tissue-specific expression pattern: in both cases the copper efflux from cells is impaired and copper-dependent enzymes are inactivated. MNKP was identified in the TGN of intestinal epithelia and most other tissues except the liver. Defective MNKP causes Menkes disease, an X-linked disorder with an incidence of

1:100 000. A primary defect is the reduced transport of dietary copper across the basolateral membrane of enterocytes into the hepatic portal circulation. This results in the entrapment of copper within the intestinal mucosa, ultimately leading to a severe copper deficiency in the peripheral organs and the central nervous system leading to skeletal abnormalities, skin laxity, hypopigmentation and neurological impairment (Lutsenko and Petris, 2002). Despite the overall copper deficiency, the intestinal cells and kidney accumulate copper (Vulpe *et al.*, 1993). Classical Menkes disease is usually lethal by the age of three, however there are two milder allelic variants, occipital horn syndrome and mild Menkes disease.

In the adult cerebellum both WNDP and MNKP are present in a cell-specific manner, where they appear to have distinct functions. Also, the expression pattern of the two proteins changes during postnatal development. In addition, in the absence of WNDP, functional compensation by MNKP was observed (Barnes *et al.*, 2005), information which supports the idea of complex regulation of copper homeostasis in the brain.

### 1.3 Structure of WNDP

All copper transporting ATPases contain the sequence motifs that characterise the P-type ATPase superfamily: DKTG, TGDN and GDGxND in the ATP-binding domain, TGE in a smaller cytoplasmic domain preceding the ATP-binding domain (Figure 3). Specific structural features of the P<sub>1</sub>-type subfamily include Cys, His and Met-rich sequences at the cytosolic N-terminal portion of the proteins that form metal binding sites, the signature sequences CPx in the transmembrane portion and the HP motif in the cytoplasmic domain (Tsivkovskii *et al.*, 2004).

In contrast to P<sub>2</sub>-type ATPases, very little is known about the structure of any of the P<sub>1</sub> group. In case of P<sub>2</sub>-type ATPases, the sequence similarity of H<sup>+</sup>/K<sup>+</sup>-, Na<sup>+</sup>/K<sup>+</sup>- and Ca<sup>2+</sup>-ATPases permits homology modeling using the high resolution structure of the Ca<sup>2+</sup>-ATPase (Toyoshima *et al.*, 2000; Toyoshima and Nomura, 2002). A high resolution structure has been determined only for an isolated metal binding site of MNKP (Gitschier *et al.*, 1998). Information about the rest of the protein was obtained by homology modeling of certain domains, which contain conserved motifs of all P-type ATPases, with the structure of the Ca<sup>2+</sup> ATPase (Efremov *et al.*, 2004; Morgan *et al.*, 2004). Consequently, the intracellular loop between TMS 4 and 5 is termed the 'actuator domain' and the loop between TMS 6 and 7 the



‘ATP binding domain’ similarly to those of the intracellular loops between TMS 2,3 and 4,5 of the  $\text{Ca}^{2+}$  ATPase.

The two human copper transporting ATPases are very similar regarding their primary sequence. In the following section only the structure of Wilson Disease Protein (WNDP) will be discussed in detail.

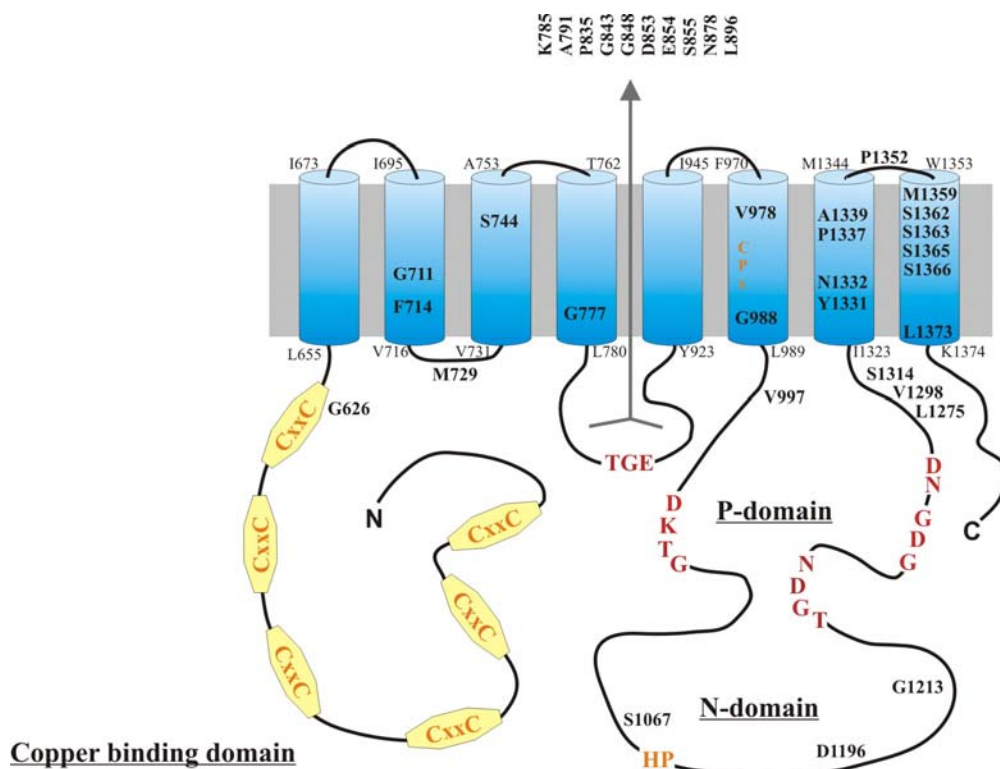


**Figure 1.3 Structure of WNDP: domain structure and sequence motifs**

from Tsivkovskii *et al.* in „Handbook of ATPases“, 2004, Wiley-VCH Verlag GmbH.

WNDP consists of 1465 amino acid residues predicted to form eight transmembrane segments (TMS), flanked by long N- and C-termini. The second and third putative cytoplasmic loops contain the conserved sequence motifs mentioned above (see **fig 1.1.3**).

The positions of the TMS in **figure 1.3** were predicted with the GCG Wisconsin Package’s TransMem program for human, mouse, rat and sheep WNDP. The boundaries of WNDP TMS were proposed based on the comparison of the predicted TMS in the alignment. Residues invariant for all ATPases are shown in red, residues conserved in the  $\text{P}_1$ -type ATPases in orange. Residues in black (bold) contribute to copper specificity, experimentally proven for several  $\text{P}_1$ -type ATPases (Argüello, 2003). The eight TMS topology was confirmed for the putative cadmium- and copper-ATPases from *Helicobacter pylori*, and the CadA protein from

*Staphylococcus aureus*. The hydropathy profiles of various members of the P<sub>1</sub>-type subfamily are similar, therefore it is likely that all copper transporting ATPases have the organisation suggested for WNDP. How the TMS are organised in respect to each other, is currently unknown (Tsivkovskii *et al.*, 2004).

The N-terminus contains six repetitive sequences with the conserved motif GMxCxxC. The Cys residues in this motif are invariant and are involved in Cu<sup>+</sup> coordination (DiDonato *et al.*, 2000; Gitschier *et al.*, 1998; Lutsenko *et al.*, 1997; Ralle *et al.*, 2004). The number of MBS in the N-terminal tail apparently correlates with the relative position of the organism on the evolutionary ladder, increasing from one (in bacteria) to six (in humans). It seems that the functional core of the copper transporting ATPases include only one or two MBS, whereas the others are important for protein regulation. In case of the mammalian proteins the MBS are not identical, in the MBS4 of mouse WNDP the second cysteine of the GMxCxxC motif is absent while MBS4 of rat WNDP lacks both cysteines. These missing residues most likely eliminate copper binding, further suggesting that not all MBS in mammalian CTAs are important for protein function. The differential role of MBS is further supported by homology modeling for all MBS using the NMR structure of MBS4 of MNKP. The overall structure resembles that of MBS4, but the distribution of the surface charges is distinct for different MBS. This could contribute to the differential function of each of the six MBS, like interaction with a copper chaperone, inter-domain interactions or regulation of WNDP.

The ATP-binding domain (ATP-BD) is located between TMS6 and TMS7 and contains the majority of the sequence motifs present in all P-type ATPases (see **fig 1.3**), similar to the cytoplasmic loop between TMS4 and -5 in the Ca<sup>2+</sup>-ATPase of the sarcoplasmic reticulum. In case of the latter protein, the crystal structure revealed that the ATP-BD is composed of two subdomains: the P-domain (phosphorylation domain) and the N-domain (nucleotide binding domain) (Toyoshima *et al.*, 2000; Toyoshima and Nomura, 2002). The primary sequence of the P-domain is not continuous, the domain is formed by the N- and C-terminal parts of the ATP-BD, which come together in the folded protein. The P-domain of WNDP shares 30% sequence identity with the corresponding domain of the Ca<sup>2+</sup>-ATPase and contains the signature motifs of P-type ATPases (**figures 1.2** and **1.3**). In contrast, the N-domain has no obvious sequence homology with any of the P-type ATPases. Homology modeling using the coordinates of the Ca<sup>2+</sup>-ATPase for the P-domain on one hand, and secondary structure predictions and threading algorithms for the N-domain on the other hand

revealed, that the entire ATP-BD of WNDP matches the fold of the  $\text{Ca}^{2+}$ -ATPase (Lutsenko *et al.*, 2002), reviewed in (Tsivkovskii *et al.*, 2004).

The actuator (A)-domain is located between the predicted TMS4 and -5 and is approximately 120 amino acids long. Its sequence is conserved among  $\text{P}_1$ -type ATPases and contains a TGE motif present in all P-type pumps. Earlier work has shown that mutations of residues within the TGE motif trap proteins in the E1-like (phosphorylated) state. Mutations in the putative A-domain of MNKP cause hyperphosphorylation of the enzyme after incubation with ATP and also affect the trafficking process of MNKP upon elevated copper concentrations (Petris *et al.*, 2002). This suggests that the A-domain could have a similar role in the human copper transporting ATPases as in the  $\text{Ca}^{2+}$ -ATPase.

The C-terminal tail of WNDP is about 100 amino acids long and contains a triple-leucine motif. MNKP has two Leu residues in its C-terminal region, which seem to be involved in copper-dependent trafficking.

#### 1.4 Functional properties of WNDP

The presence of conserved motifs in the structure of copper transporting ATPases suggests that the major steps in the catalytic cycle might be very similar for all P-type ATPases. At the same time, differences in the primary sequence and the predicted secondary structure of the copper transporting ATPases compared to the  $\text{P}_2$ -type ATPases point to the distinct structural organisation of the copper translocation pathway in copper transporting ATPases. A general model that describes the current understanding of the function of  $\text{P}_2$ -type ATPases is presented in **figure 1.4**

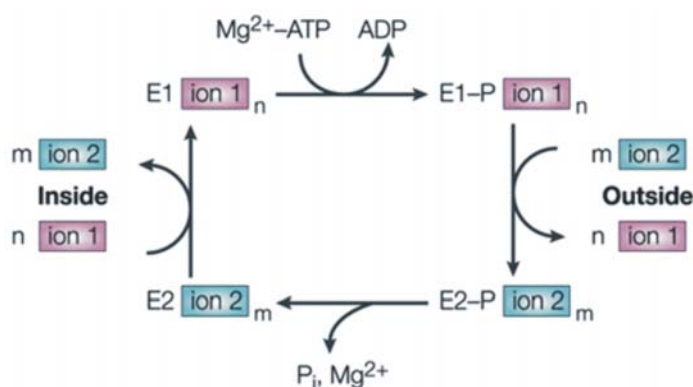


**Figure 1.4** The general ion translocation cycle of P-type ATPases based on the Albers-Post scheme of the NaK-ATPase: ion 1 from the cell interior binds to a high-affinity site in the ATPase E1 state. Ion binding triggers phosphorylation of the enzyme by  $\text{Mg}^{2+}$ -ATP, which leads to the phosphorylated E1-P state. The phosphorylated E2-P state then forms, which is unable to phosphorylate ADP, and this state has a reduced affinity for ion 1, which is released to the outside. Ion 2 binds from the outside and, on hydrolysis

of the phosphorylated Asp, the enzyme releases ion 2 to the interior and re-binds ion 1. The enzyme is then ready to start another cycle. As a net result of this process,  $n$  ions of type 1 are expelled and  $m$  ions of type 2 are imported per molecule of ATP consumed —  $n$  and  $m$  are small integral numbers between 1 and 3.  $\text{P}_i$  inorganic phosphate. From Kühlbrandt, (2004) *Nature Reviews Molecular Cell Biology* 5, 282-295.

In the case of CTAs the only transported ion identified is  $\text{Cu}^+$ , but the existence of a counterion or an auxiliary subunit like in the case of the NaK-ATPase can not be excluded.

Over the last years several *in vitro* and *in vivo* assays have been developed to investigate the functional properties of copper transporting ATPases. For a complete review see Tsivkovskii *et al.* in the *Handbook of ATPases* (2004).

Functional characterisation of WNDP endogenously expressed in human cells is difficult due to its low expression level [ $\sim 0.005\%$  of total membrane protein, (Tsivkovskii *et al.*, 2002)] and because the predominant localisation of the protein is in the intracellular membranes. Initial studies were carried out using the  $\Delta ccc2$  yeast strain heterologously expressing WNDP where their ability to complement the function of the deleted yeast homologue was followed (Forbes and Cox, 2000; Forbes *et al.*, 1999; Hsi *et al.*, 2004; Hung *et al.*, 1997). Voskoboinik *et al.* (2001) characterised the transport of copper using membrane preparations of the mammalian CHO cells heterologously expressing WNDP, and  $^{64}\text{Cu}$ :  $V_{\max} = 1.4 \text{ nmol/mg/min}$  and  $K_m = 8.4 \mu\text{M}$ , values very similar to those obtained for MNKP (Voskoboinik *et al.*, 1998). Transient phosphorylation of the invariant Asp residue in the DKTG motif is the signature event required for transmembrane ion-transport by all P-type ATPases and it is also present in all copper transporting ATPases. The enzymatic steps which accompany Cu transport were extensively studied by Lutsenko and coworkers using the *Sf9*/baculovirus system (Huster and Lutsenko, 2003; Lutsenko and Cooper M., 1998; Lutsenko *et al.*, 2002; Lutsenko and Petris, 2002; Lutsenko *et al.*, 2003; Tsivkovskii *et al.*, 2001; Tsivkovskii *et al.*, 2003; Tsivkovskii *et al.*, 2002; Vanderwerf *et al.*, 2001; Vanderwerf and Lutsenko, 2002; Walker *et al.*, 2004; Walker *et al.*, 2002). They characterised several steps of the catalytic cycle, rates of phosphorylation, apparent affinities for nucleotides and Cu and the conformational state of the enzyme by analyzing the effect of various ligands (Cu, ATP, ADP, inorganic phosphate, vanadate). The kinetics of phosphoenzyme formation for WNDP is considerably slower than those of other P-type ATPases:  $T_{1/2} = 60 \text{ s}$  (Tsivkovskii *et al.*, 2002). As other P-type ATPases, WNDP can be phosphorylated in the presence of inorganic phosphate ( $\text{P}_i$ ) and  $\text{Mg}^{2+}$ , starting from the  $\text{E}_2$  state. The copper chelator bathocuproine disulfonate (BCS) inhibits this reaction, supporting the general reaction cycle for P-type ATPases proposed by Albers and Post (Albers, 1967; Post *et al.*, 1969) – see **figure 1.4**. The affinity of WNDP for Cu is  $\sim 1.5 \mu\text{M}$  and this concentration is sufficient for maximum phosphorylation. Additionally, the effect of Cu on WNDP activity is cooperative which suggests that more than one copper-binding site is involved in stimulation of phosphoenzyme formation. According to Huster *et al.* (2003) the MBS 5 or -6 are involved: mutating Cys residues in either MBS5 or -6 eliminates the cooperative effect of copper but the protein can still be phosphorylated.

Although much is known about isolated steps in WNDP's catalytic cycle, there is no information available yet about the entire turnover of the protein. It is also not clear whether and how the use of different expression systems could influence the experimental data [e.g. transport characteristics of MNKP expressed in mammalian or yeast cells are different (Voskoboinik *et al.*, 2001; Voskoboinik *et al.*, 1999)].

### 1.5 The copper-dependent localisation of WNDP and MNKP

The subcellular distribution of WNDP and MNKP in cultured mammalian cell lines was investigated using immunohistochemistry (Forbes and Cox, 2000; La Fontaine *et al.*, 1999; Lutsenko and Petris, 2002; Petris *et al.*, 1996), confocal microscopy (Harada *et al.*, 2000; Huster and Lutsenko, 2003) and electron microscopy (Huster and Lutsenko, 2003; La Fontaine *et al.*, 2001; Petris *et al.*, 1996; Roelofsen *et al.*, 2000). In addition, Huster *et al.* (Huster *et al.*, 2003) presented electron microscopy images of normal and Wilson Disease-affected human liver.

In human and rodent cell lines MNKP was shown to localise under normal copper concentrations to the TGN, confirmed *in vivo* in human breast tissue sections (Lutsenko and Petris, 2002). Similar studies have shown, that WNDP is located in the TGN of hepatoma cell lines, primary hepatocytes and in rat and human liver sections (Hung *et al.*, 1997; Huster *et al.*, 2003; Roelofsen *et al.*, 2000; Schaefer *et al.*, 1999). The location of WNDP and MNKP in the TGN presumably enables the supply of copper to cuproenzymes synthesised in the secretory compartments. The TGN is a critical cellular compartment where proteins are segregated into different transport packages and dispatched to their final destination in the cell (Alberts *et al.*, 2004).

A novel post-translational mechanism for regulating copper export via the Cu<sup>+</sup>-ATPases has been identified, involving the copper-dependent exocytic trafficking of these proteins from the TGN (Hung *et al.*, 1997; La Fontaine *et al.*, 2001; Petris *et al.*, 1996; Petris *et al.*, 2002; Roelofsen *et al.*, 2000; Schaefer *et al.*, 1999; Strausak *et al.*, 1999). The trafficking of WNDP and MNKP does not involve *de novo* protein synthesis, and occurs at intermediate copper levels in the 20-40 µM range (MNKP) but can be triggered already at 1 µM (WNDP). In the case of MNKP, elevated copper induces relocation from the TGN to the plasma membrane of CHO cells (Petris *et al.*, 1996) or to the basolateral membrane of polarised MDCK cells (Greenough *et al.*, 2004).

Studies of WNDP expressed in different cell lines suggest, that unlike MNKP, WNDP might not reach the plasma membrane, but cycles to cytoplasmic vesicles in hepatoma cell lines (Hung *et al.*, 1997; Huster and Lutsenko, 2003; Schaefer *et al.*, 1999), or to apical vacuoles reminiscent of bile canaliculi (Roelofsen *et al.*, 2000). This latter observation suggests that WNDP can relocate to the apical membrane and thus directly contribute to the biliary copper excretion when copper is elevated. In non-hepatic CHO cells WNDP was found in a vesicular compartment devoid of marker proteins for late endosomes and lysosomes that may represent a novel compartment for storing excess copper (Forbes and Cox, 2000; La Fontaine *et al.*, 2001). Copper-induced trafficking of WNDP to vesicles located in proximity to the canalicular membrane has been observed in liver sections derived from rats injected with excess copper (Schaefer *et al.*, 1999; Schaefer and Gitlin, 1999). In contrast to these studies, Harada *et al.* (2000) identified WNDP-GFP chimaeras only in late endosomes, under both basal and elevated copper concentrations (Harada *et al.*, 2000).

An alternative mechanism of copper clearance from cells is exocytosis of vesicles containing copper transported by WNDP, while WNDP itself returns to the TGN (Payne *et al.*, 1998). Strong evidence supporting either model is currently lacking and the molecular mechanism of WNDP relocalisation within cells and the involved protein machinery remain to be determined.

The copper-induced trafficking of WNDP and MNKP is a reversible process, since both proteins return to the TGN when cells are returned from high copper to basal media. This ability to recycle probably serves to reinstall the copper supply to secreted cuproenzymes once basal copper levels are restored. Interestingly, MNKP constitutively cycles between the plasma membrane without addition of copper (Petris and Mercer, 1999). It is unknown, whether this cycling is induced by basal copper levels in the media, or simply a corrective mechanism for retrieving molecules that escaped TGN retention. The restoration of TGN localisation of both WNDP and MNKP upon changing to low copper-containing media suggests the existence of sorting signals for endocytic retrieval to the TGN. In case of MNKP a di-leucine motif in the C-terminal region has been identified as endocytotic retrieval signal. Di-leucine motifs are known to function in the endocytosis of proteins via clathrin-coated vesicles (Alberts *et al.*, 2004). Petris and Mercer have shown that these leucine residues are involved in the endocytosis of MNKP and that the retrieval of MNKP from the plasma membrane occurs into the transferrin-containing endosomal pathway (Petris *et al.*, 1998; Petris and Mercer, 1999). In addition, Lane *et al.* suggest that MNKP can utilise both clathrin-dependent and independent endocytosis (Lane *et al.*, 2004). The mechanism by which copper

influences the ATPase cycling is not entirely clear, but it seems that inhibition of MNKP internalisation is not the mechanism. Only the kinetics of MNKP internalisation is affected by copper (Petris and Mercer, 1999). The retention of MNKP in the TGN might involve sequence elements within the third transmembrane region of MNKP (Francis *et al.*, 1998).

WNDP has three leucine residues in homologous position to MNKP in the C-terminal domain. This sequence similarity suggests that WNDP may also cycle via the plasma membrane. Difficulties with detection of WNDP at the plasma membrane could reflect low amounts of WNDP in this location at any given time (Lutsenko and Petris, 2002; Schaefer *et al.*, 1999).

### **1.6 Molecular mechanism of copper-dependent trafficking**

As other aspects related to the characterisation of the human copper ATPases, the molecular mechanism of copper-dependent trafficking has been studied in more detail for MNKP. Two approaches have been used: site-directed and deletion mutagenesis in the copper binding region of MNKP and various mutations found in Menkes disease patients.

In the N-terminal region only MBS5 or MBS6 seems necessary and sufficient for the copper-dependent redistribution of MNKP (Strausak *et al.*, 1999). Earlier experiments demonstrated that MBS5 or MBS6 are also important for the copper ATPase function, so the trafficking studies raise the question of whether the ability of mammalian copper ATPases to traffick is coupled to their functional activity.

This issue has been addressed using MNKP and WNDP with single amino-acid mutations. Several disease-causing mutations were shown to disrupt normal localisation and trafficking of both MNKP and WNDP (Forbes and Cox, 2000; Huster *et al.*, 2003; Kim *et al.*, 2002; Payne *et al.*, 1998; Voskoboinik *et al.*, 2003). These mutations are located in various parts of the ATPases, suggesting that their effect on copper-induced trafficking is probably indirect. Consequently it was hypothesised that trafficking of MNKP and WNDP depends on copper transport activity. In case of MNKP, this conclusion was supported by the finding that the mutations within the conserved CPC, SEHPL and DKTG sequences disrupted the copper-induced relocalisation from the TGN (Petris *et al.*, 2002). Similarly, mutations in the CPC motif of WNDP cause mislocalisation of the protein upon addition of copper (Forbes and Cox, 2000). Interestingly, mutations of the TGE motif (of both MNKP and WNDP), and residues in its proximity (MNKP) resulted in the constitutive relocalisation to the plasma

membrane even in the absence of additional copper (Petris *et al.*, 2002). The TGE motif of P-type ATPases is thought to facilitate conformational transitions during the catalytic cycle and dephosphorylation of the phospho-catalytic intermediate. Petris *et al.* have found that both the TGE>AAA and L873R mutations have a 2-3-fold higher level of phosphorylation compared to the wild-type MNKP, which is consistent with the predicted stabilisation of the E1-like state. Neither of these two mutants can transport copper, suggesting that a certain conformational state rather than the ability to go through the entire cycle is necessary for relocalisation of the copper transporting ATPases (Petris *et al.*, 2002). Based on experiments with the MNKP double mutant 1044DKTG-EKTG and 875TGE-AAA, Petris *et al.* suggest that the formation of the phosphorylated intermediate during MNKP catalysis triggers the exocytic trafficking of the protein from the TGN. The double mutant had an exclusively perinuclear localisation and failed to undergo relocalisation to the plasma membrane in cells exposed to elevated copper. It was concluded that the D1044E mutation suppressed the TGE>AAA mutation and therefore copper-induced trafficking of MNKP required the formation of a phosphorylated catalytic intermediate. According to the catalysis-dependent trafficking model formulated by the authors, the steady state TGN localisation of MNKP and WNDP under low copper conditions is a reflection of the small proportion of molecules cycling through phosphorylated catalytic intermediates. The shift in distribution of MNKP and WNDP from the TGN upon exposure to elevated copper can be explained by an increase in the proportion of catalytically active proteins and thus the number of transporters cycling through the phosphorylated conformation (Petris *et al.*, 2002). This model seems to neglect the importance of the WNDP and MNKP in supplying copper for enzymes in the secretory pathway. Another explanation could be that the copper ATPases need to adopt a certain conformation to become trafficking-competent; however, this conformation is not directly linked to the catalytic cycle: the above results with the mutants indicate that this trafficking-competent conformation resembles the E1 or E1P state of the enzyme.

Kim *et al.* recently demonstrated that the trafficking and catalytic activity can be uncoupled (Kim *et al.*, 2003). The authors characterised a mutation found in Menkes disease patients, which resulted in a shorter linker connecting MBS6 to the TM1. This mutant localises correctly to the TGN and can transport copper to tyrosinase (a copper dependent enzyme in the secretory pathway) but fails to relocalise to the plasma membrane in response to elevated copper. This means that the linker region between the last MBS and the first transmembrane helix could contribute to an important trafficking signal. This idea is further supported by the experiments Mercer *et al.* have done with chimaeras of MNKP and WNDP expressed in CHO



cells, to identify the regions of these proteins responsible for their differential trafficking: MNKP to the plasma membrane and WNDP to a not clearly defined cytosolic compartment. Chimeras in which the N-terminal MBSs of MNKP were replaced with the corresponding MBSs of WNDP localised to a vesicular compartment, similarly to WNDP in elevated copper, pointing to the important role of the N-terminal domain in protein targeting. Further deletions of various MBSs of the chimaera indicate that the targeting signal which directs the chimera to the vesicular compartment is present in the region of MBS6 and may involve the small segment close to the membrane (Mercer *et al.*, 2003). Whether the signaling sequence works by itself or in the context of the entire protein sequence is still unclear (Tsivkovskii *et al.*, 2004).

Trafficking of WNDP is less well characterised. In basal copper concentrations, WNDP is localised primarily in the plasma membrane. WNDP shows a more diffuse staining than MNKP suggesting that lower amounts of copper may trigger relocalisation. The sequences of the WNDP homologues from mouse, rat and sheep each include three consecutive leucines at a position corresponding to the dileucine motif of MNKP. This triple-leucine motif might function in TGN targeting of WNDP similarly to the L1487-L1488 in MNKP. Ultrastructural studies on cultured cells (Huster and Lutsenko, 2003; La Fontaine *et al.*, 2001) and liver sections of WND patients (Huster *et al.*, 2003) suggest that increasing copper concentrations determine the relocalisation of WNDP to large multi-vesicular structures resembling late endosomes. The molecular nature of this compartment is not yet known, it might represent a novel compartment for copper transport. Gou *et al.* identified the first 63 amino acids in the amino-terminus to be important for the targeting of WNDP to the appropriate cellular compartment in polarised cells when the copper concentration increases (Guo *et al.*, 2005).

The effect of mutations on both activity and trafficking of WNDP has been investigated. The catalytically inactive mutants of WNDP R778L and CPC>SPS were unable to traffic in response to copper and R778L was also mislocalised under basal copper conditions, presumably to the ER. G943S was shown to localise normally to the TGN but unable to redistribute in elevated copper conditions. Together with two other mutants, D965N and L776V, which are initially mislocalised throughout the cell, these mutants show almost normal function in the yeast complementation assay. These findings further illustrate that activity and trafficking in human copper transporting ATPases can be uncoupled (Forbes and Cox, 2000).

Altogether, the general mechanism of copper-stimulated trafficking appears to be similar for WNDP and MNKP.

Recent studies suggest that the copper concentration, the presence of the copper chaperone Atox1, and the phosphorylation level are involved in the copper-dependent relocation of copper ATPases (Cobbold *et al.*, 2002; Hamza *et al.*, 2003; Vanderwerf *et al.*, 2001; Voskoboynik *et al.*, 2003).

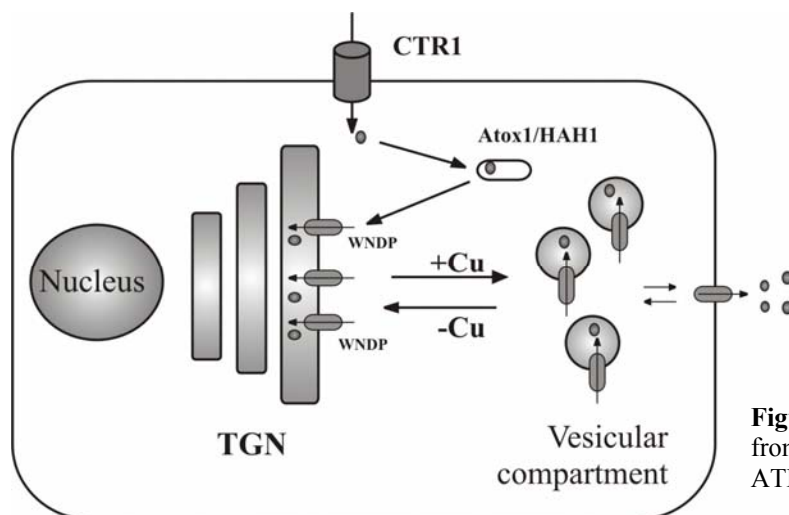


**Figure 1.5 Trafficking of WNDP in a cell** from Tsivkovskii *et al.* in „Handbook of ATPases“, 2004, Wiley-VCH Verlag GmbH.

The current model of regulation of human copper transporting ATPases (**figure 1.5**) can be summarised as follows: the activities of WNDP and MNKP are copper dependent and are likely to be regulated by their N-terminal domain. The copper chaperone Atox1 controls the copper-occupancy of the N-terminal domain through a reversible delivery of copper. At copper concentrations exceeding a certain threshold the N-terminal domain of mammalian copper ATPases binds copper and undergoes conformational transitions, which result in alterations of both the N-terminal domain and the ATP binding domain and possibly the C-terminal tail as well. These events initiate the trafficking steps either directly or following phosphorylation of WNDP by a kinase. A decrease in copper concentration drives these reactions in reverse (Tsivkovskii *et al.*, 2004).

### 1.7 Disease mutations that affect the function of WNDP and MNKP

Mutations in the ATP7A and ATP7B genes cause two severe genetic disorders in humans: Menkes disease and Wilson's disease, described earlier in this chapter. Currently over 200 disease-causing mutations have been described for human copper ATPases, particularly for WNDP. These are documented in the NCBI Protein database (<http://www.ncbi.nlm.nih.gov/entrez/dispomim.cgi?id=277900>), and at the Univ. of Alberta (<http://www.uofa-medical-genetics.org/wilson/index.php>) and some of them are listed in

Tsivkovskii *et al* (2004). The mutations are of several types: *missense* (single amino acid substitutions in the protein), *non-sense* (insertion of a stop-codon and premature termination of the translation), *frame-shift* (deletion or insertion of several nucleotides), *splice site* mutations, and *large gene rearrangements* (gross modification or loss of the transcript).

The mutations are found in all structural domains of WNDP, suggesting that all domains are likely to contribute to protein stability, activity, or regulation. Also, the distribution of mutations is not uniform over the protein sequence, the ATP-binding domain, the A-domain and the transmembrane segments have on average more mutations per number of residues than the N-domain, consistent with the idea that these three domains with a high mutation content form a “catalytic core” present in all P-type ATPases. The N- and C-terminal regions might be involved in regulation rather than function (Tsivkovskii *et al.*, 2004).

A comparative analysis of all mutations in WNDP and MNKP shows an almost equal distribution of mutations throughout the genes. The number of mutations lying within the copper-binding domain, the transmembrane helices, the conserved CPC motif, the transduction domain and the C-terminus are comparable. A difference is seen in the linker region between MBS6 and TMS1, with an abundance of MNK patient mutations in this region compared with only 3% of WND patient mutations. The phosphorylation and ATP-binding domains of WNDP are also more affected by mutations. The less affected regions are the C-termini of both proteins (Hsi and Cox, 2004).

Mutations in both WNDP and MNKP occur with various frequencies and depend on the ethnic background of particular populations. The **H1069Q** mutation is the most frequent cause of Wilson disease in northern European populations and one of the most frequent found in others (Butler *et al.*, 2001). His1069 belongs to the conserved SEHPL motif in the putative large cytoplasmic loop between TMS 6-7 (N-domain), HP occurring in all P-type ATPases. Several groups tried to characterise the effect of the H1069Q substitution. Initial studies using the yeast complementation assay provided inconsistent results regarding the ability of the H1069Q mutant to rescue the  $\Delta ccc2$  yeast phenotype [yes: Iida *et al*, 1998; no: Hung *et al.*, 1998, reviewed in (Tsivkovskii *et al.*, 2004)]. Payne *et al.* (Payne *et al.*, 1998) showed that in a fibroblast cell line H1069Q and H1069A disrupt WNDP function and the transcripts are localised mainly in the ER instead of the TGN. Interestingly, mislocalisation of H1069 mutants could be corrected by growing the fibroblasts at lower temperature (28°C versus 37°C), suggesting that misfolding of the mutated protein could be a temperature-sensitive defect. Analysis of endogenous WNDP in biopsy samples from humans confirmed the mislocalisation of the H1069Q mutant (Huster *et al.*, 2003).

Tsivkovskii *et al.* employed the *Sf9* insect cell system to investigate the role of His1069. Substitution of His1069 with Gln, Cys and Ala and analysis of these mutants led to the conclusion that H1069 may contribute to orientation of ATP in the active site or may play a role in organising the catalytic site by mediating domain-domain interactions. These conclusions are supported by the localisation of His1069 in the ATP-binding domain (Tsivkovskii *et al.*, 2003).

**C985Y** is a disease causing missense mutation of the second Cys in the conserved CPC motif in TMS6, predicted to be involved in copper binding within the transmembrane domain during transport (Haas *et al.*, 1999). Forbes and Cox have shown already using the yeast complementation assay that experimental replacement of Cys with Ser residues leads to a non-functional protein (Forbes and Cox, 1998). Studies of copper transporters homologous to WNDP from *Caenorhabditis elegans*, *Enterococcus hirae*, and MNKP draw similar conclusions (reviewed in Tsivkovskii *et al.*, 2004). Altogether, these studies emphasise the importance of the CPC motif for the CTAs.

In the ATP-binding domain there are few disease-causing mutations known directly to affect the conserved motifs (D1267A, D1270S from the GDG-ND motif) and no records of mutations which affect directly the DKTG motif, but there are several ones scattered in the large cytoplasmic loop between TMS6-7 pointing towards the functional importance of correct folding. Similarly, there are no mutations known of the actuator-domain of WNDP, but in case of MNKP L873R has been identified, 2 residues upstream from the TGE motif, characterised by hyperphosphorylation and inability to complement the  $\Delta ccc2$  yeast phenotype.

Non-clinical studies introduce mutations experimentally to study the structure and function of CTAs. Those known of WNDP are mentioned in the ‘*Structure of WNDP*’ section.

## 1.8 The aim of the work

The present study sought to establish the *Xenopus* oocytes – now a well-established system for the analysis of plasma membrane transporters – as an alternative expression system for WNDP. The oocytes were employed to find out whether WNDP can be found at the plasma membrane in measurable quantities, verify the topology of the protein suggested by hydropathy plots, and to investigate the effect of sequence modifications of WNDP on the plasma membrane localisation of the protein.

## 2. Results

### 2.1 Topological model of WNDP

According to hydropathy analysis WNDP encompasses 8 transmembrane segments with cytoplasmic amino- and carboxy-terminus (**fig. 2.1.A**). Amino acid positions at the membrane interface of proposed TM segments are indicated (according to protein database entry P35670). Structural parts relevant to our study are shown: the six amino-terminal heavy-metal binding sites each containing a CxxC motif, the highly conserved SEHPL motif encompassing His-1069, and the triple leucine at the far carboxy-terminus, the encircled D denotes the residue Asp-1027 transiently phosphorylated during the catalytic cycle. The positions of the HA epitope insertions are schematically drawn.

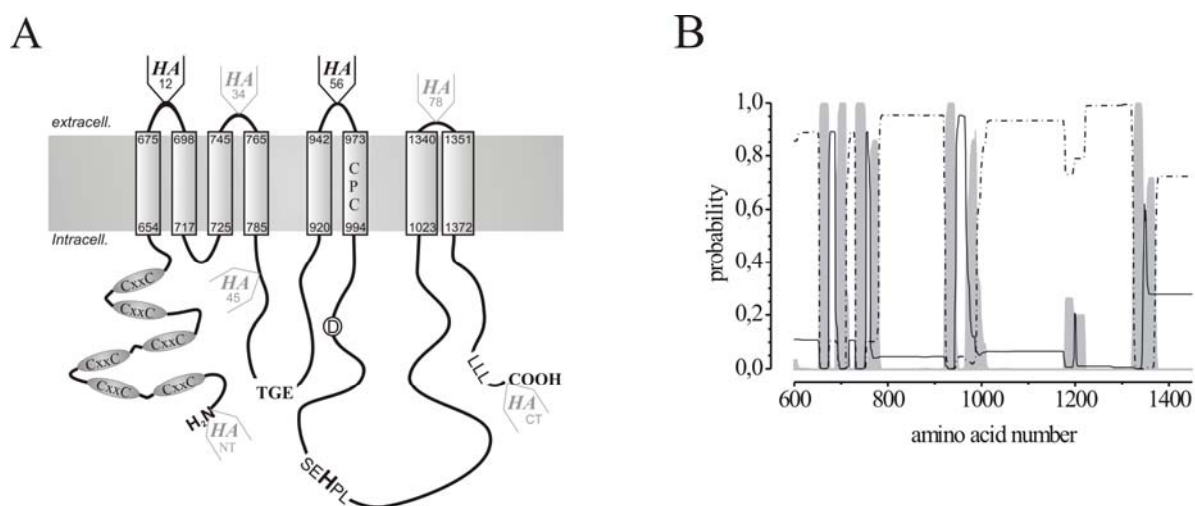


**Figure 2.1 Topology model of WNDP (A)** According to hydropathy analysis WNDP encompasses 8 transmembrane segments with cytoplasmic amino- and carboxyl termini. Amino acid positions at the membrane interface of proposed TM segments are indicated (according to the protein database entry P35670). The six amino-terminal heavy-metal binding sites each containing a CxxC motif, and a series of conserved sequences are also shown: the TGE motif, the SEHPL with the highly conserved His1069, the D1027 which is transiently phosphorylated during the catalytic cycle, part of the DKTG motif. The inserted HA epitopes are schematically depicted, in black the ones detected at the extracellular surface. **(B)** Analysis of the WNDP primary sequence with the hidden Markov modelling algorithm (Krogh et al., 2001) for prediction of the membrane topology. Only amino acids from 600 to 1450 are shown. Probabilities for intracellular (dash-dotted) or extracellular (solid) location and the resulting TM region (grey) are depicted. Difficulties in determining the extracellular location for the short loops between TMS 3-4 and TMS 7-8 are visible.

**Figure 2.1 B** shows the analysis of the WNDP primary sequence with the hidden Markov modelling algorithm TMHMM (Krogh et al., 2001) for prediction of the transmembrane topology (<http://www.cbs.dtu.dk/services/TMHMM/>).

The graph shows clearly the difficulty in determining extracellular location of the extremely short loops connecting TMS-7 and -8 (and to some extent TMS-3 and -4).

Similar results were obtained with the prediction algorithms:

TopPred (<http://bioweb.pasteur.fr/seqanal/interfaces/toppred.html>),

TMpred ([http://www.ch.embnet.org/software/TMPRED\\_form.html](http://www.ch.embnet.org/software/TMPRED_form.html)),

and DAS (<http://www.sbc.su.se/~miklos/DAS/maindas.html>) (data not shown).

The TMHMM algorithm incorporates not only hydrophobicity, but also charge bias, helix lengths, and grammatical parameters, the latter taking into account that helical membrane proteins have an alternate cytoplasmic/non-cytoplasmic loop structure (Krogh *et al.*, 2001). TMHMM predicts 8 transmembrane segments for WNDP, in accordance with a hydropathy profile published for the related CopA Cu-ATPase from *Enterococcus hirae* (Solioz and Christopher, 1996). According to the TMHMM algorithm all predicted extracellular loop regions of WNDP are very short (1-2: 14 amino acids (AA), 3-4: 9 AA, 5-6: 21 AA, 7-8: 7 AA), in case of the 7-8 loop resulting in a significantly lower probability for extracellular location.

## 2.2 Expression of the full length WNDP in oocytes

To evaluate the usefulness of the *Xenopus* oocyte system for the expression of WNDP, various amounts of WNDP cRNA were injected into oocytes and expression was quantified in Western blots of crude membrane preparations after four days. Protein bands corresponding to the 165 kDa full-length WNDP were observed in cRNA-injected oocytes, but not in control, water-injected oocytes (**fig 1.2.2**), indicating expression of the full-length WNDP. Protein expression after 4 days was maximal with 25 ng cRNA per oocyte and did not increase with prolonged expression time (data not shown).

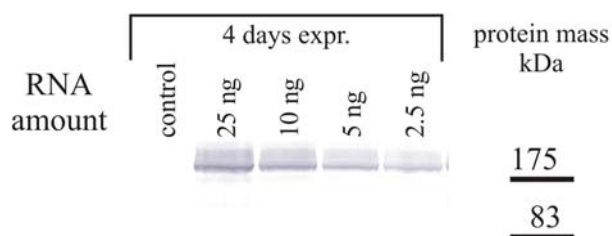


**Figure 2.2 Expression of WNDP wt in *Xenopus laevis* oocytes** Different amounts of WNDP wild-type cRNA were injected into oocytes, and cells were harvested after 4 days expression time. Samples corresponding to the amount of one oocyte were loaded in each lane, and detection was carried out with the polyclonal antibody a-ABD. Protein weight standards are marked (right).

Therefore, injections with 25 ng cRNA were used as a standard for WNDP expression, unless otherwise stated, and further analysis were carried out after four days post-injection.

### 2.3 Localisation of WNDP at the cell surface using immunoluminescence

In order to detect WNDP in the plasma membrane of oocytes and to probe for the proposed membrane topology of WNDP, HA epitopes were inserted into the putative extracellular loops between TMS 1-2, 3-4, 5-6, and 7-8 (**fig 2.1.A**). The resulting constructs (termed **WNDP-HA12** through **WNDP-HA78**) were expressed in oocytes, and the presence or absence of the HA tag at the cell surface was evaluated using a chemiluminescence detection assay originally described by (Zerangue *et al.*, 1999) for the plasma membrane localisation of inward rectifier potassium channels. The HA epitope insertions at the amino and carboxy termini (**WNDP-HA(N)**, **WNDP-HA(C)**) and within the cytoplasmic loop between TMS-4 and -5 (**WNDP-HA45**) served as negative controls.

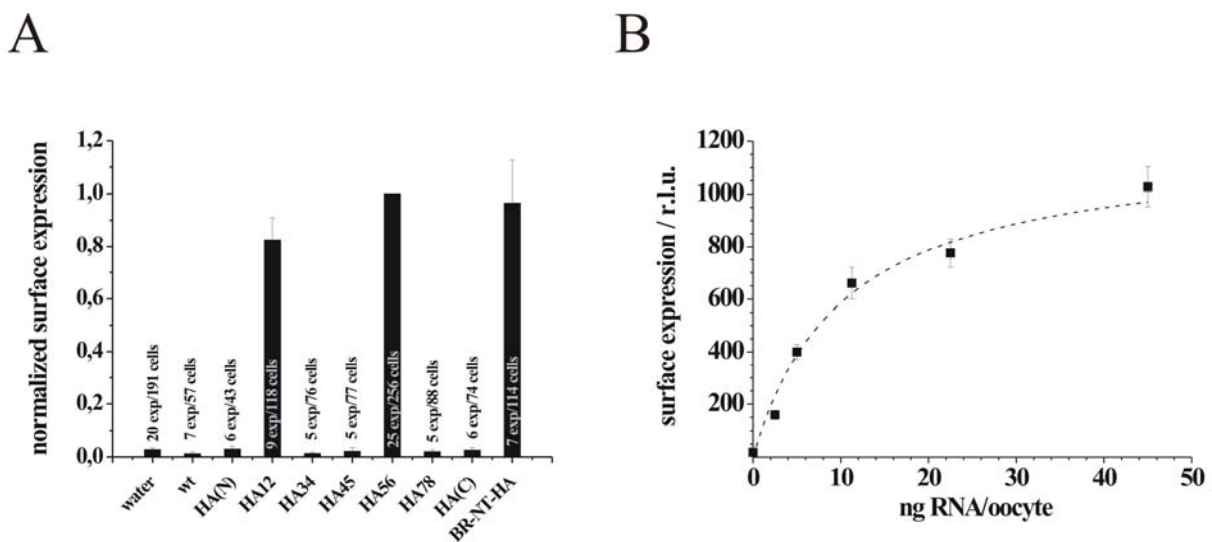


**Figure 2.3 Surface detection of WNDP construct with the HA-tag in different loops**

Surface expression of various HA-tagged WNDP constructs (A) and cRNA dependence of surface expression (B). In (A) the number of experiments and oocytes are indicated above each bar. Within each experiment original luminescence data were averaged for each construct, normalized to the mean value for WNDP-HA56 and thus averaged over several experiments. Water-injected and WNDP wild-type cRNA-injected oocytes served as background controls. For comparison also surface expression of an amino-terminally HA-tagged bacteriorhodopsin (BR-NT-HA) – a typical plasma membrane protein of the halophile archaebacterium *Halobacterium salinarum* – is shown, also normalized to the WNDP-HA56 values. (B) Dependence of WNDP-HA56 surface expression on the amount of cRNA injected. Data are averages of luminescence values from one experiment with 15 to 20 oocytes per data point.

**Figure 2.3 A** shows that the WNDP-HA12 and WNDP-HA56 constructs produce a comparable luminescence signal with amplitudes, which are several hundred-fold higher than in non-injected control oocytes. The non-tagged WNDP and WNDP with an HA tag located in the predicted cytosolic regions do not show any signal above background confirming the

specificity of the assay. To compare the extent of the WNDP surface expression with that of a known plasma membrane protein, an HA-tagged bacteriorhodopsin was used. The epitope was added to the extracellularly located amino-terminus (termed **BR-NT-HA**). The luminescence values for WNDP-HA56 and BR-NT-HA were of equal magnitude within the error limits (**fig. 2.3 A**), showing that WNDP surface expression in oocytes is comparable to that of typical plasma membrane proteins.

In contrast to the WNDP-HA12 and WNDP-HA56 constructs, two other constructs with predicted extracellular inserts, WNDP-HA34 and WNDP-HA78, did not yield luminescence signals above background (**fig. 2.3 A**). As the extracellular loops 3-4 and 7-8 of WNDP are predicted to be very short, the exposure and/or accessibility of the HA epitope to the antibody could be insufficient. Therefore we extended the HA insertions in the loops 3-4 and 7-8 by 6 additional amino acids, however these new constructs also did not yield luminescence signals above background, pointing to the lack of surface expression (data not shown). Consistent with this prediction, Western blot analysis revealed that expression was reduced for WNDP-HA34, when compared to WNDP-HA12 or WNDP-HA45. Hardly any protein was observed for WNDP-HA78 (**Fig. 2.4. A**) indicating impaired protein folding / stability for this latter construct. Similarly, in the case of WNDP-CT-HA, the gene product is absent in the Western blot (**fig 2.9 B**). Results in **figure 2.4. B** suggest that in this eukaryotic expression system the surface expression of WNDP is more efficient than that of BR, since in surface expression experiments yield similar values in case of both proteins.



**Figure 2.4 Western blot analysis of WNDP and BR constructs** Overall protein expression level of (A) HA tagged WNDP constructs and (B) WNDP HA56 construct compared to BR-NT-HA. Cell batches were previously used for surface expression

measurements. The equivalent of 1.5 oocytes was loaded in each lane. Water-injected oocytes from the same batch served as control. Detection was carried out using rat monoclonal antibody 3F10 against the HA epitope. Right lane: molecular weight standard.



## 2.4 Immunogold labelling of the surface expressed WNDP

To further confirm plasma membrane localisation of WNDP, immunogold labeling was carried out on plastic sections of embedded oocytes and on freeze-fracture replicas of the WNDP-expressing cells. **Figure 2.5** shows labelling of the oocyte plasma membrane microvilli in thin sections.

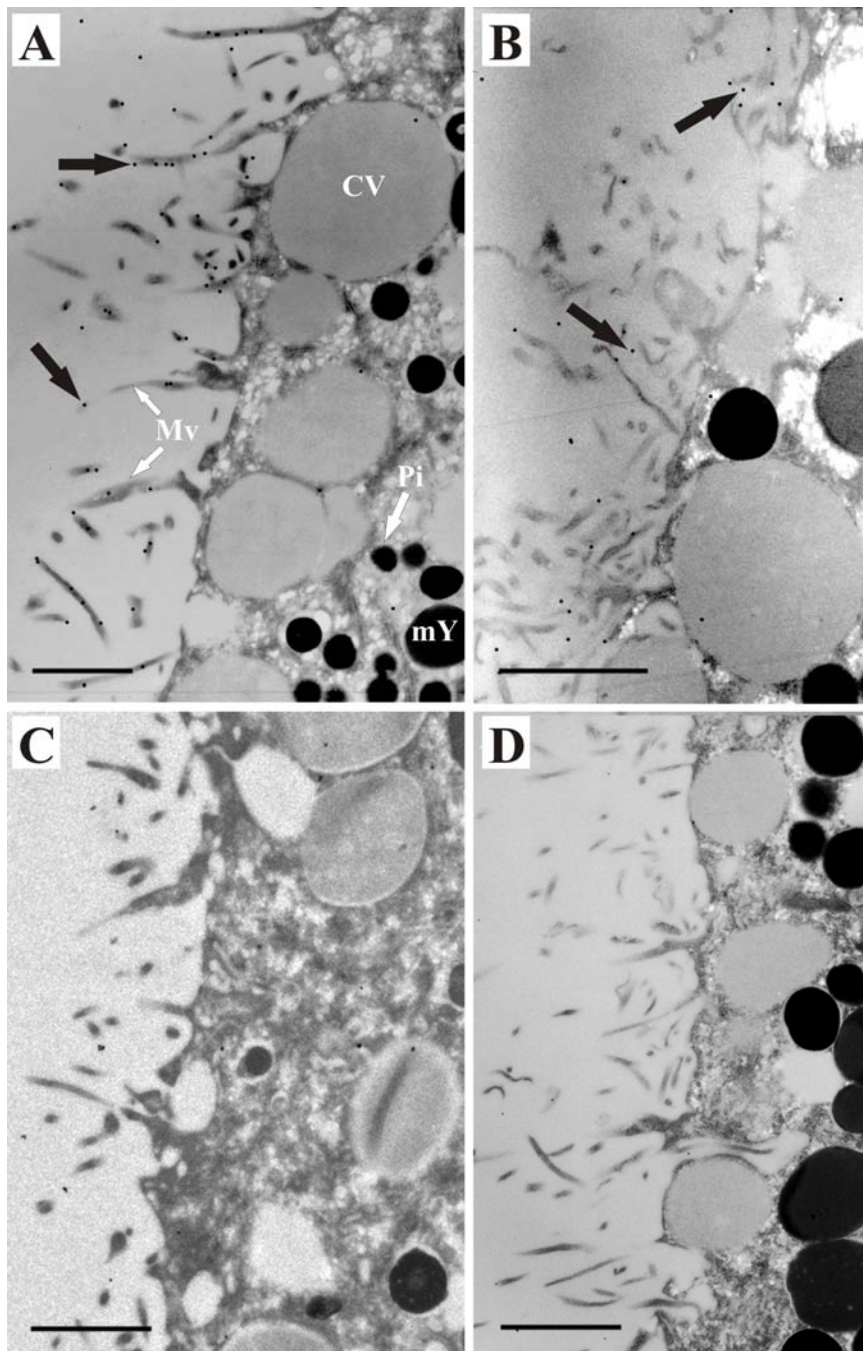


**Figure 2.5 Immunogold labelling of oocyte sections** Post-embedding immunogold labelling of oocyte sections was carried out with polyclonal antibody  $\alpha$ -ABD (A,C), or monoclonal anti-HA antibody 3F10 (B,D) of oocytes expressing either WNDP wild-type (A) or WNDP-HA(N) (B). Gold particles are present over microvilli of WNDP-expressing oocytes (A,B) but not over uninjected controls (C,D). Specific staining is exemplarily indicated by black arrows. **Scale bars = 1 $\mu$ M.** CV cortical vesicle, Pi pigment granule, mY mature yolk granule, MV microvilli [according to (Hilken et al., 1997)].

Both the polyclonal antibody a-ABD against the wild-type protein (**fig. 2.5 A**), as well as the anti-HA antibody against WNDP-HA(N) (**fig. 2.5 B**) bind to the oocyte microvillous cell membrane, demonstrating the targeting of WNDP to the cell surface. In control oocytes injected with water only, no gold marker was detected (**fig. 2.5 C,D**).

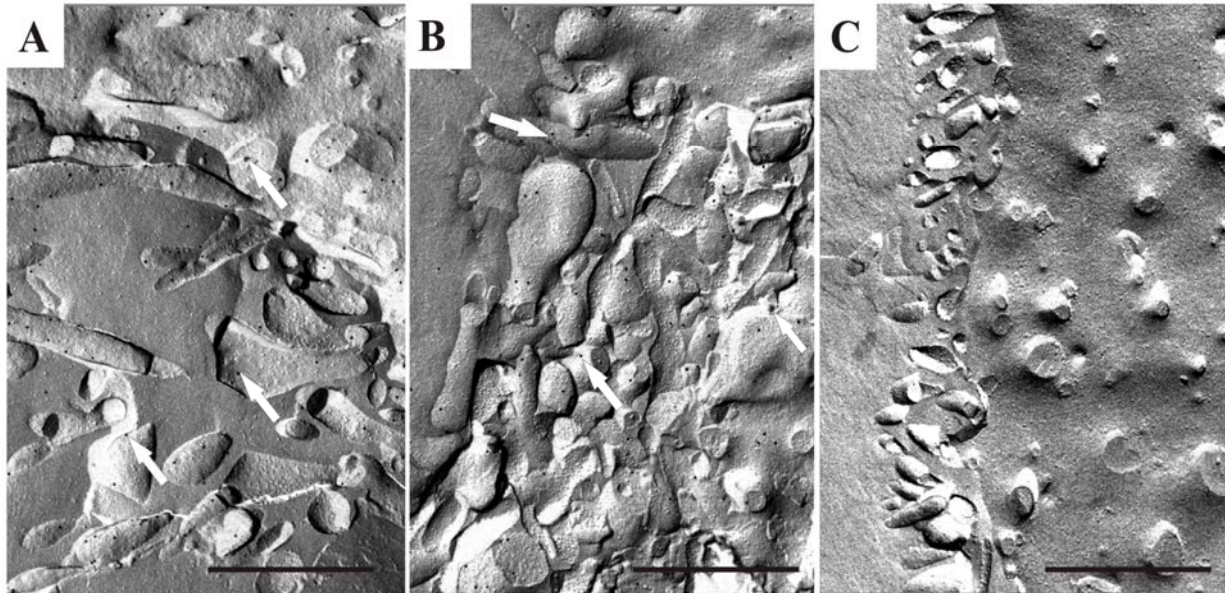


**Figure 2.6 Freeze-fracture replica labelling of *Xenopus laevis* oocytes** Polyclonal antibody a-ABD only binds to P (=plasmic)-fracture faces of WNDP wild-type-expressing oocytes (**A**), WNDP-HA(N) (**B**), and not to membranes of uninjected control oocytes (**C**). Specific staining is exemplarily indicated by white arrows. **Scale bars = 1  $\mu$ m.**

A similar result was obtained when freeze-fracture replicas were labelled using a-ABD, an antibody recognizing the nucleotide binding region of WNDP (**fig. 2.6.A**). Also for the WNDP HA(N) construct the gold label was predominantly associated with the P(= plasmic)-fracture face indicating that WNDP was present in the membrane, and confirming that the antibody binding site is located at the cytoplasmic surface of cell membrane (**fig. 2.6.B**). Replicas of control oocytes showed no labelling when treated with antibody a-ABD (**fig. 2.6.C**).

## 2.5 Functional characterisation of the HA-tagged WNDP

*A priori*, the plasma membrane localisation does not prove that the HA-tagged WNDP is correctly folded and functional. Since we intended to use the WNDP-HA56 construct in further experiments to analyze the effects of mutations/deletions on surface localisation of WNDP, it was necessary to confirm catalytic activity of WNDP-HA56. For this purpose the WNDP-HA56 construct was expressed in *Sf9* cells according to Tsivkovskii and co-workers

(Tsivkovskii *et al.*, 2002; Tsivkovskii *et al.*, 2002), and the ATP-dependent catalytic phosphorylation of the tagged protein was compared with that of the wild-type. The WNDP mutant Asp-1027-Ala in which the catalytic aspartate residue within the characteristic DKTG motif (**fig 1.3 A**) was exchanged for an alanine, served as a negative control.

**Figure 2.7 A** demonstrates that the phosphorylation levels for wild-type WNDP and WNDP-HA56 are comparable, while no phosphorylation is detected for the catalytically inactive Asp-1027-Ala mutant. Furthermore, in both cases phosphorylation is sensitive to treatment with hydroxylamine, as expected for the acyl-phosphate intermediate.

Finally, analysis of the ATP-dependence of catalytic phosphorylation of WNDP-HA56 (**fig. 2.7 B,C**) yielded an apparent  $K_M$  for ATP of  $0.5 \pm 0.15 \mu\text{M}$ . This value is comparable to the wild-type  $K_M$  for ATP ( $0.95 \pm 0.25 \mu\text{M}$ , (Tsivkovskii *et al.*, 2002) confirming proper folding of the WNDP-HA56 variant.

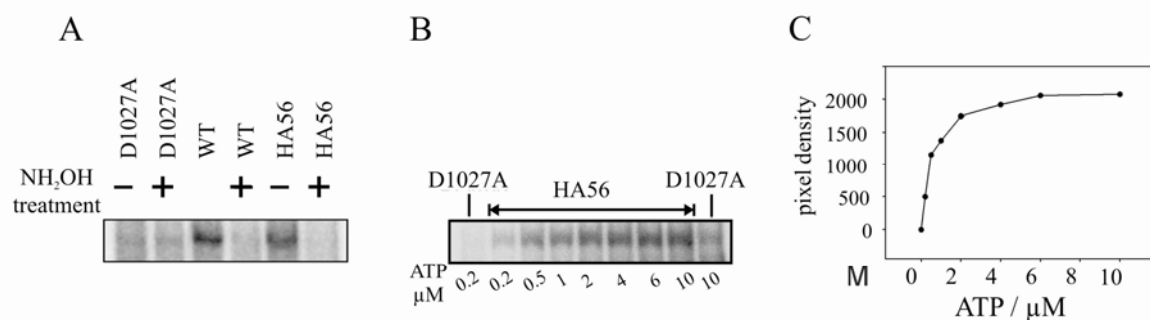


**Figure 2.7 Phosphorylation of the WNDP-HA56 construct by ATP** WNDP wild-type and WNDP-HA56 proteins were expressed and purified from *Sf9* cells. **(A)** Hydroxylamine treatment abolishes phosphorylation of either WNDP wild-type or WNDP-HA56. No phosphorylation signal is visible for the WNDP-D1027A mutant. **(B)** Dependence of phosphorylation level on the ATP concentration, again with WNDP-D1027A mutant as negative control. Densitometric evaluation of phosphorylation bands yielded an apparent  $K_M$  for phosphorylation from ATP of  $0.5 \pm 0.15 \mu\text{M}$  **(C)**.

## 2.6 The effect of sequence modifications on surface localisation of WNDP

The WNDP-HA56 construct was then used as a template to investigate the effects of sequence modifications on plasma membrane targeting of WNDP. The changes were introduced in the regions previously identified as implicated in the cellular trafficking of WNDP. First, a WNDP variant was constructed in which the first 600 amino acids including all 6 regulatory copper binding sites were deleted (**WNDP-HA56-delN600**). This deletion mutant showed a 50% increase in surface localisation (**fig. 2.8. A**), suggesting that the lack of the copper-binding sites does not impair plasma membrane targeting.

Secondly, the effect of deletion of a tri-leucine motif in the carboxy-terminus of WNDP was analysed. In MNKP, the di-leucine motif in the carboxy terminus was shown to be important for retrieval of MNKP from the plasma membrane into intracellular compartments (Petris *et al.*, 1998; Petris and Mercer, 1999). According to the working hypothesis the deletion of Leu residues in the tri-leucine motif of WNDP might have similar effects increasing the amount of WNDP present at the plasma membrane. To delete the triple-leucine motif, WNDP was truncated after Ser-1453, yielding **WNDP-HA56-delLLL**. **Figure 2.8 A** shows that the amount of WNDP-HA56-delLLL at the surface was increased by 20%.

Next, the most common Wilson's disease mutation His-1069-Gln, affecting the localisation of WNDP in cultured human cells and tissues (Cater *et al.*, 2004; Huster *et al.*, 2003; Huster and Lutsenko, 2003), was introduced resulting in a construct **WNDP-HA56-H1069Q**. Notably, the H1069Q mutation strongly reduced surface expression of WNDP by more than 50% (**fig. 2.8 A**).

Finally, the effect of disrupting the TGE motif (construct **WNDP-HA56 TGE>AAA**), which was shown to result in hyperphosphorylation and constitutive localisation to the plasma membrane even under basal copper conditions for both WNDP and MNKP (Petris *et al.*, 2002), and of disruption of the CPC motif (construct **WNDP-HA56 CPC>SPS**), which is involved in copper binding during catalytic transport, on plasma membrane localisation of the protein were investigated. Whereas the TGE>AAA mutant did not show a difference in plasma membrane expression, the transport-incompetent CPC>SPS mutant exhibited a strongly reduced surface expression (**fig. 2.8.A**).

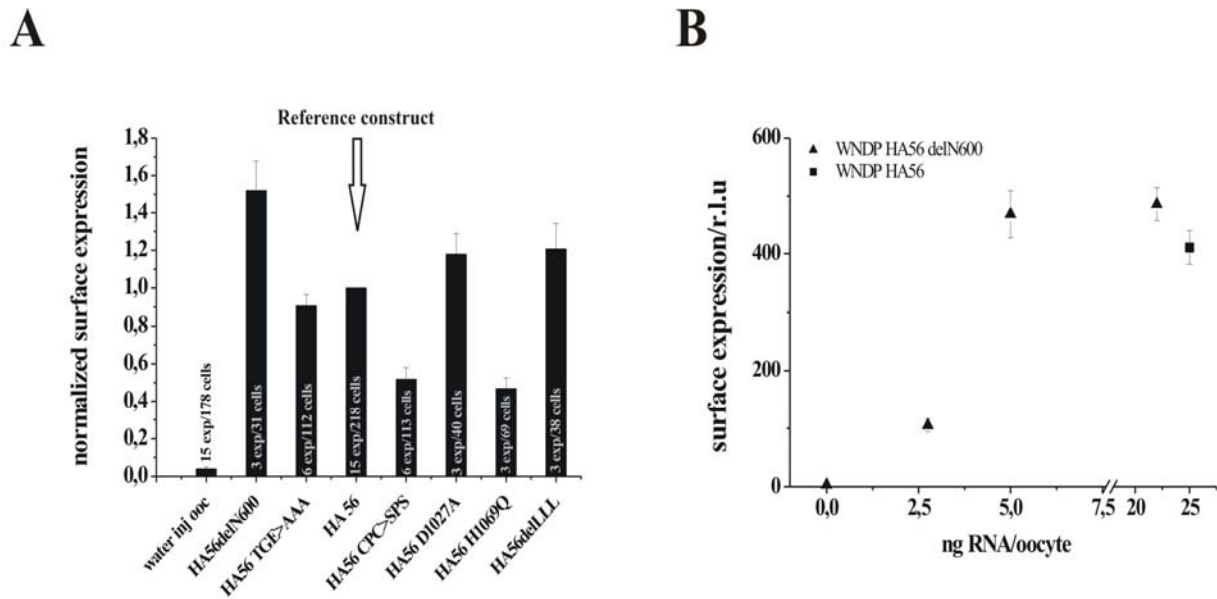


**Figure 2.8** Surface expression of sequence variants of WNDP HA56 (A) Luminescence measurements of various WNDP-HA56 sequence variants were obtained from 3 to 5 oocyte batches, with a total number of 31 to 82 oocytes, as indicated on top of each bar. Within each experiment original luminescence data were averaged for each construct, normalized to the value for WNDP-HA56 and thus averaged over several experiments. Water-injected oocytes served as a background control. (B) Results from a cRNA titration experiment to quantify the influence of the amount of cRNA injected on surface expression of construct WNDP-HA56-delN600.

Since the cRNA molecules for the WNDP-HA56-delN600 construct are significantly shorter than for WNDP-HA56, a 25 ng injection sample for WNDP-HA56-delN600 contains nearly 80% more cRNA molecules than that for WNDP-HA56. To exclude the possibility that higher surface expression of WNDP-HA56-delN600 is due to a larger number of injected cRNA molecules, we carried out a cRNA titration experiment and measured surface expression of WNDP-HA56-delN600 at lower cRNA levels. The results in **figure 2.8. B** show that surface expression of WNDP-HA56-delN600 did not decline even upon reduction of the injected cRNA amount to below 5 ng.

## 2.7 Plasma membrane localisation is not dependent on functional activity of WNDP

The effect on plasma membrane localisation of WNDP was independent from the effect of the mutation on catalytic activity. While both the Asp-1027-Ala and the His-1069-Gln mutants are phosphorylation deficient (Tsivkovskii *et al.*, 2003), the Asp-1027-Ala mutant of WNDP-HA56 showed comparable or even slightly higher surface expression than WNDP-HA56, in contrast to the His-1069-Gln mutant (**fig 2.8 A**). The whole-cell expression level was also comparable for both mutants (**fig 2.8 C**).

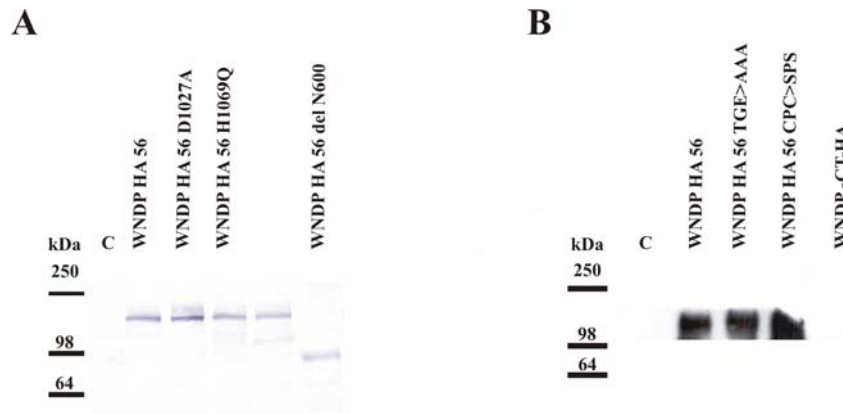


**Figure 2.9 Overall expression level of WNDP mutants** Western blots for quantification of the overall protein expression level of the various WNDP-HA56 sequence variants from **fig 2.8 A**. Detection was carried out using polyclonal antibody a-ABD on oocyte samples originating from a cell batch used for luminescence measurements. The equivalent

of 1.5 oocytes was loaded in each lane. Water-injected oocytes served as control. Left: molecular weight standard. Proteins were visualized using AP-conjugated (**A**), or HRP-conjugated (**B**) secondary antibody (see methods).

To exclude that the observed differences in surface expression were simply due to differences in the total protein expression level, Western blots using a monoclonal antibody 3F10 directed against the HA epitope were performed on oocyte samples which previously had been used for surface expression analysis. **Figure 2.9 (A, B)** shows that the expression levels for the WNDP-HA56-H1069Q, WNDP-HA56-delLLL, WNDP-HA56-delN600, WNDP-HA56 CPC>SPS, and WNDP-HA56 TGE>AAA constructs are very similar to WNDP-HA56. Thus, the different surface expression values measured for these constructs can not simply be due to differences in overall protein expression.

### 3. Discussion

This work describes expression of WNDP in *Xenopus* oocytes and the applicability of this expression system for analysis of the plasma membrane localisation of WNDP, a copper-transporting P-type ATPase mutated in Wilson Disease. Using a luminescence technique originally developed to quantify surface expression of potassium channels, WNDP was located in the plasma membrane of oocytes and shown that the loops between proposed TMS-1 and -2 and between TMS-5 and -6 are exposed to the extracellular face, in accordance with the proposed topology model (**fig 2.1. A**). Plasma membrane localisation is additionally confirmed by immuno-electron microscopy of sections and freeze-fractured oocytes expressing WNDP. Evidence is provided that the insertion of an HA-tag into the loop between TMS-5 and -6 does not alter functional activity of the WNDP-HA protein variant. These data together indicate that expression in *Xenopus* oocytes represents a valuable system for probing the effects of various WNDP mutations on delivery to the plasma membrane.

*Xenopus* oocytes have been used in numerous expression and trafficking studies of human plasma membrane proteins, for example the Na<sup>+</sup>/glucose cotransporter SGLT1 (Martin *et al.*, 1997), the glucose transporter GLUT4 (Mora *et al.*, 1997; Mora *et al.*, 1997), the GABA transporter GAT1 (Quick *et al.*, 1997; Tong *et al.*, 2001), the epithelial Na<sup>+</sup> channel ENaC (Schild *et al.*, 1996; Snyder *et al.*, 1995; Staub *et al.*, 1997), the chloride channel CFTR involved in cystic fibrosis (Denning *et al.*, 1992), and many others. Although a general proof for the equivalence of trafficking mechanisms between these amphibian cells and mammalian cells cannot be given, (Quick *et al.*, 1997) pointed out that the ease at which molecular trafficking properties can be reproduced between different cell lines suggests a mechanism for membrane trafficking which is shared by all cells. According to these authors both the protein components required for trafficking are conserved, and the actual pathway may have evolved from a more basic mechanism of membrane repair [see e.g. (Steinhardt *et al.*, 1994)]. It is well established that oocytes faithfully express exogenous proteins, target them to the correct cellular compartment (Subramanian *et al.*, 2001), and that many regulatory features of mammalian membrane protein expression are conserved, including the specialised exocytotic mechanisms for neurotransmitter release (Quick *et al.*, 1997). Furthermore, they are advantageous due to their large size (~1 µl volume) and membrane surface (due to microvilli structures), which undergoes extensive endo- and exocytotic turnover. Altered membrane

protein behaviour may only be expected from the lower ambient temperature at which oocytes are kept, as shown for trafficking defects of some CFTR mutants (e.g.  $\Delta F508$ ), which do not show up in oocytes (Denning *et al.*, 1992)).

The pathological defects observed in affected humans point to a dual role of WNDP: first, copper excretion from cells, second, copper delivery to the secretory pathway for incorporation into copper-dependent enzymes, such as ceruloplasmin. The experiments demonstrating the presence of WNDP at the plasma membrane suggest that WNDP directly contributes to cellular copper clearance by active transport across the plasma membrane, rather than sequestering copper to exocytotic vesicles.

### 3.1 WNDP is expressed in *Xenopus laevis* oocytes

Surface expression of the WNDP-HA56 construct is comparable to that of HA-tagged bacteriorhodopsin (BR-NT-HA), a typical plasma membrane protein (**fig. 2.3. A**). In contrast, when the total protein level was compared for WNDP-HA56- and BR-NT-HA-expressing oocytes, a much larger amount HA-tagged bacteriorhodopsin than WNDP-HA56 protein could be detected by Western blot using an anti-HA antibody (**fig 2.4. B**). Considering the approximately equal surface expression values for both proteins this result implies that plasma membrane targeting of the archeal membrane protein is less efficient in the eucaryotic expression system, and that the ratio between the plasma membrane portion and the total cellular protein content is much higher for WNDP than for BR. Considerable plasma membrane expression of WNDP is encouraging for future copper transport assays on oocytes, which have been initiated in our laboratory. These observations also suggest the plasma membrane as a physiologically relevant cellular locus for WNDP, where it directly contributes to cellular copper export.

### 3.2 The chemiluminescence experiments confirm the suggested topology of WNDP

Predictions of the transmembrane topology of WNDP reveal 8 transmembrane domains (TMS-1 to TMS-8) with cytoplasmic amino- and carboxy-termini, and large cytoplasmic loops between TMS-2 and -3 or TMS-4 and -5, whereas the extracellular loop regions are very short (**fig 2.1. B**). The data obtained in this work are consistent with these predictions. The luminescence technique unambiguously showed that the loops between TMS-1 and -2,



and between TMS-5 and -6 are exposed to the extracellular space, while the loop between TMS-4 and -5 is not. The HA epitope insertion failed to detect the extracellular location of the loops between TMS-3 and -4 or TMS-7 and -8. This is likely caused by steric constraints within these extremely short loops, or due to improperly folded proteins. Misfolding of the WNDP-HA78 protein is indicated by very low expression levels in Western blots (**fig. 2.4. A**).

Plasma membrane localisation of WNDP was additionally confirmed by electron microscopy. On the sections of plastic-embedded oocytes the protein was detected using two different antibodies (against the ATP-binding domain – **fig. 2.5 A**, and against the HA-tag – **fig. 2.5 B**) where the detection of the epitope does not yield information about the orientation of the protein; and on replicas of freeze-fractured oocyte membranes in which the intracellular location of the loop between TMS-4 and -5 was demonstrated (**fig. 2.6**) since with this latter method one can detect only the epitopes located on the cytoplasmic side of the membrane.

### **3.3 The effects of sequence modifications on the surface expression of WNDP in oocytes**

#### **3.3.1 The N-terminal copper binding domains are not necessary for plasma membrane localisation**

Using the catalytically active WNDP-HA56 construct as a template, the effects of mutations/deletions on surface localisation of WNDP were investigated. Deletion of the entire amino terminal domain in construct **WNDP-HA56-delN600** resulted in a 50 % increase in surface expression (**fig 2.8. A**). It was confirmed by a cRNA titration experiment that the surface expression for WNDP-HA56-delN600 did not decline upon reduction of the cRNA amount to below 5 ng (**fig 2.8. B**). Thus, the difference in surface expression is present at the saturation level for both, WNDP-HA56 and WNDP-HA56-delN600, and can be even larger with lower amounts of injected cRNA molecules.

Cater *et al.* demonstrated the important role of MBS-5 and -6 on intracellular trafficking of WNDP (Cater *et al.*, 2004) because each of these two metal binding sites was sufficient to drive copper-dependent redistribution of WNDP to vesicular compartments (Roelofsen *et al.*, 2000), in agreement with observations obtained on the homologous Menkes Disease Protein (Strausak *et al.*, 1999). The results of the present study also indicate that the WNDP amino terminus does not only modulate the catalytic properties, as pointed out by (Tsivkovskii *et al.*, 2001), but also profoundly influences the subcellular distribution of the protein. (Kim *et al.*,

2003) have shown that in the case of MNKP a mutation that results in a shorter linker region between MBS6 and TMS1, also abolishes the re-localisation of the protein to the plasma membrane under elevated copper conditions. In the present experiments in the case of the mutant WNDP-HA56-delN600 this linker region is present, only the 6 MBS deleted. Knowing this, it is tempting to speculate about the importance of this linker region: these 50 amino acids could be indispensable for the redistribution of human copper transporters in increased copper concentrations. Interestingly, Guo *et al.* (2005) identify using immunofluorescence microscopy the first 63 residues in the amino-terminus as being important for correct apical targeting in polarised hepatic cells under excess copper conditions (Guo *et al.*, 2005). In case of the WNDP-HA56-delN600 construct this sequence of 63 amino acids is missing.

Presently, it is unclear whether the delivery of WNDP to the plasma membrane in oocytes can be considered as equivalent to the copper-induced trafficking in mammalian cells. Considering the recent results of Guo *et al.* (2005), there could be differences between the trafficking machinery of mammalian cells and amphibian oocytes since in the polarised hepatic cells the truncated constructs with these 63 residues present reach the same subcellular construct as the wild-type, and oppositely, the absence of this short sequence causes constitutive targeting to a different subcellular compartment of WNDP independent of copper concentrations.

Nevertheless, it is interesting that the removal of the copper-binding regulatory domain does not impair the folding of WNDP and its interaction with the trafficking machinery of oocytes, in effect bringing more WNDP molecules to the cell surface.

### **3.3.2 The triple-Leu motif might be involved in the retrieval of WNDP from the cell surface**

Truncation of WNDP at the far carboxy terminus after amino acid Ser-1453 (construct **WNDP-HA56-delLLL**) led to a moderate elevation in surface expression by 20% (**fig 2.8. A**). This truncation deleted a triple-leucine motif of WNDP at homologous position to a di-leucine in Menkes disease protein, which is important for retrieval of the latter protein from the plasma membrane (Petris *et al.*, 1998; Petris and Mercer, 1999). The enhanced surface expression of WNDP-HA56-delLLL suggests that the triple-leucine motif of WNDP may act as an endocytotic signal in a similar way as the carboxy-terminal di-leucine motif in MNKP.

### 3.3.3 Mutations supposed to impair catalytic activity of WNDP not always affect its plasma membrane localisation

Notably, the His-1069-Gln mutation (construct **WNDP-HA56-H1069Q**) strongly reduced the surface expression of WNDP by more than 50% (**fig 2.8. A**). This result, together with previously shown effects on catalytic activity (Tsivkovskii *et al.*, 2003) or intracellular distribution (Huster and Lutsenko, 2003), provides further understanding of the loss-of-function phenotype of this mutant. Even if the observed decrease in catalytic activity (in this case: steady-state phosphorylation) were only due to a kinetic effect without severe consequences on the overall protein turnover [as e.g. found in case of some Na<sup>+</sup>/K<sup>+</sup>-ATPase mutations, e.g. Asn-779-Ala (Arguello *et al.*, 1996)], the observed decrease in plasma membrane expression would be consistent with a loss-of-function effect under physiological conditions.

A similarly strong reduction in plasma membrane expression was also found for the **WNDP-HA56 CPC>SPS** construct, which can not transport copper and was found to be unable to relocate from TGN to the plasma membrane in response to copper (Petris *et al.*, 2002). Since this effect is already present under basal copper conditions, the differences in the surface expression patterns point to structural defects rather than impaired catalytic activity. This may also serve as an explanation for the essentially unchanged surface localisation of the **WNDP-HA56 TGE>AAA** construct, which was shown to result in hyperphosphorylation and constitutive plasma membrane localisation in mammalian cell lines under basal copper conditions, which has led to the conclusion that a certain conformational state, rather than catalytic activity determines the intracellular distribution of the protein (Petris *et al.*, 2002).

Using a MNKP-deficient *mottled* fibroblast cell line Payne and coworkers showed that the His-1069-Glu mutant of WNDP, in contrast to the wild-type WNDP was neither able to sustain viability under high copper conditions nor to rescue the *mottled* phenotype of the cells (Payne *et al.*, 1998). Immunofluorescence studies indicated localisation of the His-1069-Gln mutant to the ER, whereas WNDP wild-type was found in the TGN (Payne *et al.*, 1998). However, maintenance of transfected cells at lower temperature (28 °C) resulted in TGN localisation of the His-1069-Gln mutant protein. This, together with a 5-fold decreased half-life of the mutant protein, was taken as evidence for a temperature-sensitive effect on protein folding followed by premature degradation (Payne *et al.*, 1998). Since *Xenopus* oocytes are usually kept at 18 °C the decreased surface expression is apparently not due to a temperature-

dependent misfolding of WNDP-H1069Q. In view of the observed effect on the conformation of the ATP-BD (Tsivkovskii *et al.*, 2003) the mutation probably has more subtle consequences on other regulatory interactions that influence subcellular distribution of the protein.

### **3.3.3.1 The effect on surface localisation is apparently independent from catalytic activity**

Although both, the Asp-1027-Ala and the His-1069-Gln mutants were shown to be phosphorylation deficient (Tsivkovskii *et al.*, 2003), the Asp-1027-Ala mutation transplanted into the WNDP-HA56 backbone showed comparable or even slightly higher surface expression than WNDP-HA56 in contrast to decreased surface expression of His-1069-Gln. It is important to note, that the differences in plasma membrane expression cannot be due to differences in the total protein expression level for the above mentioned constructs (**fig 2.9. A**). Therefore the conclusion drawn is that the observed effects on plasma membrane expression reflect intrinsic trafficking properties of the respective constructs. It also has to be mentioned that (Petris *et al.*, 2002) obtained different results with MNKP: the catalytic-phosphorylation deficient Asp-1044-Glu mutant (homologous to WNDP D1027) does not relocate to the plasma membrane upon increasing the copper concentration. One can speculate about the reason for this difference: it could be the difference in the proteins (WNDP versus MNKP), the nature of the point-mutation (Ala versus Glu), or the expression system (*Xenopus* oocytes versus CHO cells).

## 4. Conclusions

The above experiments show that Wilson Disease Protein was heterologously expressed in *Xenopus* oocytes and detected at the cell surface by chemiluminescence and electron microscopy. The surface detection experiments using HA-tagged WNDP confirm the proposed topology of WNDP. The HA-tag *per se* does not interfere with the function of WNDP, as shown for WNDP HA56 by ATP-dependent phosphorylation after expression in *Sf9* cells. Sequence modifications within the WNDP HA56 template-construct reveal some interesting features: **i)** the N-terminal domain, which contains the 6 metal binding sites, is not necessary for plasma membrane targeting; **ii)** elevated surface expression of WNDP was observed when the carboxy terminus containing the tri-Leu motif is missing, which suggests that this motif might be involved in the retrieval of the protein from the plasma membrane; **iii)** the mutations TGE>AAA (proposed to lock the protein in the E1 conformation and lead to constitutive plasma membrane localisation) and D1027A (phosphorylation deficient) did not interfere with the surface localisation of the protein; **iv)** the mutations CPC>SPS (copper transport deficient) and H1069Q (phosphorylation deficient, most common mutation in Wilson Disease) reduced plasma membrane expression to less than 50%. Western blot analysis shows that the overall expression level of all constructs is similar to that of the reference construct WNDP HA56.

These findings suggest that motifs involved in copper binding and catalytic activity do not interfere with plasma membrane targeting of WNDP in *Xenopus* oocytes. However, the H1069Q mutation could interfere with the distribution of WNDP protein within the cells.

The demonstrated applicability of the *Xenopus* expression system for WNDP opens a novel route for investigating the effects of mutations found in Wilson Disease patients. It should also allow for further topological studies with less invasive changes in primary sequence, like e.g. insertion of glycosylation sites. Furthermore, the high plasma membrane expression level of WNDP achieved in oocytes may facilitate studies of direct copper transport and help to clarify the intracellular components necessary for efficient copper delivery to transport sites.

# **Proteorhodopsin**

**Electrophysiological characterisation of the wild-type and  
several mutant proteins expressed in *Xenopus laevis* oocytes**



## 1. Introduction

### Retinylidene proteins

Photochemically reactive proteins that use retinal (vitamin A aldehyde) as their chromophore have been identified in both prokaryotic and eukaryotic organisms – hence their name, commonly called rhodopsins. A common feature of these proteins is that they contain seven transmembrane  $\alpha$ -helices (termed A-F) which form a pocket, where the retinal is bound. Based on their primary sequence, the group of retinylidene proteins is split in two families: *type I*, consisting of light-driven ion pumps (e.g. bacteriorhodopsin), phototaxis receptors (sensory rhodopsins I and II) and yet undiscovered functions (fungal rhodopsins) and *type II*, which includes the photosensitive receptor proteins in animal eyes (like human rod and cone visual pigments), receptor proteins in the pineal gland, hypothalamus and other tissues of lower vertebrates (Spudich *et al.*, 2000). In addition, the first light-gated ion channels have been identified, termed channelrhodopsins (Nagel *et al.*, 2002; Nagel *et al.*, 2003). An extensive description of photosensitive proteins can be found in (Spudich and Briggs, 2005).

### 1.1 Bacteriorhodopsin

Bacteriorhodopsin (BR) has been the subject of nearly three decades of intense investigation, yielding a wealth of biochemical, spectroscopic, mutational and structural information (reviewed in (Haupts *et al.*, 1999; Kühlbrandt, 2000; Lanyi and Schobert, 2004; Lanyi, 2001; Luecke, 2000; Spudich and Jung, 2005) making it the best understood ion pump (Luecke, 2000), and a model system for seven-helical membrane proteins. This small, 26 kDa protein – with 248 amino acid residues – is described as a light-driven pump that transports  $H^+$  against an electrochemical gradient from the cytoplasmic to the extracellular side. The generated  $H^+$  gradient can be subsequently converted into chemical energy by other membrane proteins, like ATP synthase. The pumping process is energized by photoisomerization of the covalently attached all-*trans* retinal chromophore to the 13-*cis*, 15-*anti* configuration.



### 1.1.1 Photocycle, spectral characteristics, structure and photocurrents: a summary\*

The conformational change of the retinal triggers the photocycle: the formation of a series of intermediates which can be identified based on their spectral characteristics, which ends with the return to the ground state conformation (**fig 1.1**). For some of the intermediates the crystal structure have been determined which greatly contribute to the understanding of the pumping mechanism [reviewed in (Luecke, 2000)].

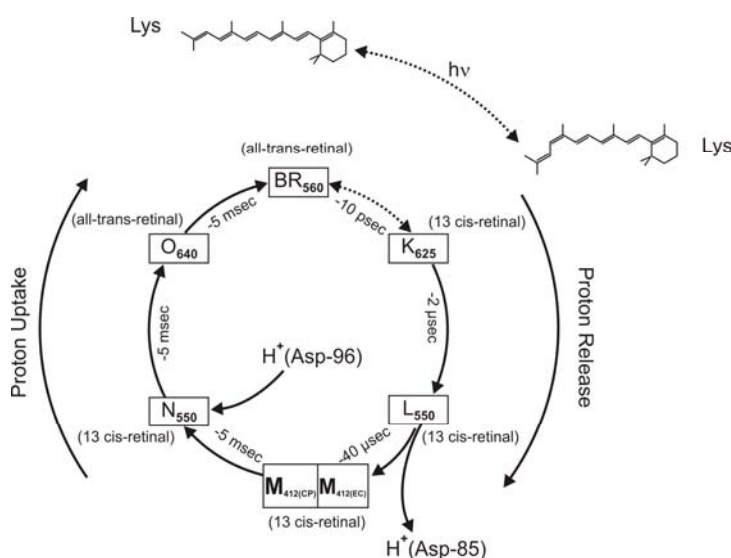


**Figure 1.1. Simplified photocycle of BR**  
Upon illumination, isomerisation of the retinal (all-*trans* – 13-*cis*) triggers a series of conformational changes, the photointermediates K, L, M, N and O. During the L → M transition a H<sup>+</sup> is transferred from the Schiff base to Asp85. In the M state the accessibility of the Schiff base changes from extracellular (EC) to intracellular (CP), and will be reprotonated from the cytoplasmic side during the M → N transition by the proton donor Asp96. The conformation of the retinal is shown next to each photocycle intermediate. Based on ref. (Geibel, 2003).

The structure of BR in its ground state solved by Luecke *et al* (1999) is presented in **figure 1.2**.

\* In the present work bacteriorhodopsin is used as a reference for the study of proteorhodopsin, so it is not presented in detail. There is a series of review articles which summarise the large amount of information collected since the first description of this pump (Oesterhelt and Stoekenius, 1971) – see (Haupts *et al.*, 1999; Kühlbrandt, 2000; Lanyi, 2001; Luecke, 2000; Pebay-Peyroula *et al.*, 2000; Schäfer *et al.*, 1999; Spudich *et al.*, 2000; Spudich and Jung, 2005).

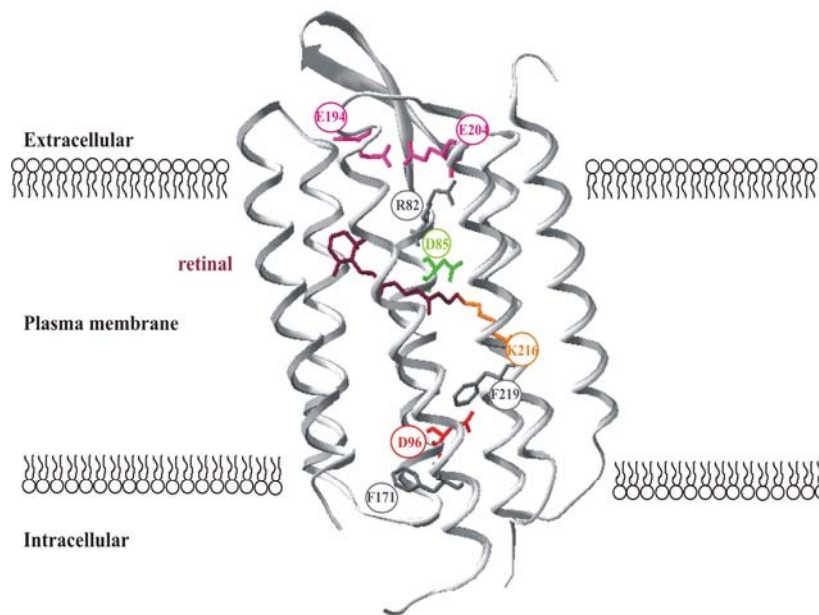


**Figure 1.2. Structural model of BR in the ground state**

The retinal chromophore (purple) forms a Schiff base bond with Lys216 (orange) in helix F. H<sup>+</sup> donor D96 (red) and acceptor D85 (green) are in helix C. Residues E194 and E204 (pink) close to the extracellular surface belong to the proton release group. Another residue important for H<sup>+</sup> release is R82 (grey). Mutations of D96 lead to an accumulation of the M-state, mutations of F171 and F219 (both in grey) lead to an accumulation of the N-state [based on refs. (Geibel, 2003; Luecke, 2000)].

During the photocycle the pK<sub>a</sub> of the Schiff base changes from 13 in the ground state to less than 4 and in the M state back to more than 10. These changes enable the transfer of a H<sup>+</sup> from the intracellular to the extracellular side upon absorption of a photon and against a transmembrane potential of up to -280 mV (Geibel, 2003).

The most important features of the photocycle intermediates, as summarised in (Luecke, 2000):

- The **ground (or 'BR') state** ( $\lambda_{\max} \sim 568$  nm) is the best characterised state, both regarding ionisation states and structure. The light-adapted form contains an active site with the all-*trans* retinal in tight contact with surrounding protein residues. The *Schiff base is protonated*. Towards the extracellular side, an extensive hydrogen-bonded network leads from the Schiff base, *deprotonated Asp85*, Arg82 to the initially *protonated* terminal *proton-release group (Glu204/Glu194)* near the extracellular surface. In marked contrast, the cytoplasmic side is very hydrophobic, with no polar residues or ordered waters between the Schiff base and *protonated Asp96*.
- The **K state** ( $\lambda_{\max} \sim 590$  nm) arises within a few picoseconds of photon absorption, depositing about 50 kcal/mol of energy into the retinal. The K state has a reported  $\Delta H$  of 11.6 kcal/mol, thus about 20% of the photon energy is converted to enthalpy and a substantial portion of this enthalpy gain is due to charge separation. Spectroscopic methods have determined a highly strained 13-*cis*, 15-*anti* configuration of the retinal.

- In the **L state** ( $\lambda_{\max} \sim 550$  nm), the retinal strain has partly relaxed and hydrogen bonds of the retinal, protein groups and bound water begin to change. The active site is now primed for the decisive event in the photocycle, the deprotonation of the Schiff base (L→M reaction) and protonation of Asp85.
- The **M state** ( $\lambda_{\max} \sim 412$  nm) is defined by a deprotonated Schiff base and consists of at least two sub-states, often referred to as  $M_1$  and  $M_2$ . For this reaction to proceed, the large initial  $pK_a$  difference of over 11 units between the proton donor (Schiff base, ground state  $pK_a$  over 13) and acceptor (Asp85, ground state  $pK_a$  of 2) has to be reduced to less than 1 unit. Kinetic studies on purple membrane suspensions have suggested that in these sub-states the retinal Schiff base comes to two sequential protonation equilibria with the proton acceptor toward the extracellular side, Asp85, equilibria that are shifted further to deprotonation of the Schiff base in  $M_2$ . At this point, reprotonation of the Schiff base from Asp85 is no longer possible.
- In the **N state** ( $\lambda_{\max} \sim 560$  nm) the Schiff base is reprotonated and the Asp96 on the cytoplasmic side is deprotonated. With Asp85 still protonated and Asp96 now deprotonated, the retinal binding site is relaxed and preferentially accommodates the 13-cis, 15-anti configuration.
- The **O state** ( $\lambda_{\max} \sim 610$  nm) occurs after both reprotonation of Asp96 from the cytoplasmic side and thermal reisomerisation of the retinal. The driving force for its transition to the ground state is not clear, but it is the last and unidirectional step of the photocycle in which the initially very low  $pK_a$  of Asp85 is re-established, and this residue deprotonates in a strongly downhill reaction to reprotonate the extracellular proton release site.

The conformational change that takes place during the M state, when the accessibility of the Schiff base changes from extracellular to intracellular side, can be also regarded as a *molecular switch*, which divides the M state into two substates,  $M_1$  ( $M_{412\text{ EC}}$ ) and  $M_2$  ( $M_{412\text{ CP}}$ ). The study of photocycle intermediates by X-ray crystallography has shown that in the first part of the photocycle (BR → L) only small conformational changes occur, the larger structural changes take place during the relaxation from the excited to the ground state by the movement of helices (B), G and F (Kühlbrandt, 2000; Luecke, 2000) – presented simplified in **figure 1.3**.

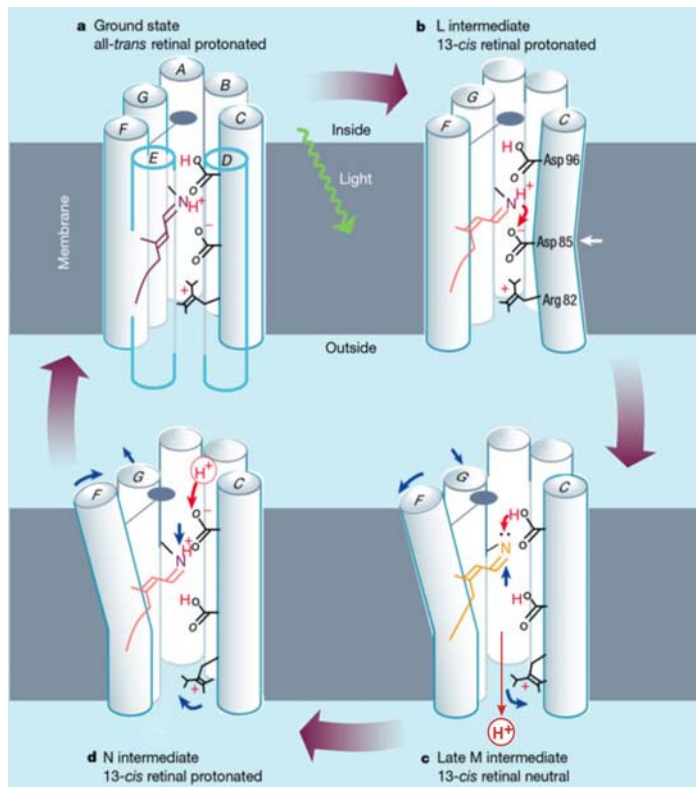


**Figure 1.3 Structural, spectroscopic and proton transfer steps in the photocycle of BR** (a) light induced isomerisation of the protonated retinal from all-*trans* (purple) to 13-*cis* (pink) determines the H<sup>+</sup> transfer from the Schiff base to Asp85, aided by a slight movement of this residue in the L-intermediate (b) towards the nitrogen atom of the Schiff base. In the M state (c), the deprotonated retinal (yellow) straightens, pushing against helix F and causing it to tilt. This opens the channel on the inner, cytoplasmic side of the membrane through which Asp96 is reprotonated (d), having given up its proton to the Schiff base. Asp85 transfers its H<sup>+</sup> through a network of hydrogen bonds and water molecules to the outside medium, past Arg82, which has moved slightly. Red arrows show H<sup>+</sup> movement, blue arrows movements by groups of atoms. Helices D and E are omitted in b-d for clarity. The ‘paddle’ attached to helix F represents the bulky side chains, which move to open the cytoplasmic proton channel (based on refs (Geibel, 2003; Kühlbrandt, 2000; Luecke, 2000)).

Continuous illumination leads to an outward current mediated by BR. Photocurrents of BR have been studied electrophysiologically using the **Black Lipid Membrane (BLM)** technique (Bamberg *et al.*, 1979; Butt *et al.*, 1989), voltage- and patch-clamp of *Xenopus laevis* oocytes and HEK293 cells heterologously expressing BR (Geibel, 2003; Geibel *et al.*, 2001; Nagel *et al.*, 1998; Nagel *et al.*, 1995). The first technique allows an easy control of the transmembrane pH, the latter two the control of the transmembrane potential, i.e. the electric field. After expressing BR in oocytes for the first time and determining its current-voltage (I-V) behaviour over the range of -160 to +60mV (Nagel *et al.*, 1995), Nagel *et al.* (1998) also showed that the pump current is governed by the ratio of M<sub>1</sub>/M<sub>2</sub> states. The M<sub>1</sub> state can be arrested by hyperpolarising potentials and as such, to allow accessibility to the Schiff base only from the extracellular side. At hyperpolarising potentials a non-transporting cycle may develop by increased population of M<sub>1</sub>. Nagel *et al.* observed for the first time the existence of a long-lived M state with a decay time of ~ 300 ms in addition to the usual ~ 5 and ~ 20ms. Complementary BLM experiments showed that the M-decay is pH dependent, faster at pH 6 than at pH 8, which supports the idea of reprotonation of the Schiff base from the extracellular side (Nagel *et al.*, 1998). Under improved experimental conditions Geibel *et al.* (2001) could show that the decay of this long-lived M state is also voltage dependent. In addition, these authors also showed that the slope of the I-V relation changes in a similar manner to the slope of the rate (1/τ) of the M-decay over the range of -160 to +60 mV and

two pH units (from 5.5 to 7.5), meaning that the I-V relationship under their experimental conditions is determined by this process.

BR mutants with known crystal structures were studied by means of two-electrode voltage-clamp by (Geibel, 2003), grouped depending on their properties of stabilising or destabilising the M state. Residue changes which affect the H<sup>+</sup> donor D96 (D96N, D96G and the triple mutation D96G/F171C/F219L), slow down the decay of the M intermediate; the mutations F171C and F219L accelerate it.

### 1.1.2 Probing the photocycle of BR with blue light

The photocycle of BR contains one intermediate with a blue-shifted absorption maximum, the M state. Consequently, blue light applied during continuous illumination could be absorbed by molecules which are in the M state. Indeed, blue laser flashes applied during stationary illumination result in charge translocation, directed oppositely to the stationary pump current ('quenching effect of blue-light'). The underlying mechanism is the photoisomerisation of 13-*cis* retinal to the all-*trans* form upon absorption of a blue photon in the M state, followed by the reprotonation of the Schiff base from the extracellular side (i.e. a shortcut of the photocycle without net transported charge), demonstrated originally by Ormos *et al.* (1978) (Keszthelyi and Ormos, 1980; Ormos *et al.*, 1978; Ormos *et al.*, 1980). The amplitude of these currents reflects the amount of the M intermediate (Nagel *et al.*, 1998).

Light protocols combining continuous illumination with transient laser flashes were employed by Geibel *et al.* to study the long lived M intermediate of BR wild type (Geibel *et al.*, 2001) and the lifetime of the M intermediates of BR mutants (Geibel, 2003).

## 1.2 Proteorhodopsin

First described in 2000, proteorhodopsin (PR) belongs to the type I retinylidene proteins. It has been identified through genomic analysis of naturally occurring marine bacterioplankton in the genome of an uncultivated  $\gamma$ -proteobacterium, with high sequence similarity to archaeal rhodopsins, like bacteriorhodopsin and sensory rhodopsins (Béjà *et al.*, 2000).

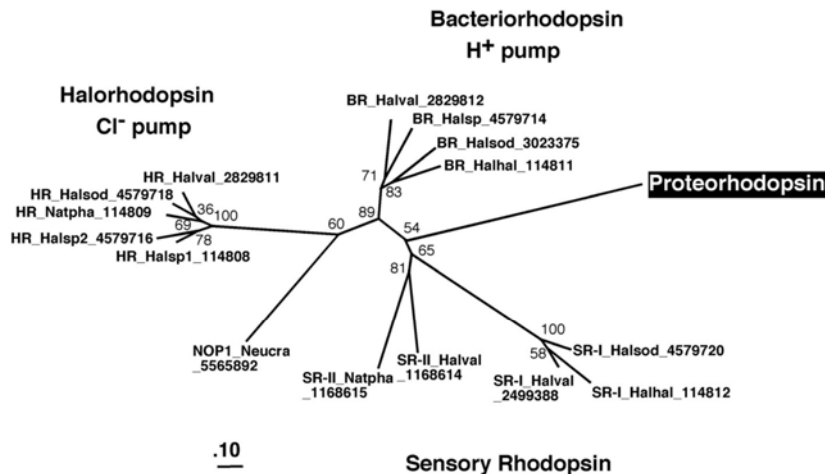


**Fig. 1.4** Phylogenetic analysis of proteorhodopsin with archaeal (BR, HR, and SR prefixes) and *Neurospora crassa* (NOP1) rhodopsins (Béjà *et al.*, 2000).

Sensory rhodopsins are generally cotranscribed with genes encoding their own transducer [e.g. Htr, (Schäfer *et al.*, 1999)]. The absence of an Htr gene in close proximity to the PR gene suggests that PR might function primarily as a light-driven ion pump. Early work by Béjà and coworkers (Béjà *et al.*, 2000; Béjà *et al.*, 2001) has shown that the proteorhodopsin gene encodes a 249 amino acid long polypeptide of 27 kDa which can be reconstituted to a functional H<sup>+</sup>-pump upon addition of all-*trans*-retinal. In membrane preparations of *E. coli* with heterologously expressed PR or in native bacterioplankton cell membranes the protein is able to generate a membrane potential after illumination; the time course of the photocycle kinetics measured in *E. coli* membrane suspension is closer to that of bacteriorhodopsin (~20 ms) than of sensory rhodopsins (>300 ms) with a blue-shifted photointermediate characteristic for unprotonated Schiff-base forms of retinylidene pigments. A phylogenetic analysis of PR, BR, HR and SR is visible in **fig 1.4** (Béjà *et al.*, 2000). These authors have also identified a number of PR variants in gene libraries derived from different depths of the Pacific ocean's photic zone, suggesting an adaptation to light conditions in the bacteria's environment and as such, a significant contribution to the cell's energy requirements and with a likely impact on the energy flux in the ocean (Béjà *et al.*, 2000; Béjà *et al.*, 2001).

### 1.2.1 Structure

PR is a membrane protein with a short history of studies and there are no high resolution structures available. Hydropathy plots and the significant degree of similarity (~22-26% sequence identity) with bacteriorhodopsin (BR) suggests that it belongs to the group of seven-transmembrane-helix proteins (Béjà *et al.*, 2000; Béjà *et al.*, 2001), see the alignment of the two proteins in **figure 1.5**.

The amino-terminus of the protein is on the extracellular-, the carboxy-terminus on the intracellular side.

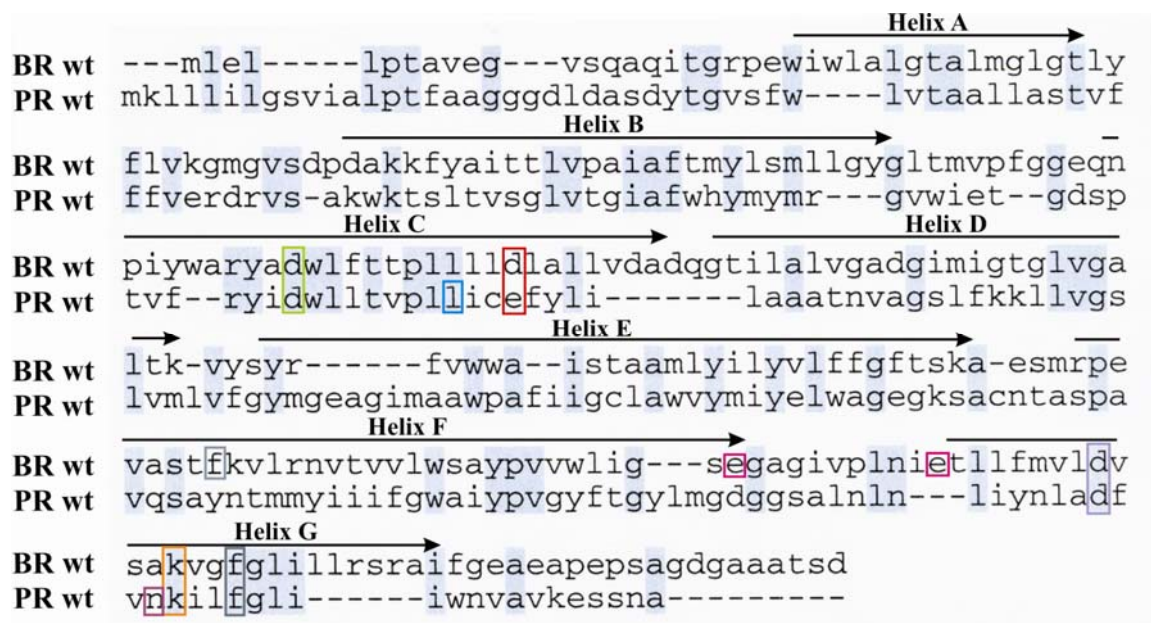


**Figure 1.5 Alignment of the amino acid sequence of BR wild-type (bacterio opsin with signal sequence, gi: 15790468 in the NCBI protein database) and PR wild-type (gi: 9971913, AF279106.2).** The two sequences show 26% overall identity, shown by the light blue background coloring. The conserved H<sup>+</sup> acceptors (D85 and D97) are depicted in green, H<sup>+</sup> donors (D96, E108) in red, the Lys residues (Lys216 and Lys231) which form the Schiff base with the retinal chromophore, in helix G, in orange. Homologous residues Asp212 (BR) and Asp227 (PR) in helix G, important for the photoisomerisation of the retinal, are highlighted in violet. In addition, in the sequence of BR the glutamate residues, members of the H<sup>+</sup> release complex (Glu194 and Glu204), are depicted in pink and Phe171 and Phe234, mutation of which cause accumulation of the N state, in grey. In the sequence of PR there is a Phe in a position homologous to Phe234 of BR, coloured also in grey. Amino acid residues of PR, which do not have homologous counterparts in the sequence of BR are Leu105 ('spectral tuning switch')(Man *et al.*, 2003) and Asn230, involved in the primary photoreaction in PR (Bergo *et al.*, 2004), both in helix G. Delimitation of the transmembrane helices as in ref. (Spudich and Jung, 2005). For sequence alignment of several microbial rhodopsin sequences see Spudich and Jung, 2005 (Spudich and Jung, 2005). Colour coding is the same as in **figure 1.6**.

The scaffold of all published structural models of PR is the 1.55 Å resolution structure of BR (Luecke *et al.*, 1999), see also (Béjà *et al.*, 2000; Béjà *et al.*, 2001; Bielawski *et al.*, 2004; Friedrich *et al.*, 2002) and **figure 1.6**.

Conserved amino acid residues include Lys231 which forms the Schiff base with the retinal; Arg94, Asp97, Thr101 and Asp227. In BR Asp96 ( $H^+$  donor) and Asp85 ( $H^+$  acceptor) are critical for  $H^+$  transfer. These are in the third transmembrane domain (C), very similar in the two proteins (**fig 1.5**). Residue Asp227 could interact with another conserved site, Tyr200, which contributes to the proton release from the Schiff base; Arg94 appears to regulate the process of  $H^+$  release that occurs before the  $H^+$  uptake from the cytoplasm. A proton-release-complex is missing in PR (Béjà *et al.*, 2000).

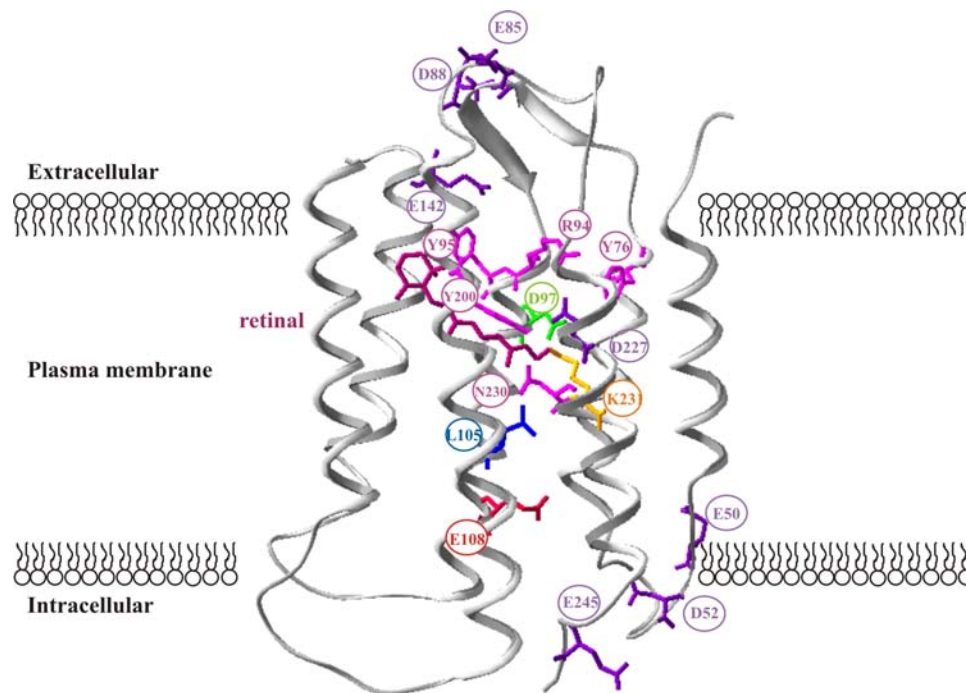


**Figure 1.6 Structural model of PR** The amino acid sequence was fitted into the X-ray structure 1C3W of BR (Luecke *et al.*, 1999). Because the 1C3W structure of BR does not cover the region between Tyr157 and Glu161, the homologous region of PR was excluded. Conserved residues are highlighted:  $H^+$  donor E108 in red, the  $H^+$  acceptor D97 in green, Lys231 which binds the retinal (purple) in yellow. Negatively charged conserved residues which could contribute to  $H^+$  transfer on the two sides of the membrane are depicted in light violet (E50, D52, E85, D88, E142, E245), positively charged residues in light magenta (Y76, R94, Y95, Y200). Also in light magenta the polar residue Asn230, which is important for the initial photoisomerisation of the retinal (Bergo *et al.*, 2004). The only residue shown here and not conserved within the microbial retinylidene protein group is L105 (blue), was identified to play the role of a spectral tuning switch (Man *et al.*, 2003). Model constructed based on ref. (Friedrich *et al.*, 2002).

Glu108 and Asp97 play the roles of primary proton donor and acceptor respectively, similarly to the homologous residues of BR.



### 1.2.2. Photocycle and spectral characteristics

Similar to bacteriorhodopsin (BR), PR undergoes a photocycle triggered by the all-*trans* to 13-*cis* conformational change of the retinal upon absorption of a photon. The photocycle intermediates can be identified based on spectral characteristics.

Absorption spectra of PR show a characteristic peak at 518 nm (pH 11.5), red-shifted to 538 nm at pH 4.0. The two forms are termed PR<sup>alkaline</sup> and PR<sup>acidic</sup> (Friedrich *et al.*, 2002) as also depicted in **figure 1.7**.

The sequence comparison of BR and PR suggested that residues homologous to BR's proton donor and acceptor (Asp96 and Asp85; Glu108 and Asp97 respectively) might play a similar role in the proton transport by proteorhodopsin and initial characterisation revealed at least two distinct intermediates with spectra like those of the M and O states of BR (Béjà *et al.*, 2000). Time resolved visible and FT-IR spectroscopy measurements confirmed this hypothesis: indeed, Asp97 and Glu108 play key roles in the deprotonation and reprotonation of the Schiff-base during the photocycle (Dioumaev *et al.*, 2002; Friedrich *et al.*, 2002; Krebs *et al.*, 2002; Váró *et al.*, 2003). Additionally, comparison of absorption spectra of wild-type PR with D97N under alkaline and acidic conditions revealed that residue D97 is responsible for the red shift of the  $A_{\max}$  of the acidic form (Dioumaev *et al.*, 2002; Dioumaev *et al.*, 2003). The photocycle intermediates resemble those of BR and in analogy are named K-like, M-like, N-like and O-like.

Under **alkaline conditions** the photocycle of PR is similar to that of BR, with the exception that *no* L-like intermediate was detectable (Friedrich *et al.*, 2002). Alternatively, the equilibrium of the  $K \leftrightarrow L$  states is strongly shifted towards K, and both are red-shifted (Dioumaev *et al.*, 2002; Friedrich *et al.*, 2002). The photocycle model based on the latter studies includes 6 intermediates comprised of four spectral states, analogous to the K, M, N, O states of the BR photocycle. With the exception of the first, K-like state (PR<sub>560</sub>), the next four are composed of temperature-dependent equilibria of at least two components. The first two represent equilibria between K and M (PR<sub>410</sub>), followed by complex mixtures of M, N-like (PR<sub>530</sub>) and O-like (PR<sub>580</sub>) (Friedrich *et al.*, 2002), see **figure 1.7**.

Deprotonation of the Schiff-base is not complete until tens of microseconds, the M-like state does not accumulate to the same extent as M in BR, and a H<sup>+</sup> is not released during the rise of the M-like state due to the absence of homologues of Glu194 and Glu204, which are involved in the H<sup>+</sup> release. Reprotonation of the Schiff-base produces an intermediate similar in its molecular properties to BR's N (containing a 13-*cis* retinal, protonated Schiff-base and

protonated Asp97) but with a red-shifted absorption maximum. Reprotonation of the Schiff-base occurs from the cytoplasmic side probably via an M-like intermediate with accessibility to the cytoplasmic side. The H<sup>+</sup>-donor Glu108 is not observed in an unprotonated state. Before returning to the ground state, the retinal is reisomerised producing a state analogous to O in BR, with a protonated Asp97 and a perturbed all-*trans* retinal with an absorption maximum similar to that of the ground state (Dioumaev *et al.*, 2002; Friedrich *et al.*, 2002).

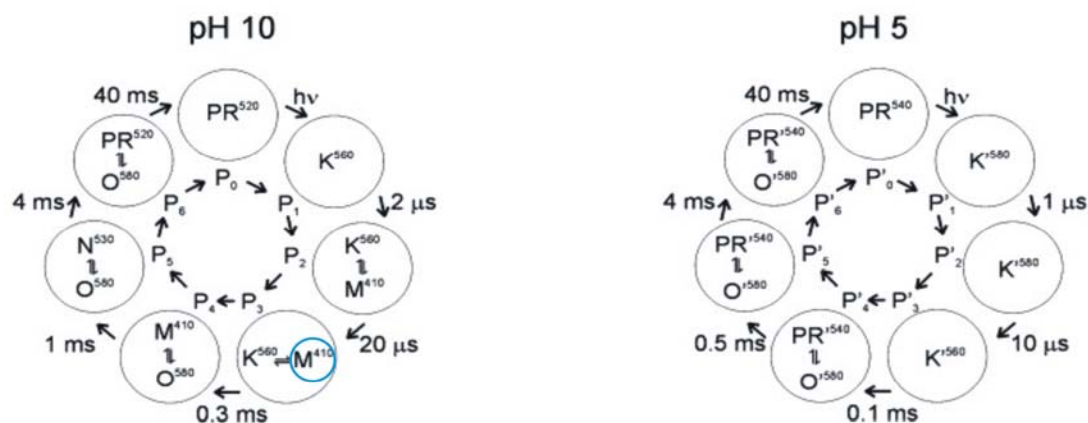


Figure 1.7 Photocycle model of PR<sup>alkaline</sup> and PR<sup>acidic</sup> (Friedrich *et al.*, 2002)

Thermodynamic parameters (the activation enthalpy  $\Delta H$  and the activation barrier  $\Delta S$ ) associated with the photocycle are similar to those measured in case of the photocycle of BR and the sensory rhodopsin SRII from *Natronobacterium pharaonis* (Friedrich *et al.*, 2002).

Under **acidic pH conditions** only red-shifted spectral states have been identified (Dioumaev *et al.*, 2002; Friedrich *et al.*, 2002; Lakatos *et al.*, 2003; Lakatos and Váró, 2004; Váró *et al.*, 2003). The M-like state – defined as a characteristic absorbance change at around 400 nm, due to the formation and decay of the deprotonated Schiff base – is missing. A reason for this can be that the reprotonation is faster, so the M-like state cannot significantly accumulate (Friedrich *et al.*, 2002). All spectroscopic studies agree about this finding, the discrepancy lies in the interpretation of the (possible) consequences. Friedrich *et al.* (2002) measure inwardly directed H<sup>+</sup>-translocation using proteoliposomes attached to black lipid membranes (BLM). In this study the key to the direction of H<sup>+</sup>-pumping is considered the protonation state of the H<sup>+</sup>-acceptor Asp97: when this site is already occupied by a H<sup>+</sup> at the moment of illumination (high H<sup>+</sup> concentration = acidic pH at least at the extracellular side where Asp97 is), the H<sup>+</sup> can leave only towards the intracellular side of the protein (Friedrich *et al.*, 2002) – see *Photocurrents of Proteorhodopsin* below.

The suggested model is:



In contrast to this model, a series of studies claim that  $H^+$  translocation across the membrane take place only under alkaline conditions, where Asp97 is anionic, at acidic pH there is no  $H^+$  pumping possible (Dioumaev *et al.*, 2003; Lakatos *et al.*, 2003; Lakatos and Váró, 2004). It is argued that similar to BR, where at pH values below the  $pK_a$  of the proton acceptor of  $\sim 2.5$ , transport cannot occur because the proton acceptor is not available and the retinal Schiff-base does not deprotonate. Thus, it should not be possible for PR to transport at pH values lower than the determined  $pK_a$ ,  $\sim 7.1$ . Lakatos *et al.* suggest that at low pH there is charge motion inside the protein, but their net transport is zero (Lakatos *et al.*, 2003).

Experiments designed by the groups that challenge inward proton transport to directly measure  $H^+$  translocation (by photoelectric current measurements using membrane fragments encapsulated in polyacrylamide gel or pH measurements in PR-containing liposome suspension) fail to achieve this under acidic conditions. Moreover, spectroscopic measurements of PR mutants where the  $H^+$  donor (Glu108) or acceptor (Asp97) were replaced behave similarly to BR mutants of the  $H^+$  donor (Asp96) and acceptor (Asp85).

Azide is a weak acid, with a delocalized charge when anionic.  $\text{HN}_3^+$  partitions into the hydrophobic cytoplasmic region of BR and dissociates there. By contributing to the proton transfer to the Schiff base, accelerates the M-decay in BR D96N. Azide has much less effect on proton release to the extracellular side of BR where the proton acceptor is, i.e. on the rise of the M state (Tittor *et al.*, 1989). Experiments in the presence of azide show that as in the case of BR, azide has little effect on the kinetics of a wild-type-like PR (a triple Cys mutant), but strongly accelerates the M-decay of E108Q ( $\sim$ BR D96N) at pH 9.5. At pH 5, if E108 is involved in  $H^+$  transport in the opposite direction, the *rise* of M-state in the E108Q mutant should be observed. The sole effect observed was an elevated accumulation of the red-shifted N state but with little change in the apparent rise and decay time constants. In conclusion, this residue-pair has the same function in the two retinal-proteins (Dioumaev *et al.*, 2002; Dioumaev *et al.*, 2003). “Thus, if there is proton transport at low pH in the direction opposite to that of the translocation at high pH, it will be based on an entirely different mechanism that does not utilise Asp97 and Glu108 as transient acceptor and donor.” (Dioumaev *et al.*, 2003)

FTIR spectroscopy measurements using proteolipid films of Imasheva *et al.* (2004) have shown that the residue Asp227 is involved in the selectivity of retinal

photosomerisation in PR. Asp227 together with Arg94 are homologous to BR's Asp212 and Arg82, components of a complex counterion to the Schiff base on the extracellular side of the protein. Continuous illumination by  $\lambda > 530\text{nm}$  at low pH induces the formation of a long-lived species that absorbs at 430 nm that contains 9-*cis* retinal. The yield of this species seems strongly pH-dependent and can be converted back to ground state PR by blue-light illumination. Light-induced formation of the 9-*cis* species is enhanced in the D227N mutant but not in D97N. This means that Asp227 facilitates the all-*trans*  $\rightarrow$  13-*cis* photoisomerisation pathway and prevents the formation of the 9-*cis* photoproduct when it is in an anionic state. The "9-*cis* photocycle" is slower as the 13-*cis*, it has a decay time of tens of minutes. The mechanism of involvement of Asp227 in the control of the retinal isomerisation or transport properties of this 9-*cis* cycle are not clear yet, but it is suggested that might be a nonfunctional side-reaction of the pigment, or could have a sensory or regulatory role (Imasheva *et al.*, 2004).

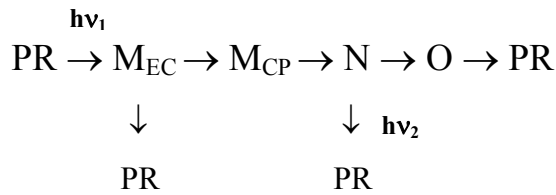
Using ultrafast pump/probe spectroscopy, Huber *et al.* show that the speed and efficiency of the primary reactions (after illumination) are controlled by the charge distribution in the vicinity of the Schiff-base (i.e. in the retinal binding pocket). The spectral and dynamic features suggest that the ultrafast dynamics of PR are highly related to those of archeal retinal proteins, bacteriorhodopsin and sensory rhodopsins I and II (Huber *et al.*, 2005). Bergo *et al.* identify Asn230 as important for the initial photoisomerisation reaction of retinal. Low-temperature FTIR spectroscopy measurements show that replacement of Asn230 with an alanine has a large effect on the structure of the chromophore, its response to light, thermal stability of the K intermediate and also the hydrogen bonding of nearby internal water molecules. Asn230 is adjacent to the Schiff-base-forming residue Lys231 in an analogous position as Ala215 in BR. The presence of the hydrophilic group of Asn230 may contribute to the differences observed between BR and PR. Furthermore, the neutralization of the proton acceptor Asp97 does not have the same strong effect on the initial all-*trans* chromophore structure as replacement of the homologous Asp85 of BR (Bergo *et al.*, 2004).

### 1.2.3 Photocurrents of Proteorhodopsin

Upon continuous illumination, PR mediates proton translocation across the membrane. This has been detected by following pH changes in an *E. coli* cell-suspension which expressed PR (Béjà *et al.*, 2000) and in oriented *E.coli* membrane fragments encased in polyacrylamide gels (Dioumaev *et al.*, 2003; Lakatos *et al.*, 2003; Váró *et al.*, 2003). Friedrich *et al.* (2002) applied the **Black-Lipid-Membrane** technique to measure directly the

currents triggered by light. PR containing proteoliposomes were attached to a BLM, which separated 2 compartments of a teflon cuvette. Upon continuous illumination characteristic signals could be observed, which reflected the charging of the electrical capacitance of the compound membrane system. After addition of ionophores which permeabilise the compound membrane system, stationary currents appeared showing continuous pumping. Additional illumination with blue light led to quenching of the stationary photocurrent, a phenomenon well known for BR. The quenching originates from a fast conversion of a blue-shifted photocycle intermediate with a deprotonated Schiff base back to the ground state (Ormos *et al.*, 1980). At pH ~10, the currents were outwardly directed and resembled that of BR, but when the same compound membrane system was titrated down to pH 5.4, the stationary current reverted its direction. This suggests that the protonation status of the primary proton acceptor Asp97 is crucial for the vectoriality of the proton transport (Friedrich *et al.*, 2002). Blue laser flashes (396 nm) during and after continuous illumination at neutral and acidic pH showed that at pH 7 PR pumps outwardly, a signature for the M state (quenching of the stationary current by the blue laser flashes) is present, and a laser flash several hundreds of milliseconds after illumination triggers a small positive transient (excites the ground state). At pH 5.2, the blue flashes during illumination with green light added a small negative transient to the negative stationary current, after illumination cause a large negative transient, compatible with inward H<sup>+</sup> pumping. These results indicate the absence of detectable concentrations of an M-like intermediate in the acidic form.

Friedrich *et al.* also observed a peculiar light-intensity dependence: at pH 7 negative transient and stationary currents could be recorded, when the yellow light was attenuated to <2%. At pH 5.4, illumination with 10% light produced the largest inward stationary current, illumination with 100% resulted in a biphasic signal with a large negative transient followed by a small positive stationary component. This indicates that the contributions of the alkaline and acidic form of PR to the pump current are superimposed and depend differently on the light intensity. Experiments with continuous illumination (>515 nm) versus laser flashes (503 nm) suggested that the outward proton transport might require the absorption of two photons, whereas the inwardly directed only one (single laser flashes allow only for single-photon excitation, continuous illumination enables the absorption of more than one photon) (Friedrich *et al.*, 2002). The way the second photon could accelerate the transport cycle is shown in the scheme below by shifting the M<sub>EC</sub> – M<sub>CP</sub> equilibrium to M<sub>CP</sub>. The cycle could also branch into a non-transporting part:



Photocurrents measured upon illumination of *Xenopus laevis* oocytes which heterologously express PR support the BLM experiments (PR containing proteoliposomes attached to the BLM are right-side-out) and show that PR is a H<sup>+</sup> pump as potent as BR (Friedrich *et al.*, 2002).

### 1.2.4 Proteorhodopsin variants

Soon after identifying PR in marine bacterioplankton, Béja *et al.* report about variants of PR in the PCR-generated Monterey Bay and Antarctic Ocean gene libraries. The changes in amino acid sequences were spread over the entire protein, including the retinal binding pocket. Interestingly, it seems that PR variants are adapted to their environment and that surface- and deep-water groups of proteorhodopsin-based phototrophs co-exist, where the energy generating pigments are spectrally tuned to either shallow or deeper water light fields (Béja *et al.*, 2001).

By comparing theoretical structural models Man *et al.* (Man *et al.*, 2003) identified the residue at position 105 responsible for spectral tuning in Blue- (Gln105) and Green (Leu105) PRs: interchanging these two residues almost interconverted the absorption spectra of Blue-PR and Green-PR, essentially complete at pH 5. Therefore the Q-L difference between Green-PR and Blue-PR pigment functions as a *single residue spectral tuning switch* (Man *et al.*, 2003). An increase in the number of dipolar side-chains near the protonated Schiff base of retinal was found to increase the ground-excited state energy gap via a long-range dipole-dipole Coulomb interaction. Such interactions may explain the blue-shift in PRs on substitution of the non-polar Leu with the polar Gln residue (Man *et al.*, 2003).

Sequence variations at position 105 were observed in PRs in the Mediterranean and Red Seas, with absorption maxima between 505nm (Glu105) and 540 nm (Val105) (Man *et al.*, 2003). Residues outside the retinal binding pocket may also influence the absorption maximum of the protein. Moreover, members of the PR family have photocycles with different speeds as measured in spectroscopic experiments, which also raises the possibility of regulatory (i.e.

sensory) rather than energy harvesting functions for some members of the PR group (Man-Aharonovich *et al.*, 2004; Sabehi *et al.*, 2003).

Phylogenetic and comparative genomic analysis of genomic fragments recovered directly from planktonic bacteria inhabiting waters where the original PR genes were identified (Californian coast, central Pacific Ocean and the Antarctic Ocean) show that PR genes are distributed among a variety of divergent bacterial taxa, including both  $\alpha$ - and  $\gamma$ -proteobacteria (De LaTorre *et al.*, 2003).

The idea that PR might play a central role in marine phototrophy due to its ubiquitous presence, is strengthened by the study of (Venter *et al.*, 2004). To the 67 closely related PR homologs (Sabehi *et al.*, 2003), this study adds about 782 new PR homologs in the Sargasso Sea. In total, they identified 13 distinct subfamilies of rhodopsin-like genes, which include 4 families of proteins known from cultured organisms (bacteriorhodopsin, halorhodopsin, sensory opsins and fungal opsin), and 9 families from uncultured species of which 7 are known only from Sargasso Sea populations. Of these subfamilies, many are quite distant from either PR or from rhodopsins in cultured species. The expression levels of these genes are not yet known (Venter *et al.*, 2004).

Sequences from all above mentioned geographical locations have been analysed by Bielawski *et al.* (Bielawski *et al.*, 2004) in order to identify evolutionary mechanisms responsible for the divergence of PRs. Their analysis of 80 sequences suggests that PRs were adapted to different light intensities in the marine environment by a process of Darwinian evolution that involved substitutions of major effect, as well as substitutions for fine-tuning of absorption maxima. In Green-PRs, the spatial distribution of amino acid positions 65, 68, 70, 101, and 105 ( $< 10 \text{ \AA}$  away from the Schiff base) is consistent with the action of natural selection to modulate the stability of the protonated Schiff-base, thus altering the energy needed for  $H^+$  absorption. In case of Blue-PRs, the amino acids at the positive selection sites appear to be unrelated to the retinal binding pocket ( $> 10 \text{ \AA}$  from the Schiff base), so functional evolution of the Blue-PRs was accomplished by different means than was the diversification of Green-PR spectral sensitivity (Bielawski *et al.*, 2004).

Recently, PR has been identified in the ubiquitous marine bacterium SAR11 (*Pelagibacter ubique*), the first cultivated member of the abundant SAR11 clade. The genes encoding this protein are most closely related to genes recovered from the Sargasso Sea by shotgun sequencing. The sequence of the protein contains the residues Asp102 and Glu113 in positions appropriate to act as putative proton acceptor and donor residues during the

photocycle. The fact that this bacteria can be cultivated under laboratory conditions opens new perspectives in the study of this protein (Giovannoni *et al.*, 2005).

### 2.3 The aim of the work

The current work proposes to study proteorhodopsin expressed heterologously in *Xenopus laevis* oocytes, and to investigate the role of conserved and non-conserved residues in proton pumping, observed in spectroscopic measurements important for the function of the protein.

The oocyte system allows the control of the transmembrane potential and also that of extra- and intracellular pH. In this way we can gain insight into the vectoriality of PR photocurrents - controversial in the literature at the moment - and its regulation by the electrochemical membrane potential (given by the potential- and pH-gradients). Similarly, the importance of the amino acid residues at positions E108 and D97 – the proton donor and acceptor – for the proton pumping process is analysed. By the replacement of these residues both charge and side-chain volume were taken into account: E108D and D97E are charge-conserving mutations with only the structure of the amino acid side-chain changed, whereas E108G, D97N and D97T not only remove the negative charge at these positions but also introduce side-chains of different length.

In the experiments presented in this work the sequence of the first identified PR is used, which later was included in the group of ‘Green-PR’-s. The residue L105, identified as a ‘spectral tuning switch’ was replaced by glutamate, to determine how the blue-shift in the absorption spectrum observed for this L105Q mutant is reflected in its action spectrum.

General electrophysiological characterisation of the generated mutants is presented.

In most cases experiments with BR were done in parallel to those designed for PR, as a reference, since data on BR in the same expression system is already available (Geibel, 2003; Geibel *et al.*, 2001; Nagel *et al.*, 1998; Nagel *et al.*, 1995).

Complementary to the electrophysiological experiments, the expression of PR in the oocyte expression system was evaluated: the presence of the protein at the cell surface was detected by means of a chemiluminescence test developed originally by (Zerangue *et al.*, 1999) and the overall expression by Western blotting, using N- or C-terminally tagged PR and BR constructs.

Altogether, these data contribute to the understanding of proton pumping by proteorhodopsin and evaluate the applicability of the oocyte system for the study of this light driven proton pump.



## 2. Results

Proteorhodopsin (PR) is one of the most recent members identified in the group of retinylidene proteins (Béjà *et al.*, 2000). Spectroscopic studies have shown that upon light stimulation the protein undergoes a photocycle similar to that of bacteriorhodopsin (BR), also characterised by only slightly larger time constants (Béjà *et al.*, 2000; Dioumaev *et al.*, 2002; Friedrich *et al.*, 2002; Krebs *et al.*, 2002). This, together with the absence in the vicinity of the PR gene of another gene encoding transducers characteristic for sensory rhodopsins, suggested that PR might function as a light-driven ion-pump. Direct measurements of the transport activity of PR were done with the BLM technique, using PR expressed and purified from *E.coli* and the authors found that at pH values lower than the pK<sub>a</sub> of the proton acceptor D97 (where this residue is protonated) transient and stationary inward proton transport is possible (Friedrich *et al.*, 2002). In case of BR, the control of the deprotonation and reprotonation steps during the photocycle is important for the overall pumping activity of the protein.

Expression in *Xenopus laevis* oocytes allows not only the study of pH effects on perfectly oriented PR molecules, but also that of the membrane potential (which together form the electrochemical potential for protons,  $\Delta\tilde{\mu}_H^+$ ). Wild-type and mutant PR expressed heterologously in this system were investigated, in order to learn more about the factors that control proton transport properties.

### 2.1 Action spectrum of PR wild-type

The response of the system as a function of the wavelength of light was measured in order to determine how the data measured in spectroscopic experiments are reflected by the active pump, under stationary illumination conditions. Oocytes expressing PR constructs were illuminated with light from a 75W XBO arc lamp, filtered by narrow bandwidth filters ( $\pm 5$  nm) between 339 nm to 615 nm in steps of  $\sim 25$  nm, at -30 mV transmembrane potential.

The action spectrum of the wild-type PR measured in oocytes fits nicely with that measured in BLM experiments (**fig. 2.1**). The data correlate with absorption spectroscopy measurements which showed a maximal absorption around 520nm (Béjà *et al.*, 2000): the current amplitudes reach the maximum at  $\sim 517$  nm – hence the name ‘green PR’.

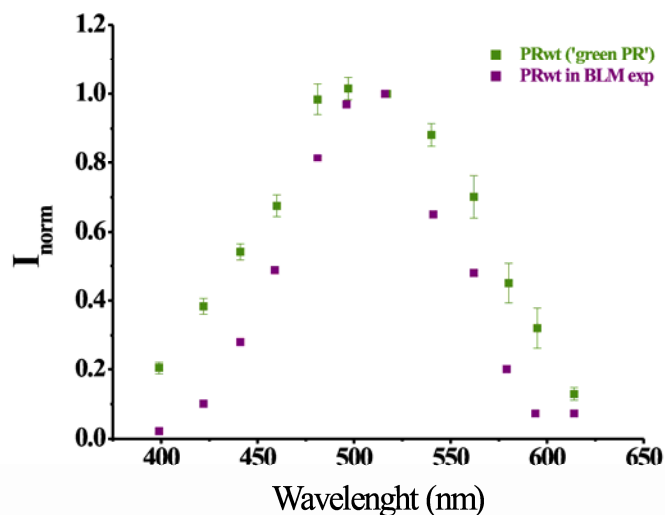


**Figure 2.1 Action spectra of PR wt expressed in oocytes and in the BLM system** Mean $\pm$ SEM of 4 (PR wt) oocytes presented. The recorded stationary current amplitudes were normalised to the quantum flux at  $\lambda=517\text{nm}$ .

## 2.2 Voltage dependence of the proton transport in the presence or absence of pH gradients

In case of proteorhodopsin the I-V relationship was studied in the presence of pH gradients, similar to bacteriorhodopsin (Geibel, 2003; Geibel *et al.*, 2001; Lauger, 1991), but also in the absence of a pH gradient by manipulating the intracellular pH of the oocytes using buffers containing organic acids.

### 2.2.1. In the presence of a pH gradient (asymmetrical pH conditions)

As it can easily be seen in **fig 2.2**, both transmembrane potential and pH have a marked effect on the photocurrents of PR. Under neutral conditions ( $\sim\text{pH } 7.4$  on both sides of the membrane, left side of **fig 2.2**), the signal has a clear peak after which the photocurrent reaches a stationary level. Decreasing the extracellular pH leads to inversion of the  $\text{H}^+$  transport at hyperpolarising potentials at pH 5.5 and at pH 4.5 only inward charge translocation can be observed, in accordance with the findings of (Friedrich *et al.*, 2002).

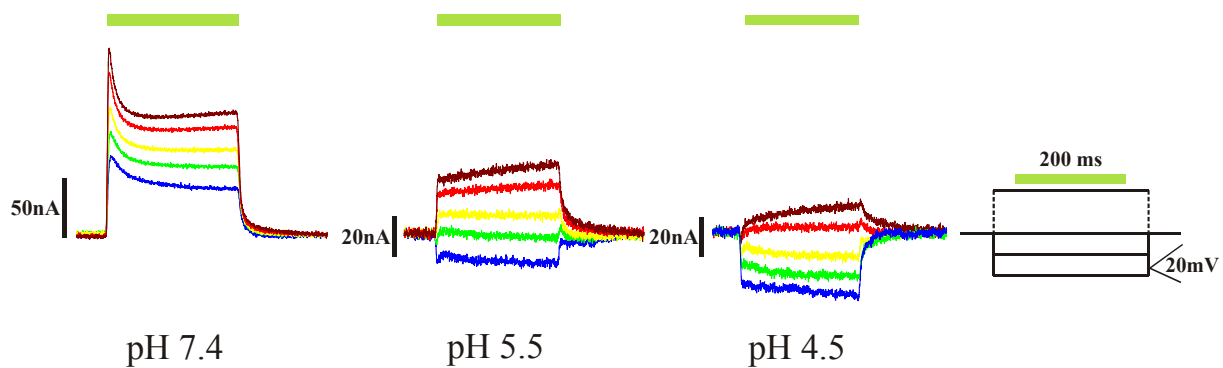


**Figure 2.2 PR wt photocurrents at three different external pH values.** 200 ms illumination (green bars) elicit currents whose direction depend on the applied transmembrane potential and pH gradient. The oocyte membrane was clamped first to a certain potential after which light with  $\lambda > 495$  nm was applied by opening a shutter for 200 ms, as shown on the far right side of this figure. The voltage protocol consisted of jumps from the holding potential of -30 mV to a test potential, starting at -140 to +40 mV in 20 mV steps. Colour coding: -140 mV (—), -100 mV (—), -60 mV (—), 0 mV (—), +40 mV (—).

The I-V relationship of PR is linear at all extracellular pH values, (**Fig 2.3. A**) over the measured range from -140 mV to +40 mV. Since the pH inside the cell is  $\sim 7.3$  (Stewart *et al.*, 2001), this means a difference of up to 3 pH units when the pH of the extracellular buffer is lowered to 4.5. At pH  $> 6.5$  only outwardly directed photocurrents can be measured at all test potential values. At pH 5.5 the currents invert at  $\sim -75$  mV and at pH 4.5 mostly inwardly directed photocurrents could be observed. A change of one pH unit determines a  $\sim 70$  mV shift in the apparent reversal potential (determined by extrapolation at pH 4.5 – 7.4). Between pH 7.4 – 8.5 this shift is only  $\sim 30$  mV.

**Table 2.1 Reversal potential values as result from fig. 2.3 A**

| Extracellular pH      | 4.5         | 5.5           | 6.5            | 7.4            | 8.5            |
|-----------------------|-------------|---------------|----------------|----------------|----------------|
| $V_{\text{reversal}}$ | $\sim 0$ mV | $\sim -75$ mV | $\sim -130$ mV | $\sim -210$ mV | $\sim -235$ mV |

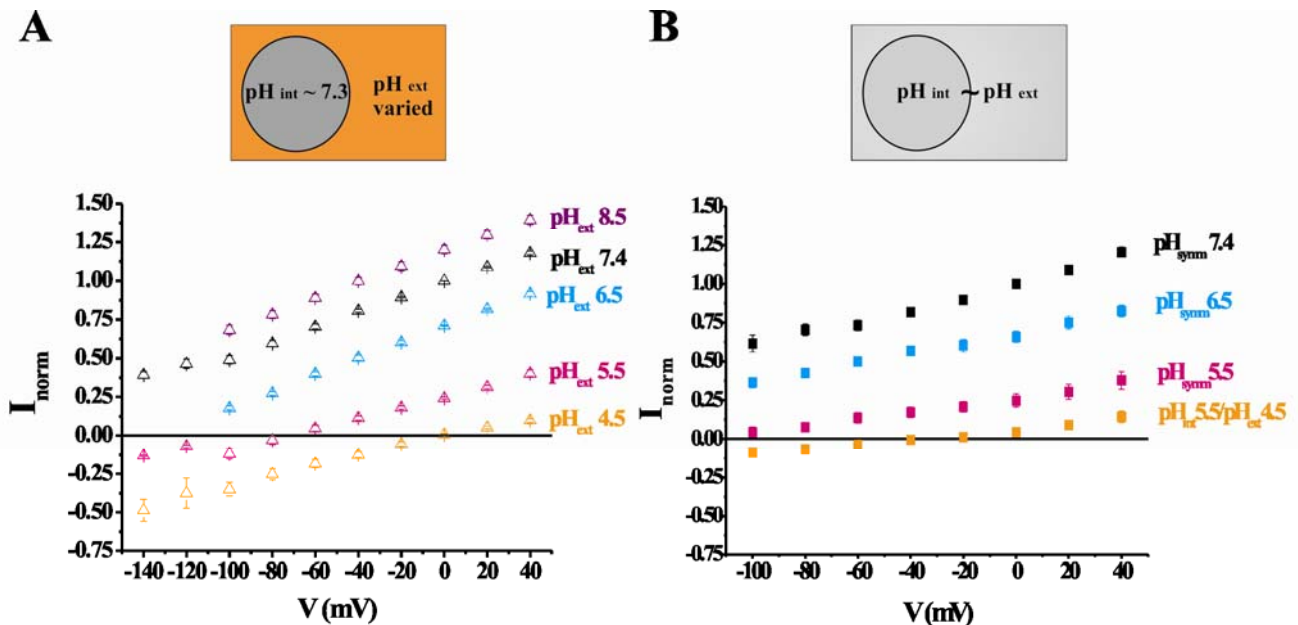


**Figure 2.3. PR wt under asymmetrical and symmetrical pH conditions** I-V curves in the presence of **A.** asymmetrical pH conditions and **B.** symmetrical pH conditions. In both cases the amplitudes of the stationary currents were evaluated and normalised to the value of the current at 0 mV, pH 7.4. In case of external pH changes the rundown of the photocurrent was taken into account by measuring photocurrents at pH 7.4 before and at the end of each experiment. Measurements were done on 3-18 cells (A) and 4-6 cells (B) and the mean  $\pm$  SEM presented.

### 2.2.2. In the absence of a pH gradient (symmetrical pH conditions)

When the intracellular pH is lowered employing organic acids (see *Materials and methods*), the slope of the I-V curves decreases and the reversal potential at each pH is shifted towards more negative values (**Fig 2.3. B**): in symmetrical pH 6.5  $V_{rev} \sim -180$  mV compared to  $\sim -130$  mV under asymmetrical pH conditions, in symmetrical pH 5.5 the current does not invert at -100 mV:  $V_{rev} \sim -120$  mV compared to  $\sim -75$  mV when there is a difference of 2 pH units facing the pumping direction. Under more acidic conditions, when  $pH_{ext} \sim 4.5$  and  $pH_{int} \sim 5.5$ , the apparent reversal potential is left-shifted with 25 mV and at positive potentials larger outward currents can be measured compared to asymmetrical pH conditions.

**Table 2.2 Reversal potential values as result from fig. 2.3 B**

|                | $pH_{ext} 4.5/pH_{int} 5.5$ | $pH_{symm} 5.5$ | $pH_{symm} 6.5$ | $pH_{symm} 7.4$ |
|----------------|-----------------------------|-----------------|-----------------|-----------------|
| $V_{reversal}$ | $\sim -20$ mV               | $\sim -120$ mV  | $\sim -180$ mV  | $\sim -210$ mV  |

To prove that the PR photocurrent is mediated by  $H^+$ , similar measurements in buffers lacking  $Na^+$ ,  $K^+$ ,  $Cl^-$  at all pH values were performed. The photocurrents measured in the NMG-containing solution were identical to those measured in ND96 at all pH values (not shown).

### 2.3. Investigating the effects of the applied electric field

As carried out previously in case of BR, the following approaches were used to study the effect of the applied transmembrane potential on proton transport mediated by PR (Geibel *et al.*, 2001):

- analysis of the on- and off-response of the stationary- or laser flash induced transient currents;
- probing the formation or decay of the M intermediate with blue laser flashes during or after illumination with green light. Blue light induces the *cis-trans* isomerisation of the retinal, followed by uptake of a proton from the extracellular side, resulting in transient inward currents, completing a non-pumping two-photon cycle (Geibel *et al.*, 2001; Nagel *et al.*, 1998; Ormos *et al.*, 1978; Ormos *et al.*, 1980).

Similarly to the case BR, it is assumed that the peak current reflects the deprotonation of the Schiff base whereby an M-like state is formed; after switching off the illumination the recovery of the ground state can be observed. Both the peak and stationary part of the PR photocurrents appear to exhibit similar voltage dependence. However, the ratio ( $I_{\text{peak}}/I_{\text{stationary}}$ ) changes from 1.7 at -140 mV to 1.5 at +40 mV (**fig 2.4**). This is different in BR, where the stationary current – the  $M_2 \rightarrow \text{BR}$  decay – is primarily influenced by the electric field, the peak current is only weakly voltage dependent (Geibel *et al.*, 2001).

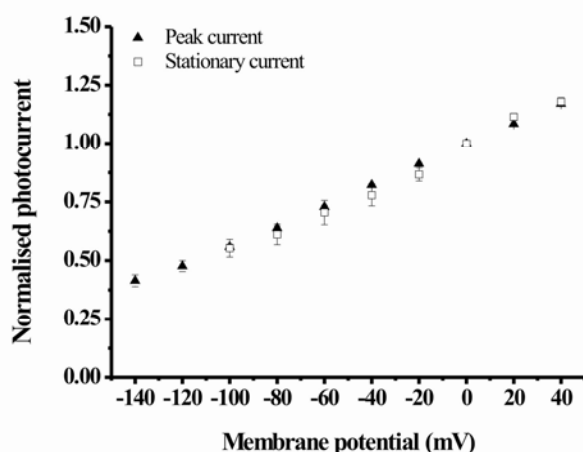


**Figure 2.4. Voltage dependence of peak and stationary currents of PR wt at pH 7.4**

In both data sets the current amplitudes are normalised to the value recorded at 0 mV. Each point represents data from 6-18 oocytes, given as Mean  $\pm$  SEM.

The photocycle of PR was probed by laser flashes during and after stationary illumination using blue light (396 nm) to detect the blue-shifted M-like state or green light (503 nm) to excite molecules in the ground state at various membrane potentials and pH values. The illumination protocol is shown in **fig 2.5**. For comparison, measurements with BR-expressing oocytes were done in parallel under the same illumination conditions.

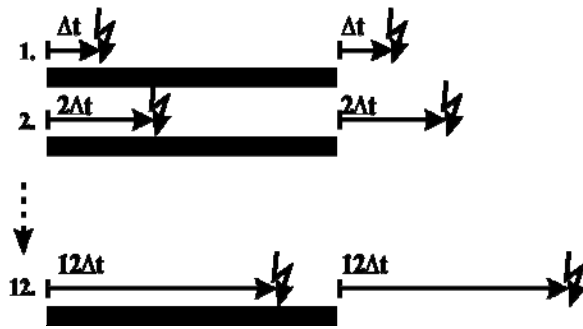


**Figure 2.5. Protocol for simultaneous stationary and transient illumination of PR and BR expressing oocytes.** Laser flashes (arrows) of  $\lambda = 396$  nm or 503 nm were applied during and after continuous illumination (bars) with  $\lambda > 495$  nm from an HBO lamp. One recording consists of 12 superimposed traces measured in the same conditions (membrane potential, pH). In one trace, the laser flashes are applied after begin or end of continuous illumination with green light:  $\Delta t = 25$  ms (BR) or 50

ms (PR). In the first trace, flashes are applied with a delay of  $1 \times \Delta t$ , delay time which increases to  $12 \times \Delta t$  in the last trace. Stationary illumination was 350 ms for BR, 700 ms for PR. The total length of the protocol is for PR two times that of BR. Protocol is similar to that used in (Geibel *et al.*, 2001).

*Green laser flashes* evoke similar transient currents for both retinal proteins, pointing in the same direction as the stationary current (**fig. 2.6 A and B**). During illumination there is no time dependent change of amplitudes, small in case of BR and large in case of PR. After continuous illumination large positive transients can be observed, increasing with  $n \times \Delta t$ , in a saturating manner.

*Blue laser flashes* trigger during stationary illumination biphasic transient current signals in case of both retinal proteins, with no time-dependent change in amplitudes (**fig. 2.6 C and D**). In BR, the transient signals have a large negative component and a small positive one, in PR the opposite case. Similar current signals measured in BR-expressing HEK293 cells were interpreted as an indication of M state accumulation (Geibel *et al.*, 2001). After continuous illumination, in the case of BR at  $\Delta t = 25$  ms the transient current is still negative, biphasic at intermediate  $n \times \Delta t$  ( $n = 2, 3$ ) and small positive transient signals are recorded at larger  $n \times \Delta t$  ( $n > 4$ ). The transient currents of PR are biphasic with large peaks at all  $n \times \Delta t$ .

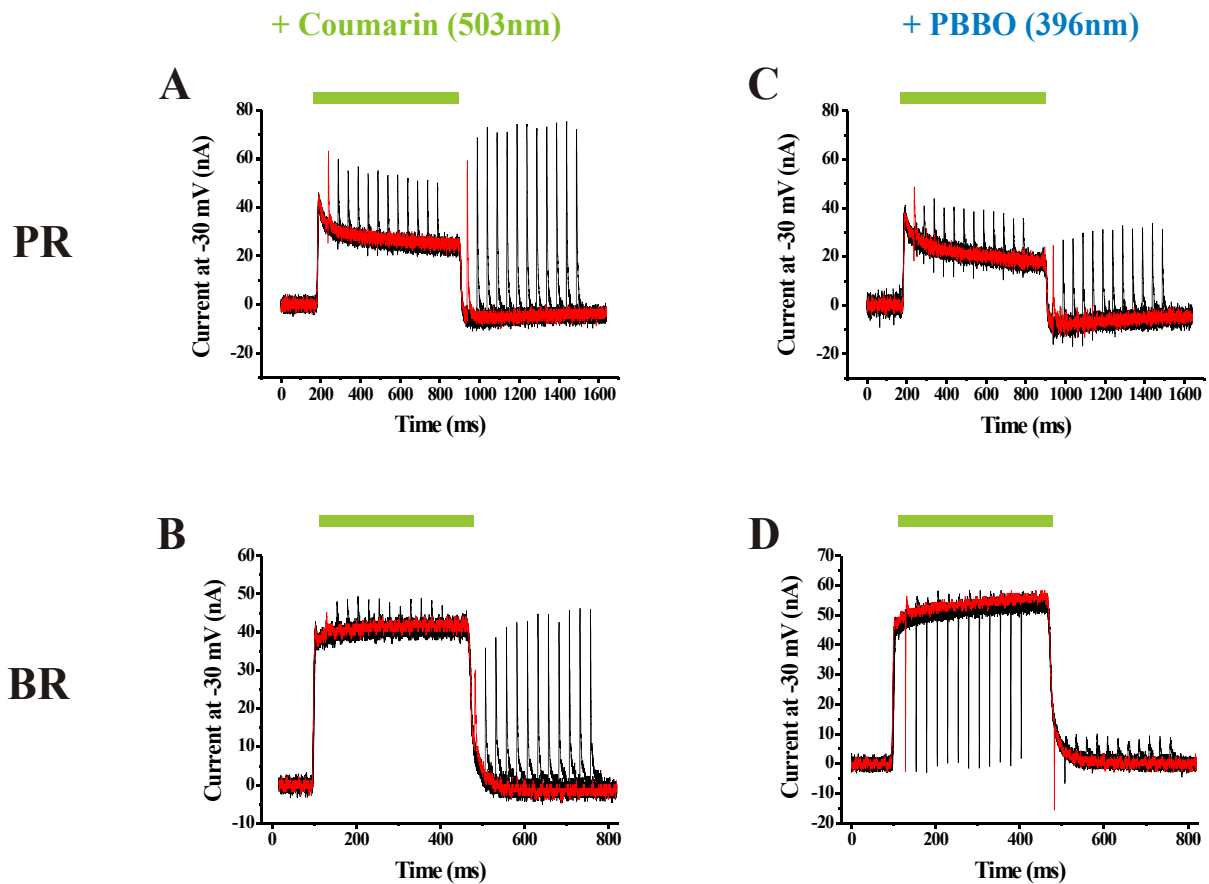


**Figure 2.6. Laser flashes during and after stationary illumination on PR wt (A and C) and BR wt (B and D) expressing oocytes at -30 mV holding potential and pH 7.4 under similar illumination conditions.** Stationary light and laser flashes were applied as described in figure 2.5. The photocurrents in case of both proteins were measured using the same cell.

To learn more about the effect of the extracellular pH on the photocurrents of PR, blue and green laser flashes were applied under acidic extracellular pH conditions, in addition to the recordings at pH 7.4. An example can be seen in **fig 2.7**, recorded at a transmembrane potential of -30 mV.

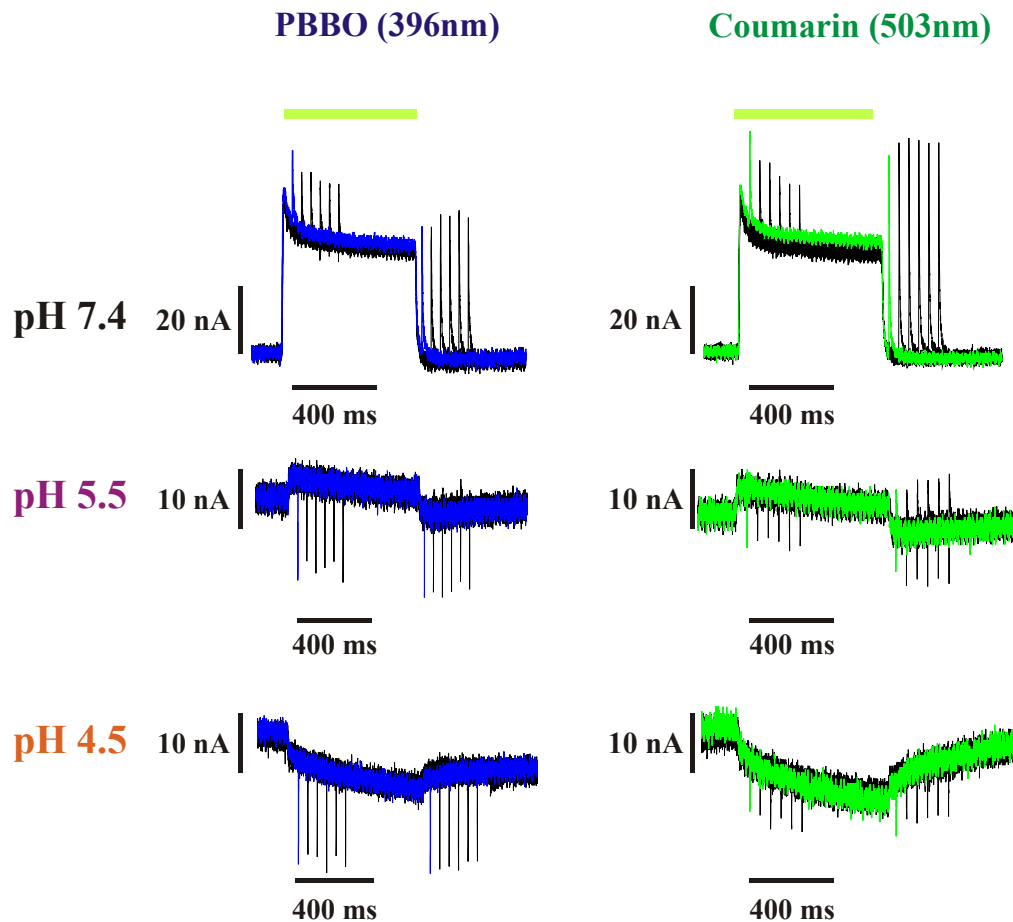


**Figure 2.7. PR wt: the effect of blue and green laser flashes changes with pH (holding potential -30 mV)** Stationary light and laser flashes were applied as described in figure 2.5, the recordings originated from the same cell.

At **pH 7.4**, the current signals are equivalent to those shown in fig 2.2.6. When the external pH is lowered, the pattern of electric signal generated by continuous and transient light excitation changes. At **pH 5.5** there is a small outward stationary current ‘quenched’ by the *blue* laser transient signals which are time independent. After continuous illumination the transients keep their inward direction, also time independent. Surprisingly and in contrast to pH 7.4, *green* laser flashes evoke inward, time-independent transient currents during stationary illumination but of smaller amplitudes, with only a small, if any, positive component; after stationary illumination the transients appear biphasic, with a negative and a positive component. At **pH 4.5** the stationary current is inwardly directed (see also **figures 2.2, 2.3**). The blue- and green-laserflash triggered transient signals are also inwardly directed and time-independent. Similarly to pH 5.5, the amplitudes of the ‘blue-transients’ are larger as those of the ‘green-transients’.



To investigate the effect of acidic pH additional to hyperpolarising transmembrane potentials on the transient currents triggered by blue flashes, the same protocol was applied at -70 mV, external pH 5.5, on both PR and BR expressing oocytes (**fig 2.8**).

In case of PR wt (upper part of **fig 2.8**), the transient currents are inwardly directed during and after stationary illumination at -30 and -70 mV. At -30 mV, the transient signals after stationary illumination also have a small positive component, which is absent at -70 mV. At -70 mV there is no stationary current detected, compatible with the reversal potential of  $\sim -75$  mV, as shown in **fig. 2.3**. The sloping baseline is an illumination artefact probably due to heating, which occurs frequently on 9-day-old oocytes. The amplitudes of transient currents measured at -70 mV are larger than at -30 mV. For comparison see also **fig 2.6**.

It is important to note the difference between the PR- and BR-generated signals: the amplitudes of transient currents triggered after continuous illumination are time-dependent in the case of BR, whereas in case of PR they are not.

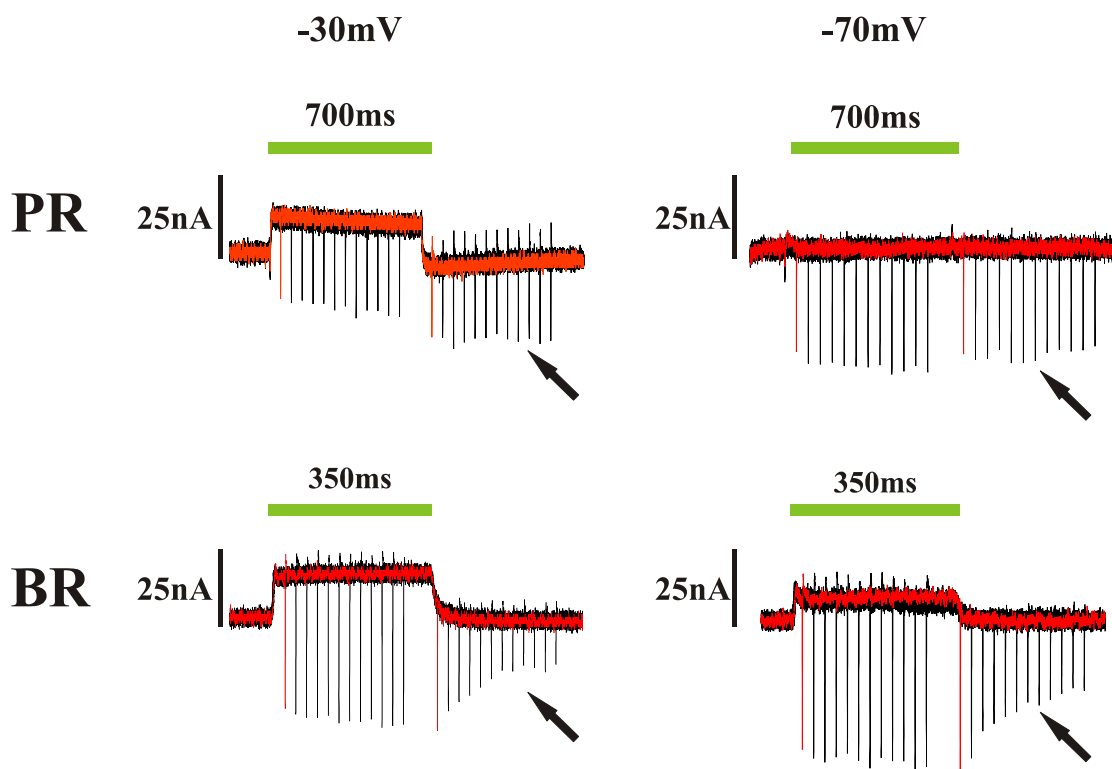


**Figure 2.8. Blue (396nm) laser flashes on PR- and BR expressing oocytes at pH 5.5 at two membrane potentials.** Stationary light and laser flashes were applied as described in figure 2.5. Recordings were obtained from the same cell expressing either PR wt or BR wt. The arrows are inserted to help noticing the difference in the pattern of laser triggered transient currents.

In case of BR wt, the results confirm the earlier observation that hyperpolarising membrane potentials prolong the lifetime of the M state (Geibel *et al.*, 2001): the amplitudes of the blue

flashes triggered transients are larger during and after stationary illumination than at pH 7.4, and at -70 mV are larger as at -30 mV. In addition, the effect of extracellular pH (or, the presence or absence of pH gradient across the membrane) was evaluated. From the recordings it seems that in the presence of a pH gradient opposing the proton pumping direction the lifetime of the M state is extended, similarly to hyperpolarising potentials.

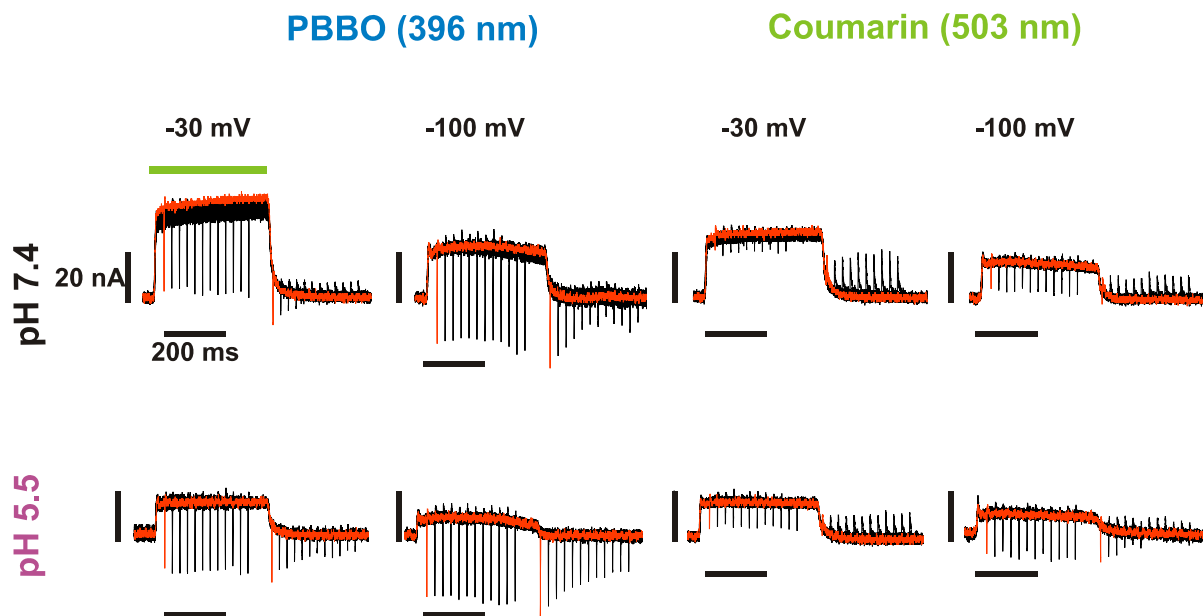


**Figure 2.9** BR wt: blue- and green laser flashes at two different membrane potentials, in the absence and presence of a pH gradient of 2 pH units across the membrane. Stationary light and laser flashes were applied as shown in figure 2.5, the recordings originate from the same cell.

**Figure 2.9** summarises the effect of membrane potential and pH on the photocurrents of BR wt probed with blue- and green laser flashes. The measurements at -30 mV are similar to those of PR in **figure 2.7**. On the left side, the quenching effect of blue laser flashes is shown again, larger under acidic conditions. Interestingly, green laser flashes may also quench the stationary current at hyperpolarising membrane potentials and/or acidic extracellular pH. At pH 5.5 and -100 mV, the pattern of green- and blue laser flashes triggered transient currents in the dark are similar, larger and negative when  $\Delta t$  between the continuous illumination and the laser flash in the dark is short, with decreasing amplitudes as this  $\Delta t$  increases. However, the amplitudes of the transient currents elicited by green laser flashes are considerably smaller compared to those triggered by blue laser flashes, and become positive even at -100 mV, pH 5.5. This latter observation suggests that there are molecules returned to the ground state excitable by green light.

To further characterise the effect of the applied electric field on the photocycle of PR, blue- and green-laser flashes were applied on the switch-off phase of the photocurrents at three transmembrane potentials, with a light-protocol similar to that described in **fig. 2.5**, but without flashing during stationary illumination.

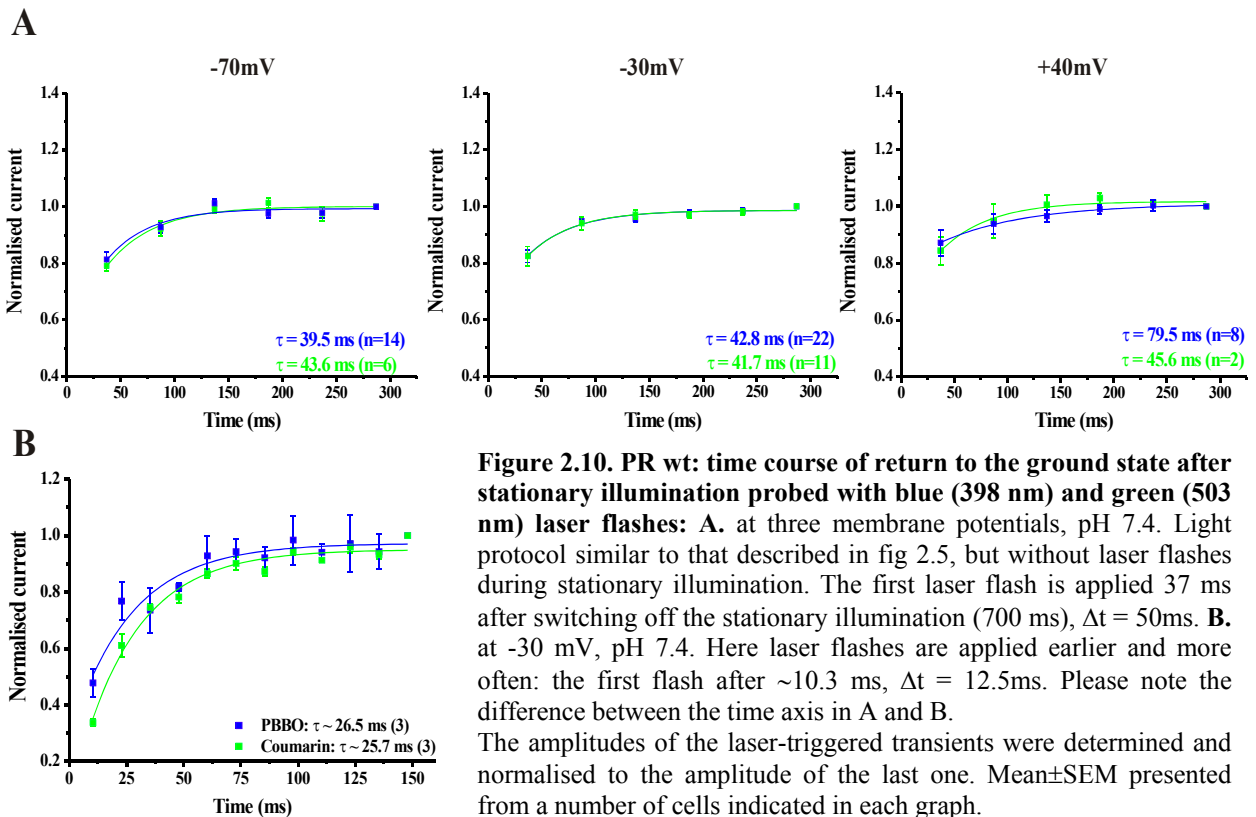


**Figure 2.10.** summarises the results of measurements performed using both blue- and green laser flashes. When probed with green flashes, the membrane potential does not seem to have much influence on the time course of the return to the ground state, since the time constants have very similar values, only the amount of molecules stimulated by the first flash appears to increase with more depolarising potentials: it is less than 80% at -70 mV and  $\sim 85\%$  at +40 mV. Blue laser flashes have a similar effect, reflected by the similar time constants. About 200 ms after switching off the stationary illumination, the transients reach the maximal amplitude which can be triggered by a certain wavelength. A similar evaluation at pH 5.5 is not possible since the transient current amplitudes seem to be time-independent.

To better resolve the switch-off phase of the stationary current of PR wt, equivalent to the M decay of BR, laser flashes of both wavelengths were applied earlier after stationary illumination and with a shorter  $\Delta t$  between subsequent traces (**fig. 2.10 B**). The results support observations made earlier:  $\sim 50$  ms after switching off the stationary illumination, 80% from the final amount of molecules excitable with a certain wavelength can be detected with both

blue and green laser flashes (see also **fig 2.10 A**, middle panel) and in  $< 200$  ms the process seems to have reached saturation.

Equivalent measurements have been done with BR wt. The results obtained by applying green laser flashes at pH 7.4 and four membrane potential values is shown in **fig 2.11**. As clearly visible, the BR molecules return faster to the ground state at depolarising potentials at both of the pH values investigated.

At pH 7.4 the process at +40 mV is more than twice (**fig. 2.11 A**), at pH 5.5 three times (**fig. 2.11 B**) faster as at -100 mV. The time window is the same as in case of PR wt.

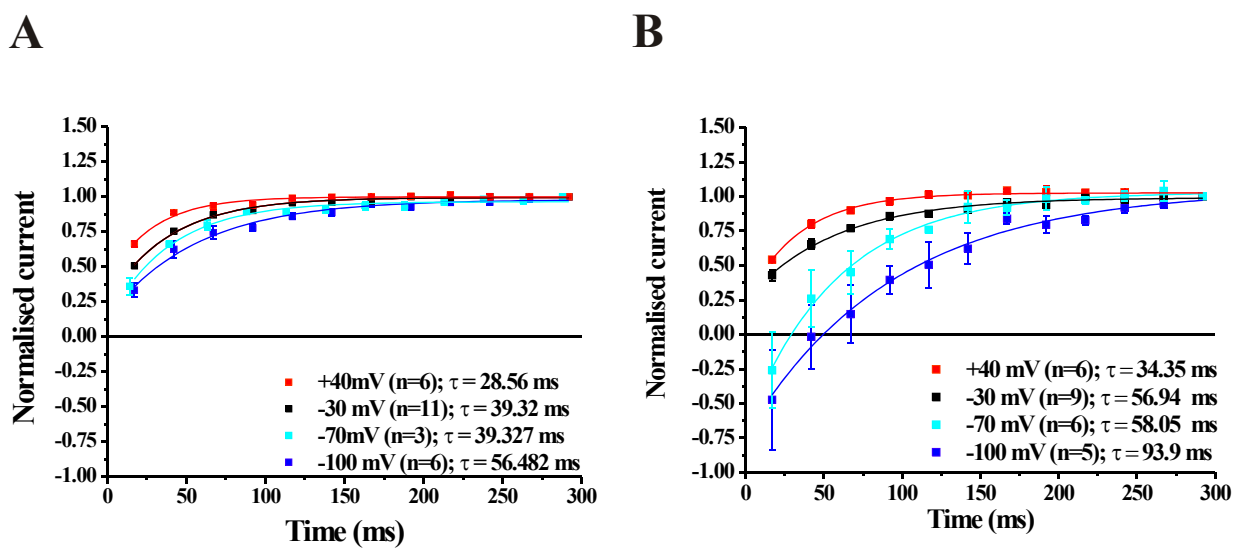


**Figure 2.11. BRwt: time course of return to the ground state after stationary illumination probed with green (503 nm) laser flashes at A. pH 7.4, B. pH 5.5** Protocol similar to that used in case of PR, the first flash applied after  $\sim 15$  ms,  $\Delta t = 25$  ms, after 350 ms stationary illumination. The amplitudes of the transients were normalised to that of the last one, mean $\pm$ SEM presented from a number of cells indicated next to each potential value.

**Figure 2.12** summarises the effect of pH on the second half of BR's photocycle, from M back to the ground state. Blue laser flashes detect the blue light absorbing M state which disappears gradually; green laser flashes detect the re-formation of the ground state.

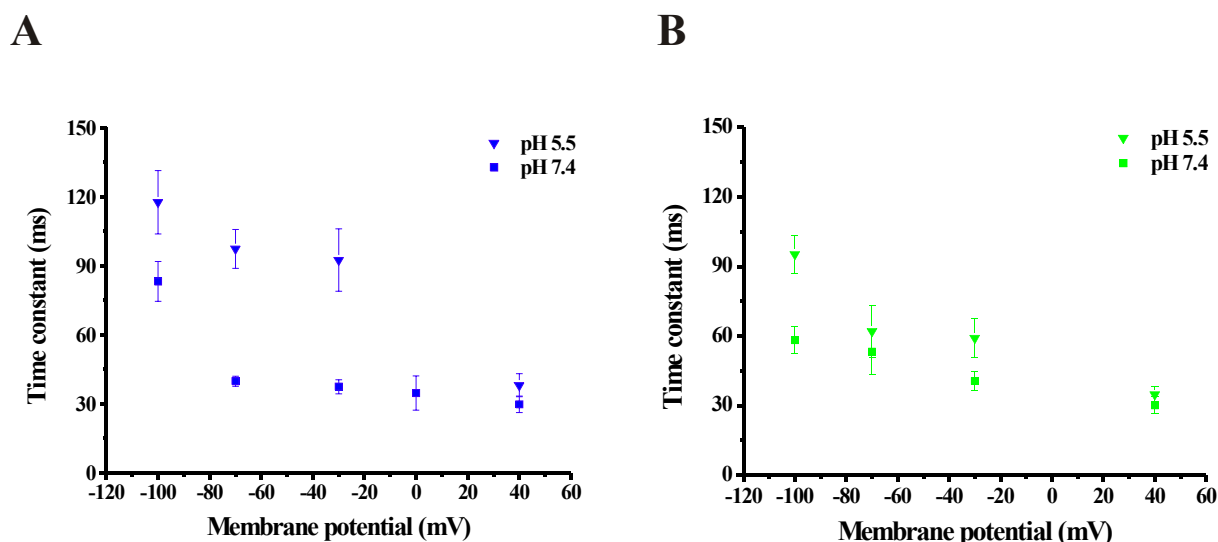


**Figure 2.12. BR wt: time course of the second half of the photocycle probed with blue = 398 nm (A) and green = 503 nm (B) laser flashes, at two extracellular pH values.** Blue flashes: 2-13 cells/data point; green flashes: 4-11 cells/ data point. Mean  $\pm$  SEM presented.

At both pH values, the M decay is slowed with more negative potentials; the gradient of 2 pH units across the cell membrane against the pumping direction causes further deceleration. The graphs in **fig 2.12** panels A and B suggests that the acidic pH has a stronger influence at more negative membrane potentials.

Information about the single turnover of the protein can be gained by applying laser flashes in the absence of stationary illumination. 10 ns long laser flashes of  $\sim 100$ -200  $\mu$ J yield a power of  $1\text{-}2 \times 10^4$  W over the area of the light guide of  $\sim 1$  mm<sup>2</sup>.

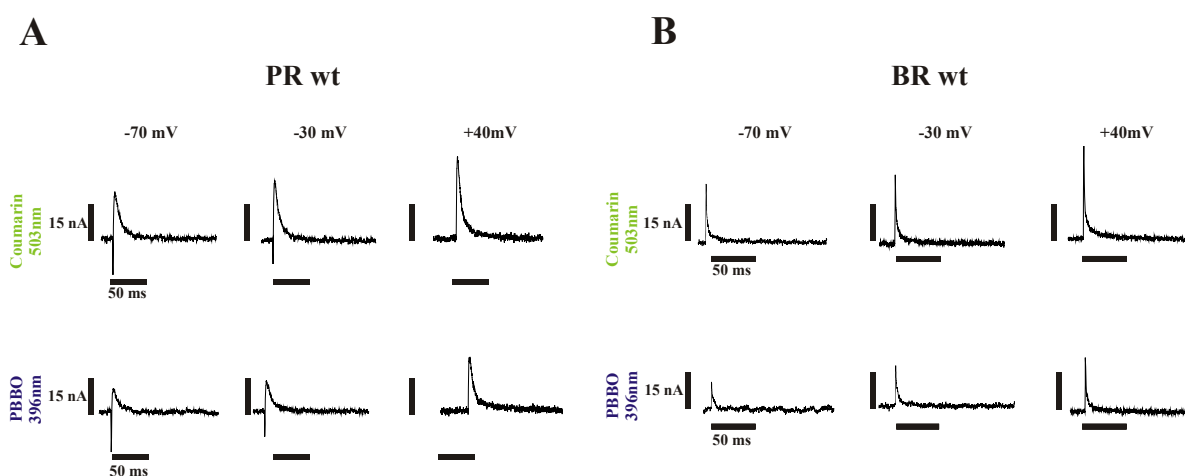


**Figure 2.13. Transients triggered by blue (396 nm) and green (503 nm) laser flashes without previous stationary illumination at three different potentials at pH 7.4. A. PR wt and B. BR wt.** The traces are averages of 3 flashes on the same cell.

At both wavelengths, PR transient currents (**fig 2.13 A**) are biphasic at -70 mV, the amplitude of the positive component increases with more depolarising potentials and the fast negative component decreases. At +40 mV only a positive component is detectable. 503 nm laser flashes trigger larger transient currents compared to those of 396 nm. The decay phase of the positive signal component can be approximated by a mono- or biexponential function and is characterised by one time constant at -70 and -30 mV of  $\tau \sim 8$  ms, at +40 mV is better approximated with two,  $\tau_1 \sim 5$  ms and  $\tau_2 \sim 40$  ms. The time constants measured are summarised in **Table 2.3**.

**Table 2.3** Time constants which characterise the decay phase of the laser triggered transients in **fig 2.2.13**.

| $V_{\text{membrane}}$ | PR               |                  |   | BR   |  |  |
|-----------------------|------------------|------------------|---|--|--|--|
|                       | -70 mV           | -30 mV           | +40 mV                                  | -70 mV                                       | -30 mV                                       | +40 mV                                       |
| <b>Coumarin</b>       | $\tau \sim 8$ ms | $\tau \sim 8$ ms | $\tau_1 \sim 5$ ms, $\tau_2 \sim 40$ ms | $\tau \sim 3$ ms                             | $\tau \sim 3$ ms                             | $\tau \sim 3$ ms                             |
| <b>PBBO</b>           | $\tau \sim 8$ ms | $\tau \sim 8$ ms | $\tau_1 \sim 5$ ms, $\tau_2 \sim 40$ ms | $\tau_1 \sim 1.5$ ms,<br>$\tau_2 \sim 13$ ms | $\tau_1 \sim 1.5$ ms,<br>$\tau_2 \sim 13$ ms | $\tau_1 \sim 1.5$ ms,<br>$\tau_2 \sim 13$ ms |

The signals generated by BR under similar conditions (**fig 2.13 B**) are decaying faster, characterised by one time constant when triggered by 396 nm of  $\sim 3$  ms, and two time constants when 503 nm is used,  $\tau_1 \sim 1.5$  ms and  $\tau_2 \sim 13$  ms at all three potential values.

The used mono- and biexponential functions have the following forms:

$$y = y_0 + A_1 \cdot \exp[-(x-x_0)/\tau_1] \quad \text{Equation (1)}$$

respectively

$$y = y_0 + A_1 \cdot \exp[-(x-x_0)/\tau_1] + A_2 \cdot \exp[-(x-x_0)/\tau_2] \quad \text{Equation (2)}$$

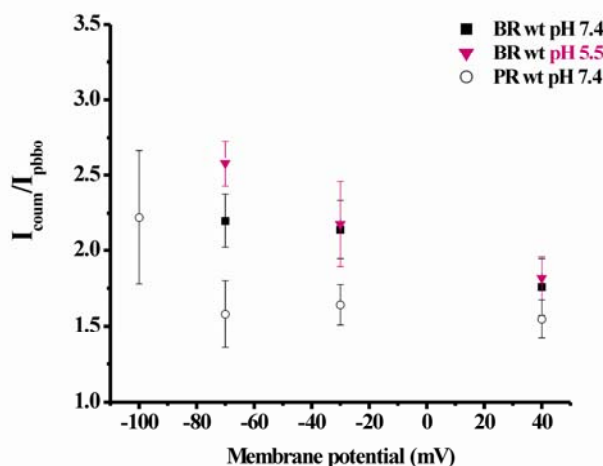


**Figure 2.14.** Ratio of the peak amplitudes of transients from **fig 2.2.12**.  $I_{\text{Coumarin}}/I_{\text{PBBO}}$  at the indicated pH values. For BR wt 3-4 cells/data point, for PR wt 2-9 cells/data point were evaluated, mean  $\pm$  SEM presented.

The ratio of the peak amplitudes ( $I_{\text{Coumarin}}/I_{\text{PBBO}}$ ) gives information about the efficiency of stimulation of the two wavelengths relative to each other. In case of BR, this ratio changes with the applied potential and also with the pH at  $-70$  mV, suggesting that at more depolarising potentials blue light can excite more protein molecules. The ratio of green- and blue light triggered transients is larger in case of BR compared to PR. In case of PR, this ratio does not seem to be affected by the applied potential over the measured range.

At pH 5.5, PR exhibits inward transients at  $-70$  mV with both green- and blue laser flashes, a small biphasic signal at  $-30$  mV with both green- and blue laser flashes and  $+40$  mV with blue flashes; green flashes trigger only a small positive current (not shown).

## 2.4 The effect of azide on photocurrents of PR wt

It is known from mutations of the proton donor group Asp96 in BR, which exhibit only very small stationary photocurrents, that azide is able to restore their pumping activity by accelerating the decay of the M intermediate (Tittor *et al.*, 1989). In order to investigate the effect of azide on the PR mutants, where either the  $\text{H}^+$  donor (E108) or the acceptor (D97) have been replaced, first the effect on the wild type was tested.

As can be seen in **figure 2.15**, both the peak and stationary current are increased by  $\sim 25\%$  upon addition of 50 mM azide. The IV curves in the presence of azide are parallel to those in its absence; the stationary current becomes slightly more voltage dependent in the presence of azide.

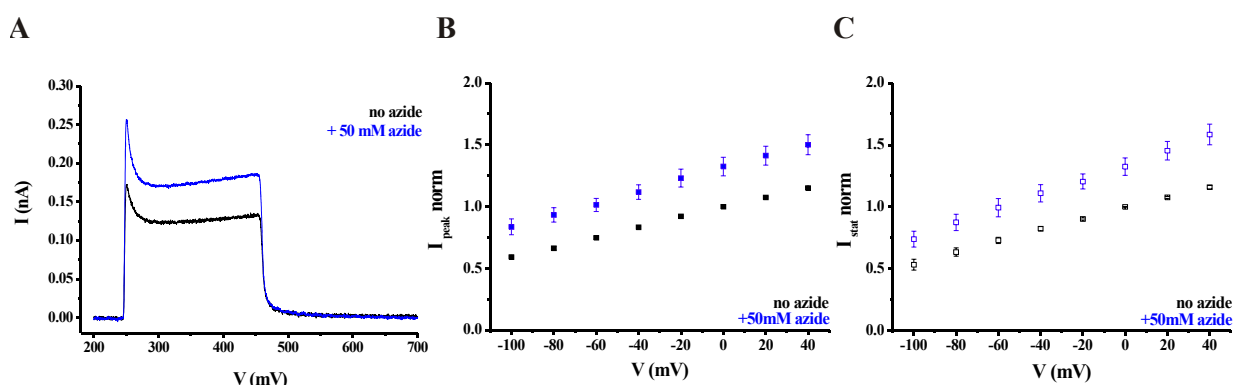


**Figure 2.15** The effect of 50 mM azide on photocurrents of PR wt at pH 7.4. **A.** Original current traces measured at 0 mV. The peak and stationary part of the photocurrent are evaluated separately, as depicted in panels **B** – respectively **C**. Current amplitudes are normalised to the value at 0 mV in the absence of azide. Mean $\pm$ SEM from 9 cells presented.

## 2.5 Light intensity dependence of PR wt

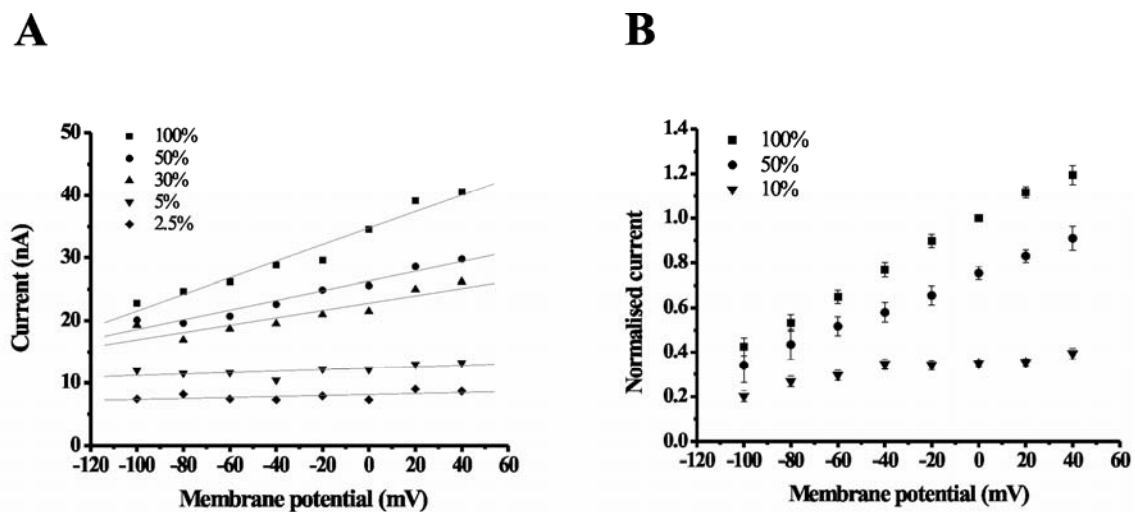


**Figure 2.16** Light intensity dependence of the stationary current of PR wt at pH 7.4 **A.** measured on one cell; **B.** summarised from 8 (100%), 4 (50%) and 5 (10%) cells, normalised to the current amplitude at 0 mV, 100% light intensity.

The effect of the intensity of applied light was investigated in the oocyte system, where in addition to the light conditions, the effect of transmembrane potentials can also be followed. The amplitude of the photocurrents increases gradually with the light intensity ( $\leq 8\text{W}/\text{cm}^2$  at 100%) – see **fig 2.16**. At low light intensities, the photocurrents lose voltage dependence. It is also visible that the amplitude of the stationary photocurrents is not proportional with the applied light: at 10% light intensity more than a tenth of the maximal amplitude is measured. The experiments, where laser flashes were applied additional to the continuous illumination, have shown that at 100% light intensity applied PR was not saturated. At pH 5.5 at low light intensities no inward current was recorded (not shown).

## 2.6 Mutants of proteorhodopsin

In order to investigate the role of residues homologous to BR's proton donor and acceptor groups, point mutants of residues E108 and D97 have been generated (**figure 2.17**).

Charge conserving mutants (E108D and D97E) exhibit similar pumping activity to the wild-type but with smaller stationary photocurrent amplitudes, especially in the case of D97E. E108G abolishes effective proton pumping but the residual stationary photocurrent is still positive, as in case of the wild-type.



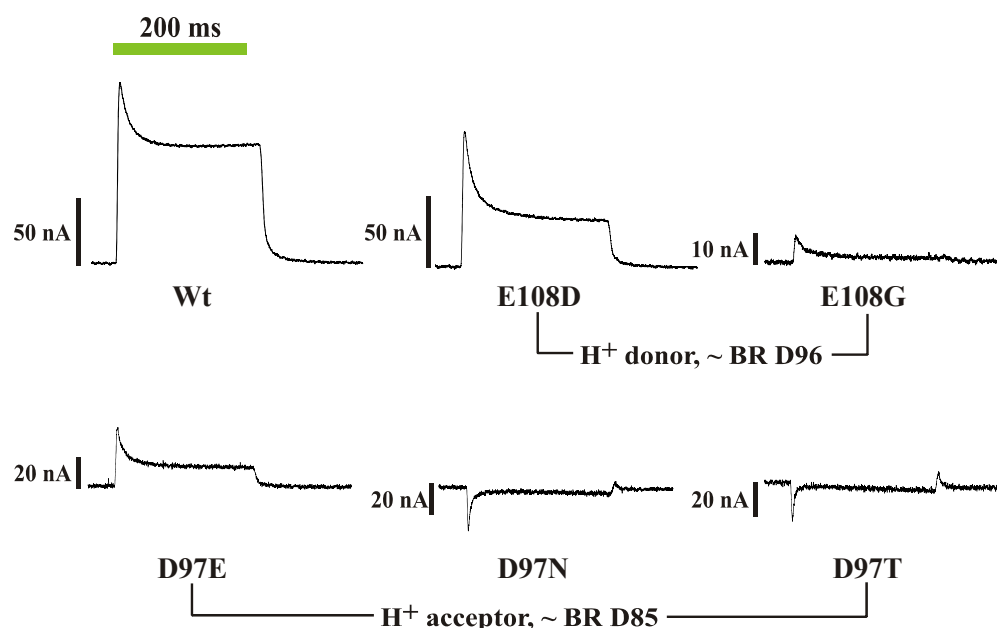


**Figure 2.17** Overview of the current signals generated by PR mutants at pH 7.4 and -30 mV by 200 ms continuous illumination with  $\lambda > 495$  nm. In the upper row mutants of the  $H^+$  donor group E108, on the lower row mutants of the  $H^+$  acceptor group D97 are shown. Please note the scale bars and the photocurrent of the wild-type for comparison.

Characteristic parameters of PR wt and the charge conserving mutants E108D and D97E are presented in **Table 2.4**. It is important to keep in mind that the ratio of peak and stationary components of the photocurrent shows voltage dependence in case of the mutants, as visible from **figures 2.4** and **2.19**. The off-response of the charge conserving mutants is quite similar to that of the wild-type at pH 7.4, -30 mV and may be fitted with a double exponential function. From the two time constants the slower is related to the rate-limiting step in the photocycle, shown in **Table 2.4** (the faster,  $\sim 3$  ms in all cases is not shown since it is at the limit of detection determined by the speed of the voltage clamp and the opening time of the shutter). Knowing the amplitude of the stationary current and the slow time constant of the switch-off signal, it is possible to set a lower limit of the expression level in one oocyte according to the formula in Table 2.4.

**Table 2.4: Characteristic parameters of PR wild type and the charge conserving mutants**

| Construct (nr. of cells)   | Wild type (18)           | E108D (18)             | D97E (6)               |
|--|--------------------------|------------------------|------------------------|
| $I_{\text{peak}}$ (nA) at -30 mV   | $136.05 \pm 15.1$        | $35.6 \pm 4.8$         | $29.25 \pm 16$         |
| $I_{\text{stat}}$ (nA) at -30 mV   | $92.4 \pm 10.7$          | $13.028 \pm 1.596$     | $25.74 \pm 5.25$       |
| $I_{\text{peak}} / I_{\text{stat}}$ at -30mV   | $1.5 \pm 0.03$           | $2.66 \pm 0.1$         | $2.48 \pm 0.26$        |
| Reversal potential (mV) of $I_{\text{peak}}$   | $\sim -195$              | $\sim -270$            | $\sim -210$            |
| Reversal potential (mV) of $I_{\text{stat}}$   | $\sim -210$              | $\sim -210$            | $\sim -165$            |
| $\tau_2$ (ms) at -30mV   | $\sim 17.5$              | $\sim 18.3$ (6)        | $\sim 24$              |
| Expression level (N)<br>[ $I_{\text{stat}}(\text{C s}^{-1}) \times \tau_2$ (s)]/ $1.602 \times 10^{-19}$ (C) | $\sim 10.12 \times 10^9$ | $\sim 1.5 \times 10^9$ | $\sim 1.5 \times 10^9$ |

Replacing the aspartate at position 97 with residues with non-charged polar side chains causes the appearance of a small asymmetric photocurrent directed oppositely to the wild-type signal (**fig. 2.17**).

The effect of 50 mM azide was tested on all mutations of the proton donor- (E108) and acceptor- (D97) groups. It is known that azide has a strong effect in restoring pumping activity on mutants of the proton donor in BR (Geibel, 2003; Tittor *et al.*, 1989), investigated also on mutants of the proton acceptor (Tittor *et al.*, 1994).

### 2.6.1 Mutations of the proton donor E108

#### E108D

Comparing the current signals at pH 7.4 and -30 mV (**fig 2.17**), it is visible that from the series of mutants studied E108D exhibits the smallest changes in the transport properties of PR. The stationary currents are clearly smaller than that of the wild-type, but the ability to pump protons is preserved, in the same direction as in case of PR wt.

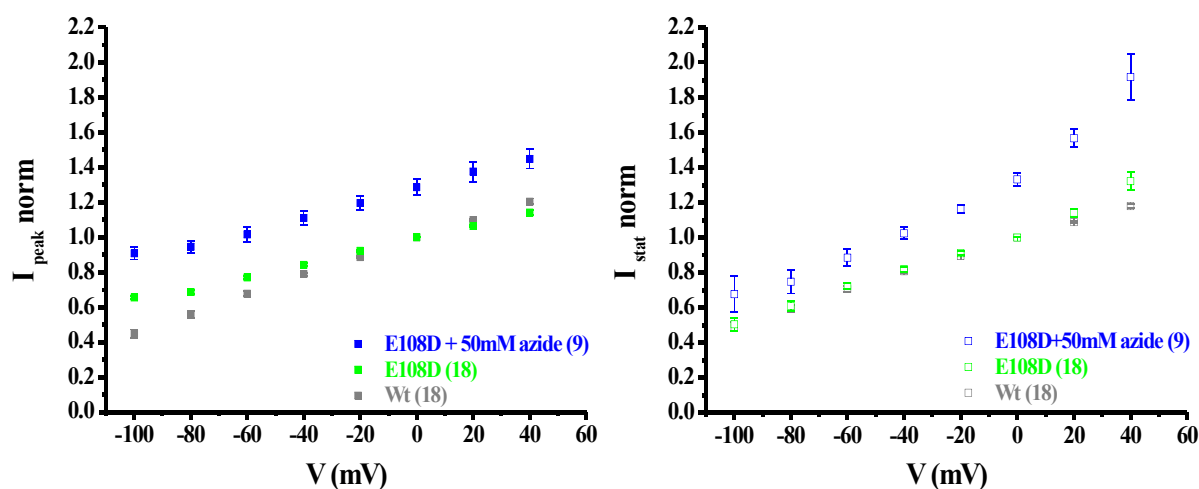


**Fig 2.18. Current-voltage relationship of PR E108D at pH 7.4, in the absence and presence of 50 mM azide** Current amplitudes normalised to the value at 0 mV in case of the mutant and wild-type protein in the absence of azide, in case of E108D+50 mM azide to the value of E108D at 0 mV in the absence of azide. The cells were illuminated with  $\lambda > 495$  nm. Mean $\pm$ SEM of a number of cells indicated in each graph is presented.

In **fig 2.18** the IV relationship of E108D is compared to that of the wild-type over the range of -100 to +40 mV, they appear to be similar, linear over the investigated potential range. The peak current is less voltage dependent at more negative potentials. If extrapolated, the reversal potential of the stationary current is  $\sim -210$  mV, similar to the wild-type. 50 mM azide increases the amplitudes of both the peak and stationary currents. The azide effect is of the

same magnitude (~20%) as for the wild type. The stationary currents gain both in amplitude and voltage dependence (fig. 2.18 right), suggesting that azide interferes more with the decay (i.e. reprotonation of the Schiff base) than with the formation of the M-like state. A similar increase in slope of the stationary current was also observed with PR wt (fig. 2.15).

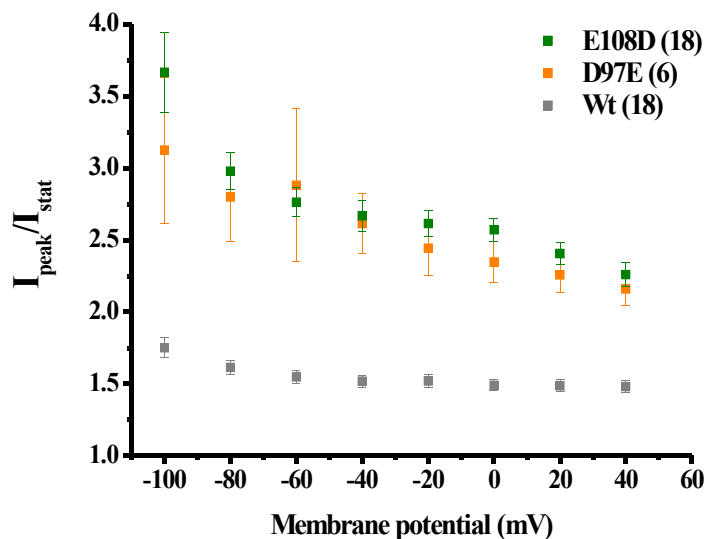


**Figure 2.19 Charge conserving mutations: the effect of the transmembrane voltage on the ratio of the peak and stationary currents compared to that of the wild-type.** Mean $\pm$ SEM of a number of cells indicated in the legend.

In figure 2.19 it is visible that although the peak and stationary part of the current signal of PR E108D changes with voltage similarly to the wild-type, their ratio shows a steeper voltage dependence, changes from 3.6 at -100 mV to 2.2 at +40 mV.

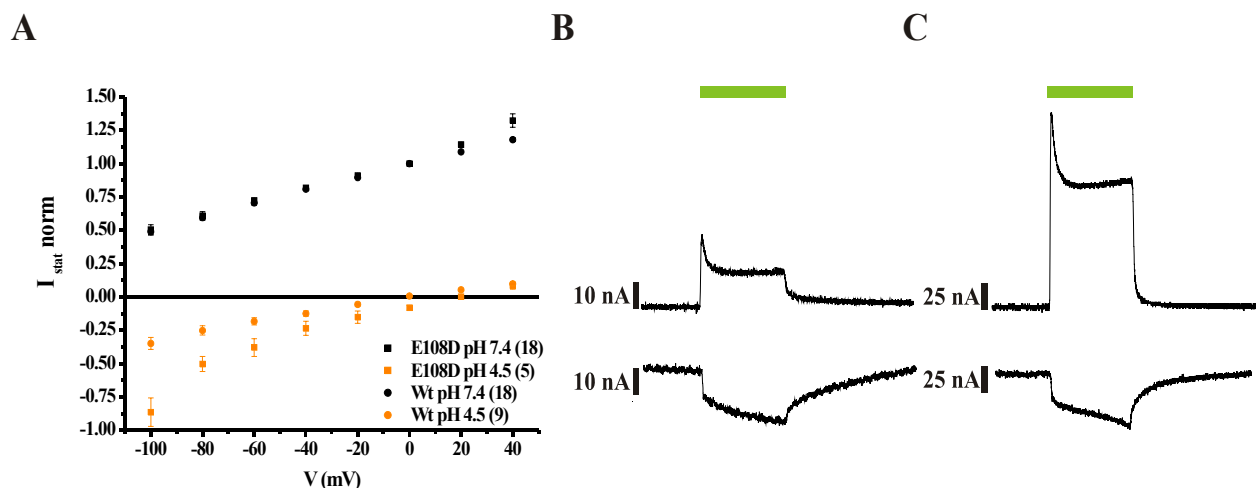


**Figure 2.20 Inward  $H^+$  translocation of E108D mutant under acidic conditions shown in comparison with the wild-type protein.** A. IV relationships of the wild-type protein and E108D under neutral and acidic extracellular pH. Current amplitudes are normalised to the value measured at 0 mV, pH 7.4 for each construct and mean $\pm$ SEM presented using a number of cells indicated in the legend. Current traces of B. E108D at pH 7.4, 0 mV (top) and pH 4.5, -100 mV (below) and C. PR wt at pH 7.4, 0 mV (top) and pH 4.5, -100 mV (below), triggered by 200 ms continuous illumination of  $\lambda \geq 495$  nm (green bars), measured on the same cell in both constructs.

Under acidic conditions (pH 4.5) only inward charge translocation by E108D can be observed, with an I-V curve significantly steeper to that of the wild-type (**fig. 2.20 A**). This behaviour is exemplified also with the current traces shown in **fig. 2.20 B** and **C**, which show that although at pH 7.4 stationary currents are much larger in case of the wild-type (upper traces), under acidic conditions the currents generated by the two constructs have similar amplitudes (lower traces).

## E108G

Replacement of the voluminous, negatively charged glutamate by glycine abolishes almost completely the stationary proton transport by PR (**fig. 2.21 A**). This effect is similar to that observed in BR mutant D96G.

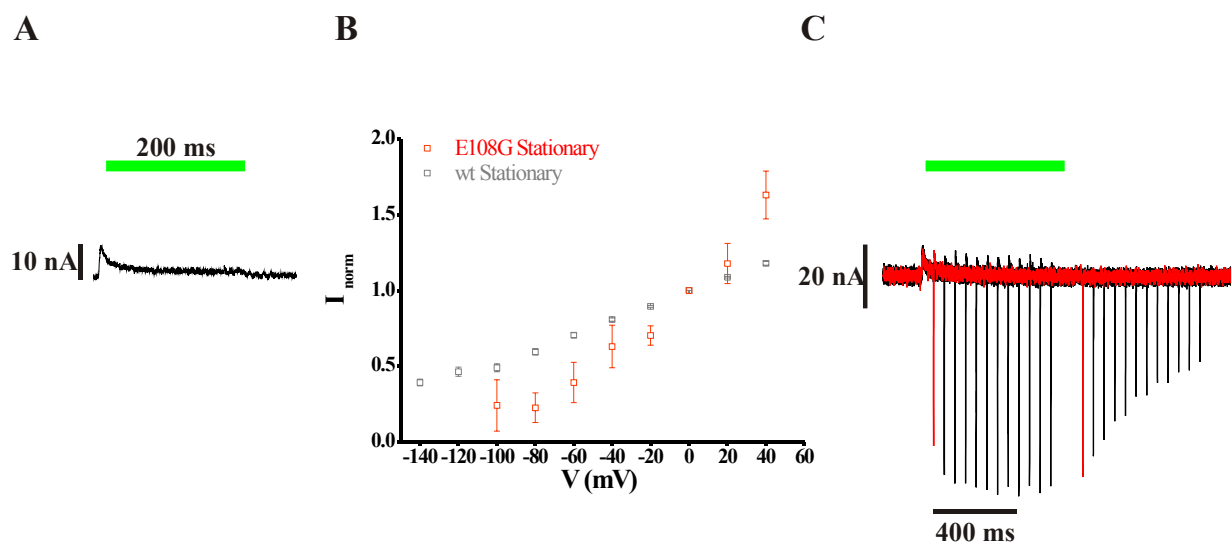


**Figure 2.21 H<sup>+</sup> transport by PR E108G.** (A) current signal at -30 mV, pH 7.4, upon 200 ms illumination with  $\lambda > 495\text{nm}$ ; (B) I-V relationship compared to the wild-type, mean $\pm$ SEM of 7 (E108G) and 18 (wild-type) cells presented; (C) the effect of 396 nm blue laser flashes applied during and after continuous illumination at pH 7.4.

The photocurrents start with a positive peak immediately after switching on the stationary illumination, but then decay to a very small stationary level. The stationary current of E108G shows a steeper voltage dependence compared to the wild-type (**fig 2.21 B**), as observed with BR D96G.

Experiments using 396 nm laser flashes aimed at detection of formation and decay of an M-like species similar to those described in case of PR wt, were done with the E108G mutant, using the same illumination protocol (**fig. 2.5**).

During continuous illumination the blue laser flashes trigger large negative transient currents, quite different from the case of the wild-type protein: compare **figure 2.21 C** with **fig 2.7** top left, and similar to those seen in BR D96G (Geibel, 2003).

The transient currents during stationary illumination increase in amplitude as the time between switching on the illumination and fall of the laser flash increases, and reach a constant level in  $\sim 325$  ms.

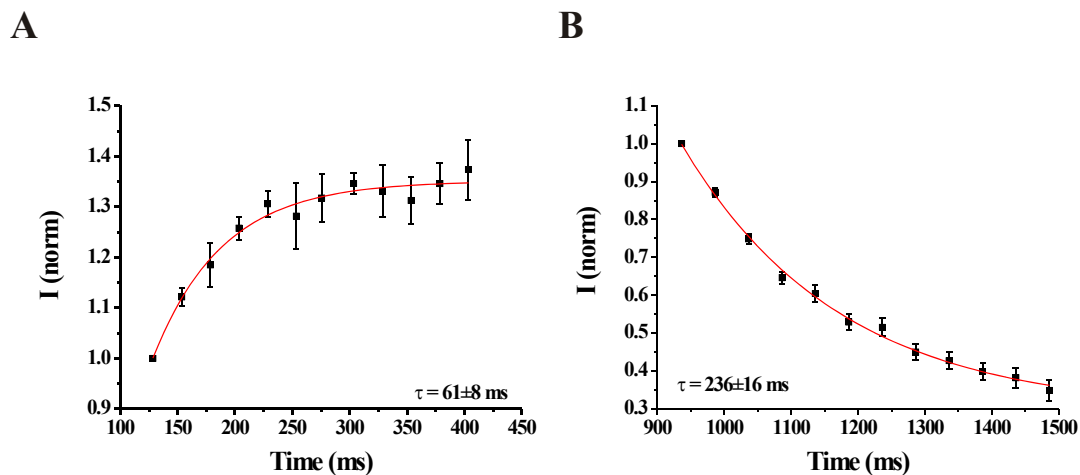


**Figure 2.22 PR E108G: accumulation (A) and decay (B) of the M-like state at pH 7.4, -30 mV.** Transient amplitudes normalised to that of the first one  $\sim 30$  ms after switch-on (A) or  $\sim 15$  ms after switch-off (B) of the stationary illumination. Data from 4 (in A), respectively 8 (in B) cells used for analysis, presented as mean  $\pm$  SEM.

The processes of formation and decay of the M-like state during, or after continuous illumination can be described with a monoexponential equation, with  $\tau \sim 61$  ms (**fig. 2.22A**), and  $\tau \sim 236$  ms (**fig 2.22 B**), respectively.

Azide has a similar effect on photocurrents of PR E108G as on those of BR mutants D96N (Tittor *et al.*, 1989) or D96G (Geibel, 2003). Addition of 50mM azide to the buffer re-establishes the proton transport in the mutated protein: compare figures **2.2A** and **2.23A**, where the measurements were performed on the same cell.

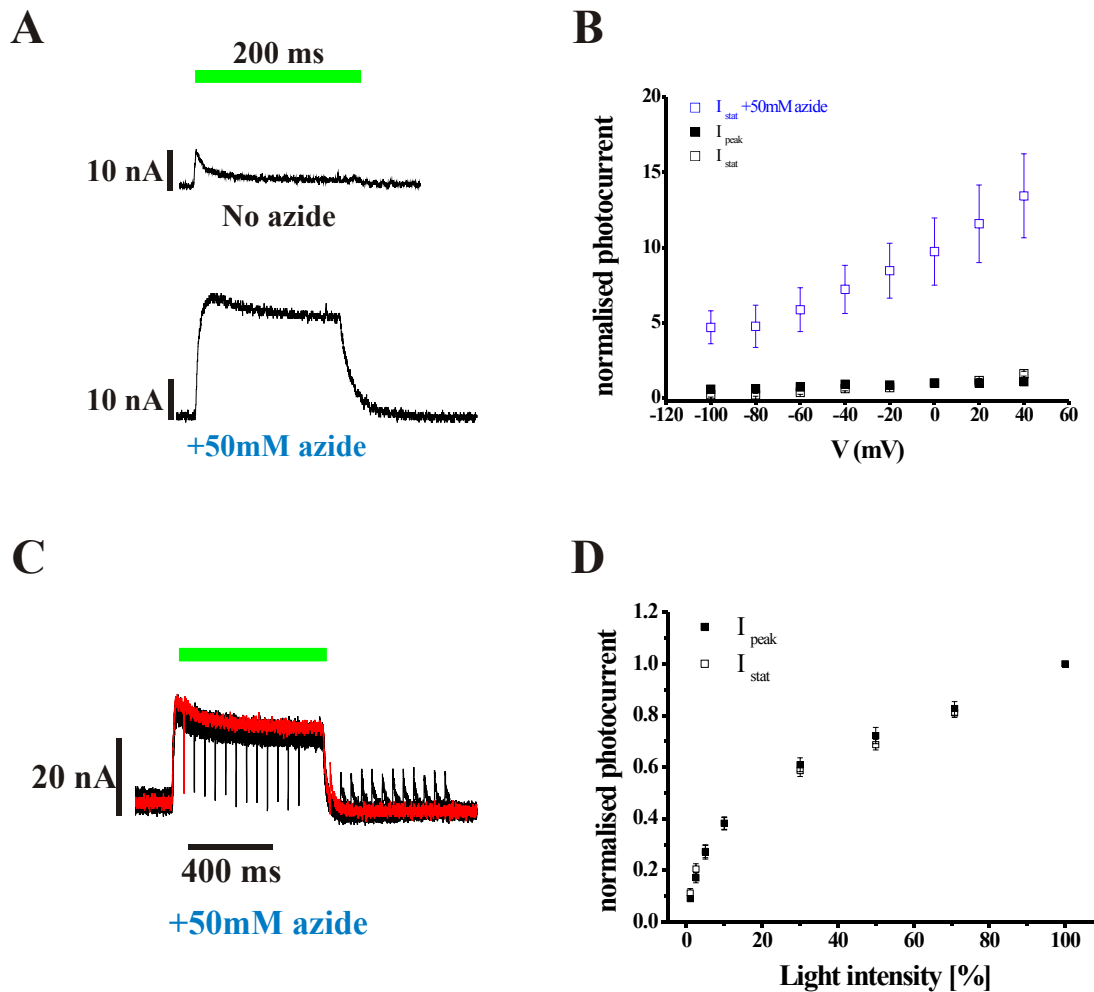


**Figure 2.23 PR E108G: the effect of 50mM azide at pH 7.4.** (A)  $H^+$  pumping by E108G is restored upon addition of azide. The current trace in the absence of azide is the same as shown in fig. 2.16. (B) IV relationship in the presence and absence of azide; data from 6, respectively 7 cells used for analysis, presented as mean $\pm$ SEM. (C) Blue laser flashes applied on the mutant E108G during and after stationary illumination in the presence of azide. (D) Light intensity dependence of the recovered photocurrent at -30 mV, 5-7 cells/data point  $\pm$  SEM.

The off-signal of the recovered proton transport can be fitted with a double exponential function, associated with  $\tau_1 = 9.33 \pm 3.55$  and  $\tau_2 = 34.57 \pm 14.8$  (over a time window of 250 ms), which indicate a slower photocycle as that of the wild type (Table 1). In the absence of azide the photocurrent decays to a very small stationary level already during illumination at the reference potential of -30 mV, consequently it is not possible to compare the photocycle of E108G in the absence and presence of 50 mM azide.

The photocurrent of E108G shows stronger voltage dependence in the presence of azide (**fig. 2.23 B**). Blue laser flashes applied in the presence of azide during stationary illumination trigger negative transient currents, similar to those in BR wild-type (**fig 2.6** bottom left). After the stationary illumination the first transient current is biphasic, similar to BR wt. Transient

currents triggered 80 ms after switching of the continuous illumination point into the same direction as the stationary current, as in case of PR wild-type (**fig. 2.6** top left).

The amplitude of the photocurrent recovered by the 50 mM azide depends on the applied light intensity (**fig. 2.23 D**).

Blue laser flashes at pH 5.5 trigger only inwardly directed transient currents, both during and after stationary illumination. At this pH, no stationary photocurrent is detectable (**fig 2.24 A**). When azide is added, a stationary photocurrent becomes visible during continuous illumination (**fig 2.24 B**) and blue laser flashes trigger biphasic signals, as indicated in the inset. After switching off the continuous illumination, the blue laser flashes trigger positive transients similar to those at pH 7.4 (**fig 2.23 C**).

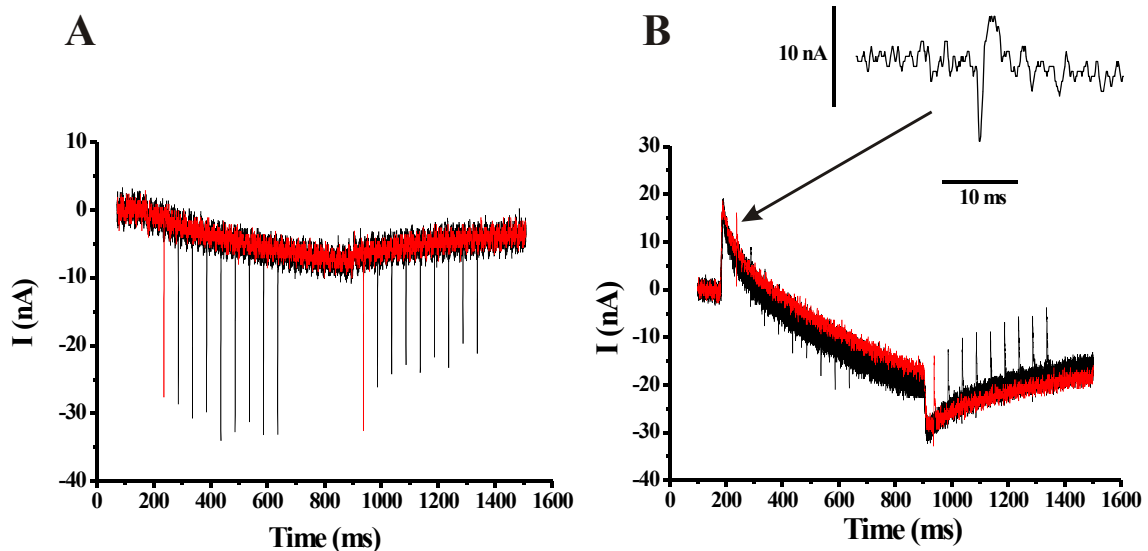


**Figure 2.24 PR E108G: blue laser flashes at pH 5.5, -30 mV membrane potential in the absence (A) and presence (B) of 50mM azide, recorded on the same cell. Illumination protocol as shown in fig. 2.5.**

## 2.6.2 Mutations of the proton acceptor D97

### D97E

Although in this mutant the charge is preserved at position 97, the replacement of the aspartate residue with a glutamate has strong effects on the pumping abilities of PR (**fig 2.17**).

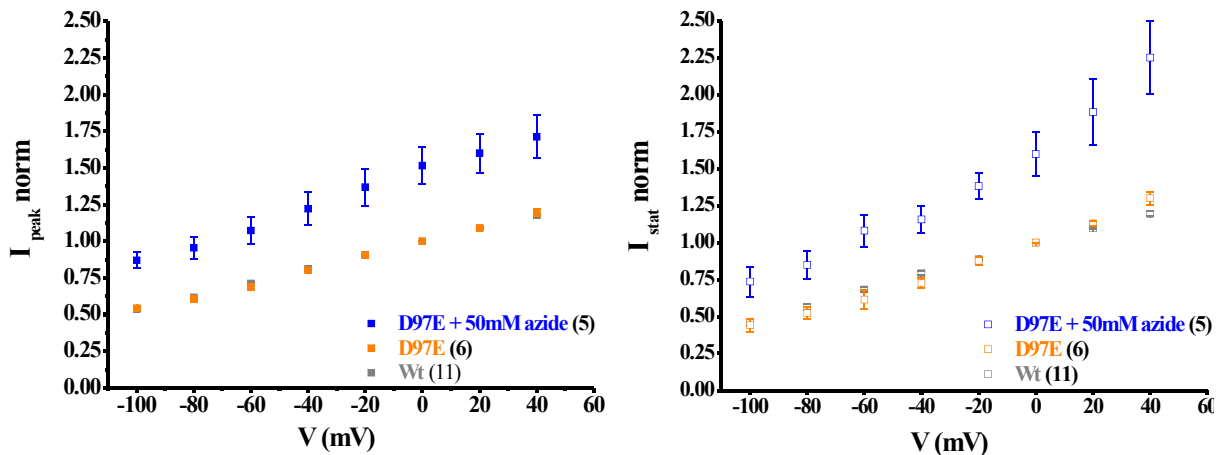


**Figure 2.25** PR D97E I-V relationship of the peak and stationary current at pH 7.4 shown in comparison with the wild-type. The effect of azide on these two components of the current signal. Current amplitudes normalised to the value at 0 mV in case of D97E and the wild-type, in case of D97E + 50 mM azide the same value used as in the absence of azide. Mean $\pm$ SEM presented using a number of cells indicated in each graph.

The I-V relationship in **fig 2.25** shows that the voltage dependences of both peak – and stationary parts of the signal are very similar to that of the wild-type. On the other hand, their ratio, as in case of the mutant E108D, is different (**fig. 2.19**). **50 mM azide** increases both the peak and stationary components of the electric signal, with  $\sim 25\%$  at more negative transmembrane potentials and  $\sim 50\%$  at  $V_m > 0$  mV. This results in a steeper the I-V curve in the presence of azide, similarly to the mutant E108D.

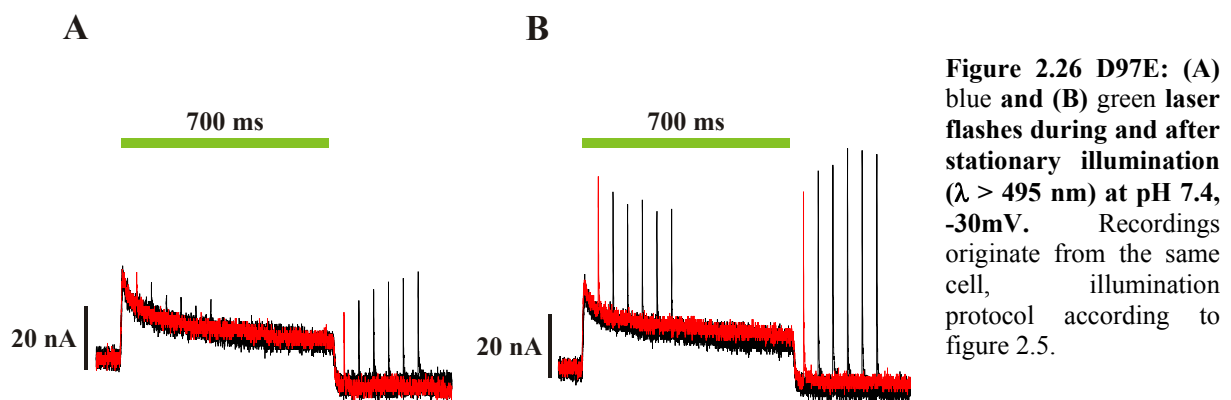


**Figure 2.26** D97E: (A) blue and (B) green laser flashes during and after stationary illumination ( $\lambda > 495$  nm) at pH 7.4,  $-30$  mV. Recordings originate from the same cell, illumination protocol according to figure 2.5.



Preliminary experiments with laser flashes during and after continuous illumination show that this mutant behaves similarly to the wild type PR, which is not saturated under the same light conditions as BR. Both wavelengths trigger positive transients during and after continuous illumination at -30 mV, pH 7.4 (**fig. 2.26**). Blue laser flashes trigger transients with smaller amplitudes as green laser flashes, in agreement with the absorption maximum of the protein.

### D97N

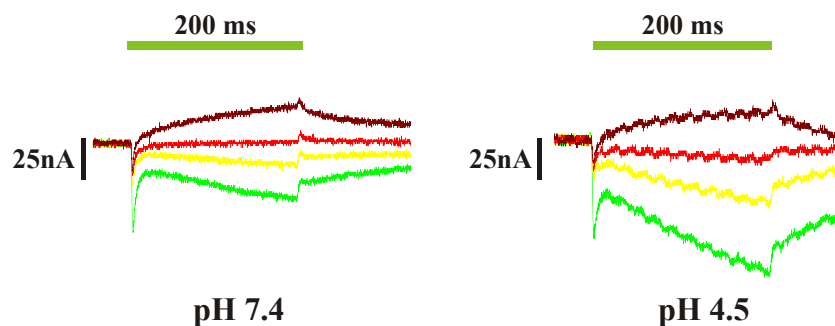


**Figure 2.27 Photocurrent signals of PR mutant D97N in the absence or presence of a pH gradient at four membrane potentials.** Illumination and voltage clamp protocol as presented in **fig. 2.2**. -100 mV (—), -60 mV (—), +20 mV (—), +40 mV (—). Both recordings originate from the same cell.

Removal of the negative charge at position 97 dramatically alters proton pumping. For this mutant only transient and stationary inward currents are observed (**fig. 2.17**). The recorded signal starts with a negative peak and decays to a negative stationary level. The amplitude of the transient and stationary current signals depends on the membrane potential and pH (**figures 2.2.26 and 2.2.27**).

Decreasing the pH on the extracellular side of the cell means increasing the proton gradient against the normal pumping direction of PR. In case of D97N reducing the extracellular pH causes a slight increase of the inwardly directed peak current and has a stronger effect on the stationary component. The voltage dependence of the effect of pH on the activity of D97N is summarised in **fig. 2.28**.

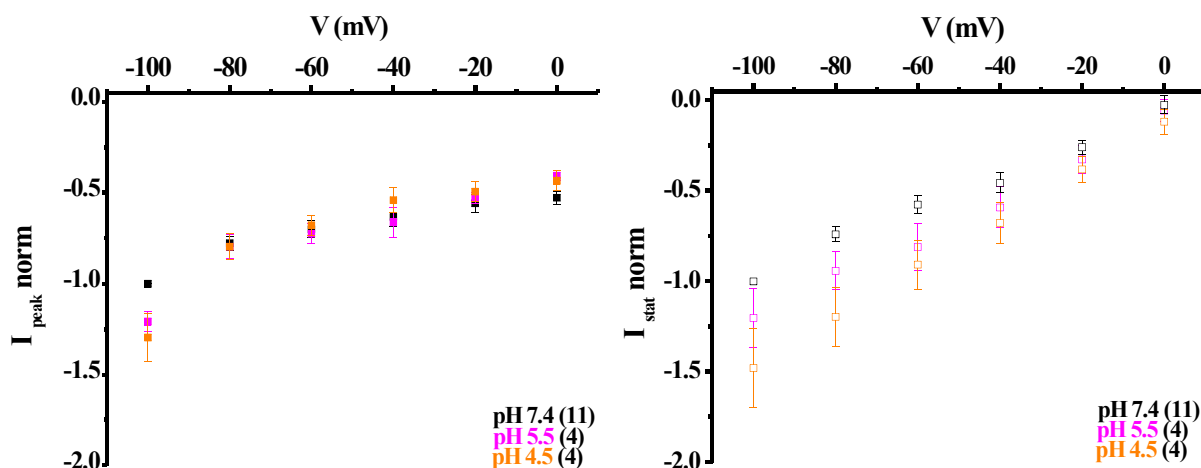


**Figure 2.28** The effect of extracellular pH on the current signal of D97N. Current amplitudes normalised to the value at -100 mV, pH 7.4. Mean $\pm$ SEM from a number of cells indicated on each graph presented.

**Figure 2.29** summarises the effect of 50 mM azide on the current signal generated by D97N. On the left panel is visible that the amplitude of the peak current is decreased, while that of the stationary component is not significantly changed in the presence of azide.

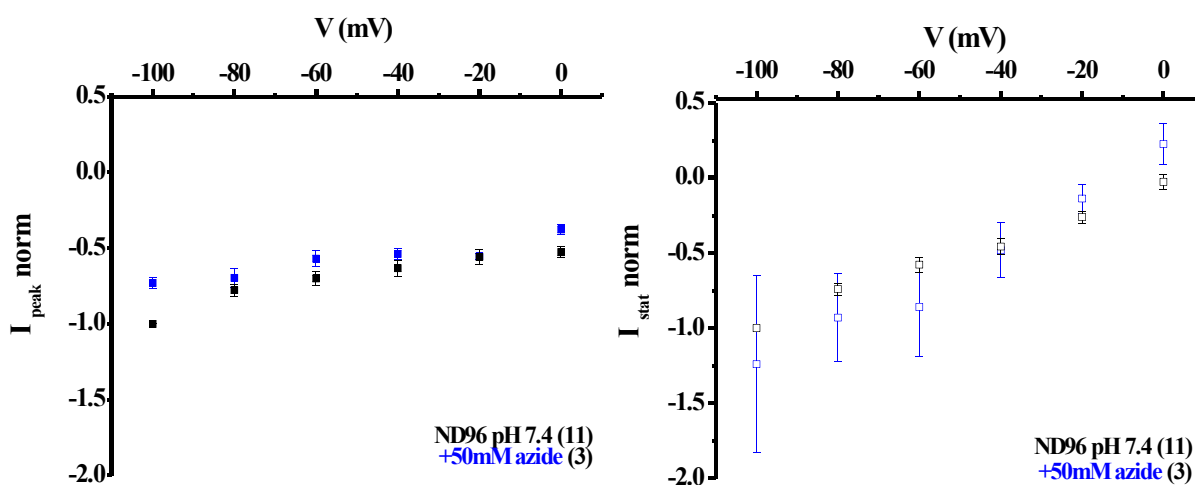


**Figure 2.29** PR D97N: the effect of azide on the peak- and stationary part of the current signal. Current amplitudes normalised to the value at -100 mV, pH 7.4. Mean $\pm$ SEM from a number of cells indicated on each graph presented.

## D97T

The electric signals generated by the D97T mutant upon illumination with  $\lambda \geq 495$  nm are very similar to those of D97N, with only negative peak and stationary components.

Similarly to D97N, in the presence of azide the amplitude of the peak currents decrease and stationary photocurrents virtually remain the same over the measured range.

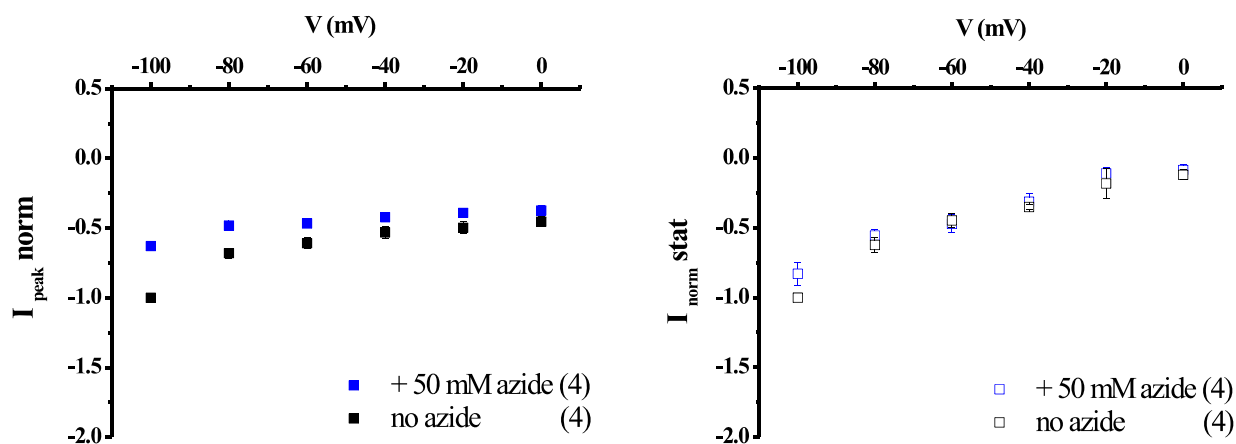


**Figure 2.30 PR D97T: the effect of azide on the peak- and stationary part of the current signal.** Current amplitudes normalised to the value at -100 mV, pH 7.4. Mean $\pm$ SEM from a number of cells indicated on each graph presented.

In the case of BR a complex behaviour has been observed for the D85T mutant (Tittor *et al.*, 1997): the mutated protein displays four different transport modes at pH  $\sim$  6.8, dependent on the light conditions. Blue light drives  $H^+$  extrusion; white light determines inward  $H^+$  transport in a 2-photon process (shown also previously in (Tittor *et al.*, 1994)) and in green light  $Cl^-$  is transported inwardly,  $H^+$  outwardly. The transport modes can occur simultaneously but not within a single catalytic cycle of one molecule (Tittor *et al.*, 1997).

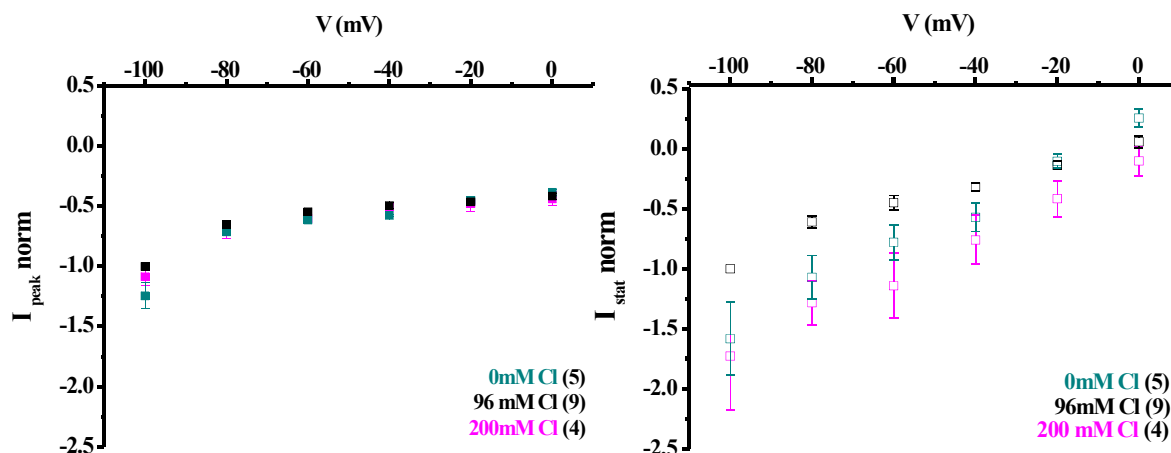


**Figure 2.31 PR D97T: the effect of chloride on the peak- and stationary part of the current signal triggered by continuous green light  $\lambda > 495\text{nm}$ .** Current amplitudes normalised to the value at -100 mV, pH 7.4. Mean $\pm$ SEM from a number of cells indicated on each graph presented.

To investigate the effect of chloride on transport properties of PR, chloride was replaced with aspartic acid (“0 mM  $Cl^-$ ”) or the concentration of NaCl of the usual measuring buffer was doubled (“200 mM  $Cl^-$ ”). The results in **figure 2.30** do not support the possibility that PR

transports chloride: although the amplitudes of the current in the absence of  $\text{Cl}^-$  are larger than with 96 mM  $\text{Cl}^-$ , 200 mM  $\text{Cl}^-$  does not further decrease the signal amplitudes.

Similar experiments were performed in blue [ $375 \text{ nm} < \lambda < 425 \text{ nm}$ ] and white light ( $\lambda > 360 \text{ nm}$ ), but no effect upon changes in chloride concentrations were observed (not shown), suggesting that over the measured concentration range from 0-200 mM, no substantial  $\text{Cl}^-$  transport takes place in blue, green or white light.

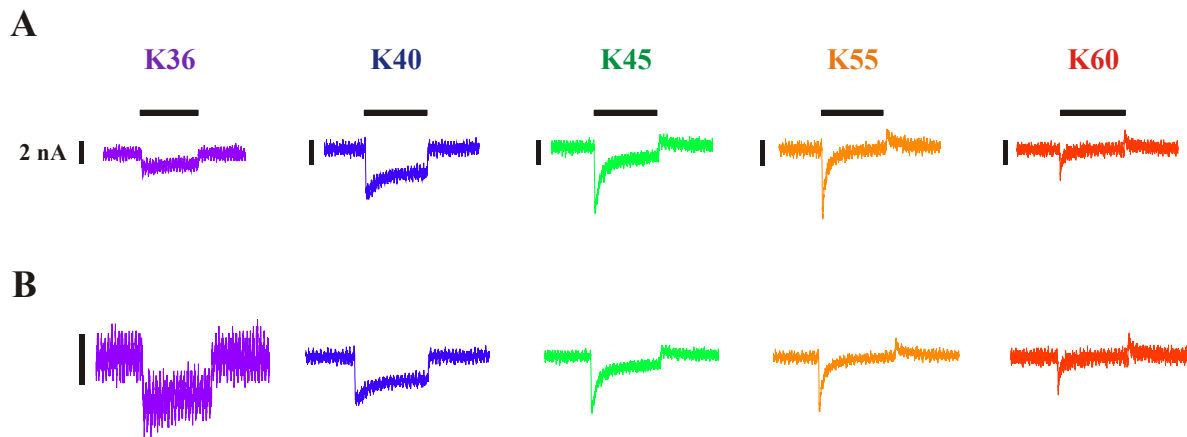


**Figure 2.32 PR D97T: the effect of the wavelength of light on the photocurrents at -30 mV and pH 7.4.** Measurements recorded on the same cell, by illumination for 200 ms using an HBO lamp and broad band interference filters ( $\lambda \pm 25 \text{ nm}$ ): K36 – 360 nm, K40 – 400 nm, K45 – 450 nm, K55 – 550 nm, K60 – 600 nm with transmission values of (in  $\text{mW}/\text{mm}^2$ ) 3.95; 13.55; 14.68; 16.38; 10.17, measured at the end of a optical fibre with 1.5 mm diameter. **A.** direct current recordings; **B.** current amplitudes scaled to the transmission values of the interference filters shown in A with arbitrary scaling.

The inward current generated by D97T has different shape depending on the wavelength of illumination, as shown in **figure 2.32**. It also has to be considered that the broad band interference filters have different transmission values. In the presence of  $335 \text{ nm} < \lambda < 385 \text{ nm}$  the signal looks like a very small stationary inward current. When  $375 \text{ nm} < \lambda < 425 \text{ nm}$  the inward current increases, with a clear stationary component; with  $425 \text{ nm} < \lambda < 475 \text{ nm}$  the peak component is more prominent and the stationary one decreases. At  $525 \text{ nm} < \lambda < 575 \text{ nm}$  the signal consists of a rapidly decreasing negative spike and at  $575 \text{ nm} < \lambda < 625 \text{ nm}$  almost no current signal is visible. Scaling of the current signal to the transmission values of the interference filters, the differences in the amplitudes of the peak component disappear and the changes in the shape of the photocurrent can be followed more directly (**fig. 2.32. B**).

The intensity of light on the transport properties of D97T was another parameter investigated. In **figure 2.33A** current traces at three wavelength of interest are presented. **Figure 2.33 B**

shows that independent of the light conditions, both peak- and stationary currents change in a similar manner with the light intensity applied.

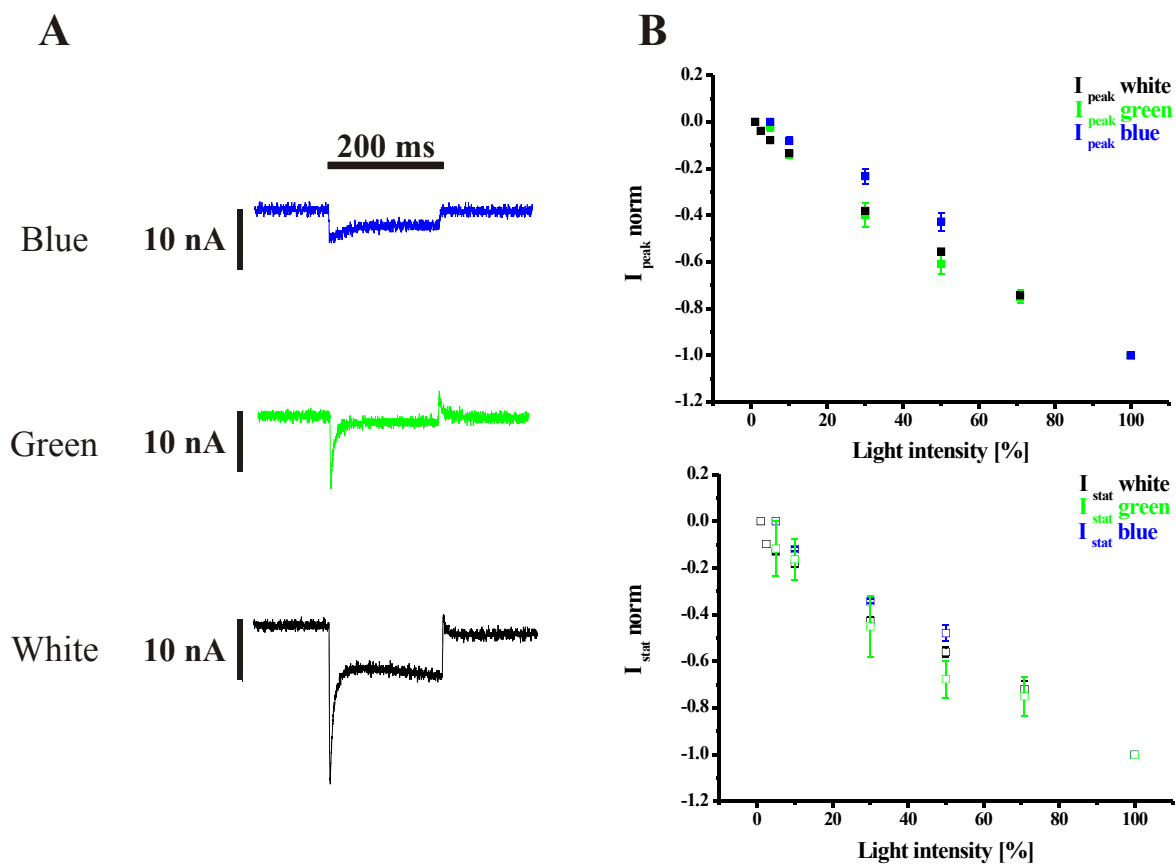


**Figure 2.33 PR D97T: light intensity dependence of the peak- and stationary currents at three different wavelengths, pH 7.4, -30 mV.** (A) Current signals recorded on the same cell in blue light using the K40 interference filter, green light  $\lambda > 495$  nm and white light  $\lambda > 360$  nm. The intensity at 100% of each  $\lambda$  in  $\text{mW}/\text{mm}^2$ :  $\sim 88$  (white),  $\sim 34$  ( $> 495$  nm),  $\sim 14$  (K40). (B) Current signals normalised to the value at 100%. Mean  $\pm$  SEM of 7 (white light), 3 ( $> 495$  nm) and 2 (K40) cells are presented.

The effect of laser flashes in addition to the continuous illumination is illustrated by the preliminary recordings in **figure 2.34**. The laser triggered transients at -30 mV point into the same direction as the small inward current in case of both wavelengths used, blue (396 nm) and green (503 nm).

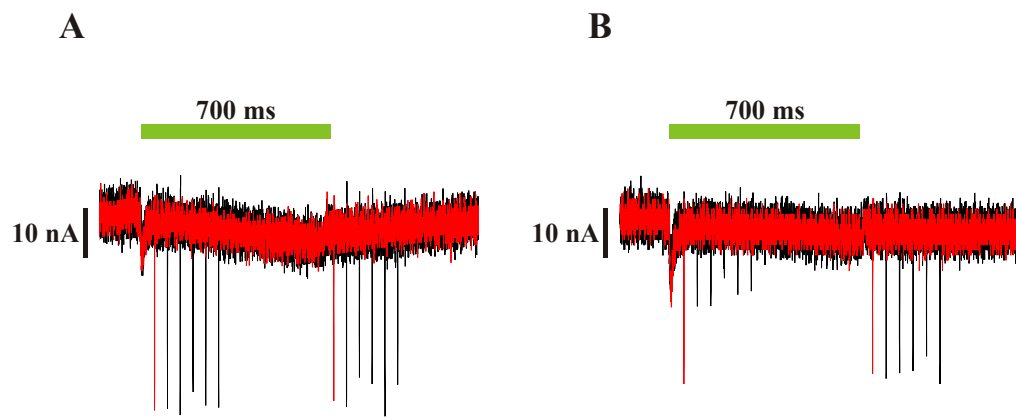


Figure 2.34 D97T: (A) blue and (B) green laser flashes during and after stationary illumination ( $\lambda > 495$  nm) at pH 7.4, -30 mV. Recordings on the same cell, illumination protocol according to figure 2.5.

## 2.6.3 L105Q, the spectral tuning switch

### 2.6.3.1 Action spectra of the wild type ('green') and L105Q ('blue') proteorhodopsin

The sequence of the protein termed 'wild type' in this work is identical to that first bacterial clone identified, EBAC31A08. Since then, many naturally occurring variants have been identified, and soon the idea that the residue at position 105 plays the role of a 'spectral tuning switch' emerged (Man *et al.*, 2003). In 'green PR' this position is occupied by a Leu residue, in 'blue PR' - with a 30 nm blue-shifted absorption maximum - by a Glu.

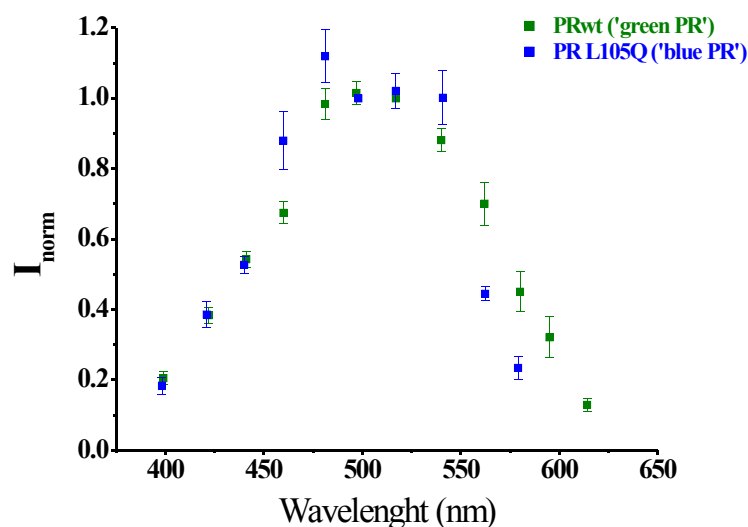


Figure 2.35. Action spectra of PR wt and PR L105Q. Mean $\pm$ SEM of 4 (PR wt) and 5 (PR L105Q) oocytes presented. The recorded stationary current amplitudes were normalised to the quantum flux at  $\lambda=517$  nm.

To see whether we could shift the maximal activity of PR to shorter wavelengths, we introduced the L105Q mutation into the sequence of 'green PR'. The effect of this point

mutation is shown in **fig 2.2.35** and **2.2.36**. The action spectrum shows a blue shift, but less than 30 nm.

The response of PR wt and PR L105Q to 200 ms illumination shows that the mutant protein is a less efficient proton pump (**fig 2.36 A**). The off-response of the photocurrent of L105Q is characterised by time constants similar to that of the wild type (data not shown).

The IV relationship of the two constructs shows that the stationary current (i.e. the decay of the M-like state, where most of the charge translocation takes place) is most affected by the L>Q replacement by increasing its voltage dependence, the peak component is similar to that of the wild type (**Fig 2.36 B**).

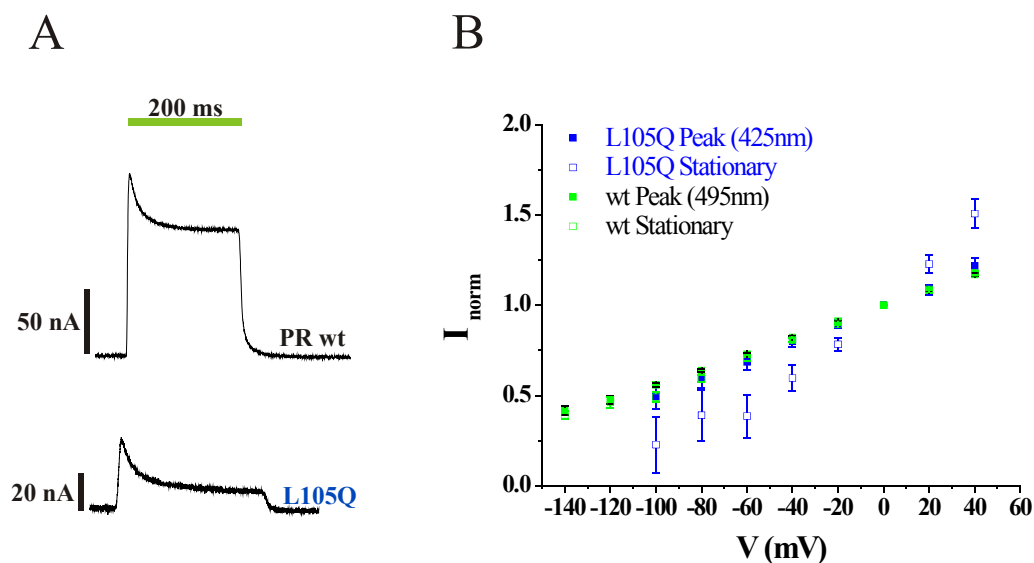


**Figure 2.36. Photocurrent and IV relationship of PR L105Q compared to PR wt** (A) PR wt-expressing oocytes were illuminated with  $\lambda > 495$  nm, for PR L105Q  $\lambda > 425$  nm was used. (B) Current amplitudes normalised to that recorded at 0 mV. Mean $\pm$ SEM of 4 (L105Q) and 18 (wt) cells are presented.

## 2.7 Localisation of bacteriorhodopsin (BR) and proteorhodopsin (PR) at the surface of the oocyte membrane, investigated by chemiluminescence

Previous studies have shown already that bacteriorhodopsin is functionally expressed in the plasma membrane of *Xenopus* oocytes (Geibel, 2003; Geibel *et al.*, 2001; Nagel *et al.*, 1998; Nagel *et al.*, 1995). HA-tagged BR served as comparison for the plasma membrane expression of Wilson Disease Protein (W NDP) and PR. The HA-tag was fused to the N-terminus of both retinal proteins, which is on the extracellular side of the membrane (termed BR-NT-HA and PR-NT-HA). Expressed in oocytes, the presence or absence of the HA tag at the cell surface was evaluated using the same luminescence detection assay as for the surface expression of W NDP and its mutants.

As already shown in Part I, **fig. 2.3 A**, WNDP-HA56 and BR-NT-HA are present to similar extent in the plasma membrane of oocytes. In the case of PR-NT-HA similar results have been obtained where all oocytes were incubated for 4 days after cRNA injection (**fig. 2.37**, below).

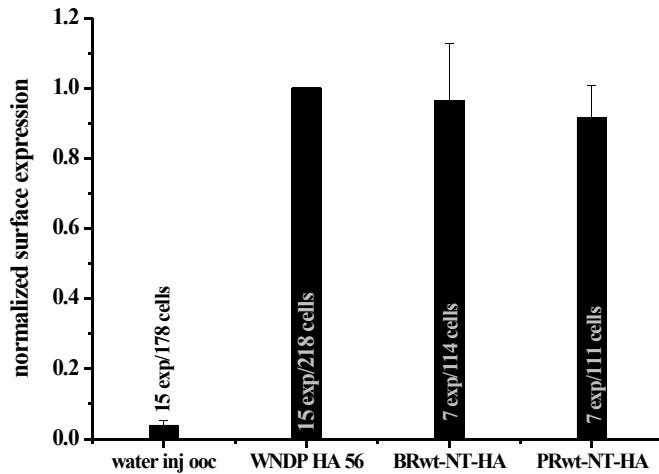


**Figure 2.37 Surface detection of HA-tagged BRwt and PRwt, compared to WNDP HA56** Four days after cRNA injection the expression level of the three proteins were similar. Water-injected oocytes from the same batch served as controls.

However, the plasma membrane targeting of WNDP seems to be more effective, since in Western blots the same amount of total membrane preparation yields a much stronger signal in the case of BR (**fig. 2.3 B**, Part I).

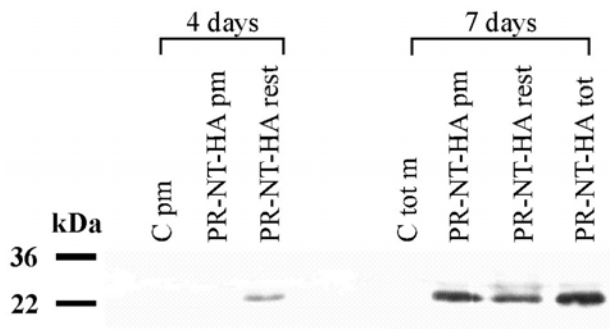


**Figure 2.38 Western blot analysis of PR-NT-HA** Membrane preparation, where the plasma membrane was separated from the rest, was loaded on 10% SDS-acrylamide gel 2 oocytes/lane. Water-injected oocytes from the same batch served as a control. Detection was carried out using rat monoclonal antibody 3F10 against the HA epitope. On the left: molecular weight standard. C=control, **pm**=plasma membrane, **rest**=all membranes with the plasma membrane depleted; **tot**=crude membrane preparation.

**Figure 2.38** shows a comparison between the expression of PR-NT-HA at 4 and at 7 days after cRNA injection, where the plasma membrane was separated from the rest of the oocyte membranes. Four days after cRNA injection PR-NT-HA apparently is only detectable below the oocyte surface by this method (**fig 2.38** left, lanes 2, 3). After seven days of expression, the amount of PR-NT-HA strongly increases in the plasma membrane, and the amount of protein at the plasma membrane seems to be larger than in the rest of the membranes. Interestingly, PR-NT-HA can be clearly detected at the oocyte surface after 4 days of expression time by the chemiluminescence method. However, the Western blot shows that the



amount of protein increases with time, which supports observations made during voltage clamp experiments.

C-terminally tagged bacterio- and proteorhodopsin were generated to serve as negative controls in luminescence measurements and detection on Western blots.

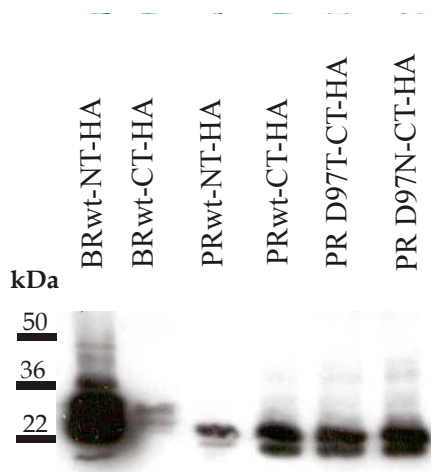


**Figure 2.39 HA-tagged BR and PR construct expressed in oocytes.** Cells harvested 4 days after cRNA injection. Total membrane preparation equivalent of 0.5 oocyte loaded on each lane of a 12% gel. Detection was carried out using rat monoclonal antibody 3F10 against the HA epitope. On the left: molecular weight standard.

All HA-tagged constructs are visible on Western blots, using total oocyte membrane preparations. Each construct demonstrates a propensity for oligomerisation, strongest in BR-NT-HA, which results in a double-banded pattern (**fig. 2.39**).

### 2.7.1 Functional assessment of HA-tagged retinylidene proteins

As the example of BR-NT-HA in **fig 2.40** shows, the presence of the HA-tag attached to the amino-terminus does not impair the function of the protein. The behaviour of the N-terminally tagged BR is similar to that of the wild-type. At neutral pH, where there is no pH gradient across the plasma membrane, there is a stronger voltage dependency for BR wt as the HA-tagged construct. Under extracellular acidic conditions the reversal potentials are almost identical.

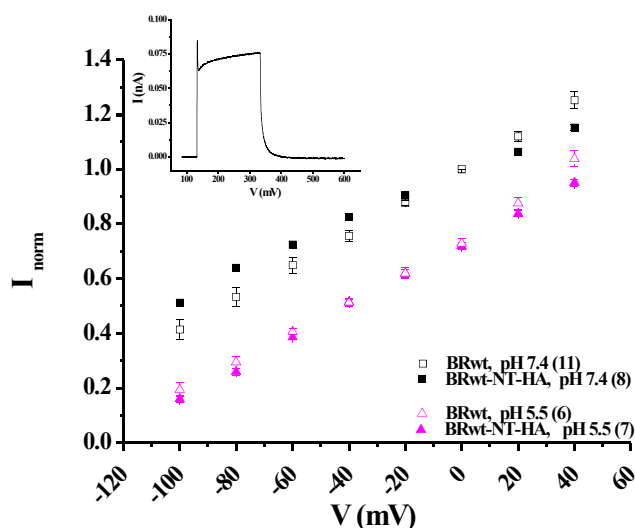


**Figure 2.40 Comparison of BR wt and BR-NT-HA: IV relationship in the absence and presence of a transmembrane pH gradient.** Cells expressing BR-NT-HA were tested for surface expression with the chemiluminescence assay in the opsin form eventually incubated with 5  $\mu$ M retinal for voltage clamp experiments. Normalised to the current amplitude at 0mV, mean  $\pm$  SEM presented, of a number of cells indicated in the graph. Inset: photocurrent at -30mV, pH 7.4.

| Extracellular pH | pH 7.4  | pH 5.5  |
|------------------|---------|---------|
| BR wt            | -170 mV | -130 mV |
| BR-NT-HA         | -220 mV | -130 mV |

Tabel 2.5 Reversal potential of the BR constructs in fig. 2.2.38.

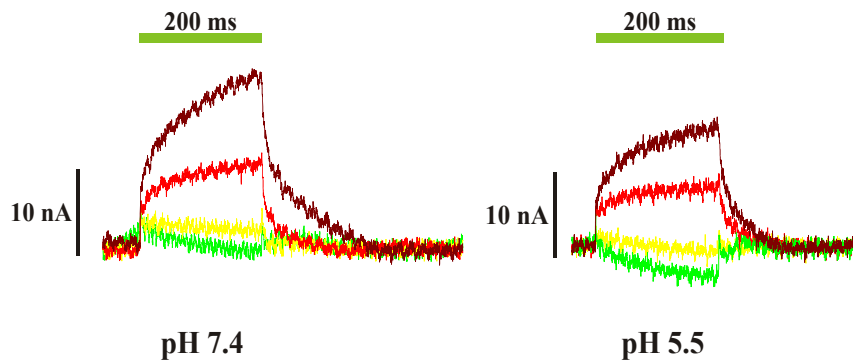


**Figure 2.41 BR-CT-HA: IVs without and with a pH gradient across the cell membrane.** Photocurrents were measured 7 days after cRNA injection, in the presence of 5  $\mu$ M retinal upon illumination with  $\lambda > 495$  nm for 200 ms on the same cell. The voltage protocol consists of jumps from a -30 mV holding potential to test potentials starting from -100 mV to +40 mV in 20 mV increments.

Colour coding: -100 mV (—), -60 mV (—), 0 mV (—), and +40 mV (—).

**Figure 2.41** shows that contrary to BR-NT-HA, when the HA-tag is attached to the C-terminus, photocurrents of BR are different from those of the wild type (compare with **fig. 2.6** left) under both pH conditions applied: the photocurrents do not reach a stationary level during illumination, both the switch-on and -off phase of the signal are slower; and the overall amplitude of the currents is also much smaller as in the wild type. Consequently, the C-terminal HA-tag impairs the function of the protein. Moreover, in the case of PR-CT-HA this effect is even stronger: no photocurrents are observed (not shown), the activity of the protein is abolished.

### 3. Discussion

The functional expression of proteorhodopsin (PR) in *Xenopus laevis* oocytes allows direct investigation of its pumping activity under the control of the potential across the plasma membrane and pH.

Transport properties of wild type PR and mutants of residues in the retinal binding pocket were studied under various potential and pH conditions. The electrophysiologic data in this work were carried out to complete information on this recently identified bacterial rhodopsin, available mostly from spectroscopic experiments.

Data interpretation in case of PR is somewhat complicated by the observation made in spectroscopic experiments, that H<sup>+</sup> uptake (from the cytoplasmic side) and release (to the extracellular side) during the photocycle are temporally not as separated as in case of BR (Dioumaev *et al.*, 2002) which makes assignment of electrical signal components to specific steps in the photocycle approximate. In the case of BR, the switch-on phase of the photocurrent is assigned to the formation of the M state (the rate limiting step of the photocycle), while the switch-off phase to its decay (Geibel *et al.*, 2001).

In PR the H<sup>+</sup> release is slowed down by the missing ‘release complex’ homologous to BR’s E194 and E204, deprotonation of the Schiff base is complex and, according to spectroscopic experiments, not completed for tens of ms. Uptake of H<sup>+</sup> from the cytoplasmic side follows shortly after reprotonation of the Schiff base (Dioumaev *et al.*, 2002). As a consequence, an M-like state as known from BR, is present for a shorter time.

In analogy to BR experiments, the effect of azide on PR and its mutants has been investigated, discussed together for all constructs in section 2.3.6 towards the end of this chapter.

#### 3.1 Action spectrum of PR wild-type

**Figure 2.1** shows the action spectra of PR wild type measured under two different experimental conditions: two-electrode voltage-clamp of oocytes heterologously expressing the protein, and in BLM experiments with PR reconstituted into proteoliposomes\*. The maxima of both datasets is ~ 517nm, 10 nm blue-shifted compared to the absorption maximum of the Monterey Bay PR clone, the first described (Béjà *et al.*, 2000). However, the width of distributions is different. The higher activity between 400-450 nm could be due

---

\* courtesy of Dr. Thomas Friedrich, unpublished results

either to differences in the light saturation between the BLM and oocyte experiments and/or to the controlled transmembrane potential in oocytes, kept at -30 mV.

### 3.2 Regulation of H<sup>+</sup> translocation by pH and transmembrane potential in PR wt

The total driving force generated by a proton pump consists of an electrical potential difference ( $\Delta\Psi$ ) and an osmotic gradient, which are equivalent from a thermodynamic point of view (Läuger, 1991):

$$\Delta\tilde{\mu}_{H^+} = \Delta\Psi + \frac{RT}{zF} \ln \frac{c_o}{c_i}, \quad \text{Equation (3)}$$

a relationship, which can be also written in the form:

$$\Delta\tilde{\mu}_{H^+} = \Delta\Psi - (59\text{mV}) * (\Delta\text{pH}) \quad \text{Equation (4)}$$

[where R = molar gas constant, T = absolute temperature (K),  $c_o$  = ion concentration outside the cell,  $c_i$  = ion concentration inside the cell, z = valence of the ion, F = Faraday constant and  $\Delta\Psi$  = electrical potential difference]

For kinetic reasons the influence of the concentration gradient may differ from that of the applied electrical potential: under many conditions  $\Delta\Psi$  will be kinetically more efficient as a driving force for secondary active transport than  $\Delta\text{pH}$  (Läuger, 1991).

Two electrode voltage clamp experiments allow the simultaneous observation of the effect of pH and membrane potential on the photocurrents generated by PR. Over the range of measured potentials between -140 to +40 mV under asymmetric -, and -100 to +40 mV under symmetric pH conditions the IV relationships at each measured pH value are linear. From this linearity the apparent reversal potentials can be estimated by extrapolation.

Upon extracellular acidification (**fig. 2.3 A**) the observed shift in the apparent reversal potential upon one pH unit change is  $\sim 70\text{mV}$ , value not far from the 59 mV calculated using the Nernst equation (equations 5 and 6):

$$E_{H^+} = \frac{RT}{zF} \ln \frac{c_o}{c_i} \quad \text{Equation (5)}$$

or in the form

$$E_{H^+} = (59\text{mV}) * (\Delta\text{pH}) \quad \text{Equation (6)}$$

[where R = molar gas constant, T = absolute temperature (K),  $c_o$  = ion concentration outside the cell,  $c_i$  = ion concentration inside the cell, z = valence of the ion, F = Faraday constant]

In the case of bacteriorhodopsin (BR), over a similar pH range only a shift of 34 mV/pH unit was seen, the difference being explained by possible charge movements inside the protein influenced mainly by the electric field (Geibel, 2003; Geibel *et al.*, 2001).

At extracellular pH 8.5, when the pH gradient would favor proton pumping, the apparent reversal potential shift is markedly smaller ( $\sim 30\text{mV}$ ) than when the pH gradient opposed the pumping direction, although no saturation effect can be observed at extreme positive membrane potentials [as in case of BR (Geibel, 2003; Geibel *et al.*, 2001)]. The explanation for this behaviour could be - similarly to BR - that charge movements inside the protein become more evident when there is no chemical gradient opposed to the pumping direction. It is important to note that measurements at pH 7.4 and 8.5 are physiologically most relevant, since the pH of seawater is between 7.4 and 8.4 (Clayton and Byrne, 1993).

When the pH gradient across the membrane is decreased by manipulating the intracellular pH of the oocytes, the photocurrents are less voltage dependent (**fig. 2.3 B**) and the apparent reversal potential values are left-shifted compared to the values under asymmetrical pH conditions (**fig. 2.3 A**). This, on one hand, extends the range of potentials over which PR can pump outwardly, on the other the pump currents become smaller due to a possibly reduced pH sensitivity on the cytoplasmic side.

Altogether these results imply that the activity of the pump can be modulated by both the extracellular and the intracellular pH.

### 3.3 The photocycles of PR and BR probed by potential changes and laser flash experiments

From **figure 2.4**, it is evident that at pH 7.4 the transmembrane potential affects both the peak and stationary components of PR photocurrents. Their ratio ( $I_{\text{peak}}/I_{\text{stationary}}$ ) does not change significantly over the tested range from  $-140$  to  $+40$  mV, which means that both components, i.e. at least the formation and decay of the M-like state might be influenced by the applied potential. This is to be expected already from the shape of the PR-generated photocurrent, which has, at neutral-to-alkaline pH values, a clear peak at the beginning of illumination, decaying to a stationary level during continuous illumination. In BR the peak component of the photocurrent (steps leading to the deprotonation of the Schiff base) contributes only a small fraction to the translocated charge during the pump cycle, and displays a weak voltage dependence, as observed by Geibel *et al* (2001), in accordance with the decay of the  $M_2$  state being the main electrogenic and rate-limiting step of the photocycle (Geibel *et al.*, 2001) (compare electric signals in **fig. 2.6**).

In the case of BR, experiments with blue laser flashes applied during and after continuous illumination at various membrane potentials and neutral pH greatly contributed to

the understanding of the photocycle (e.g. identification of a long lived M intermediate, (Geibel *et al.*, 2001)). The M state is important for the vectoriality of H<sup>+</sup> pumping: during the M<sub>1</sub>→M<sub>2</sub> transition the accessibility of the Schiff base changes from the extracellular side to the cytoplasmic side, so this key position can be reprotonated only from the cytoplasmic side (from D96) during the following steps of the photocycle (Kataoka and Kamikubo, 2000; Luecke, 2000). If the protein is arrested in the M<sub>1</sub> form – Schiff base accessibility from the outside – by the chosen conditions (membrane potential, pH) or mutagenesis, additional blue laser flashes will shortcut the photocycle by inducing *cis*→*trans* isomerisation of the retinal followed by reprotonation of the Schiff base from the extracellular side and return to the ground state (Geibel, 2003; Geibel *et al.*, 2001; Nagel *et al.*, 1998). For BR wt it was concluded that the amplitudes of the blue light induced transients reflect the amount of M (Geibel *et al.*, 2001).

In this work, BR expressing oocytes were used as a control for PR, under the same experimental conditions: the measurements at neutral pH conform earlier observations that **i**) the M state is clearly detectable when the protein is expressed in oocytes (**fig. 2.6**) similarly to HEK cells (Geibel *et al.*, 2001); **ii**) the lifetime of the detected M state is prolonged by hyperpolarising potentials (**fig. 2.8**); **iii**) return to the ground state is accelerated by more positive potentials (**fig. 2.11, 2.12**). In addition, the effect of acidic pH on the photocycle was investigated (**fig. 2.9, 2.10 B, 2.11**). The measurements where instead of blue, green flashes were used, confirm the *additive nature* of pH and transmembrane potential on the activity of BR, i.e. a pH gradient opposed to the proton pumping direction extends – similarly to hyperpolarising membrane potentials – the lifetime an intermediate (presumably M1) where the deprotonated Schiff base is accessible from the extracellular side. They also suggest that the *extracellular reprotonation of the Schiff base can be triggered also by green light*, although less efficiently compared to blue (**fig 2.9**), since the absorption maximum of the M intermediate with deprotonated Schiff base is ~ 410 nm.

The total electrochemical gradient ( $\Delta\tilde{\mu}_{H^+}$ ) which acts on the pump under each experimental condition is summarised in the Table 2.6 below. The values, similar at pH 7.4, -100 mV, and pH 5.5, -30 mV, also explain why the recordings under these conditions are alike (**fig 2.9**).

| V <sub>hold</sub> | pH 7.4  | pH 5.5  |
|-------------------|---------|---------|
| -30 mV            | -89 mV  | -148 mV |
| -100 mV           | -159 mV | -218 mV |

**Table 2.6 Theoretical values of  $\Delta\tilde{\mu}_{H^+}$  calculated using Equation 4.**

The same idea has been employed for PR to probe for the properties and life time of an M-like state with blue laser flashes and the ground state by green laser flashes.

Obviously, at neutral pH, illumination conditions which saturate BR do not have the same effect on PR: blue laser flashes additional to continuous green illumination further excite the pump, generating biphasic signals, with a small negative and a large positive component. Transient currents triggered by blue flashes have smaller amplitudes as those triggered by green flashes (**fig 2.6** and **2.7** top) due to the higher efficiency of green light (see action spectrum in **fig. 2.1**).

Another important difference between the two H<sup>+</sup>-pumps is that there is *no sign of a long lived M-like intermediate* in case of PR because the transient currents after switching off the continuous illumination at pH 7.4 are always positive as the photocurrent during illumination, not negative as in case of BR.

Dioumaev *et al.* suggested, based on spectroscopic experiments, that the deprotonation of the Schiff base in PR's photocycle is more complex than in BR, and an M-like intermediate does not accumulate to the same extent as in case of BR (Dioumaev *et al.*, 2002). A BR mutant, F171C, was shown by X-ray crystallography to accumulate the N-state during the photocycle (Kamikubo *et al.*, 1996; Kataoka and Kamikubo, 2000). In oocytes, no quenching by blue laser flashes can be observed during continuous illumination (Geibel, 2003), which means that the M state does not accumulate to the same extent as in the wild-type protein. The measurements with wild-type PR could reflect a similar situation (less accumulation of M-like state) in addition to the non-saturating light conditions (**figures 2.6** and **2.7** top). As a result, laser flashes applied during continuous illumination trigger transient currents in addition to the stationary currents, whose amplitude depends on the wavelength of the applied flash. The absence of blue flashes-triggered large *negative* transient currents suggests that an M-like state does not accumulate, or, that the insufficiently stimulating light conditions interfere with its detection.

Application of laser flashes at three different membrane potentials (-70, -30, and +40 mV) shows that the time course for the molecules to return to the ground state is very similar (**fig 2.10**). With both green (503 nm) and blue (396 nm) laser flashes, the same process can be detected, due to the similar time constants resulted from fitting the data points with a monoexponential function [Eq. (1)]. It is interesting, that at +40 mV the process seems slower when probed by blue laser flashes, however the first flash applied ~ 37 ms after the continuous illumination excites more molecules compared to more negative potentials.

Application of laser flashes in shorter time intervals during the switch-off phase of the stationary current of PR (**2.10 B**) confirms the results at -30 mV.

From the increasing amplitudes of the transient currents triggered by the blue- and green laser flashes one could think about a possible mechanism which would prevent the PR molecules from rapidly populating the ground state after switching off the stationary illumination. Since in PR the M-like state does not accumulate to the extent comparable of BR (Dioumaev *et al.*, 2002), this could also be considered an *indirect evidence of the detection of an M-like state*.

The effect of the transmembrane potential is much more evident in case of BR (**fig 2.11**) suggesting that the potential has a stronger effect on the decay of the M state in BR as in PR, possibly because there are more BR molecules in this state compared to PR.

Laser flashes under **acidic pH conditions** strengthen the evidence that active proton translocation in PR involves different mechanisms as in case of BR. The pattern of laser induced inward transients is different: *their amplitude stays constant after switching off the continuous illumination (fig. 2.7)* and increases at more negative potential values (**fig. 2.8**). In addition, at pH 4.5 the laser induced transient currents - independent of the wavelength used - point into the same direction as stationary current, inward already at -30 mV (**fig. 2.7**). This means, that there is a substantial fraction which can mediate transient inward H<sup>+</sup> transport at acidic pH, in the same fashion as the deprotonated BR species would do (described as 'blue light quenching' of the stationary photocurrent). The difference is that this species in PR is present also *in the absence of illumination*.

By applying laser flashes without previous continuous illumination, one can gain information about a single turnover of the protein upon absorption of photons. In BLM experiments laser flashes trigger negative or positive transient currents dependent on the pH (Friedrich *et al.*, 2002). This behaviour is explained by the necessity of two photons for an efficient forward transport, the acidic form being more efficient than the alkaline form upon absorption of a single photon. When PR was expressed in oocytes, under voltage clamp conditions most of the charge was transported outwardly at all tested membrane potentials at pH 7.4 (**fig. 2.13 A**). At -70 and -30 mV the current signal also showed a negative component, larger when PR was excited with blue light. At all three membrane potentials the amplitude of the green-light triggered transient currents is larger, in agreement with the action spectrum of the protein (**fig. 2.1**). The decay phase of the positive component can be approximated by one time constant,  $\tau \sim 8$  ms at -70 and -30 mV, at +40 mV by two -  $\tau_1 \sim 5$  ms and  $\tau_2 \sim 40$  ms. Inward transient currents as seen on the BLM at pH 7.4 are observed in case of the oocytes



only at pH 5.5 at -70 and -30 mV (not shown). This suggests that the transmembrane potential, when present, has an important contribution to the population of the two forms, alkaline and acidic of PR.

For comparison, similar experiments were done also with BR expressed in oocytes (**fig 2.13 B**). The laser flashes generate similar transient currents as described in the case of PR only faster, characterised by one time constant when excited with blue light of  $\tau \sim 3$  ms and two time constants when excited with green light  $\tau_1 \sim 1.5$  ms and  $\tau_2 \sim 13$  ms. Here, the membrane potential is important in determining the amplitude of the transient currents with both wavelengths. However, it is also possible in case of transient currents of low amplitudes (e.g. stimulated with blue laser flashes, or at negative membrane potentials) that a longer time constant is not detected during the fitting procedure. The small time constants determined for both proteins are at the detection limit (determined by the system time constant –  $\tau = RC$  – necessary to clamp the oocyte membrane to a certain potential, in the millisecond range), the long time constant is the same order of magnitude as the rate limiting step during the photocycle,  $\sim 20$  ms in case of BR wt, depending on the transmembrane potential (Geibel *et al.*, 2001). In the case of two time constants detected, the detected rate limiting step is twice slower in case of PR compared to BR (40 ms versus 13 ms).

It is important to note that earlier experiments on BR, using the BLM method, detected a fast negative component in the  $\mu$ s range (Fahr *et al.*, 1981), which is not seen in the oocyte experiments, possibly due to limitations imposed by the experimental setup (e.g. shutter opening). The fast negative component in BR is associated with the K $\rightarrow$ L transition of the protein, where the isomerisation of the retinal takes place (Fahr *et al.*, 1981). If in case of PR the negative component is related to the similar event, this must be slower since it is readily detectable.

In **figure 2.14**, the ratio of positive amplitudes triggered by the green- and blue laser flashes is compared. This does not change significantly with potential in case of PR suggesting that the membrane potential influences the excitability of PR by blue and green wavelengths in a similar manner. In case of BR this ratio appears to be voltage dependent in the absence or presence of a proton gradient. At pH 5.5 the laser triggered transient currents in PR have a positive component only at +40mV, and consist of a negative transient current at more negative membrane potentials which makes such a comparison not feasible.

### 3.4 Light intensity dependence of PR wild-type

Current measurements of PR using the BLM method have shown that the intensity of the applied light has different effects on the alkaline and acidic form of the protein (Friedrich *et al.*, 2002). In the oocyte system under neutral pH conditions (pH 7.4), the amplitudes of the outward photocurrent depend primarily on the intensity of stimulating light while voltage dependence develops only at strong intensities (**fig. 2.16**). Interestingly, the current amplitudes are not proportional with the applied light: at 10% light intensity the amplitude of the photocurrents are more than a tenth of current triggered by 100% intensity, at any membrane potential applied between -100 and +40 mV, although the effect is stronger at more hyperpolarising potentials. This is further evidence for the modulation of PR's activity by the electric field, which at negative potentials could arrest the protein in an M-like state, similar to BR (Geibel *et al.*, 2001; Nagel *et al.*, 1998), leading to less efficient proton pumping.

The fact that inward currents under acidic conditions at low light intensities are missing (not shown) when PR is expressed in oocytes suggests that the oocyte- and BLM experiments are not entirely comparable.

Proteorhodopsin appears to be a protein which is difficult to saturate with light: laser flashes applied during continuous illumination trigger transients additional to the stationary current (**figs. 2.6, 2.7**) – this is further evidence for the two-photon-process required for outward proton transport by the alkaline form suggested by Friedrich *et al* (2002).

### 3.5 Mutants of proteorhodopsin

Since the first description of bacteriorhodopsin (BR) in 1971 (Oesterhelt and Stoekenius, 1971), spectroscopic, crystallographic and electrophysiologic experiments revealed many of its functionally important amino acid residues. The recently identified (Béjà *et al.*, 2000) proteorhodopsin is just starting to be characterised, mainly by spectroscopy (Béjà *et al.*, 2000; Béjà *et al.*, 2001; Bergo *et al.*, 2004; Dioumaev *et al.*, 2002; Dioumaev *et al.*, 2003; Friedrich *et al.*, 2002; Huber *et al.*, 2005; Imasheva *et al.*, 2004; Imasheva *et al.*, 2005; Krebs *et al.*, 2002; Lakatos *et al.*, 2003; Lakatos and Váró, 2004; Man *et al.*, 2003; Man-Aharonovich *et al.*, 2004; Váró *et al.*, 2003). Residues in homologous positions to BR's D85 and D96 have been found important for function by spectroscopic characterisation of mutants in which these positions were occupied by different amino acid residues (Dioumaev *et al.*, 2002; Dioumaev *et al.*, 2003). A series of other residues in the vicinity of the retinal binding pocket were

identified to be implicated in PR's function either by restricting the formation of a long-lived photoproduct like Asp 227 (Imasheva *et al.*, 2004; Imasheva *et al.*, 2005), or by conferring adaptation to the host bacteria's natural environment, like residues at positions 65, 68, 70, and 105 (Bielawski *et al.*, 2004; Man *et al.*, 2003; Man-Aharonovich *et al.*, 2004; Wang *et al.*, 2003). This work is the first survey of consequences of mutations on the photocurrents of PR and the direct transport measurements of PR mutants are intended to supplement the available spectroscopic information.

It is possible that the expression level of PR mutants in *Xenopus* oocytes is ten-fold lower than that of the wild type (Table 2.4). However, the recorded current signals still reflect the effect of the mutations on the shape of the photocurrents.

### 3.5.1 Mutations of the proton donor E108

#### E108D

This charge-conserving mutation has the smallest effects on the activity of PR. In this mutant, both the proton donor and acceptor positions are occupied by aspartate residues, like in BR (Asp96 and 85). Comparing the shape of the signals at pH 7.4 of the BR and PR wild type constructs suggest that the residues which are directly involved in proton translocation (in- and also possibly outside the retinal binding pocket) are different in these two retinylidene ion pumps.

Following the IV relationship at pH 7.4 (**fig 2.18**), the E to D replacement causes a slightly stronger voltage dependence of the peak current and no change in the voltage dependence of the stationary current over the measured range between +40 to -100 mV. As a consequence, their ratio shows also changed voltage dependence: compared to the wild type, it is steeper, similar to that of D97E construct (**fig 2.19**). Since E108 plays the role of proton donor, the E to D mutation could affect the reprotonation step in the photocycle, most likely by slowing it down. This possibility is supported by the effect of azide on this mutant, the voltage dependence of the stationary current being stronger affected as that of the peak current. It is known that azide acts mainly within the cytoplasmic channel of the protein in BR (Butt *et al.*, 1989), where E108 is located in PR. Nevertheless, azide increases the amplitudes of both the peak and stationary current components of PR E108D.

Under acidic conditions the photocurrents of E108D are inverted and show a stronger voltage dependence compared to the wild type (**fig. 2.20**). This suggests that the presence of the

aspartate residue at position 108 does not interfere with inward charge translocation under conditions where this was observed in wild type PR. Comparing the size of the photocurrents of wild-type PR and E108D under neutral and acidic extracellular pH conditions, it appears that the mutation affects more the outward charge translocation, since under identical experimental conditions the outward currents generated by E108D are smaller compared to those of the wild-type, but the inward currents at hyperpolarising potentials are similar (**fig. 2.20 B, C**). The role of the shorter side-chain at the proton donor position for charge translocation by E108D is not entirely clear.

### E108G

Removing the primary proton donor group for reprotonation of the Schiff base has the same effect as observed in case of BR D96N or -G (Butt *et al.*, 1989; Tittor *et al.*, 1989); this mutation reduces H<sup>+</sup> transport due to an impaired reprotonation of the Schiff base from the cytoplasmic side (**fig 2.21 A**). For BR D96G it was shown that the mutation causes the accumulation of the M state by slowing down its decay (Geibel, 2003), an effect similar to that described in D96N (Luecke *et al.*, 1999). The amount of the accumulated M state can be detected by applying blue laser flashes during and/or after stationary illumination as described in (Geibel *et al.*, 2001) and in this work, in case of the wild-type.

The experiments with blue laser flashes confirm this assumption for PR (**fig 2.21 C**): the data with PR E108G are similar to those of BR D96G (Geibel, 2003). The amplitudes of the transient currents applied during continuous illumination increase with time between the onset of continuous illumination and application of the blue flashes, and reach a constant level after ~ 325 ms (**fig. 2.21 C and 2.22 A**). This suggests that the blue light absorbing state accumulates within the time of continuous illumination and could be considered as the formation of an M-like state, characterised by a time constant  $\tau \sim 61$  ms. After switching off the continuous illumination the electrical measurements resemble the mirror image of the process detected during continuous illumination, with amplitudes larger when the laser flash is applied shortly after the continuous illumination and which decay as the time between the continuous illumination and laser flash illumination increases (**fig. 2.21 C**). This process is characterised by a time constant  $\tau \sim 236$  ms (**fig. 2.22 B**). From similarities with BR wild-type, the experimental protocol which combines continuous and transient illumination **detects directly the formation and decay of an M-like state, for the first time in case of PR**. The data also support the conclusions of spectroscopic experiments of Dioumaev *et al.*, according

to which M-like state does not largely accumulate unless the proton donor E108 is removed (Dioumaev *et al.*, 2002).

Using the quenching effect of blue laser flashes during continuous illumination on the BR mutants D96N and D96G it was shown that the life time of the M intermediate for D96N is shorter than D96G, the M-decay process being characterised by long time constants compared to BR wild-type ( $V_m = 0$  mV):  $\tau > 300$  ms (D96N) and  $\tau > 1200$  ms (D96G) (Geibel, 2003). Although both mutants prolong the lifetime of the M state, the longer side chain of asparagine allows a more open channel on the cytoplasmic side, so protons could reach the Schiff base by diffusion easier than with glycine at the same position.

In case of PR, an M-like state similar to that observed in BR becomes directly detectable only after replacement of the negatively charged glutamate at position 108 with glycine and its lifetime is clearly shorter than in case of the homologous mutation in BR, D96G [PR E108G:  $\tau \sim 236$  ms at  $V_m = -30$  mV (this work); BR D96G:  $\tau > 1200$  ms at  $V_m = 0$  mV (Geibel, 2003)].

H<sup>+</sup> transport by E108G in the presence of azide is discussed in section 3.6.

### 3.5.2 Mutations of the proton acceptor D97

#### D97E

In BR, the D85E replacement of the proton acceptor accelerates the first steps in the photocycle which lead to protonation of the Schiff base, compared to the wild type (Butt *et al.*, 1989; Tittor *et al.*, 1994). Dioumaev *et al.* report a similar effect in D97E, where the apparent rate of M formation in the mutant is 10 times faster than in PR wild type (Dioumaev *et al.*, 2002). From the photocurrents measured in D97E expressing oocytes it is visible that the ratio of peak and stationary current is larger (**figures 2.17 and 2.19**). This could originate from the acceleration of M-like state formation (switch-on phase of the signal) or slowing down the decay of M-like state. Considering the observations of Dioumaev *et al.*, the first possibility is more likely. Still, by accelerating the deprotonation reaction, the D>E mutation does not create a more effective pump, so the equilibrium between the deprotonation/reprotonation reactions appears to be important. As apparent from experiments where laser flashes were applied in addition to the continuous illumination (**fig. 2.26**), the

D97E mutant is not saturated by continuous illumination, the recordings are similar to those made with the wild type protein (**fig 2.6** top). Similar to the wild type PR, transient currents triggered by green laser flashes are larger as those triggered by blue flashes, likely because the mutant protein is more efficiently stimulated by green light compared to blue. Further experiments are needed to characterise laser flash induced transient currents of D97E under acidic conditions to see how the similarities with BR D85E (Friedrich *et al.*, 2002) are reflected in the oocyte system.

### D97N

When position 97 is occupied by neutral, polar amino acids (e.g. asparagine, threonine), the deprotonation of the Schiff base by the same mechanism as in wild-type PR cannot occur (**figure 2.17**). During both continuous and transient illumination **only inward charge translocation can be observed**, in the presence or absence of background green illumination ( $\lambda > 495$  nm). In addition, changes in membrane potential (between -100 mV and +40 mV), pH and buffer composition did not elicit outward photocurrents. This is in agreement with the suggestion of Dioumaev *et al.*, that for outward  $H^+$  pumping activity under neutral (i.e. natural) conditions the presence of a negatively charged residue at position 97 is necessary (Dioumaev *et al.*, 2003).

For the homologous mutation in BR, D85N, a decrease of the  $pK_a$  value of the Schiff base was reported, from 13 to  $\sim 8$ , depending on the ionic strength. As a consequence at physiological pH a mixture of chromophores absorbing at  $\sim 410$  nm (deprotonated form) and  $\sim 610$  nm (protonated form) coexist (Kataoka *et al.*, 1994; Tittor *et al.*, 1994). Experiments employing the **black lipid membrane (BLM)** method resulted in the observation that D85N is able to transport protons in both directions, depending on the surrounding pH (i.e. the protonated or unprotonated state of the Schiff base), ionic strength and light conditions. In yellow light ( $\lambda > 515$  nm) an inward transient current due to proton transport to the cytoplasmic side of the protein and small outward stationary current enhanced by low pH and high chloride concentrations were reported (Ganea *et al.*, 1998).

When the extracellular pH is lowered, the amplitude of the PR D97N mediated inward currents increase (**fig. 2.27** right). The peak and stationary components of the photocurrent both increase, in a pH- and voltage dependent manner (**fig. 2.28**), suggesting that the inward current is enhanced by acidification on the extracellular side. Since the negative photocurrents

in mutants D97N and D97T are small compared to the wild-type signals (the peak amplitude 5-10 times smaller) and the decay is fast after the onset of continuous illumination to a very small stationary level, it is also possible that the charge movement takes place only around the Schiff base, which undergoes a conformational change from all-*trans* to 13-*cis* upon illumination.

### D97T

Introduction of a threonine residue at the site of the proton acceptor (D97T) at neutral pH (7.4) has the same effect as the presence of another neutral polar residue, asparagine (D97N). In the case of BR D85T, the mutation expands the range of transported ions of the protein, turning the protein into a chloride pump. A change from chloride to proton transport was seen in another retinylidene pump, halorhodopsin (Bamberg *et al.*, 1993). The transport modes in BR D85T also depend on the light conditions: in green light H<sup>+</sup> are outwardly, Cl<sup>-</sup> inwardly transported; in blue light H<sup>+</sup> are transported outwardly like in the wild type; in white light inward H<sup>+</sup> translocation was observed (Tittor *et al.*, 1997). The D>T replacement introduces an anion binding site whose occupational state is important (Tittor *et al.*, 1997). At higher NaCl concentrations is more likely to have the binding site occupied. In BLM experiments, the authors used up to 1 M NaCl and the half maximal chloride dependent current-changes in green light occur in the range between 100-150 mM NaCl.

To test this possibility in PR D97T, the ND96 buffer was supplemented with NaCl up to 300 mM final concentration. In oocytes, it is not possible to use high concentrations of salts and measurements in 300 mM Cl<sup>-</sup> did not appear reliable due to the osmotic pressure on the cell membrane which caused high background conductance. Although in the absence of Cl<sup>-</sup> both the peak and stationary components of the currents appear larger as at 96 mM NaCl, since at 200 mM Cl<sup>-</sup> causes a further increase, the signal cannot be clearly associated with chloride transport in green light ( $\lambda > 495\text{nm}$ ).

As shown in **figures 2.32** and **2.33**, the *wavelength* of light has a notable effect, although only the shape of the signal and not the vectoriality of the charge translocation changes. The photocurrent triggered by white light appears like the cumulative result of blue and green light induced currents.

According to these experiments, in white light the vectoriality of H<sup>+</sup> transport of PR D97T does not change as in case of BR D85T, although the peak and stationary components of the photocurrent become larger, which suggests a cooperative effect of blue and green light (**fig.**

**2.33 A**). This observation is further supported by the results with additional laser flashes during and after continuous illumination (**fig. 2.34 A, B**) and the dependence of the photocurrents on the relative intensity of the three wavelengths tested (**fig. 2.33 B**), conditions under which the vectoriality of charge translocation does not change upon increased light intensity. An explanation for the additive effect of the applied light could be a two-photon-driven photocycle in the inward direction. When the protein is illuminated with blue light, the resulting photocurrent is dominated by a stationary component because the blue photons are absorbed efficiently only by the deprotonated Schiff base, helping in its reprotonation (**fig. 2.33 A top**). On the other hand, the protonated Schiff base in the ground state is efficiently deprotonated by green light giving rise to a sharp peak current (**fig. 2.33 A middle**). Proton transport by D97T is favoured if the protein absorbs sequentially photons of both wavelengths resulting in inward photocurrent with clear peak and stationary components (**fig. 2.33 A bottom**). The sequence of events could be explained using the elements of the **IST model** (Haupts *et al.*, 1997) (see in ‘Inward transport by proteorhodopsin’).

Still, further experiments under different transmembrane potential and pH conditions are needed to elucidate the transport properties of this mutant and also, whether the nature of the neutral amino acid residue introduced influences inward transport.

Similar to the BR mutant D85N, the homologous mutant D85T has also been extensively studied using the **black-lipid-membrane** technique (Ganea *et al.*, 1998; Tittor *et al.*, 1994). According to the authors’ observations, the direction of transient and stationary photocurrents – which may take place in both directions - depends on the experimental conditions (light intensity and wavelength, pH), i.e. the mutations do not determine the direction of H<sup>+</sup> pumping.

Unfortunately there are no data available with the same mutants in the oocyte system, which makes the comparison of results more difficult due to differences in experimental methods. The BLM system allows an exact control of the pH and light conditions; the oocyte system insures a natural orientation of protein molecules and allows precise control of the transmembrane potential or current. The pH can only be precisely determined on the extracellular side. Experiments with PR D97N and -T using the BLM technique and/or BR D85N, -T in oocytes are necessary for a better comparison of the results.



So far, all experiments with the mutants D97N, and -T in the oocyte system support the idea that when the proton acceptor is not available, only inward currents can be observed and Schiff base deprotonation is restricted to the cytoplasmic part of the proton transfer channel.

### 3.5.3 L105Q, the spectral tuning switch

Shortly after the first description of PR, Bèjà *et al.* published observations on the variability in absorption maximum among different environmental samples. In species from 75 m depth in the Monterey Bay and in Antarctic bacterioplankton the absorption maximum was blue-shifted to 490 nm (Bèjà *et al.*, 2001). Later, comparing PR sequences of different origins, Man *et al.* identified residue 105, as the ‘spectral tuning switch’ responsible for determining the absorption maximum of the protein (Man *et al.*, 2003). For PRs in which this position is occupied by a leucine, the absorption maximum is in the green range of visible light, with Gln at position 105 and the absorption maximum is blue-shifted. This property can be almost entirely interchanged between PR groups by exchanging the amino acid residues at position 105 (Kelemen *et al.*, 2003; Man *et al.*, 2003; Man-Aharonovich *et al.*, 2004; Wang *et al.*, 2003). Beside Leu and Gln, the position 105 can be occupied by other residues, like Val or Glu (Man *et al.*, 2003). Additionally, other residues, e.g. at positions 65 and 70, outside the retinal binding pocket, were shown to contribute to the fine-tuning of the absorption maximum in PRs (Man-Aharonovich *et al.*, 2004).

Comparison of the action spectra of wild type PR (‘green PR’) and PR L105Q (‘blue PR’) shows a blue-shift in case of the mutant. The distribution of data points reveals this blue shift more clearly on the right flank of the graph (**fig 2.35**), with no clear separation of the action spectra maxima at blue and green wavelengths. However, these direct measurements of the proteins activity support the hypothesis that residue 105 contributes to the determination of the absorption maximum of the protein, as previously suggested (Man *et al.*, 2003; Man-Aharonovich *et al.*, 2004; Wang *et al.*, 2003), also within a cellular context.

#### 3.5.3.1 Transport properties of PR L105Q

The photocurrents of PR L105Q are smaller than those of the wild type (**fig. 2.37 A**). The amplitude of photocurrents currents is determined by the turnover number of the protein and the number of molecules (i.e. the level of expression) in the oocyte membrane. However, in the case of L105Q, the photocycle in the oocyte expression system is characterised by similar time constants over the measuring range (200 ms continuous illumination flanked by 200 and

330 ms dark periods at a certain holding potential), which leaves another possibility – low expression levels – as a reason for the small stationary currents. Indeed, using the values of  $\tau_2 \sim 21.91$  ms,  $I_{\text{stationary}} = 9.225 \pm 3.4$  nA and the formula in **Table 2.4** to evaluate the expression level, it appears that the expression level of L105Q mutant in oocytes is, similarly to the other mutants, ten fold lower as that of the wild-type ( $N_{\text{L105Q}} \sim 1.262 \times 10^9$  compared to  $N_{\text{wt}} \sim 10.118 \times 10^9$ ).

According to earlier observations of spectroscopic experiments, PR clones with Gln at position 105 are characterised by a slower photocycle (Man-Aharonovich *et al.*, 2004; Wang *et al.*, 2003). A possible mechanism to explain the effect of Gln at this position is, that the polar glutamine sidechain stabilizes the Schiff-base proton and creates a higher energy gap between excited and ground states (Man *et al.*, 2003). At water depths where Q105 – bearing PR variants (‘blue-PRs’) have been identified, the available light intensity is very low. Since the light with  $\lambda > 500$  nm is sharply attenuated, there is no selective pressure for a faster photocycle (Wang *et al.*, 2003). In addition, a regulatory rather than energy-harvesting function has been suggested for BPRs with photocycle more than 10-fold slower than that of GPRs (Man-Aharonovich *et al.*, 2004; Wang *et al.*, 2003).

The results obtained in the oocyte system suggest that further experiments are needed to clarify the role of the amino acid residue at position 105 in a putative deceleration of the photocycle in blue PRs. It is likely that both residue 105 and the rest of 20-30% difference between sequences of green- and blue PR’s (Man *et al.*, 2003; Wang *et al.*, 2003) are important in the determination of absorption spectral maxima.

### 3.6 The effect of azide on the photocurrents of proteorhodopsin

Azide is an inorganic base with pK of 4.7. Its effect on the chloride pump halorhodopsin (HR) has been studied earlier and shown to accelerate de- and reprotonation reactions of the Schiff base (Hegemann *et al.*, 1985; Lanyi, 1986). The same effect has been observed in case of the photocycle of certain BR mutants by Tittor *et al.* who described the reactivating effect of azide on D96 mutants. Testing other anions as well, apparently the efficiency of regeneration of the H<sup>+</sup>-pump’s activity is dependent on the size and pK<sub>a</sub> of the inorganic base used (Tittor *et al.*, 1989). Azide is able to replace D96, thereby acting as a catalyst for reprotonation of the Schiff base. As a consequence, the decay of the M state is accelerated. Azide occupies a binding site close to that of the proton donor (replaced in the mutants), accepts a proton from

the cytoplasmic side and transfers it to the Schiff base (Tittor *et al.*, 1989). The molecule(s) integrate(s) into the hydrogen-bond-system of the proton-transfer pathway of the BR molecule (Tittor *et al.*, 1994). Azide enhances not only the reprotonation (from D96) but also the deprotonation (to D85) of the Schiff base (Ganea *et al.*, 1998; Tittor *et al.*, 1994; Tittor *et al.*, 1994), a conclusion which was also supported by electron paramagnetic resonance spectroscopy measurements of Steinhoff *et al.* In this study it, is concluded that azide decreases the hydrophobic barrier in the proton transfer channel around both, the proton donor and acceptor (Steinhoff *et al.*, 1999). In the case of BR, based on pH titration experiments it was proposed that azide acts in its protonated form (Ganea *et al.*, 1998; Tittor *et al.*, 1994; Tittor *et al.*, 1994). BLM experiments have shown that the effect of azide saturates around 60 mM at pH 6.4 and almost fully restores the activity of the D96N mutant to wild-type level (Tittor *et al.*, 1989). Based on pH-dependence measurements Tittor *et al.* concluded that azide exerts its effect in its protonated form (Tittor *et al.*, 1994). Azide concentrations of 50 mM azide were also used in later reports on BR mutants (Ganea *et al.*, 1998; Tittor *et al.*, 1994), therefore this concentration served as a starting point for evaluating its possible effects on proteorhodopsin.

At pH 7.4 azide is almost entirely in the  $\text{N}_3^-$  form (99.8%), at pH 5.5 ~ 86.3%  $\text{N}_3^-$  and 13.7%  $\text{HN}_3$ . At 50 mM and pH 7.4 there are ~ 0.1 mM  $\text{HN}_3$  and 49.9 mM  $\text{N}_3^-$ , at pH 5.5 ~ 6.85 mM  $\text{HN}_3$  and 43.15 mM  $\text{N}_3^-$  present.

As clearly visible in **figure 2.15**, at pH 7.4, 50 mM azide increases both the peak and stationary components of the photocurrent in **PR wt** by 25% over the range of membrane potentials tested. This observation suggests that azide facilitates the transfer of protons during more than one step in the photocycle. In the case of wild type BR, azide does not seem to have any effect (Tittor *et al.*, 1989; Tittor *et al.*, 1994).

50 mM azide (pH 7.4) has the same effect on the **E108D** mutant, and the stationary currents increase in amplitude (~30%) and the slope of the IV curve (**fig. 2.18** right). It is possible that the passage of protons (and azide molecules) between the cytoplasmic side of the protein and Schiff base is easier in the presence of the aspartate residue with a shorter side-chain and higher polarity than glutamate. The increased amplitude of inward currents at pH 4.5 supports this idea (**fig. 2.21**).

Azide exerts a large effect on the PR mutant **E108G**. In presence of 50 mM azide at pH 7.4, the amplitude of the photocurrent increases by more than 20 times (**fig. 2.23 A**). Although the stationary photocurrent is largely enhanced, the signal shape is different from that of the wild-type, starting with a very slow transient current which settles to a stationary level much larger as in the absence of azide. The time constants which characterise the off-signal of the recovered photocurrent of E108G are still slower than those of the wild type ( $\tau_1 \sim 9.3$  ms versus 3 ms and  $\tau_2 \sim 34.5$  ms versus 17.5 ms) – this also suggests that azide at pH 7.4, cannot activate E108G to wild-type level. The light dependence of the azide-effect shows that its effect is genuine, i.e. azide affects the activity of the light-triggered protein (**fig. 2.24 D**).

The negative transient currents elicited on PR E108G by blue laser flashes in the presence of 50 mM azide during continuous illumination (**fig. 2.23 C**) resemble the photocurrents of BR wild-type in the absence of azide (**fig. 2.6** bottom left), where the amplitudes of transients are associated with the amount of M state at the moment of the blue flash. This means that **in case of the mutant with an accelerated photocycle (but still slower compared to wild-type PR) an M-like state can be detected, similarly to BR wt.**

Dioumaev *et al.* suggest, based on FTIR spectroscopy experiments, that the E108Q mutation produces a photocycle with a long-lived M, which accumulates under constant illumination because reprotonation of the Schiff base (from E108) is slowed down (Dioumaev *et al.*, 2002). It is very likely that the same happens in case of E108G (**fig. 2.21 C**). The presence of azide speeds up the photocycle, but not to values observed in the wild type, so the M-like state still accumulates in amounts detectable by the blue laser flashes (**fig. 2.23 C**). Although the photocurrents of E108G in presence of 50 mM azide resemble the current signal of the wild type without azide, a notable difference is the amplitude of blue laser flash triggered *negative* transient currents (compare **figures 2.6** top left with **2.23 C**). However, the similarity to the behaviour of PR wt at pH 7.4 is even stronger, when azide is applied at pH 5.5 (**fig. 2.24 B**), although the photocurrents are small due to the existing pH gradient against the pumping direction. The blue laser flash triggered transient currents become clearly biphasic (see inset in **fig. 2.24 B**), as in the wild type, and their amplitude after continuous illumination is positive throughout as well. At pH 5.5 the amount of  $\text{HN}_3$  increases from 0.1 mM (pH 7.4) to 6.85 mM – this suggests that the active species is  $\text{HN}_3$ , as in case of proton donor and/or acceptor deficient BR molecules.

Comparing several proton donor mutants of BR, Tittor *et al* reported that the M-decay of D96G is slower than that of D96N and that D96N has a higher affinity for azide than D96G (Tittor *et al.*, 1989). In BLM experiments saturation of the system with azide (hundreds of

mM in case of D96G) causes an increase in the rate of M-decay in the mutants to values measured in the wild-type. In the oocyte system, it is difficult to test this aspect due to high background conductances observed in the presence of high azide concentrations.

The measurements with PR wild type, E108D and E108G suggest that not only the decay of M, but also its formation is accelerated by the presence of azide, suggested by the increase in the switch-on part of the photocurrent in all three cases, ~ 25% for PR wt and E108D (**fig. 2.15 A, B** and **2.18 A**) and more than 20 times in case of E108G.

When the proton acceptor D97 is replaced, the charge of the newly introduced residue appears to be important. In the presence of the negatively charged glutamate (**D97E**) which also does not change the pumping direction, azide increases the peak and stationary components of the photocurrent similarly to the wild type and E108D but to a larger extent, of about 50%. The effect on the voltage dependence of the stationary current is stronger as in the wild type or the E108D mutant (see **fig. 2.25** left). This suggests that the access of the active form of azide is similar to both residues 108 and 97 and that azide acts on both de- and reprotonation reactions in the photocycle.

When position 97 is occupied by the neutral, polar amino acid residues glutamine (**D97N**) or threonine (**D97T**), azide causes a *decrease* of the peak of the small inward photocurrent and almost no change in the amplitude and voltage dependence of the stationary component. In similar mutants of BR it was observed that azide in its protonated form accelerates not only the re- but also the deprotonation step in D85N (Ganea *et al.*, 1998; Tittor *et al.*, 1994). In contrast, azide has no effect under any illumination condition on D85T (Tittor *et al.*, 1994). In PR D97N and -T azide seems to have similar effects at pH 7.4 and  $\lambda > 495$  nm, but more detailed experiments are needed to fully characterise them.

For BR it was suggested that azide integrates into the H-bonding-network (Tittor *et al.*, 1994), whether this is valid also in the case of PR, or azide acts by a different mechanism, remains to be elucidated.

Altogether, experiments with PR wt at low pH and the mutants with no negatively charged proton acceptor (D97N, T) suggest that unlike in case of BR, in PR D97 defines the vectoriality of the H<sup>+</sup> translocation. In the absence of a protonatable side-chain in this position only inward transport of H<sup>+</sup> can take place, by a mechanism which is most likely present in PR wt under conditions in which D97 is neutral (i.e. protonated), e.g. at acidic pH.

### 3.7 Inward pumping by proteorhodopsin

Spectroscopic studies have identified an M-like state in the photocycle of PR similar to that of BR, but only under conditions where  $\text{pH} \geq 6$ . At  $\text{pH} \leq 6$  no absorption changes could be detected in the blue spectral range (Dioumaev *et al.*, 2002; Friedrich *et al.*, 2002; Lakatos *et al.*, 2003). From purely spectroscopic studies it was concluded that an M-like state is absent under acidic conditions and that proton transport cannot take place due to the absence of evidence for a deprotonated Schiff base (Dioumaev *et al.*, 2002; Lakatos *et al.*, 2003). Another argument to support the hypothesis that proton transport is absent under acidic conditions refers to the  $\text{pK}_a$  of the proton acceptor, which is much higher in PR (7.1-7.6) than in BR (~2.5). When the pH is below this value in the case of BR, the proton acceptor is not available and transport is thought to be blocked (Lakatos *et al.*, 2003).

In electrical measurements, PR shows the unique behaviour among known retinylidene  $\text{H}^+$  pumps that it is able to change transport direction depending on pH and transmembrane voltage (**figures 2.2 and 2.3**). The change in vectoriality is attributed to the protonation state of the proton acceptor, Asp97 (Friedrich *et al.*, 2002). The protonated and unprotonated forms of PR are present as two different populations of transporters: the alkaline form with deprotonated Asp97, and the acidic form with Asp97 protonated in the ground state. A possible model to explain this complex behaviour was already proposed by Friedrich *et al.*, based on photocurrent measurements using the BLM method and spectroscopic measurements (Friedrich *et al.*, 2002). According to this model, stationary illumination triggers large outward photocurrents at pH values where the alkaline form is prevalent ( $> 7.5$ ). This is most probably due to a two-photon-process. The first photon triggers the photocycle by inducing the isomerisation of the retinal, the second accelerates proton transport by shifting the equilibrium towards an M-like state with the Schiff-base accessible from the cytoplasmic side, to facilitate reprotonation of the Schiff base from the cytoplasmic side (see the *Introduction* chapter on proteorhodopsin).

The data in this work agree with previous results obtained by electrophysiologic and spectroscopic techniques, especially as inward  $\text{H}^+$  transport at low pH was investigated in more detail in a cellular expression system.

When the proton acceptor Asp97 is protonated in the ground state, upon illumination the  $\text{H}^+$  can leave only towards the cytoplasmic side. Voltage clamp experiments at low pH show that at external pH 5.5 the outward stationary currents reach ~ 25% of those at pH 7.4 and inward

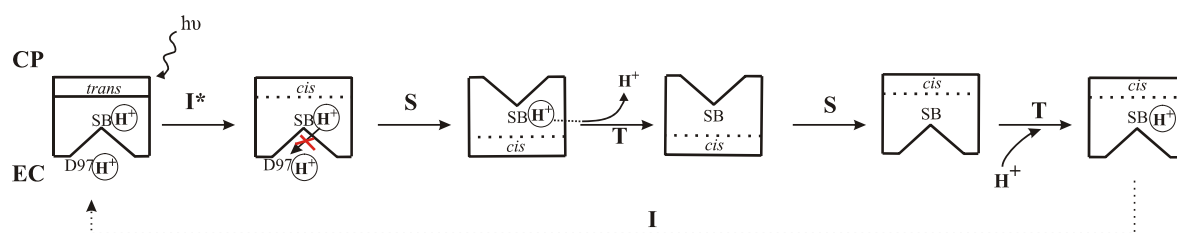
currents can be measured below -80 mV. At pH 5.5 only ~ 5% of the protein is in the alkaline form, the recorded photocurrents are the sum of charge movements generated by both, alkaline – and acidic forms. At pH 4.5, most of the protein is in the acidic form and inward currents are clearly detected, already at less negative potential values. Compared to recordings where the intracellular pH was reduced, the pH gradient across the cell membrane appears to be more important than the membrane potential to drive inward H<sup>+</sup> transport.

Experiments with mutants of D97 in which the negative charge was neutralised (D97N, T) results in a situation similar to a protonated acceptor. Photocurrent measurements of these mutants support the data obtained on PR wt at low pH. Since charge translocation to the extracellular side of the protein is blocked, only inward currents can occur (**fig 2.17**).

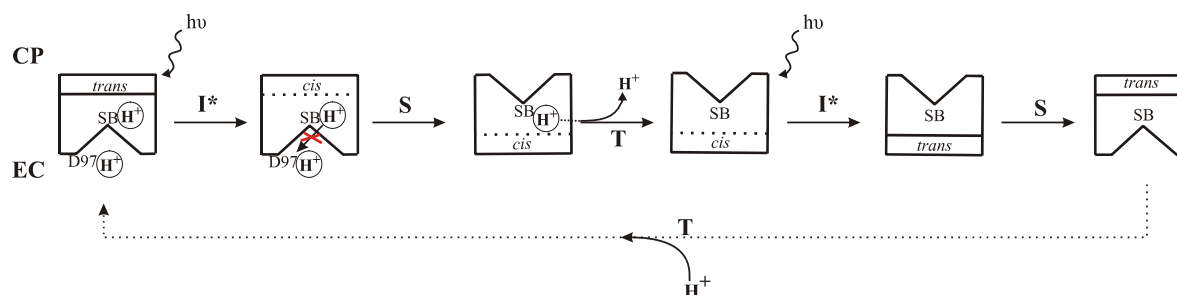
The mechanism of this inward proton translocation is not yet clear. Since it is triggered by light, it most probably involves the *trans-cis* isomerisation of the retinal. The larger side-chain of Glu108 compared to Asp96 (in BR) and its stronger hydrogen bonding could contribute to a different structural organisation of the H<sup>+</sup>-pathway in PR compared to BR, especially on the cytoplasmic side (Friedrich *et al.*, 2002). The H<sup>+</sup>-pathway is clearly disturbed in the absence of the glutamate side-chain, since azide has stronger effect on the stationary photocurrents of the E108D mutant compared to the wild-type (**fig 2.17** right), and under acidic conditions the smaller aspartate residue at the H<sup>+</sup>- donor position appears to facilitate inward charge translocation (**fig. 2.20**). In the case of BR it was proposed that the two aspartate residues at the H<sup>+</sup>-donor and acceptor positions do not sufficiently define the vectoriality of proton pumping (Tittor *et al.*, 1994). This is a likely possibility for PR as well, but more experiments are needed to validate it.

Friedrich *et al.* (2002) suggested that the inward charge translocation could be driven by a one-photon- and the outward transport by a two-photon-process. Such a sequence could be explained using the kinetic model proposed by Haupts *et al* (1997) to describe ion translocation by halobacterial retinal proteins. According to the **IST** (= isomerisation/switch/transfer) **model** the light-induced isomerisation of the retinal induces not only a change in the accessibility of the Schiff base but also an ion transfer reaction in the protein, which are *kinetically independent* and may compete with each other. In addition, thermal isomerisation of the retinal is considered possible only for a protonated Schiff base. The vectoriality of the active transport is determined by the relative rate constants in a given molecule (Haupts *et al.*, 1997). The authors exemplified their model with extensively studied archeal ion pumps (bacteriorhodopsin, halorhodopsin and sensory rhodopsin I) and mutants thereof.

A

1-photon-process (inward  $H^+$  transport under extracellular acidic conditions by PR wt)

B

2-photon-process (inward  $H^+$  transport by D97T)

**Figure 2.42 Models of inward proton translocation by PR in the absence of a charged proton acceptor**

**A.** under extracellular acidic conditions; **B.** when the proton acceptor D97 is replaced by a neutral amino acid residue. From the residues known to play an important role in proton transfer by PR, only the proton acceptor and the Schiff base are shown, since the experiments performed here do not allow conclusions about all steps of the photocycle. Model based on Haupts *et al.* (1997). CP=cytoplasmic side; EC=extracellular side; I\*=isomerisation induced by absorption of a photon ( $h\nu$ ), I=thermal isomerisation; SB=deprotonated Schiff base, SBH<sup>+</sup> = protonated Schiff base; S=switch in the accessibility of the SB; T=transfer of a proton to- or from the Schiff base. The straight and dotted lined denote the difference in the isomerisation state of the retinal.

In the case of wild-type PR the IST model could be applied as follows: at *acidic pH* the  $H^+$  acceptor D97 is protonated in the ground state. Upon incident light, the retinal isomerises (I<sup>\*</sup>) but the transfer (T) of the Schiff base proton towards the extracellular side cannot take place because D97 is not available, and as such the change in the accessibility of the Schiff base ('switch') happens earlier. Now the Schiff base is accessible from the cytoplasmic side and the Schiff base proton leaves in this direction (T). Since it is considered, that the retinal cannot undergo a thermal reversion, the switch in accessibility of the Schiff base (S) happens first, followed by the transfer (T) of a proton to the Schiff base from the extracellular side. With the Schiff base protonated, after thermal isomerisation of the retinal (I) the molecule is ready to start another photocycle. The sequence of events would be **I\*STSTI** (Figure 2.42 A). However, the sequence of events may change depending on the illumination conditions: with more light available a second photon might induce the isomerisation of the retinal earlier, before the switch step (I\*STI\*ST). Experiments with laser flashes support this



possibility: blue and green laser flashes applied during and after continuous illumination at pH 4.5 trigger negative transient currents in the same direction as the inward stationary currents (**fig. 2.7** bottom) suggesting that the light intensity used for continuous illumination might not be saturating and that there is still a substantial fraction of molecules in the ground state ready to be excited. At pH 5.5, in the absence of continuous illumination both blue and green laser flashes trigger inward transient currents already at  $V_m = -30$  mV i.e. one photon is enough for inward charge translocation. And interestingly, the pattern of laser induced transient currents is also very similar to that observed with E108G mutant at pH 5.5, suggesting similarities between proton translocation by PR wild-type and mutant E108G when the proton acceptor is not available and the electrochemical gradient opposes the direction of proton pumping.

When the laser flashes are applied during continuous illumination at  $V_m = -30$  mV the current signal resembles a superposition of the inward transients and small outward stationary current, the former due to the acidic form (but smaller fraction compared to pH 4.5), the latter to the alkaline form still present at pH 5.5. After switching off the continuous illumination, green laser flashes trigger biphasic transient currents probably due to the superposition of the photocurrents generated by the alkaline and acidic forms (**fig. 2.7** middle).

Throughout the experiments, the energies of single flashes were adjusted to similar values for both wavelengths. Under acidic conditions blue laser flashes trigger transient currents of larger amplitudes than green flashes.

In D97T the proton acceptor is also not available, as under acidic conditions. White light triggers a photocurrent which is apparently the cumulative effect of blue and green photon absorption (see '*Mutants of proteorhodopsin*', D97T, **fig 2.33**). A two photon driven photocycle in the inward direction, using the elements of the IST model, could be explained as follows (**figure 2.42 B**): in the ground state the Schiff base is protonated, accessible from the extracellular side, the retinal is most likely in the all-*trans* configuration. Upon illumination ( $I^*$ ) the retinal undergoes a conformational change (all-*trans*  $\rightarrow$  13-*cis*). From the proton transfer and Schiff base accessibility switch which compete, in the absence of the proton acceptor the switch takes place earlier (S), followed by release of a proton on the cytoplasmic side (T). Upon absorption of a second photon ( $I^*$ ) the retinal isomerises again, from 13-*cis*  $\rightarrow$  all-*trans*, followed again first by a switch in the Schiff base accessibility (S) and then by uptake of a proton from the extracellular side (T) re-forming the ground state. The sequence of events would be  $I^*STI^*ST$ , as for the 2-photon-driven photocycle in case of the alkaline form of PR wt. If only blue light is applied, the photocurrent has only a clear

stationary component because the deprotonated Schiff base absorbs blue photons efficiently. If only green light stimulates the protein, the Schiff base in the ground state is efficiently deprotonated, but reprotonation is slowed because the deprotonated Schiff base does not absorb green light, resulting in an asymmetric electric signal with a sharp peak current (**fig. 2.33 A**). Ideally the first photon could be green, the second blue, both available when white light is used for illumination. The light intensity dependence at all three wavelengths supports this idea (**fig. 2.33 B**).

According to spectroscopic studies (Dioumaev *et al.*, 2002; Dioumaev *et al.*, 2003; Friedrich *et al.*, 2002; Lakatos *et al.*, 2003; Váró *et al.*, 2003), the photocycle of PR at low pH is marked by the absence of a detectable signature for an M state, because no absorption *change* is observed at 400 nm, characteristic for the intermediate with deprotonated Schiff base. On the other hand, for a model that uses the same transport pathway for both directions it is necessary that the Schiff base becomes transiently deprotonated and reprotonated during the photocycle.

Although the mutants D97N, -T resemble the case of the protonated, i.e. neutral, D97 (acidic form), one has to keep in mind that the mutations probably change the  $pK_a$  of the Schiff base, as observed for D85 mutants of BR. Consequently, charge translocation in the mutants might be different than in the wild type under acidic conditions. Further spectroscopic and structural data is necessary to characterise the nature of the proton transfer pathway through the protein.

Another possibility is that at low pH – when D97 is protonated – a state exists with an already deprotonated Schiff base. This will be reprotonated from the extracellular side (as in BR upon incident blue laser flashes), but because the acceptor site is likely to be protonated, the proton will be released towards the intracellular side of the protein, resulting in inward charge translocation. Since the deprotonated Schiff base absorbs blue light more efficiently than green light, the transient currents should have larger amplitudes when triggered by blue laser flashes. This has actually been recorded, and visible in **figure 2.7**, where at pH 5.5 and 4.5 blue laser flashes trigger transients of larger amplitudes compared to green flashes, both during and after continuous illumination. The fact that at low pH the *amplitude of the laser triggered transient currents changes only with potential, but not time*, independent of the wavelengths used (**figures 2.7, 2.8**) suggests that there are differences in the proton translocation steps between the alkaline and acidic forms of PR. However, experiments employing other methods are necessary to confirm or invalidate the existence of a state with deprotonated Schiff base and characterise the two forms of proteorhodopsin.

### 3.8 Localisation of bacteriorhodopsin (BR) and proteorhodopsin (PR) at the surface of the oocyte membrane, investigated by chemiluminescence

The BR-NT-HA construct was originally generated as a control for surface expression of Wilson Disease Protein (W NDP) and its mutants, since it is a membrane protein already functionally expressed in the plasma membrane oocytes (Geibel, 2003; Geibel *et al.*, 2001; Nagel *et al.*, 1998; Nagel *et al.*, 1995). Later the N-terminally tagged PR construct was added (PR-NT-HA) in order to gain more insight into the expression of proteorhodopsin in this model system.

In the case of W NDP the surface detection assays have been performed 4 days after injection because Western blot analysis demonstrated no increase of the amount of protein beyond this period (not shown). As visible in **figure 2.37**, after 4 days the three proteins are detectable to the same extent at the surface of oocytes. At a first glance this means that the three membrane proteins of different origins (W NDP-human, BR-archeal and PR-bacterial) are expressed in similar amounts in the plasma membrane of the oocytes. Looking at Western blots prepared from total membranes of oocytes expressing W NDP and BR it becomes clear that the copper-ATPase is more efficiently expressed at the cell surface since the BR signal is much stronger, i.e. most of the protein molecules did not reach the plasma membrane (**fig 2.4 B**).

Also the expression of PR-NT-HA on Western blots was assessed, using a preparation where the plasma membrane of the oocytes was separated from the rest of membranes. Although in the chemiluminescence assay there is a clear signal coming from the presence of the PR molecules in the plasma membrane, these are detected on the Western blot only under the oocyte surface (**fig. 2.38**, 4 days). Only after 7 days, when large currents can be measured, is PR detected in the plasma membrane. Now more protein seems to be present at the plasma membrane as below it (**fig. 2.38**, 7 days). Although the difference in the outcome of the two different approaches (chemiluminescence versus Western blot) is puzzling, it is possible that the lower amount of protein present after four days expression time in the plasma membrane is detected only by chemiluminescence because some of the material is lost during the membrane-preparation steps (see *Materials and Methods* section 3).

Protein molecules which are below the oocyte surface may affect the recorded electric signal if they react to the exciting light and build up a potential against the pumping gradient (Geibel *et al.*, 2001).

### 3.8.1 Whether the HA-tag interferes with the function of an HA-tagged retinal H<sup>+</sup> pump depends on its position

Similarly to Wilson Disease Protein, the effect of the HA-tag on the protein was investigated in the case of BR (**fig. 2.41**). The photocurrents of the N-terminally tagged protein are identical to those of the wild type (**fig. 2.41** inset) and only small differences can be observed in its IV relationship under neutral pH conditions. A previous study (Geibel *et al.*, 2001) reports similar values for BR wt to those measured here: the reversal potential at pH 7.5 is -220 mV (like in case of BR-NT-HA) and at pH 5.5 -157 mV.

Interestingly, when the HA-tag is inserted at the C-terminal end of both bacterio- and proteorhodopsin, the currents are much smaller and show a different kinetic behaviour in BR (**fig. 2.40**), and no photocurrents at all can be recorded in PR constructs, wild type or mutants (not shown). However, all C-terminally tagged constructs are detectable on Western blots (**fig. 2.38**), suggesting that the synthesis of the proteins is not impaired, only their function.

## 4. Conclusions

Data presented in this work support earlier observations according to which proteorhodopsin can operate as an outwardly and inwardly directed light-driven ion pump (Friedrich *et al.*, 2002). The residues proposed to play the roles of proton donor (E108) and acceptor (D97) are important for proton translocation. In the absence of an anionic residue at position 97 no outward pumping takes place, as suggested (Dioumaev *et al.*, 2003), but inward charge translocation may occur under appropriate conditions. An M-like state similar to that known from BR detectably accumulates under neutral pH conditions or under conditions where reprotonation of the Schiff base from the cytoplasmic side is slowed down, as in case of the mutants at position 108. Under acidic conditions PR pumps inwardly under the concerted action of pH and transmembrane potential.

The experiments performed in parallel with PR and BR wild-types brought not only interesting information about similarities and differences between the two retinylidene ion pumps, but also led to the observation that the life-time of the M state in BR wild-type can be extended in addition to hyperpolarising transmembrane potentials (Geibel *et al.*, 2001) also by extracellular acidic pH, when the proton gradient through the cell membrane is directed opposite to the ion transport (i.e. when the electrochemical gradient opposing the direction of proton transport increases). Direct photocurrent measurements of HA-tagged PR and BR have shown that the inserted tag may interfere with the functionality of the protein.

Next to E108 and D97 in PR other residues in the vicinity of the retinal binding pocket contribute to the translocation of protons, as exemplified by the mutant L105Q: additionally to changing the absorption maximum of the protein, this mutant is a less effective proton pump than the wild type. The example of PR suggests that transduction of light energy by – and reaction mechanisms of retinylidene ion pumps have not been entirely deciphered by the extensive studies of bacteriorhodopsin.

In a natural seawater environment, the pH is generally between 7.4 and 8.1 (Clayton and Byrne, 1993). Since the pK<sub>a</sub> of naturally occurring PR variants is close to that of the environmental pH, both alkaline (outwardly pumping) and acidic (involved in inward charge translocation) forms of PR are present in considerable amounts. As it was hypothesised by Kelemen *et al.*, cells expressing PR might use this pK<sub>a</sub> for regulatory purposes, otherwise significant amounts of light energy could be lost, considering the large variety of PRs suggested (Béjà *et al.*, 2001; De LaTorre *et al.*, 2003; Kelemen *et al.*, 2003; Sabehi *et al.*, 2005; Venter *et al.*, 2004). This is even more likely since based on sequence homology the

closest relatives of PR are sensory rhodopsins of *Natronobacterium pharonis* (Béjà *et al.*, 2000), which are primary receptors. The observed two-photon process reported by Friedrich *et al.* (Friedrich *et al.*, 2002) which allows the processing of information over a large range of intensities, has been also postulated for SRII (Schmies *et al.*, 2000).

PR can also serve as an energy converter and provide the electrochemical gradient for ATP synthesis (Béjà *et al.*, 2001; Friedrich *et al.*, 2002). Since PR confers autotrophy to marine bacteria harbouring it, the large variety of PR-like proteins in marine microorganisms (Giovannoni *et al.*, 2005; Venter *et al.*, 2004) suggests that these molecules play an important role in marine ecosystems.

## **Materials and Methods**

## **On the use of *Xenopus laevis* oocytes for the heterologous expression of membrane proteins**

The oocytes of *Xenopus laevis* were first introduced to modern biology in the late 1950s by John Gurdon and employed for developmental biology studies (Brown, 2004). Later, it was observed that oocytes translate exogenous messenger RNA injected into the cytoplasm (Gurdon *et al.*, 1971). However, only after the functional expression of the *Torpedo* acetylcholine receptor (Barnard *et al.*, 1982) were oocytes used as an *in vitro* expression system to study membrane proteins. Due to the ease of frog housekeeping (Hilken *et al.*, 1997) and preparation of oocytes (Bröer, 2003; Sigel and Miniér, 2005; Stühmer, 1998; Wagner *et al.*, 2000; Weber, 1999) oocytes became a popular tool in the study of ion channels, receptors and carriers of different origins, such as: human glucose transporters (Gould *et al.*, 1991), the human Na<sup>+</sup>/glucose cotransporter SGLT1 (Martin *et al.*, 1997), the rat GAT1 GABA-transporter (Quick *et al.*, 1997), the human RFC reduced folate carrier (Subramanian *et al.*, 2001), murine AE2 anion exchanger (Stewart *et al.*, 2001), rat Na<sup>+</sup>K<sup>+</sup> (Koenderink *et al.*, 2003) and H<sup>+</sup> K<sup>+</sup>-ATPases (Geibel *et al.*, 2003) and the archeal bacteriorhodopsin BR (Nagel *et al.*, 1995).

The heterologously expressed proteins can be studied with a variety of methods, including biochemistry, cell biology and electrophysiology (Bröer, 2003; Sigel and Miniér, 2005; Stühmer, 1998; Wagner *et al.*, 2000). The exogenous proteins are faithfully expressed in the sub-cellular compartments where they are localised in the native environment, which makes the oocyte a useful system for trafficking studies (Denning *et al.*, 1992; Martin *et al.*, 1997; Mora *et al.*, 1997; Quick *et al.*, 1997; Schild *et al.*, 1996; Staub *et al.*, 1997; Subramanian *et al.*, 2001; Tong *et al.*, 2001). It is important to keep in mind, that although the oocyte has relatively few endogenous proteins, these might influence the experimental results, especially in electrophysiologic experiments (Weber, 1999).



## 1. Molecular biology

### 1.1 cDNA constructs and cRNA synthesis

#### Wilson Disease Protein (WNDP)

WNDP cDNA was subcloned into the oocyte expression vector pTNPN (a derivative of pTLN containing the *PacI* restriction site within the multiple cloning region). For this purpose, a pMT2-WNDP construct (originally from K. Petrukhin, Columbia University) was cut by a *SallI* (complete) and *EcoRI* (partial) digest and the resulting 4.4 kb fragment ligated into *EcoRI/XhoI* restricted pTNPN, yielding WNDP-plasmid-1. A *PacI* site and a Kozak sequence for optimal eukaryotic translation initiation (GCCACCATGG) were added amino terminally immediately preceding the start-ATG. The resulting PCR fragment was cut with *PacI/BspI* (another unique restriction site) and ligated into the appropriately cut WNDP-plasmid-1, yielding the final WNDP-pTNPN construct.

The HA epitope (YPYDVPDYA) and the extended HA-epitope (SEHYDYDVPDYAVTF) - derived from the hemagglutinin A protein of the human influenza virus- as well as deletions and mutations were introduced using overlap extension PCR at the following positions: WNDP HA(N) (after Met1) WNDP HA12 (after Val683), WNDP HA34 (after Ala756), WNDP HA45 (after Ser797), WNDP HA56 (after Asn958), WNDP HA78 (after Ile1346), WNDP delN600 (deletion of Pro2 to Ala600), WNDP delLLL (truncation after Ser1453), WNDP HA(C) (after I1465). Point mutations and multiple mutations were introduced into the WNDP HA56 construct: D1027A, H1069Q, respectively CPC>SPS; TGE>AAA. Within the bacteriorhodopsin (BR) cDNA sequence which was subcloned into the vector pTLN the HA epitope was introduced after the propeptide sequence at Ser13. All PCR-derived fragments were verified by sequencing (MWG Biotech AG, Ebersberg, Germany).

#### Proteorhodopsin (PR) and Bacteriorhodopsin (BR)

The cDNA of PRwt - 249 amino acids - (GeneBank accession number AF279106) was used, as described (Friedrich et al, 2002).

The point mutants PR D97E, D97N, D97T, E108D, E108G and L105Q have been generated by site directed mutagenesis, overlap-extension PCR. Similarly to PR, BR - 248 amino acids - was also expressed using the pTLN vector as described in (Geibel, 2003).

Amino- and carboxy-terminally HA-tagged constructs PRwt-NT-HA PRwt-CT-HA, PR D97N-CT-HA, PR D97T-CT-HA/pTLN  $\phi$  Nco, BR-NT-HA and BR-CT-HA were generated with a recombinant PCR strategy, for the purpose of detecting the protein on the oocyte surface by a chemiluminescence assay and in Western blots.

cRNA synthesis was carried out using the SP6 mMessage mMachine Kit (Ambion, Austin, TX) after linearisation of the plasmid DNA with *Mlu* I.

### **1.2 Heterologous expression in *Xenopus laevis* oocytes**

Oocyte preparation and injection: individual stage V and VI oocytes were isolated by collagenase treatment after surgical removal of ovarian lobes from anaesthetised *Xenopus laevis* females, as described in (Grygorczyk *et al.*, 1989).

2.5 to 50 ng - WNDP constructs – or 25-75 ng of cRNA - PR and BR constructs - were injected into the oocytes (50 nl injection volume). Following injection the oocytes were kept at 18 °C in MBS solution (in mM: 88 NaCl, 2.4 NaHCO<sub>3</sub>, 1 KCl, 0.41 CaCl<sub>2</sub>, 0.33 Ca(NO<sub>3</sub>)<sub>2</sub>, 0.82 MgSO<sub>4</sub>, 10 HEPES, pH 7.6) or ORi solution (in mM: 115 NaCl, 5 KCl, 2 CaCl<sub>2</sub>, 5 HEPES, pH 7.5) both buffers supplemented with 1 mg ml<sup>-1</sup> gentamycin and 5  $\mu$ M all-trans retinal for PR and BR to reconstitute the functional retinylidene proteins. The cells were used for the luminescence assay and Western blotting 4 days after cRNA injection (all three membrane proteins), and for voltage-clamp measurements 5 – 8 (BR) or 7-10 (PR) days later.

**1.3 Heterologous expression in *Sf9* cells** is described below – see section 5.

## **2. Surface detection using chemiluminescence (WNDP HA-constructs, PR- and BR-NT-HA)**

The principle of the test is the chemiluminescence reaction between the HRP moiety of the secondary antibody and the substrate. The oocytes are placed one by one into the luminometer tubes containing 50  $\mu$ l of the reaction cocktail, prepared in advance and then introduced fast into the sample chamber of the counter. The reading starts with a delay period, followed by

the integration period (actual reading) both user-defined, in our case 5 s and 10 s, respectively. Data are recorded directly into the computer by means of a software interface. The experiments have all been performed at room temperature (20-22 °C).

*Oocyte preparation* (as described in (Zerangue *et al.*, 1999)): Oocytes (5-27/determination) have been incubated in ND96 + 1% BSA at 4 °C for 30 min to block unspecific binding sites, followed by incubation in the primary antibody solution (high affinity rat-anti-HA, Boehringer Dignostics, Mannheim, Germany, diluted according to the manufacturers instructions to 1 µg/ml) for 1 hour at 4 °C. After this, the oocytes are washed three times in ND96 + 1% BSA, on ice. The oocytes are now incubated in the secondary antibodies (HRP conjugated goat-anti-rat, Jackson ImmunoResearch Laboratories West Grove, PA, USA), the original 0.6 mg/ml diluted 1:5000, for 1 hour at 4 °C. In both antibody incubation steps, 96 well Nunclon plates have been used, 3-5 oocytes/well in 50 µl antibody solution. The oocytes are washed again three times in ND96 + 1% BSA and several times in ND96.

Individual oocytes were placed in 50 µl Super Signal® ELISA Femto Maximum Sensitivity Substrate (Pierce Biotechnologies, Rockford, IL, USA) and warmed to room temperature. Chemiluminescence was detected with a TD-20/20 Luminometer (Turner Designs, Sunnyvale, CA, USA), quantified in relative luminescence units (rlu).

### 3. Western Blot (W NDP-, PR-, BR- HA-constructs)

**Crude membrane preparations** were obtained by homogenizing oocytes in ice-cold lysis-buffer (in mM: 250 Sucrose, 0.5 EDTA, 5 Tris-HCl pH 7.4; 10µl/oocyte), containing Complete Protease Inhibitor (Boehringer Mannheim) and removal of yolk platelets by three low centrifugation steps.

**Differential membrane preparation of oocytes**, where the plasma membrane was isolated from the rest, was done based on ref. (Kamsteeg and Deen, 2001). Shortly, oocytes (8-12), with their follicular layer removed, were rotated in 1% positively charged colloidal silica in freshly prepared MBSS buffer (20 mM MES, 80 mM NaCl) for 30 min at 4 °C. After two washing steps in MBSS buffer, the oocytes were again rotated in 1% polyacrylic acid in MBSS, 30 min at 4 °C, followed by two washing steps in MBS solution. The oocytes are homogenised in 0.5 ml ice-cold HbA buffer (in mM: 20 Tris, 5 MgCl<sub>2</sub> 6H<sub>2</sub>O, 5 NaH<sub>2</sub>PO<sub>4</sub> H<sub>2</sub>O, 1 EDTA, 80 sucrose, pH 7.4) containing protease inhibitor, centrifuged 30 sec at 10g, at

4 °C. The top 1300 µl are removed (contain the rest of the membranes), the last two steps repeated at 10g, 20g and 40g, always 1000 µl removed. Finally, the membranes are spun down 30 min at 16000g and the plasma membrane pellet resuspended in 4 µl SDS-PAGE sample buffer.

After addition of SDS-Laemmli sample buffer (37.5 mM Tris pH 6.8, 5% SDS v/v, 33% Glycerol v/v, 5% mercaptoethanol v/v, 160mM DTT, bromphenol blue) added 1:1 to the total membrane preparation and heated to 50 °C for 30 min, the equivalent of 1.5 – 2 oocytes per lane was loaded on 10% SDS polyacrylamide gels (Laemmli, 1970), separated by electrophoresis and transferred to polyvinylidene fluoride (PVDF) membranes. Immunodetection was carried out using rabbit polyclonal antibody anti-ABD directed against the central hydrophilic domain (Lys1005 to Lys1321) of the wild-type WNDP (Lutsenko & Cooper, 1998) (1:20000) or, in the case of the HA epitope-tagged constructs, using rat monoclonal anti-HA antibody 3F10 (Roche) (200 ng/ml), and secondary AP- or HRP - conjugated goat anti-rabbit/anti-rat IgG (Jackson) antibodies (1:5000), respectively. Reacting proteins were visualised using the AP color reagent (BioRad Laboratories, Hercules, CA, USA) or the ECL chemiluminescence method (substrate cocktail from Roche, BioMax film from Kodak, developed using AGFA Curix 60, everything according to the manufacturer's instructions).

#### **4. Electron microscopy (WNDP constructs)\***

##### **4.1 Postembedding immunogold labelling**

*Xenopus laevis* oocytes expressing different constructs of WNDP were fixed at room temperature with 4% paraformaldehyde in combination with 0.1% or 0.5% or 1% glutaraldehyde either in PBS or in MBS – HEPES, pH 7.6. After about 3 hours, the fixative was removed and oocytes washed with PBS and thereafter incubated overnight in 2% glycine PBS. Cells were dehydrated in a series of increasing ethanol concentrations, were infiltrated with LRWhite (London Resin Company Ltd, Reading, England), transferred to gelatine capsules and polymerised at 55-60 °C. Thin sections were cut with the Ultracut (Reichert, Vienna, Austria) and placed on Formwar® (poly vinyl formal) coated nickel grids (Plano GmbH, Wetzlar, Germany).

---

\* Dr. Winfried Haase, Max-Planck-Institute of Biophysics, Dept of Structural Biology, Frankfurt am Main.

For immunogold labeling, sections were first incubated with saturated sodium metaperiodate (60 min), washed in water, treated sequentially with PBS + 2% glycine, PBS, PBS + 1% BSA + 1% Tween 20, PBS + 0.1% BSA + 0.05 Tween 20 and then reacted with the primary anti-WNDP,  $\alpha$ -ABD antibody or, for the HA-tagged constructs, with the rat monoclonal anti-HA antibody. Binding sites of the primary antibodies were visualised with secondary antibodies coupled to gold-particles (diameters 10-12 nm, dilutes 1:50 with PBS + 0.1 BSA), goat-anti-rabbit (Amersham Buchler, Braunschweig, Germany) or goat-anti-rat (Aurion, Wageningen, The Netherlands), respectively. After washing off the unbound secondary antibodies with PBS, sections were shortly treated with 1% glutaraldehyde in PBS, washed with water and dried. Before sections were analysed in the electron microscope (EM208S, Philips, The Netherlands) they were contrasted with 2% uranyl acetate followed by 1% lead citrate.

#### **4.2 Freeze-fracture replica labelling**

For freeze-fracturing, unfixed oocytes were used. Parts of the oocyte membranes were placed between two copper sheets and frozen in liquid nitrogen cooled ethane. Fracturing and shadowing were carried out in a BAF T400 freeze-fracture machine (Balzers, Lichtenstein) with a pressure of  $2 \cdot 10^{-7}$  bar and keeping the specimen stage at  $-140$  °C. Platinum/carbon shadowing was performed using an angle of  $45^\circ$  and pure carbon evaporation was at an angle of  $90^\circ$ . Immunogold labeling of freeze-fracture replicas was performed according to (Fujimoto K, 1997, *Histochem Cell Biol* 107, 87-96). Briefly, replicas were thawed in 2.5% SDS in 10 mM Tris and 30 mM sucrose, pH 8.3 and after two changes of the SDS solution replicas were stirred overnight to dissolve organic material not in direct contact with the heavy metal replica sheet. Pieces of the replica were washed in PBS, then transferred to PBS + 1% BSA and incubated for 2 hours with the  $\alpha$ -ABD antibody diluted 1:1000- 1:2000 in PBS + 0.1 % BSA. To visualize the binding of  $\alpha$ -ABD they were reacted with the secondary gold-ligated antibodies. After a washing step, the replicas were treated with 1% glutaraldehyde/PBS, washed with water and placed on Formwar® coated copper grids to be viewed in the electron microscope. Images were taken with a CCD camera (TVIPS 1Kx1K slow scan CCD camera, Tietz, Munich, Germany).

## 5. Expression of WNDP constructs in *Sf9* cells<sup>§</sup>

*DNA constructs:* a 4.4-kb fragment containing the full-length WNDP cDNA was excised from the pMT2 or WNDP-pTNPN plasmids using digestion with the restriction nuclease *SalI* and partial digestion with *EcoRI* (due to the presence of another *EcoRI* site inside the WNDP cDNA). The obtained fragments were cloned into the appropriately cut pFastBacDual vector (Invitrogen, Carlsbad CA) under the control of the polH promoter. The resultant plasmid pFastBacDual-WNDP (pWNDP) was then utilized to generate the recombinant WNDP-expressing baculovirus using the commercially available Bac-to-Bac kit (Invitrogen) and previously described protocols (Hu *et al.*, 2000). DH10 Bac cells were transformed with pWNDP and allowed to generate bacmids via a transposition mechanism as previously described (Luckow *et al.*, 1993). The WNDP bacmids were then used to transfect *Spodoptera frugiperda* 9 (*Sf9*) cells and produce baculovirus expressing WNDP. Baculovirus was amplified as described in the Bac-to-Bac<sup>TM</sup> manual and in (Hu *et al.*, 2000).

*Preparation of Membrane Fractions:* *Sf9* cells (Invitrogen) were maintained at 27 °C in 150-ml suspension cultures in the Ex-Cell<sup>TM</sup> 420 growth medium (JRH Biosciences Inc., Lenexa, KS) and were split every 2-3 days with fresh medium to maintain cell densities between  $0.5 \times 10^6$  and  $4 \times 10^6$  cells/ml. Cells were infected with recombinant virus as previously described (Gatto *et al.*, 2001; Hu *et al.*, 2000), and harvested 3 days post-infection. To obtain a total membrane preparation, the cells were centrifuged at  $500 \times g$  for 10 min and the cell pellet was frozen at -20 °C and then thawed to facilitate lysis. Cells from a 50-ml culture were pelleted and resuspended in 4 ml of homogenizing buffer (HB): 25 mM imidazole, pH 7.4, 0.25 M sucrose, 1 mM dithiothreitol (1 tablet of Roche complete protease inhibitor mixture was added per 50 ml of buffer solution).

Cell were lysed by a 20-stock homogenization in a Dounce homogenizer, and then centrifuged for 10 min at  $500 \times g$ . The pellet was discarded and the soluble fraction was subjected to an additional centrifugation for 30 min at  $20,000 \times g$  to sediment cell membranes. The pelleted cell membranes were then resuspended in 0.5 ml of HB and stored frozen at -80 °C until further use.

*Phosphorylation of WNDP from [ $\gamma$ <sup>32</sup>P]ATP:* 50  $\mu$ g of total membrane protein was resuspended in 200  $\mu$ l of the assay buffer: 20 mM bis-Tris propane, pH 6.0, 200 mM KCl, 5 mM MgCl<sub>2</sub>. Radioactive [ $\gamma$ <sup>32</sup>P]ATP (5  $\mu$ Ci, specific activity 20 mCi/ $\mu$ mol) was added to a final concentration of 1  $\mu$ M and the reaction mixture was incubated on ice for 4 min. The

---

<sup>§</sup> Dr. Ruslan Tsivkovskii, Oregon Health and Science University, Portland OR.

reaction was stopped by addition of 50  $\mu$ l of ice-cold 1 mM  $\text{NaH}_2\text{PO}_4$  in 50 % trichloroacetic acid and then centrifuged for 10 min at  $20,000 \times g$ . The protein pellet was washed once with ice-cold water and resuspended in 40  $\mu$ l of sample buffer (5 mM Tris- $\text{PO}_4$ , pH 5.8, 6.7 M urea, 0.4 M dithiothreitol, 5% SDS) and loaded on the acidic 7.5 % polyacrylamide gel (Sarkadi *et al.*, 1986). After electrophoresis, the gels were fixed in 10% acetic acid for 10 min and dried on a blotting paper. The dried gels were exposed either overnight to the Molecular Imaging screen CS (Bio-Rad) or for several hours at  $-80^\circ\text{C}$  to the Kodak BioMax MS film and the intensity of the bands was quantified using a Bio-Rad Molecular Imager or Bio-Rad densitometer, respectively.

## 6. Electrophysiology: two-electrode voltage clamp<sup>#</sup> (PR- and BR constructs)

Proteorhodopsin and bacteriorhodopsin mediated currents were recorded in the two-electrode voltage clamp configuration on *Xenopus* oocytes with a Turbo TEC-10X amplifier (npi electronic GmbH, Tamm, Germany) in the following buffers:

**ND 96:** 96 mM NaCl, 2 mM KCl, 0.2 mM  $\text{CaCl}_2$ , 2 mM  $\text{MgCl}_2$ , buffered with 5 mM MES for pH 4.5 and 5.5, and 5 mM Hepes for pH 6.5, 7.4 and 8.5, up to a total of 200 mM NaCl;

**ND 96 with 50mM sodium azide** pH 5.5 and 7.4;

**ND 96 0mM Cl<sup>-</sup>** : 96 mM  $\text{NaNO}_3$ , 2 mM KOH, 0.2 mM  $\text{Ca}(\text{NO}_3)_2$ , 2 mM  $\text{MgSO}_4$ , 2-4 mM L-Glutamic acid, pH 5.5 or 7.4.

For changing the internal pH of the oocyte, organic acid – containing buffers have been used (Stewart *et al.*, 2001):

**‘acetate solution’:** 32.4 mM Na acetate, 67.6 mM NaCl, 2 mM  $\text{MgCl}_2$ , 0.2 mM  $\text{CaCl}_2$ , 5 mM MES, pH 5.5 (HCl);

**‘butyrate solution’:** 6.3 mM Na butyrate, 93.7 NaCl, 2 mM  $\text{MgCl}_2$ , 0.2 mM  $\text{CaCl}_2$ , 5 mM MES, pH 6.6 (NaOH).

**‘NMG-containing solution’** : 50 mM NMG, 50 mM aspartic acid, 100 mM sucrose, buffered with 5 mM Hepes (pH 5.5, 6.5, 7.4, 8.5) or 5 mM MES (pH 4.5). The osmolarity of the usual measuring buffer ND96 and NMG-containing solution was the same.

All buffers were applied externally to the voltage-clamped oocytes.

---

<sup>#</sup> The TEVC method is extensively described in the following references: The Axon Guide (1993), (Stühmer and Parekh, 1995), (Stühmer, 1998).

The amplitudes of the photocurrents were in general not biased by background conductances, since the oocyte membrane was first clamped to the desired membrane potential before illumination (see **fig. 2.2** in the ‘Results’ section on *Proteorhodopsin*).

The pipettes used in the TEVC experiments were prepared from borosilicate glass (Harvard Apparatus LTD, Edenbridge, Kent, UK), filled with 3 M KCl, and had a typical resistance of 0.3 – 2 M $\Omega$ .

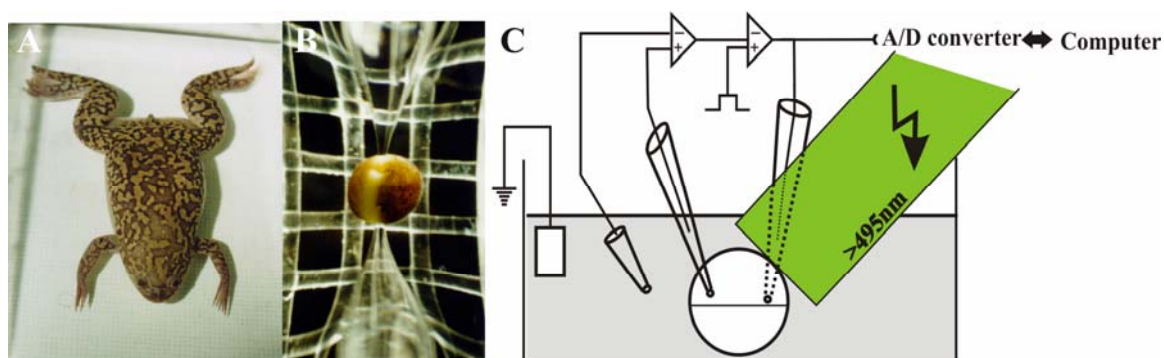


**Figure 6.1** Experimental setup of the two-electrode voltage clamp

(A) *Xenopus laevis* female; (B) voltage-clamped oocyte; (C) schematic representation of all elements needed for measurements.

Data acquisition, shutter triggering and control of the transmembrane potential were performed with pCLAMP7 software *via* a Digidata 1200 B interface (Axon Instruments Inc, Union City, CA, USA). Current traces were recorded at 10 kHz after filtering to 1 kHz using the amplifiers built-in filtering circuits. Data traces recorded were averages of 3-5 runs. All experiments were carried out at room temperature (20-22 °C).

#### *Optical equipment*

To induce photocurrents, cells were illuminated with light from a mercury or xenon arc lamp (Osram HBO 103W/2 or XBO 75W, respectively), filtered through two IR filters and a short wavelength cutoff filter (Schott GG 495 = ‘green light’, or 425) and coupled into an optical light guide. The output measured at the tip of the light-guide was ~ 16.38 mW/mm<sup>2</sup>. Illumination was controlled by a Uniblitz LS6ZM2 shutter (Vincent Associates, Rochester, NY) with a response time of < 1ms, or a slower shutter (~ 4 ms).

Other filters used to create more defined light conditions: narrow band interference filters ( $\lambda \pm 5$  nm), for recording the action spectrum of PRwt and L105Q and broad band interference filters ( $\lambda \pm 25$  nm) for experiments with PR D97T, all from Schott.



Laser flashes during or after continuous illumination were applied from a XeCl excimer laser over a pumped dye-dye laser setup, with PBBO (396 nm = “blue light”) or Coumarin 307 (503 nm = “green light”), with 10 ns pulse duration, which yielded an average light energy of ~ 0.1 - 0.2 mJ per flash at the output of the optical light guide. The laser flashes were coupled into the same optical fibre which brought the continuous light from the HBO mercury arc lamp via a prism.

## Zusammenfassung

Transportproteine sind integrale Membranproteine von großer Bedeutung für die zelluläre Homöostase. Sie erleichtern den Durchtritt von Ionen und Molekülen, für die die Lipidmembran eine niedrige Permeabilität hat. Dadurch können elektrische und/oder chemische Gradienten über die Membran auf- oder abgebaut werden. Diese Gradienten sind wichtig für den Energiehaushalt, Zellstoffwechsel, Erregbarkeit, epithelialer Transport, Osmo- und Volumenregulation der Zelle.

Transportproteine können in zwei große Gruppen eingeteilt werden: *Kanäle*, die ihre Substrate in Richtung des elektrochemischen Gradienten transportieren, und *Transporter*, von denen die meisten ihr Substrat entgegen dem Konzentrationsgradienten transportieren. Dieser Transport verbraucht Energie, da damit eine Reihe von Konformationsänderungen einhergehen („Aktiver Transport“). Beim primär aktiven Transport wird die Energie einer primären Energiequelle verwendet, wie zum Beispiel Licht, Redox-Reaktionen oder Energie aus der Hydrolyse von ATP. Sekundär aktiver Transport liegt vor, wenn der energetisch „bergauf“ gerichtete Transport eines Substrats ermöglicht wird durch Kopplung an einen „bergab“ gerichteten Transport eines zweiten Substrates (Adam *et al.*, 1995; Bröer and Wagner, 2003; Läger, 1991).

Die vorliegende Arbeit beinhaltet Experimente zum Studium zweier primär aktiver, in der Membran lokalisierter Transportproteinen. Sie wurden heterolog in Oozyten von *Xenopus laevis* exprimiert. Hierbei handelt es sich um eine Schwermetall-ATPase, das „Wilson Disease Protein“, und eine lichtgetriebene Protonenpumpe, Proteorhodopsin.

Das „**Wilson Disease Protein**“ (WNDP) ist eine P<sub>1</sub>-Typ Cu<sup>+</sup>-ATPase, die wichtig ist, um während der Proteinsynthese im Trans-Golgi-Netzwerk (TGN) Kupfer Ionen (Cu<sup>+</sup>) bereitzustellen. Cu<sup>+</sup> wird von einigen Proteinen als essentieller Kofaktor benötigt, wie z. B. Ceruloplasmin, Cytochrom c Oxidase, Superoxid Dismutase, Dopamine-β-monooxygenase. WNDP konnte in Geweben wie Leber, Niere, Gehirn und Plazenta identifiziert werden. Das Protein besteht aus 1465 Aminosäuren, und Hydropathie-Analysen lassen an 8 Transmembrandomänen schließen, die von intrazellulären Amino- und Carboxi-termini flankiert werden. Der Sequenz von WNDP enthält Motive die typisch sowohl für alle P-Typ ATPasen (z. B. TGE, DKTG, SEHPL), als auch nur für Schwermetall-ATPasen sind (z. B. die cystein-reichen Motive im Bereich des ~ 600 Aminosäuren lange N-Terminus und die siebte Transmembrandomäne) – siehe **Abbildung 1.3** (Seite 17).

Es konnte beobachtet werden, dass es bei einem Anstieg der intrazellulären Cu-Konzentration über einen physiologischen Schwellenwert zu einer Relokalisation des Proteins vom TGN an die Zelloberfläche und/oder in subzelluläre Kompartimente in Nachbarschaft der Zelloberfläche kommt. Diese Mechanismen tragen zu einer Wiederherstellung des physiologischen Cu-Spiegels bei. Durch Mutationen bedingte Fehlfunktionen von WNDP führen zu Morbus Wilson, einer Erbkrankheit mit einer Inzidenz von 1:30 000, die durch unter anderem, Leberschädigung und neurologische Degeneration gekennzeichnet ist.

Trotz der Fortschritte in Expression und Charakterisierung von WNDP in den letzten Jahren sind viele Einzelheiten des molekularen Mechanismus, Kupfer-abhängigen Regulation und der Zielsteuerung (*trafficking*) innerhalb der Zelle immer noch weitgehend unklar. Aus diesem Grund besteht ein Bedarf zur Etablierung neuer Expressionssysteme und experimenteller Methoden.

Die vorliegende Arbeit versucht, die *Xenopus*-Oozyten – ein bekanntes System zum Studium von Transportproteinen der Plasmamembran – als ein alternatives Expressionssystem zu evaluieren. Mit Hilfe der Oozyten wurde untersucht, ob WNDP in messbaren Mengen in der Plasmamembran exprimiert wird. Außerdem wurde die anhand von Hydropathie-Analysen erstellte Topologie verifiziert und der Effekt von Sequenzänderungen auf die Lokalisation des Proteins in der Plasmamembran untersucht.

Die Sequenzen für die Mutagenese wurden nach folgenden Kriterien ausgewählt (1) konservierte Motiven in P-Typ ATPasen (**TGE**, **DKTG**, **SEHPL**); (2) Motive für die kupferabhängige Zielsteuerung von MNKP („Menkes Disease Protein“, ebenfalls eine eng verwandte  $\text{Cu}^+$ -ATPase die in der Carboxy-terminus ein di-Leucin-Motiv enthält); und (3) Aminosäurenreste die bei beiden  $\text{Cu}^+$ -ATPasen für die Cu-bindung wichtig sind (N-terminale CxxC-Motive und **CPC** in der sechsten Transmembrandomäne). Darüber hinaus wurde die Mutation **H1069Q** untersucht, die die häufigste Ursache für Morbus Wilson in Bevölkerungen nordeuropäischer Herkunft ist, aber auch in anderen Populationen häufig auftritt.

Die Experimente zeigen, dass das Wilson Disease Protein in *Xenopus*-Oozyten exprimiert werden kann. Es befindet sich auf der Oberfläche der Oozyten und kann durch Chemilumineszenz und Elektronenmikroskopie detektiert werden. Die Experimente zu Oberflächenexpression, bei denen mit HA-Epitopen markiertes WNDP verwendet wurde, bestätigen die für WNDP vorgeschlagene Topologie. Das HA-Epitop *per se* interferiert nicht mit der Funktion des Proteins. Dieses wurde gezeigt für das Konstrukt WNDP HA56 durch ATP-abhängige Phosphorylierung nach Expression in Sf9 Zellen.

Sequenzänderungen, die in das Konstrukt WNDP HA56 eingefügt wurden, offenbaren einige interessante Eigenschaften des Proteins: **i)** Die N-terminale Domäne, die 6 Metall-Bindestellen enthält, ist offensichtlich für die Zielsteuerung in die Plasmamembran *targeting* nicht notwendig. **ii)** Bei fehlendem Carboxy-terminus – wodurch das triple-Leucin-Motiv deletiert wird – kommt es zu einer verstärkten Oberflächenexpression von WNDP, woraus sich Hinweise auf eine Beteiligung dieses Motives bei der Relokalisation des Proteins aus der Plasmamembran zum TGN ergeben. **iii)** Die Mutationen TGE>AAA (welche das Protein in der E1 Konformation fixieren, und zu einer konstitutiven Lokalisation in der Plasmamembran führen soll) und D1027A (phosphorylierung-defizient) interferieren nicht mit der Proteinlokalisierung an der Plasmamembran. **iv)** Die Mutationen CPC>SPS (Kupfer-Transport defizient) und H1069Q (phosphorylierung-defizient; häufigste Mutation bei Morbus Wilson) verringern die Plasmamembran- Expression auf weniger als 50%. *Western blot* Analysen zeigen, dass die Höhe der Gesamtexpression aller Konstrukte der des Referenz-Konstrukts WNDP HA56 vergleichbar ist.

Diese Resultate weisen darauf hin, dass die Motive, die für die Kupferbindung und die katalytische Aktivität wichtig sind in *Xenopus*-Oozyten, keinen Einfluss auf Zielsteuerung zur Plasmamembran von WNDP haben. Allerdings könnte die Mutation H1069Q mit der Verteilung von WNDP innerhalb der Zellen interferieren.

Die gezeigte Anwendbarkeit des *Xenopus*-Expressionssystems für WNDP eröffnet neue Wege für die Untersuchung verschiedener, bei Patienten mit Morbus Wilson identifizierter Mutationen auf ihre Effekte. Weiterhin sollten eingehendere Untersuchungen der Topologie möglich werden, bei denen die primäre Proteinsequenz weniger invasiv verändert wird, beispielsweise durch Einführung von Glycosylierungsstellen. Außerdem könnte das hohe Expressionsniveau von WNDP in Oozyten die direkte Untersuchung des Kupfer-Transports erleichtern. Damit könnten auch wichtige intrazelluläre Komponenten identifiziert werden, die für eine effiziente Heranführung von Kupfer an die  $\text{Cu}^+$ -ATPase notwendig sind.

**Proteorhodopsin (PR)**, das erste “Bakterio-Rhodopsin“ im eigentlichen Sinne, ist eine lichtgetriebene, auswärtsgerichtete Protonenpumpe, die in Meeresbakterien identifiziert werden konnte. Das Protein besteht aus 249 Aminosäuren und zeigt eine erhebliche Sequenzähnlichkeit mit Bakteriorhodopsin (BR). Die entscheidenden Elemente für die Translokation der Protonen sind konserviert: die Schiff’sche Base wird durch kovalente Bindung zwischen dem Retinal und K231 gebildet, und Aminosäurenreste E108 und D97

spielen die Rolle des Protonendonors und – akzeptors wie die homologen Gruppen K216, beziehungsweise D96 und D85 in BR – siehe **Abbildungen 1.5** und **1.6** (Seiten 55, 56).

Absorption eines Photons führt ähnlich wie im Falle von BR zu der all-*trans* zu 13-*cis* Isomerisierung des Retinals, welche den Photozyklus auslöst. Ein wichtiger Unterschied zwischen den beiden Protonenpumpen ist der  $pK_a$ -Wert der Protonen-Akzeptorgruppe,  $\sim 2.5$  bei BR (D85) und  $\sim 7$  bei PR (D97). Der Photozyklus von PR ähnelt hinsichtlich spektraler Eigenschaften und Zeitverlauf bei neutralem pH dem von BR, einschließlich der Bildung eines blauverschobenen M-Intermediates, welcher durch eine deprotonierte Schiff'sche Base gekennzeichnet. Obwohl bei saurem pH für PR kein M-ähnlicher Zustand spektroskopisch (Dioumaev *et al*, 2002, 2003; Friedrich *et al*, 2002) detektierbar ist, wurde eine invertierte Protonenpumpenaktivität beobachtet (Friedrich *et al*, 2002), die allerdings von anderen Gruppen in Frage gestellt wurde (Dioumaev *et al*, 2003, Lakatos *et al*, 2003).

Obwohl in den vergangenen Jahren eine Vielzahl neuer PR-Varianten mit weiter Verbreitung in den Weltmeeren entdeckt wurde, wurde der Pumpmechanismus meist indirekt aus spektroskopische Experimenten abgeleitet.

Die Expression in *Xenopus-laevis*-Oozyten erlaubt nicht nur die Untersuchung des pH-Einflusses auf perfekt orientierte PR Moleküle, sondern auch die des Membranpotentials (beide zusammen bilden das elektrochemische Potential für Protonen,  $\Delta\tilde{\mu}_H^+$ ). Wildtyp und PR-Mutanten wurden in diesem System heterolog exprimiert und untersucht, um mehr über die Faktoren, die die Eigenschaften des Protontransfers kontrollieren, zu erfahren.

Mittels des *Two-Electrode Voltage-Clamp* Methode (Zwei-Elektroden Spannungsklemme), wurde das Aktionsspektrum vom PR Wildtyp aufgenommen und mit früheren Messungen an künstlichen Lipid Membranen (BLM) verglichen. Außerdem wurden die Spannungsabhängigkeit der stationären Photoströme von PR Wild-Typ (I-V Kennlinien) bei verschiedene intra- und extrazellulären pH-Werten bestimmt. Die resultierende I-V Kennlinien sind bei allen pH-Bedingungen linear. Die beobachtete Umkehrung des Photostromes ist deutlich abhängig vom Membranpotential und dem pH-Wert. Wenn der pH-Gradient der Pumprichtung der Protonen entgegengesetzt ist, wird das Umkehrpotential mit  $\sim 70$  mV pro pH-Einheit verschoben. Im umgekehrten Fall aber, wenn der chemische Gradient dieselbe Richtung wie die Pumprichtung aufweist ( $pH_{\text{ext}} 8,5$ ), wird das apparente Umkehrpotential nur um  $\sim 30$  mV verschoben.

Mutationen der Proton-Akzeptor und –Donor-Gruppen D97 und E108 wurden ebenfalls auf ihre Auswirkungen untersucht. Stationäre Belichtung bei neutralem pH löst bei den Mutanten D97N und D97T keinen Auswärtsstrom aus, eine Tatsache, die die wichtige Rolle

des Protonenakzeptors D97 für das Auswärtspumpen bestätigt. Stattdessen zeigen sie nur transiente und stationäre Einwärtsströme. Die Mutante E108G zeigt im Vergleich zum Wild-Typ viel kleinere auswärts gerichtete transiente und stationäre Ströme. Die stationäre Pumpfunktion wird in Anwesenheit von Azid deutlich stimuliert, in Analogie zur BR Mutanten D96G. Wenn Azid bei einem pH unter 5,5 eingesetzt wird (wobei die Konzentration der protonierten Form  $\text{HN}_3$  erhöht wird), ist der Anstieg und Abfall der Photoströme schneller. Das deutet auf die Möglichkeit hin, dass die protonierte Form von Azid wichtig ist für die Stimulierung des Protonentransports. Außerdem wurde der Einfluss von Azid auf PR Wildtyp und Mutanten untersucht.

Die Lebenszeit des M-ähnlichen Intermediates von PR Wildtyp und E108G wurde mittels eines speziellen Belichtungsprotokolls studiert, wobei während der stationären grünen Belichtung ( $\lambda > 495 \text{ nm}$ ) zusätzliche blaue oder grüne Laserblitze eingesetzt wurden. Mit einer ähnlichen Methode wurde für BR die Existenz eines langlebigen M-Intermediates nachgewiesen: blaue Laserblitze rufen transiente Ströme hervor, die dem Auswärtsstrom entgegengerichtet sind, und als Reprotonierung der Schiff'schen Base von der extrazelluläre Seite her interpretiert werden (Geibel *et al*, 2001).

Die Eigenschaften von PR und BR Photoströmen unter identischen Bedingungen wurden verglichen. Die Ergebnisse zeigen, dass während der stationären Belichtung bei pH 7.4 blaue Laserblitze deutliche auswärtsgerichtete transiente Ströme bei PR hervorrufen, im Gegensatz zu BR, was darauf hinweist, dass unter gleichen experimentellen Bedingungen immer noch weitere PR-Moleküle angeregt werden können. Die Richtung der transienten Ladungstranslokation ist bei negativen Membranpotentialen invertiert (einwärtsgerichtet).

Bei extrazellulär saurem pH konnten einwärtsgerichtete transiente Ströme sowohl bei blauen als auch bei grünen Laserblitzen beobachtet werden. Ein M-ähnlicher Zustand wie im Falle von BR kann spektroskopischen Messungen zufolge bei PR nur bei neutralem pH-Wert akkumulieren, oder unter Bedingungen unter denen die Reprotonierung der Schiff'schen Base von der zytoplasmatischen Seite her verlangsamt ist, wie im Fall der Mutationen des Protonendonors E108. Diese Ergebnisse bestätigen die früheren Aussagen von Friedrich *et al.* (2002), dass die Richtung des Protonentransports durch den Protonenkonzentrationsgradienten und das Membranpotential bestimmt wird.

Außer E108 und D97 haben auch andere Aminosäurenreste in der Nähe der Schiff'schen Base einen Einfluss auf die Protonentranslokation in PR. Dieses konnte beispielhaft anhand der Mutante L105Q gezeigt werden: Zusätzlich zur Veränderung des Absorptionsmaximums des Proteins ist diese Mutante auch eine weniger effektive

Protonenpumpe als der Wildtyp. Der Beispiel von PR weist darauf hin, dass die Transduktion von Lichtenergie durch und die Reaktionsmechanismen von Retinyliden-Ionenpumpen durch die umfangreichen Studien an BR noch nicht vollkommen entschlüsselt sind.

Die Experimente, die parallel an PR- und BR-Wildtypen ausgeführt wurden, haben nicht nur interessante Informationen über Ähnlichkeiten und Unterschiede zwischen den beiden Retinyliden-Ionenpumpen gebracht. Außerdem führten sie zu der Beobachtung, dass die Lebenszeit des M-Zustand in BR – außer durch hyperpolarisierende Membranpotentiale (Geibel *et al.*, 2001) - auch durch einen der Richtung der Ionenpumpe entgegengesetzten Protonengradienten verlängert werden kann. Direkte Photostrom-Messungen von HA-Epitop markiertem PR und BR haben gezeigt, dass das HA-Epitop abhängig von der Insertionsstelle die Funktion des Proteins beeinträchtigen kann.

Die Bedeutung des einwärts gerichteten Photostroms für die Zellphysiologie der Proteobacteria ist noch unklar. In Meerwasser liegt der pH-Wert generell zwischen 7,4 und 8,1 (Clayton and Byrne, 1993). Da der  $pK_a$  der Protonen-Akzeptor-Gruppe von natürlich vorkommenden PR-Varianten nah am pH der Umgebung ist, sind beide PR-Formen – alkalisch (auswärts pumpend) und azidisch (einwärts pumpend) - in erheblichen Mengen vorhanden. Es wäre nicht effizient ein signifikanter Anteil des Proteins in der ‚nicht funktionierende Form‘ (azidisch) zu haben da ansonsten wesentliche Lichtmengen verloren gehen könnten durch die große Vielfalt an PRs (Béjà *et al.*, 2001; De LaTorre *et al.*, 2003; Kelemen *et al.*, 2003; Sabehi *et al.*, 2005; Venter *et al.*, 2004). Von Kelemen *et al.* (2003) wurde vorgeschlagen, dass Zellen, die PR exprimieren, die Azidische Form für Regulationszwecken verwenden könnten. Diese Hypothese wird dadurch unterstützt, dass Sequenzhomologien das Sensorische Rhodopsin aus *Natronobacterium pharaonis* als den nächsten Verwandten von PR ausweisen (Béjà *et al.*, 2000). Der Zwei-Photonen-Prozess, beobachtet von Friedrich *et al.*, erlaubt eine Informationsverarbeitung auf einer breiten Intensitätsskala und wurde auch für *Sensory Rhodopsin II* postuliert (Schmies *et al.*, 2000).

Darüber hinaus kann PR auch als Energiewandler dienen und den elektrochemischen Gradienten für die ATP-Synthese herstellen (Béjà *et al.*, 2000; Friedrich *et al.*, 2002). Weil PR in der Lage ist, den Meeresbakterien von denen es exprimiert wird Autotrophie zu verleihen, deutet die große Vielfalt an PR-ähnlichen Proteinen in marinen Mikroorganismen (Venter *et al.*, 2004; Giovannoni *et al.*, 2005) auf eine wichtige Rolle dieser Moleküle in marinen Ökosystemen hin .

## Bibliography

- Adam, G., Lauger, P. and Stark, G. (1995). **Physikalische Chemie und Biophysik**. 3rd ed. Springer, Berlin, Heidelberg, New York.
- Albers, R. W. (1967). **Biochemical aspects of active transport**. *Annu. Rev. Biochem.*, **36**:727-756.
- Alberts, B., Johnson, A., Lewis, J., Raff, M., Roberts, K. and Walter, P. (2004). **Molecular Biology of the Cell**, pp. 1463. Garland Science.
- Arguello, J. M. (2003). **Identification of ion-selectivity determinants in heavy-metal transport P1B-type ATPases**. *Journal of Membrane Biology*, **195**:93-108.
- Arguello, J. M., Peluffo, R. D., Feng, J., Lingrel, J. B. and Berlin, J. R. (1996). **Substitution of glutamic 779 with alanine in the Na,K-ATPase alpha subunit removes voltage dependence of ion transport**. *J Biol Chem*, **271**:24610-6.
- Bamberg, E., Apell, H.-J., Dencher, N. A., Sperling, W., Stieve, H. and Lauger, P. (1979). **Photocurrents Generated by Bacteriorhodopsin on Planar Lipid Bilayers**. *Biophys.Struct. Mechanism*, **5**:277 - 292.
- Bamberg, E., Tittor, J. and Oesterhelt, D. (1993). **Light driven proton or chloride pumping by halorhodopsin**. *PNAS*, **90**:639-643.
- Barnard, E. A., Miledi, R. and Sumikawa, K. (1982). **Translation of exogenous messenger RNA coding for nicotinic acetylcholine receptors produces functional receptors in *Xenopus* oocytes**. *Proc. R. Soc. Lond*, **215**:241-246.
- Barnes, N., Tsivkovskii, R., Tsivkovskaia, N. and Lutsenko, S. (2005). **The copper-transporting ATPases, Menkes and Wilson disease proteins, have distinct roles in adult and developing cerebellum**. *J. Biol. Chem.*, **280**:9640-5.
- Beja, O., Aravind, L., Koonin, E., Suzuki, M., Hadd, A., Nguyen, L., Jovanovich, S., Gates, C., Feldman, R., Spudich, J., Spudich, E. and DeLong, E. (2000). **Bacterial Rhodopsin: Evidence for a new type of phototrophy in the sea**. *Science*, **289**:1902-1906.
- Beja, O., Spudich, E., Spudich, J., Leclerc, M. and DeLong, E. (2001). **Proteorhodopsin phototrophy in the ocean**. *Nature*, **411**:786-789.
- Bergo, V., Amsden, J., Spudich, E. N., Spudich John, L. and Rotschild, K. (2004). **Structural changes in the photoactive site of Proteorhodopsin during the primary photoreaction**. *Biochemistry*, **43**:9075-9083.
- Bielawski, J. P., Dunn, K. A., Sabehi, G. and Beja, O. (2004). **Darwinian adaptation of proteorhodopsin to different light intensities in the marine environment**. *PNAS*, **101**:14824-9.
- Bray, P. F. (1965). **Sex-linked neurodegenerative disease associated with monilethrix**. *Pediatrics*, **36**:417-420.
- Broer, S. 2003. ***Xenopus laevis* oocytes**. In Yan, Q. (ed.), *Methods in Molecular Biology*, Vol. 227: Membrane Transporters: Methods and Protocols, pp. 245-257. Humana Press Inc.
- Broer, S. and Wagner, C. A. (2003). **Membrane Transporter Diseases**. Kluwer Academic/Plenum Publishers, New York.
- Brown, D. D. (2004). **A Tribute to the *Xenopus laevis* Oocyte and Egg**. *J. Biol. Chem.*, **279**:45291-45299.
- Butler, P., McIntyre, N. and Mistry, P. (2001). **Molecular Diagnosis of Wilson Disease**. *Molecular Genetics and Metabolism*, **72**:223-230.
- Butt, H., Fendler, K., Bamberg, E., Tittor, J. and Oesterhelt, D. (1989). **Aspartic acids 96 and 85 play a central role in the function of bacteriorhodopsin as a proton pump**. *EMBO J.*, **8**:1657-1663.



- Cater, M. A., Forbes, J., La Fontaine, S., Cox, D. and Mercer, J. F. (2004). **Intracellular trafficking of the human Wilson protein: the role of the six N-terminal metal-binding sites.** *Biochem. J.*, **380**:805-13.
- Clayton, T. D. and Byrne, R. H. (1993). **Spectrophotometric seawater pH measurements: total hydrogen ion concentration scale calibration of m-cresol purple and at-sea results.** *Deep Sea Research Part I: Oceanographic Research Papers*, **40**:2115-2129.
- Cobbold, C., Ponnambalam, S., Francis, M. J. and Monaco, A. P. (2002). **Novel membrane traffic steps regulate the exocytosis of the Menkes disease ATPase.** *Hum. Mol. Genet.*, **11**:2855-2866.
- Cox, D. W. and Moore, S. D. P. (2002). **Copper transporting P-type ATPases and human disease.** *Journal of Bioenergetics and Biomembranes*, **34**:333-338.
- Danks, D. M. and Cartwright, E. (1973). **Menkes' kinky hair disease: further definition of the defect in copper transport.** *Science*, **179**:1140-1141.
- De LaTorre, J. R., Christianson, L. M., Béja, O., Suzuki, M. T., Karl, D., Heidelberg, J. and DeLong, E. F. (2003). **Proteorhodopsin genes are distributed among divergent marine bacterial taxa.** *PNAS*, **100**:12830-12835.
- Denning, G., Anderson, M., Amara, J., Marshall, J., Smith, A. and Welsh, M. (1992). **Processing of mutant cystic fibrosis transmembrane conductance regulator is temperature-sensitive.** *Nature*, **358**:761-4.
- Denning, G. M., Anderson, M. P., Amara, J. F., Marshall, J., Smith, A. E. and Welsh, M. J. (1992). **Processing of mutant cystic fibrosis transmembrane conductance regulator is temperature-sensitive.** *Nature*, **358**:761-4.
- DiDonato, Hsu, Narindrasorasak, Que and Sarkar. (2000). **Copper-induced conformational changes in the N-terminal domain of the Wilson disease copper-transporting ATPase.** *Biochemistry*, **39**:1890-1896.
- Dioumaev, A. K., Brown, L. S., Shih, J., Spudich, E. N., Spudich John, L. and Lanyi, J. K. (2002). **Proton Transfers in the photochemical reaction cycle of proteorhodopsin.** *Biochemistry*, **41**:5348-5358.
- Dioumaev, A. K., Wang, J., Bálint, Z., Váró, G. and Lanyi, J. K. (2003). **Proton Transport by Proteorhodopsin Requires that the Retinal Schiff Base Counterion Asp-97 Be Anionic.** *Biochemistry*, **42**:6582-6587.
- Efremov, R., Kosinsky YA, Nolde DE, Tsivkovskii R, AS, A. and Lutsenko, S. (2004). **Molecular modelling of the nucleotide-binding domain of Wilson's disease protein: location of the ATP-binding site, domain dynamics and potential effects of the major disease mutations.** *Biochem J.*, **15**:293-305.
- Fahr, A., Läger, P. and Bamberg, E. (1981). **Photocurrent Kinetics of Purple-Membrane Sheets Bound to Planar Bilayer Membranes.** *J. Membrane Biology*, **60**:51 - 62.
- Forbes, J. and Cox, D. W. (1998). **Functional Characterization of Missense Mutations in ATP7B: Wilson Disease Mutation or Normal Variant?** *Am. J. Hum. Genet.*, **63**:1663-1674.
- Forbes, J. R. and Cox, D. W. (2000). **Copper-dependent trafficking of Wilson disease mutant ATP7B proteins.** *Hum. Mol. Genet.*, **9**:1927-1935.
- Forbes, J. R., Hsi, G. and Cox, D. W. (1999). **Role of the Copper-binding Domain in the Copper Transport Function of ATP7B, the P-type ATPase defective in Wilson Disease.** *The Journal of Biological Chemistry*, **274**:12408-12413.
- Francis, M., Jones, E., Levy, E., Ponnambalam, S., Chelly, J. and Monaco, A. (1998). **A Golgi localization signal identified in the Menkes recombinant protein.** *Hum. Mol. Genet.*, **7**:1245-1252.
- Friedrich, T., Geibel, S., Kalmbach, R., Chizov, I., Ataka, K., Heberle, J., Engelhard, M. and Bamberg, E. (2002). **Proteorhodopsin is a light driven proton pump with variable vectoriality.** *Journal of Molecular Biology*, **321**:821-838.

- Ganea, C., Tittor, J., Bamberg, E. and Oesterhelt, D. (1998). **Chloride- and pH-dependent proton transport by BR mutant D85N.** *Biochim Biophys Acta*, **1368**:84-96.
- Gatto, C., McCloud, S. M. and Kaplan, J. H. (2001). **Heterologous expression of Na(+)-K(+)-ATPase in insect cells: intracellular distribution of pump subunits.** *Am J Physiol Cell Physiol*, **281**:C982-92.
- Geibel, S. (2003). **Electrophysiologische Charakterisierung der Konformationsdynamik von Ionenpumpen *in situ*.** PhD thesis, Johann Wolfgang Goethe Universität.
- Geibel, S., Friedrich, T., Ormos, P., Wood, P. G., Nagel, G. and Bamberg, E. (2001). **The Voltage-Dependent Proton Pumping in Bacteriorhodopsin Is Characterized by Optoelectric Behavior.** *Biophys. J.*, **81**:2059-2068.
- Geibel, S., Zimmermann, D., Zifarelli, G., Becker, A., Koenderink, J., Hu, Y., Kaplan, J., Friedrich, T. and E., B. (2003). **Conformational dynamics of Na<sup>+</sup>/K<sup>+</sup>- and H<sup>+</sup>/K<sup>+</sup>-ATPase probed by voltage clamp fluorometry.** *Ann N Y Acad Sci.*, **986**:31-8.
- Giovannoni, S. J., Bibbs, L., Cho, J.-C., Stapels, M. D., Desiderio, R., Vergin, K. L., Rappe, M. S., Laney, S., Wilhelm, L. J., Tripp, H. J., Mathur, E. J. and Barofsky, D. F. (2005). **Proteorhodopsin in the ubiquitous marine bacterium SAR11.** *438*:82-85.
- Gitschier, J., Moffat, B., Reilly, D., Wood, W. I. and Fairbrother, W. J. (1998). **Solution structure of the fourth metal-binding domain from the Menkes copper-transporting ATPase.** *5*:47-54.
- Gould, G. W., Thomas, H. M., Jess, T. J. and Bell, G. I. (1991). **Expression of human glucose transporters in *Xenopus oocytes*. - Kinetic characterization and substrate specificities of the erythrocyte, liver, and brain isoforms.** *Biochemistry*, **30**:5139-45.
- Greenough, M., Pase, L., Voskoboinik, I., Petris, M. J., O'Brien, A. W. and Camakaris, J. (2004). **Signals regulating trafficking of Menkes (MNK; ATP7A) copper-translocating P-type ATPase in polarized MDCK cells.** *Am J Physiol Cell Physiol*, **287**:C1463-1471.
- Grygorczyk, R., Hanke-Baier, P., Schwarz, W. and Passow, H. (1989). **Measurement of erythroid band 3 protein-mediated anion transport in mRNA-injected oocytes of *Xenopus laevis*.** *Methods Enzymol*, **173**:453-466.
- Guo, Y., Nyasae, L., Braiterman, L. T. and Hubbard, A. L. (2005). **NH<sub>2</sub>-terminal signals in ATP7B Cu-ATPase mediate its Cu-dependent anterograde traffic in polarized hepatic cells.** *Am J Physiol Gastrointest Liver Physiol*, **289**:G904-916.
- Gurdon, G. B., C.D., L., Woodland, H. R. and Marbaix, G. (1971). **Use of frog eggs and oocytes for the study of messenger RNA and its translation in living cells.** *Nature*, **233**:177-182.
- Haas, R., Gutierrez-Rivero, B., Knoche, J., Boker, K., Manns, M. and Schmidt, H. (1999). **Mutation analysis in patients with Wilson disease: identification of 4 novel mutations. Mutation in brief no. 250. Online.** *Hum. Mut.*, **14**:88-96.
- Hamza, I., Prohaska, J. and Gitlin, J. D. (2003). **Essential role for Atox1 in the copper-mediated intracellular trafficking of the Menkes ATPase.** *PNAS*, **100**:1215-1220.
- Harada, M., Sakisaka, S., Kawaguchi, T., Kimura, R., Taniguchi, E., Koga, H., Hanada, S., Baba, S., Furuta, K., Kumashiro, R., Sugiyama, T. and Sata, M. (2000). **Copper does not alter the intracellular distribution of ATP7B, a copper transporting ATPase.** *Biochemical and Biophysical Research Communications*, **275**:871-876.
- Haupts, U., Tittor, J., Bamberg, E. and Oesterhelt, D. (1997). **General Concept for Ion Translocation by Halobacterial Retinal Proteins: The Isomerization/Switch/Transfer (IST) Model.** *Biochemistry*, **36**:2-7.
- Haupts, U., Tittor, J. and Oesterhelt, D. (1999). **Closing in on Bacteriorhodopsin: Progress in Understanding the Molecule.** *Annu. Rev. Biophys. Biomol. Struct.*, **28**:367-399.

- Hegemann, P., Oesterhelt, D. and Steiner, M. (1985). **The photocycle of the chloride pump halorhodopsin. I: Azide-catalyzed deprotonation of the chromophore is a side reaction of photocycle intermediates inactivating the pump.** *EMBO J.*, **4**:2347-50.
- Hilken, G., Iglauer, F. and Richter, H.-P. (1997). **Der Krallenfrosch *Xenopus laevis* als Labortier (Biologie, Haltung, Zucht und Experimentelle Nutzung).** Ferdinand Enke Verlag, Stuttgart.
- Hsi, G. and Cox, D. W. (2004). **A comparison of the mutation spectra of Menkes disease and Wilson disease.** *Human Genetics*, **114**:165-172.
- Hsi, G., Cullen, L. M., Glerum, D. M. and Cox, D. W. (2004). **Functional assessment of the carboxy-terminus of the Wilson disease copper-transporting ATPase, ATP7B.** *Genomics*, **83**: 473-481.
- Hu, Y. K., Eisses, J. F. and Kaplan, J. H. (2000). **Expression of an active Na,K-ATPase with an alpha-subunit lacking all twenty-three native cysteine residues.** *J Biol Chem*, **275**:30734-9.
- Huber, R., Kohler, T., Lenz, M., Bamberg, E., Kalmbach, R., Engelhard, M. and Wachtveitl, J. (2005). **pH-Dependent Photoisomerization of Retinal in Proteorhodopsin.** *Biochemistry*, **44**:1800-6.
- Hung, I. H., Suzuki, M., Yamaguchi, Y., Yuan, D. S., Klausner, R. D. and Gitlin, J. D. (1997). **Biochemical Characterization of the Wilson Disease Protein and Functional Expression in the Yeast *Saccharomyces cerevisiae*.** *J. Biol. Chem.*, **272**:21461-21466.
- Huster, D., Hoppert, M., Lutsenko, S., Zinke, J., Lehmann, C., Mössner, J., Berr, F. and Caca, K. (2003). **Defective Cellular Localisation of Mutant ATP7B in Wilson's disease Patients and Hepatoma Cell Lines.** *Gastroenterology*, **124**:335 - 345.
- Huster, D. and Lutsenko, S. (2003). **The distinct roles of the N-terminal copper-binding sites in regulation of catalytic activity of the Wilson's disease protein.** *J Biol Chem*, **278**:32212-8.
- Huster, D. and Lutsenko, S. (2003). **The Distinct Roles of the N-terminal Copper-binding Sites in Regulation of Catalytic Activity of the Wilson's Disease Protein.** *J. Biol. Chem.*, **278**:32212-32218.
- Imasheva, E. S., Balashov, S. P., Wang, J., Dioumaev, A. K. and Lanyi, J. K. (2004). **Selectivity of Retinal Photoisomerization in Proteorhodopsin is controlled by Aspartic Acid 227.** *Biochemistry*, **43**:1648 - 1655.
- Imasheva, E. S., Shimono, K., Balashov, S. P., JM, W., Zadok, U., Sheves, M., Kamo, N. and Lanyi, J. K. (2005). **Formation of a Long-Lived Photoproduct with a Deprotonated Schiff Base in Proteorhodopsin, and Its Enhancement by Mutation of Asp227.** *Biochemistry*, **44**:10828-10838.
- Kamikubo, H., Kataoka, M., Váró, G., Oka, T., Tokunaga, F., Needleman, R. and Lanyi, J. (1996). **Structure of the N intermediate of bacteriorhodopsin revealed by x-ray diffraction.** *PNAS*, **93**:1386-90.
- Kamsteeg, E.-J. and Deen, P. M. T. (2001). **Detection of Aquaporin-2 in the Plasma Membranes of Oocytes: A Novel Isolation Method with Improved Yield and Purity.** *Biochemical and Biophysical Research Communications*, **282**:683-690.
- Kataoka, M. and Kamikubo, H. (2000). **Structures of photointermediates and their implications for the proton pump mechanism.** *Biochimica et Biophysica Acta (BBA) - Bioenergetics*, **1460**:166-176.
- Kataoka, M., Kamikubo, H., Tokunaga, F., Brown, L. S., Yamazaki, Y., Maeda, A., Sheves, M., Needleman, R. and Lanyi, J. (1994). **Energy coupling in an ion pump. The reprotonation switch of bacteriorhodopsin.** *J. Mol. Biol.*, **243**:621-38.

- Kelemen, B., Du, M. and Jensen, R., B. (2003). **Proteorhodopsin in living color: diversity of spectral properties within living bacterial cells.** *Biochimica et Biophysica Acta (BBA) - Biomembranes*, **1618**:25 - 32.
- Keszthelyi, L. and Ormos, P. (1980). **Electric signals associated with the photocycle of bacteriorhodopsin.** *FEBS Letters*, **109**:189-193.
- Kim, B.-E., Smith, K., Meagher, C. K. and Petris, M. J. (2002). **A Conditional Mutation Affecting Localization of the Menkes Disease Copper ATPase. suppression by copper supplementation.** *J. Biol. Chem.*, **277**:44079-44084.
- Kim, B.-E., Smith, K. and Petris, M. J. (2003). **A copper treatable Menkes disease mutation associated with defective trafficking of a functional Menkes copper ATPase.** *J Med Genet*, **40**:290-295.
- Koenderink, J. B., Geibel, S., Grabsch, E., De Pont, J. J. H. H. M., Bamberg, E. and Friedrich, T. (2003). **Electrophysiological Analysis of the Mutated Na,K-ATPase Cation Binding Pocket.** *J. Biol. Chem.*, **278**:51213-51222.
- Krebs, R. A., Alexiev, U., Partha, R., DeVita, A. M. and Braiman, M. (2002). **Detection of fast light-activated H release and M intermediate formation from proteorhodopsin.** *BioMedCentral Physiology*.
- Krogh, A., Larsson, B., von Heijne, G. and Sonnhammer, E. (2001). **Predicting transmembrane protein topology with a hidden Markov model: application to complete genomes.** *J. Mol. Biol.*, **305**:567-80.
- Kühlbrandt, W. (2000). **Bacteriorhodopsin - the movie.** *Nature*, **406**:569 - 570.
- La Fontaine, S., Firth, S., Lockhart, P., Brooks, H., Camakaris, J. and Mercer, J. (1999). **Intracellular localization and loss of copper responsiveness of Mnk, the murine homologue of the Menkes protein, in cells from blotchy (Mo blo) and brindled (Mo br) mouse mutants.** *Hum. Mol. Genet.*, **8**:1069-1075.
- La Fontaine, S., Theophilos, M. B., Firth, S. D., Gould, R., Parton, R. G. and Mercer, J. F. B. (2001). **Effect of the toxic milk mutation (tx) on the function and intracellular localization of Wnd, the murine homologue of the Wilson copper ATPase.** *Hum. Mol. Genet.*, **10**:361-370.
- Lakatos, M., Lanyi, J. K., Szakacs, J. and Varo, G. (2003). **The Photochemical Reaction Cycle of Proteorhodopsin at Low pH.** *Biophys. J.*, **84**:3252-3256.
- Lakatos, M. and Váró, G. (2004). **The influence of water on the photochemical reaction cycle of proteorhodopsin at low pH and high pH.** *Journal of Photochemistry and Photobiology*, **73**:177-182.
- Lane, C., Petris MJ, Benmerah A, Greenough M and J., C. (2004). **Studies on endocytic mechanisms of the menkes copper-translocating P-type ATPase (ATP7A; MNK). Endocytosis of the menkes protein.** *Biometals*, **17**:87-98.
- Langner, C. and Denk, H. (2004). **Wilson's Disease.** *Virchows Arch*, **445**:111-8.
- Lanyi, J. K. (1986). **Mechanism of base-catalyzed Schiff base deprotonation in halorhodopsin.** *Biochemistry*, **25**:6706-11.
- Lanyi, J. K. and Schobert, B. (2004). **Local-Global conformational Coupling in a Heptahelical Membrane Protein: Transport Mechanism from Crystal Structures of the Nine States in the Bacteriorhodopsin Photocycle.** *Biochemistry*, **43**:3 - 8.
- Lanyi, J. K. a. L., H. (2001). **Bacteriorhodopsin.** *Current Opinion in Structural Biology*, **11**:415-419.
- Läuger, P. (1991). **Electrogenic ion pumps.** Sinauer Associates, Inc., Sunderland, Massachusetts, USA.
- Luckow, V. A., Lee, S. C., Barry, G. F. and Olins, P. O. (1993). **Efficient generation of infectious recombinant baculoviruses by site-specific transposon-mediated insertion of foreign genes into a baculovirus genome propagated in Escherichia coli.** *J Virol*, **67**:4566-79.

- Luecke, H. (2000). **Atomic resolution structures of bacteriorhodopsin photocycle intermediates: the role of discrete water molecules in the function of this light-driven pump.** *Biochimica et Biophysica Acta (BBA) - Bioenergetics*, **1460**:133-156.
- Luecke, H., Schobert, B., Richter, H.-T., Cartailler, J.-P. and Lanyi, J. K. (1999). **Structural Changes in Bacteriorhodopsin During Ion Transport at 2 Angstrom Resolution.** *Science*, **286**:255-260.
- Luecke, H., Schobert, B., Richter, H.-T., Cartailler, J.-P. and Lanyi, J. K. (1999). **Structure of Bacteriorhodopsin at 1.55 Å Resolution.** *Journal of Molecular Biology*, **291**:899 - 911.
- Lutsenko, S. and Cooper M., J. (1998). **Localization of the Wilson's disease protein product to mitochondria.** *PNAS*, **95**:6004-6009.
- Lutsenko, S., Efremov, R., Tsivkovskii, R. and Walker, J. (2002). **Human Copper-Transporting ATPase ATP7B (The Wilson's Disease Protein): Biochemical Properties and Regulation.** *Journal of Bioenergetics and Biomembranes*, **34**:351-362.
- Lutsenko, S. and Petris, M. J. (2002). **Function and Regulation of the Mammalian Copper-transporting ATPases: insights from Biochemical and Cell Biological Approaches.** *Journal of Membrane Biology*, **191**:1 - 12.
- Lutsenko, S., Petrukhin K, Gilliam TC and Kaplan, J. (1997). **Heterologous expression of the metal-binding domains of human copper-transporting ATPases (P1-ATPases).** *Ann N Y Acad Sci.*, **834**:155-7.
- Lutsenko, S., Tsivkovskii, R. and Walker, J. (2003). **Functional Properties of the Human Copper-Transporting ATPase ATP7B (the Wilson's Disease Protein) and Regulation by Metallochaperone Atox1.** *Ann NY Acad Sci*, **986**:204-211.
- Malmström and Leckner. (1998). **The chemical biology of copper.** *Current Opinion in Chemical Biology*, **2**:286-292.
- Man, D., Wang, W., Sabehi, G., Aravind, L., Post, A. F., Massana, R., Spudich, E. N., Spudich, J. L. and Beja, O. (2003). **Diversification and spectral tuning in marine proteorhodopsins.** *EMBO J.*, **22**:1725-1731.
- Man-Aharonovich, D., Sabehi, G., Sineshchekov, O., Spudich, E., Spudich, J. and Béja, O. (2004). **Characterization of RS29, a blue-green proteorhodopsin variant from the Red Sea.** *Photochem Photobiol Sci.*, **3**:459-62.
- Martin, M., Lostao, M., Turk, E., Lam, J., Kreman, M. and Wright, E. (1997). **Compound missense mutations in the sodium/D-glucose cotransporter result in trafficking defects.** *Gastroenterology*, **112**:1206-12.
- Martin, M. G., Lostao, M. P., Turk, E., Lam, J., Kreman, M. and Wright, E. M. (1997). **Compound missense mutations in the sodium/D-glucose cotransporter result in trafficking defects.** *Gastroenterology*, **112**:1206-12.
- Menkes, J. H., Alter, M., Steigleder, G. K., Weakley, D. R. and Sung, J. H. (1962). **A sex-linked recessive disorder with retardation of growth, peculiar hair and focal cerebral and cerebellar degeneration.** *Pediatrics*, **29**:764-779.
- Mercer, J. (2001). **The molecular basis of copper-transport diseases.** *Trends in Molecular Medicine*, **7**:64-69.
- Mercer, J., Barnes, N., Stevenson J, Strausak D and RM., L. (2003). **Copper-induced trafficking of the cU-ATPases: a key mechanism for copper homeostasis.** *Biometals*, **16**:175-84.
- Mora, S., Monden, I., Zorzano, A. and K., K. (1997). **Heterologous expression of rab4 reduces glucose transport and GLUT4 abundance at the cell surface in oocytes.** *Biochem J.*, **324**:455-9.

- Mora, S., Monden, I., Zorzano, A. and Keller, K. (1997). **Heterologous expression of rab4 reduces glucose transport and GLUT4 abundance at the cell surface in oocytes.** *Biochem. J.*, **324**:455-9.
- Morgan, C. T., Tsivkovskii, R., Kosinsky, Y. A., Efremov, R. G. and Lutsenko, S. (2004). **The Distinct Functional Properties of the Nucleotide-binding Domain of ATP7B, the Human Copper-transporting ATPase: Analysis of the Wilson Disease Mutations E1064A, H1069Q, R1151H, AND C1104F.** *J. Biol. Chem.*, **279**:36363-36371.
- Nagel, G., Kelety, B., Mockel, B., Buldt, G. and Bamberg, E. (1998). **Voltage dependence of proton pumping by bacteriorhodopsin is regulated by the voltage-sensitive ratio of M<sub>1</sub> to M<sub>2</sub>.** *Biophys. J.*, **74**:403-412.
- Nagel, G., Möckel, B., Büldt, G. and Bamberg, E. (1995). **Functional expression of bacteriorhodopsin in oocytes allows direct measurement of voltage dependence of light induced H<sup>+</sup> pumping.** *FEBS Letters*, **377**:263-266.
- Nagel, G., Ollig, D., Fuhrmann, M., Kateriya, S., Musti, A. M., Bamberg, E. and Hegemann, P. (2002). **Channelrhodopsin-1: A Light-Gated Proton Channel in Green Algae.** *Science*, **296**:2395-2398.
- Nagel, G., Szellas, T., Huhn, W., Kateriya, S., Adeishvili, N., Berthold, P., Ollig, D., Hegemann, P. and Bamberg, E. (2003). **Channelrhodopsin-2, a directly light-gated cation-selective membrane channel.** *PNAS*, **100**:13940-13945.
- Oesterhelt, D. and Stoekenius, W. (1971). **Rhodopsin-like protein from the purple membrane of Halobacterium halobium.** *Nat New Biol*, **233**:149-152.
- Ormos, P., Dancshazy, Z. and Karvaly, B. (1978). **Mechanism of generation and regulation of photopotential by bacteriorhodopsin in bimolecular lipid membrane.** *Biochim Biophys Acta*, **503**:304-15.
- Ormos, P., Dancshazy, Z. and Keszthelyi, L. (1980). **Electric response of a back photoreaction in the bacteriorhodopsin photocycle.** *Biophys J.*, **31**:207-13.
- Ormos, P., Dancsházy, Z. and Keszthelyi, L. (1980). **Electric response of a back photoreaction in the bacteriorhodopsin photocycle.** *Biophys. J.*, **31**:207-213.
- Palmgren, M. and Axelsen, K. (1998). **Evolution of P-type ATPases.** *Biochim Biophys Acta*, **1365**:37-45.
- Payne, A. S., Kelly and Gitlin, J. D. (1998). **Functional expression of the Wilson disease protein reveals mislocalization and impaired trafficking of the common H1069Q mutation.** *PNAS*, **95**:10854-10859.
- Payne, A. S., Kelly, E. J. and Gitlin, J. D. (1998). **Functional expression of the Wilson disease protein reveals mislocalization and impaired copper-dependent trafficking of the common H1069Q mutation.** *Proc Natl Acad Sci U S A*, **95**:10854-9.
- Pebay-Peyroula, E., Neutze, R. and Landau, E. M. (2000). **Lipidic cubic phase crystallisation of bacteriorhodopsin and cryotrapping of intermediates: towards resolving a revolving photocycle.** *Biochimica et Biophysica Acta (BBA) - Bioenergetics*, **1460**:119-132.
- Petris, M., Camakaris, J., Greenough, M., LaFontaine, S. and Mercer, J. (1998). **A C-terminal di-leucine is required for localization of the Menkes protein in the trans-Golgi network.** *Hum. Mol. Genet.*, **7**:2063-2071.
- Petris, M., Mercer, J., Culvenor, J., Lockhart, P., Gleeson, P. and Camakaris, J. (1996). **Ligand-regulated transport of the Menkes copper P-type ATPase efflux pump from the Golgi apparatus to the plasma membrane: a novel mechanism of regulated trafficking.** *EMBO J.*, **15**:6084-6095.

- Petris, M. J., Camakaris, J., Greenough, M., LaFontaine, S. and Mercer, J. F. (1998). **A C-terminal di-leucine is required for localization of the Menkes protein in the trans-Golgi network.** *Hum Mol Genet*, **7**:2063-71.
- Petris, M. J. and Mercer, J. F. (1999). **The Menkes protein (ATP7A; MNK) cycles via the plasma membrane both in basal and elevated extracellular copper using a C-terminal di-leucine endocytic signal.** *Hum Mol Genet*, **8**:2107-15.
- Petris, M. J. and Mercer, J. F. B. (1999). **The Menkes protein (ATP7A; MNK) cycles via the plasma membrane both in basal and elevated extracellular copper using a C-terminal di-leucine endocytic signal.** *Human Molecular Genetics*, **8**:2107-2115.
- Petris, M. J., Voskoboinik, I., Cater, M., Smith, K., Kim, B. E., Llanos, R. M., Strausak, D., Camakaris, J. and Mercer, J. F. (2002). **Copper-regulated trafficking of the Menkes disease copper ATPase is associated with formation of a phosphorylated catalytic intermediate.** *J. Biol. Chem.*, **277**:46736-42.
- Petris, M. J., Voskoboinik, I., Cater, M., Smith, K., Kim, B.-E., Llanos, R. M., Strausak, D., Camakaris, J. and Mercer, J. F. B. (2002). **Copper-regulated Trafficking of the Menkes Disease Copper ATPase Is Associated with Formation of a Phosphorylated Catalytic Intermediate.** *J. Biol. Chem.*, **277**:46736-46742.
- Post, R. L., Kume, S., Tobin, T., Orcutt, B. and Sen, A. K. (1969). **Flexibility of an active center in sodium-plus-potassium adenosine triphosphatase.** *J. Gen. Physiol.*, **54**:306s-326s.
- Puig, S. and Thiele, D. (2002). **Molecular mechanisms of copper uptake and distribution.** *Current Opinion in Chemical Biology*, **6**:171-180.
- Quick, M. W., Corey, J. L., Davidson, N. and Lester, H. A. (1997). **Second messengers, trafficking-related proteins, and amino acid residues that contribute to the functional regulation of the rat brain GABA transporter GAT1.** *J. Neurosci.*, **17**:2967-79.
- Quick, M. W., Corey, J. L., Davidson, N. and Lester, H. A. (1997). **Second Messengers, Trafficking-Related Proteins, and Amino Acid Residues that Contribute to the Functional Regulation of the Rat Brain GABA Transporter GAT1.** *J. Neurosci.*, **17**:2967-2979.
- Ralle, M., Lutsenko, S. and Blackburn, N. (2004). **Copper transfer to the N-terminal domain of the Wilson disease protein (ATP7B): X-ray absorption spectroscopy of reconstituted and chaperone-loaded metal binding domains and their interaction with exogenous ligands.**
- Roelofsen, H., Wolters, H., Van Luyn, M., Miura, N., Kuipers, F. and Vonk, R. (2000). **Copper-induced Apical Trafficking of ATP7B in Polarized Hepatoma Cells Provides a Mechanism for Biliary Copper Excretion.** *Gastroenterology*, **119**:782-793.
- Roelofsen, H., Wolters, H., Van Luyn, M. J., Miura, N., Kuipers, F. and Vonk, R. J. (2000). **Copper-induced apical trafficking of ATP7B in polarized hepatoma cells provides a mechanism for biliary copper excretion.** *Gastroenterology*, **119**:782-93.
- Sabehi, G., Loy, A., Jung, K.-H., Partha, R., Spudich, J. L., Isaacson, T., Hirschberg, J., Wagner, M. and Béjà, O. (2005). **New Insights into Metabolic Properties of Marine Bacteria Encoding Proteorhodopsins.** *PLoS Biology*, **3**.
- Sabehi, G., Massana, R., Bielawski, J. P., Delong, E. F. and O., B. (2003). **Novel Proteorhodopsin variants from the Mediterranean and Red Seas.** *Environmental Microbiology*, **5**:842-849.
- Sarkadi, B., Enyedi, A., Foldes-Papp, Z. and Gardos, G. (1986). **Molecular characterization of the in situ red cell membrane calcium pump by limited proteolysis.** *J Biol Chem*, **261**:9552-7.

- Schaefer, Hopkins, Failla and Gitlin. (1999). **Hepatocyte-specific localization and copper-dependent trafficking of the Wilson's disease protein in the liver.** *Am. J. of Physiology (Gastrointest. Liver Physiol. 39)*, **276**:G639-G646.
- Schaefer, M. and Gitlin, J., D. (1999). **Genetic Disorders of Membrane Transport IV. Wilson's Disease and Menkes Disease.** *American J. of Physiology (Gastrointest. Liver Physiol. 39)*, **276**:G311-G314.
- Schäfer, G., Engelhard, M. and Müller, V. (1999). **Bioenergetics of the Archaea.** *Microbiol. Mol. Biol. Rev.*, **63**:570-620.
- Schild, L., Lu, Y., Gautschi, I., Schneeberger, E., Lifton, R. and BC., R. (1996). **Identification of a PY motif in the epithelial Na channel subunits as a target sequence for mutations causing channel activation found in Liddle syndrome.** *EMBO J.*, **15**:2381-7.
- Schild, L., Lu, Y., Gautschi, I., Schneeberger, E., Lifton, R. P. and Rossier, B. C. (1996). **Identification of a PY motif in the epithelial Na channel subunits as a target sequence for mutations causing channel activation found in Liddle syndrome.** *EMBO J.*, **15**:2381-7.
- Schmies, G., Lüttenberg, B., Chizov, I., Engelhard, M., Becker, A. and Bamberg, E. (2000). **Sensory rhodopsin II from the haloalkaliphilic Natronobacterium pharaonis: light activated proton transfer reactions.** *Biophys J.*, **78**:967-976.
- Sigel, E. and Miniér, F. (2005). **The Xenopus oocyte: system for the study of functional expression and modulation of proteins.** *Mol. Nutr. Food Res.*, **49**:228-234.
- Singer, S. J. and Nicolson, G. L. (1972). **The fluid mosaic model of the structure of cell membranes.** *Science.*, **175**:720-31.
- Snyder, P. M., Price, M. P., McDonald, F. J., Adams, C. M., Volk, K. A., Zeiher, B. G., Stokes, J. B. and Welsh, M. J. (1995). **Mechanism by which Liddle's syndrome mutations increase activity of a human epithelial Na<sup>+</sup> channel.** *Cell*, **83**:969-78.
- Solioz, M. and Christopher, V. (1996). **CPx-type ATPases: a class of P-type ATPases that pump heavy metals.** *Trends Biochem Sci.*, **21**:237-41.
- Spudich, J., Yang, C., Jung, K. and Spudich, E. (2000). **Retinylidene proteins: structures and functions from Archea to Humans.** *Annu. Rev. Cell Dev. Biol.*, **16**:365-92.
- Spudich, J. L. and Briggs, W. R. (2005). **Handbook of Photosensory Receptors.** Wiley-VCH Verlag GmbH & Co. KGaA, Weinheim.
- Spudich, J. L. and Jung, K.-H. 2005. **Microbial Rhodopsins: Phylogenetic and Functional Diversity.** In Briggs, W. R. and Spudich, J. L. (eds.), *Handbook of photosensory receptors*, pp. 1-23. Wiley-VCH Verlag GmbH & Co. KGaA, Weinheim.
- Staub, O., Gautschi, I., Ishikawa, T., Breitschopf, K., Ciechanover, A., Schild, L. and Rotin, D. (1997). **Regulation of stability and function of the epithelial Na<sup>+</sup> channel (ENaC) by ubiquitination.** *EMBO J.*, **16**:6325-36.
- Staub, O., Gautschi, I., Ishikawa, T., Breitschopf, K., Ciechanover, A., Schild, L. and Rotin, D. (1997). **Regulation of stability and function of the epithelial Na<sup>+</sup> channel (ENaC) by ubiquitination.** *EMBO J.*, **16**:6325-6336.
- Steinhardt, R. A., Bi, G. and Alderton, J. M. (1994). **Cell membrane resealing by a vesicular mechanism similar to neurotransmitter release.** *Science*, **263**:390-3.
- Steinhoff, H.-J., Pfeiffer, M., Rink, T., Burlon, O., Kurz, M., Riesle, J., Heuberger, E., Gerwert, K. and Oesterhelt, D. (1999). **Azide Reduces the Hydrophobic Barrier of the Bacteriorhodopsin Proton Channel.** *Biophys. J.*, **76**:2702-2710.
- Stewart, A. K., Chernova, M. N., Kunes, Y. Z. and Alper, S. L. (2001). **Regulation of AE2 anion exchanger by intracellular pH: critical regions of the NH<sub>2</sub>-terminal cytoplasmic domain.** *Am J Physiol Cell Physiol*, **281**:C1344-1354.
- Strausak, D., La Fontaine, S., Hill, J., Firth, S., Lockhart, P. and Mercer, J. F. B. (1999). **The Role of the GMXCXXC Metal Binding Sites in the Copper-induced**



- Redistribution of the Menkes Protein.** *The Journal of Biological Chemistry*, **274**:11170 - 77.
- Strausak, D., La Fontaine, S., Hill, J., Firth, S. D., Lockhart, P. J. and Mercer, J. F. (1999). **The role of GMXCXXC metal binding sites in the copper-induced redistribution of the Menkes protein.** *J Biol Chem*, **274**:11170-7.
- Stühmer, W. 1998. **Electrophysiologic recordings from *Xenopus* oocytes.** In Conn, M. (ed.), *Methods in Enzymology Ion Channels Part B*, Vol. 293, pp. 280-300. Academic Press.
- Stühmer, W. and Parekh, A. B. 1995. **Electrophysiological recordings from *Xenopus* oocytes.** In Sakmann, B. and Neher, E. (eds.), *Single channel recording*, pp. 341-355. Plenum Press, New York and London.
- Subramanian, V. S., Marchant, J. S., Parker, I. and Said, H. M. (2001). **Intracellular trafficking/membrane targeting of human reduced folate carrier expressed in *Xenopus* oocytes.** *Am. J. Physiol. Gastrointest. Liver Physiol.*, **281**:G1477-86.
- Subramanian, V. S., Marchant, J. S., Parker, I. and Said, H. M. (2001). **Intracellular trafficking/membrane targeting of human reduced folate carrier expressed in *Xenopus* oocytes.** *Am J Physiol Gastrointest Liver Physiol*, **281**:G1477-1486.
- Tapiero, H., Townsend, D. M. and Tew, K. D. (2003). **Trace elements in human physiology and pathology. Copper.** *Biomedicine & Pharmacotherapy*, **57**:386-398.
- Tittor, J., Haupts, U., Haupts, C., Oesterhelt, D., Becker, A. and Bamberg, E. (1997). **Chloride and Proton Transport in Bacteriorhodopsin Mutant D85T: Different Modes of Ion Translocation in a Retinal Protein.** *J. Mol. Biol*, **271**:405-416.
- Tittor, J., Schweiger, U., Oesterhelt, D. and Bamberg, E. (1994). **Inversion of proton translocation in bacteriorhodopsin mutants D85N, D85T, and D85,96N.** *Biophys J.*, **67**:1682-90.
- Tittor, J., Soell, C., Oesterhelt, D., Butt, H. and Bamberg, E. (1989). **A defective proton pump, point-mutated bacteriorhodopsin Asp96Asn is fully reactivated by azide.** *EMBO J.*, **8**:3477-3482.
- Tittor, J., Wahl, M., Schweiger, U. and Oesterhelt, D. (1994). **Specific acceleration of de- and reprotonation steps by azide in mutated bacteriorhodopsins.** *Biochimica et Biophysica Acta (BBA) - Bioenergetics*, **1187**:191-197.
- Tong, Y., Brandt, G. S., Li, M., Shapovalov, G., Slimko, E., Karschin, A., Dougherty, D. A. and Lester, H. A. (2001). **Tyrosine decaging leads to substantial membrane trafficking during modulation of an inward rectifier potassium channel.** *J. Gen. Physiol.*, **117**:103-18.
- Tong, Y., Brandt, G. S., Li, M., Shapovalov, G., Slimko, E., Karschin, A., Dougherty, D. A. and Lester, H. A. (2001). **Tyrosine Decaging Leads to Substantial Membrane Trafficking during Modulation of an Inward Rectifier Potassium Channel.** *J. Gen. Physiol.*, **117**:103-118.
- Toyoshima, C., Nakasako M, Nomura H and H., O. (2000). **Crystal structure of the calcium pump of sarcoplasmic reticulum at 2.6 Å resolution.** *Nature*, **405**:647-55.
- Toyoshima, C. and Nomura, H. (2002). **Structural changes in the calcium pump accompanying the dissociation of calcium.** *Nature*, **418**:605-11.
- Tsivkovskii, MacArthur and Lutsenko. (2001). **The Lys 1010-Lys1325 fragment of the Wilson's disease protein binds nucleotides and interacts with the N-terminal domain of this protein in a copper-dependent manner.** *The Journal of Biological Chemistry*, **276**:2234-2242.
- Tsivkovskii, R., Efremov, R. and Lutsenko, S. (2003). **The Role of the Invariant His-1069 in Folding and Function of the Wilson's Disease Protein, the Human Copper-transoprtng ATPase ATP7B.** *The Journal of Biological Chemistry*, **278**:13302-13308.

- Tsivkovskii, R., Efremov, R. G. and Lutsenko, S. (2003). **The role of the invariant His-1069 in folding and function of the Wilson's disease protein, the human copper-transporting ATPase ATP7B.** *J Biol Chem*, **278**:13302-8.
- Tsivkovskii, R., Eisses, J. F., Kaplan, J. H. and Lutsenko, S. (2002). **Functional properties of the copper-transporting ATPase ATP7B (the Wilson's disease protein) expressed in insect cells.** *J Biol Chem*, **277**:976-83.
- Tsivkovskii, R., Eisses, J. F., Kaplan, J. H. and Lutsenko, S. (2002). **Functional Properties of the Copper-transporting ATPase ATP7B (The Wilson's Disease Protein) Expressed in Insect Cells.** *J. Biol. Chem.*, **277**:976-983.
- Tsivkovskii, R., MacArthur, B. C. and Lutsenko, S. (2001). **The Lys1010-Lys1325 fragment of the Wilson's disease protein binds nucleotides and interacts with the N-terminal domain of this protein in a copper-dependent manner.** *J Biol Chem*, **276**:2234-42.
- Tsivkovskii, R., Purnat, T. and Lutsenko, S. 2004. **Copper-transporting ATPases: key regulators of intracellular copper concentration.** In Masamitsu Futai, Y. W., Jack H. Kaplan (ed.), *Handbook of ATPases Biochemistry, cell biology, pathophysiology*, pp. 99-156. Wiley-VCH Verlag GmbH & Co KGaA, Weinheim.
- Vanderwerf, S. M., Cooper, M. J., Stetsenko, I. V. and Lutsenko, S. (2001). **Copper Specifically Regulates Intracellular Phosphorylation of the Wilson's Disease Protein, a Human Copper-transporting ATPase.** *J. Biol. Chem.*, **276**:36289-36294.
- Vanderwerf, S. M. and Lutsenko, S. (2002). **The Wilson's disease protein expressed in Sf9 cells is phosphorylated,** *Biometals 2002: Third International Biometals Symposium*, pp. 739-741.
- Váró, G., Brown, L. S., Lakatos, M. and Lanyi, J. K. (2003). **Characterization of the Photochemical Reaction Cycle of Proteorhodopsin.** *Biophys. J.*, **84**:1202-1207.
- Venter, J. C., Remington, K., Heidelberg, J. F., Halpern, A. L., Rusch, D., Eisen, J. A., Wu, D., Paulsen, I., Nelson, K. E., Nelson, W., Fouts, D. E., Levy, S., Knap, A. H., Lomas, M. W., Nealson, K., White, O., Peterson, J., Hoffman, J., Parsons, R., Baden-Tillson, H., Pfannkoch, C., Rogers, Y.-H. and Smith, H. O. (2004). **Environmental Genome Shotgun Sequencing of the Sargasso Sea.** *Science*, **304**:66-74.
- Voskoboinik, I., Brooks H, Smith S, Shen P and J., C. (1998). **ATP-dependent copper transport by the Menkes protein in membrane vesicles isolated from cultured Chinese hamster ovary cells.** *FEBS Letters*, **435**:178-182.
- Voskoboinik, I., Greenough, S., LaFontaine, S., Mercer, J. F. and Camakaris, J. (2001). **Functional Studies on the Wilson Copper P-type ATPase and Toxic Milk Mutant.** *Biochemical and Biophysical Research Communications*, **281**:966-970.
- Voskoboinik, I., Mar, J. and Camakaris, J. (2003). **Mutational analysis of the Menkes copper P-type ATPase (ATP7A).** *Biochemical and Biophysical Research Communications*, **301**:488-494.
- Voskoboinik, I., Strausak, D., Greenough, M., Brooks, H., Petris, M., Smith, S., Mercer, J. F. and Camakaris, J. (1999). **Functional Analysis of the N-terminal CXXC Metal-binding Motifs in the Human Menkes Copper-transporting P-type ATPase Expressed in Cultured Mammalian Cells.** *J. Biol. Chem.*, **274**:22008-22012.
- Vulpe, C., Levinson B, Whitney S, Packman S and J., G. (1993). **Isolation of a candidate gene for Menkes disease and evidence that it encodes a copper-transporting ATPase.** *Nat. Genetics*, **3**:7-13.
- Wagner, C. A., Friedrich, B., Setiawan, I., Lang, F. and Bröer, S. (2000). **The Use of *Xenopus laevis* Oocytes for the Functional Characterization of Heterologously Expressed Membrane Proteins.** *Cellular Physiology and Biochemistry*, **10**:1-12.

- 
- Walker, J. M., Huster, D., Ralle, M., Morgan, C. T., Blackburn, N. J. and Lutsenko, S. (2004). **The N-terminal metal-binding site 2 of the Wilsons disease protein plays a key role in the transfer of copper from Atox1.** *J. Biol. Chem.*, **279**:15376-84.
- Walker, J. M., Tsivkovskii, R. and Lutsenko, S. (2002). **Metallochaperone Atox1 Transfers Copper to the NH<sub>2</sub>-terminal Domain of the Wilson's Disease Protein and Regulates Its Catalytic Activity.** *J. Biol. Chem.*, **277**:27953-27959.
- Wang, W.-W., Sineshchekov, O., Spudich, E. N. and Spudich John, L. (2003). **Spectroscopic and Photochemical Characterisation of a Deep Ocean Proteorhodopsin.** *J. Biol. Chem.*, **278**:33985-33991.
- Weber, W. M. (1999). **Ion currents of *Xenopus laevis* oocytes: state of the art.** *Biochim Biophys Acta*, **1421**:213-233.
- Wilson, S. A. K. (1912). **Progressive lenticular degeneration: a familial nervous disease associated with the cirrhosis of the liver.** *Brain*, **34**:295-307.
- Zerangue, N., Schwappach, B., Jan, Y. N. and Jan, L. Y. (1999). **A New ER Trafficking Signal Regulates the Subunit Stoichiometry of Plasma Membrane K<sub>ATP</sub> Channels.** *Neuron*, **22**:537-548.

## Acknowledgements

I wish to thank Prof. Dr. Ernst Bamberg for the opportunity to work at the MPI of Biophysics and for all his accorded support.

Prof. Dr. Thomas Friedrich I would like to thank for accepting to supervise my work, challenging discussions and ingenious ideas.

I thank Prof. Dr. Klaus Fendler for his patience in ‘unfogging’ enzyme kinetics, help with the laser and interesting discussions in- and outside the institute; Dr. Klaus Hartung for help with the electronics behind electrophysiology and helpful discussions about many topics, including German literature.

I would like to thank Prof. Dr. Svetlana Lutsenko for the prompt answers and many ideas related to the *Wilson Disease Protein* project, and for organising my visit at the OHSU in Portland, OR; and Dr. Ruslan Tsivkovskii for the experiments with WNDP expressed in insect cells.

Dr. Winfried Haase collected impressive images of oocytes expressing WNDP and introduced me to electron microscopy – thank you for the cooperation!

To Dr. Sven Geibel I would like to thank for the initial help with the *Proteorhodopsin* project and Dr. Robert Dempski for the critical reading of this manuscript.

Many thanks to Anja Becker, Eva Kaindl, Barbara Legrum and Verena Pintschovius for all the help around the lab, whether molecular biology, the secrets of BLM or cell culture – always there to answer questions.

Many thanks to Heidi Bergemann for all the help during these years and being there whenever needed!

Solveigh McCormack and Rosemarie Schmidtell I would like to thank for making many articles accessible and Helga Volk for introducing me to the secrets of Corel Draw and her professional touch to my posters. From Stefan Eberhardt I learned many things about PCs. Thank you all!

For the enjoyable atmosphere I would like to thank all my former and present colleagues, and guests of the Bamberg group, it made all the difference!

Special thanks to my husband Christian, for all the travelling and support!

I would also like to express my gratitude to my parents, who accepted and supported my choice of exploring ‘new territories’.

## Glossary

|                              |   |
|------------------------------|---|
| ABD                          | ATP-binding domain (also N – or <u>n</u> ucleotide – binding domain in P-type ATPases)                                      |
| ADP                          | adenosine-5'-diphosphate  |
| ATP                          | adenosine-5'-triphosphate   |
| [ $\gamma^{32}\text{P}$ ]ATP | ATP where the radioactive isotope $^{32}\text{P}$ is incorporated into the phosphate radical at the $\gamma$ position       |
| ATPase                       | ATP-hydrolysing enzyme  |
| BLM                          | black lipid membrane  |
| BR                           | Bacteriorhodopsin   |
| BSA                          | Bovine Serum Albumin  |
| cDNA                         | coding DNA sequence   |
| Coumarin 307                 | 7-Ethylamino-6-methyl-4-trifluoromethylcoumarin   |
| CP                           | cytoplasmic   |
| cRNA                         | coding RNA sequence   |
| CTA                          | copper transporting ATPase  |
| DNA                          | deoxyribonucleic acid   |
| DTT                          | Dithiothreitol  |
| EC                           | extracellular   |
| EDTA                         | ethylenediaminetetraacetic acid   |
| HA epitope                   | identification peptide derived from the hemagglutinin A protein of the human influenza virus, amino acid sequence YPYDVPDYA |
| HEK 293                      | cell line derived from human embryonic kidney cells   |
| HepG2                        | human hepatoma cells  |
| HEPES                        | N-(2-hydroxyethylen) piperazin-N'-(2-ethansulfonic acid)  |
| HRP                          | horseradish peroxidase  |
| kDa                          | kilodalton  |
| MBS                          | metal binding site  |
| MES                          | 2-(N-Morpholino) ethane sulphonic acid  |
| MNKP                         | Menkes Disease Protein  |
| NMG                          | N-methyl-glucamine  |
| PAGE                         | polyacrylamide gel electrophoresis  |

---

|                 |   |
|-----------------|---|
| PBBO            | 2-(4-Biphenyl)-6-phenylbenoxazon-1,3  |
| PCR             | polymerase chain reaction   |
| PDB             | protein data base   |
| pH              | the negative logarithm (to the basis 10) of proton concentration (in moles/liter) |
| pK <sub>a</sub> | the negative logarithm (to the basis 10) of the dissociation constant of an acid  |
| PR              | Proteorhodopsin   |
| RNA             | ribonucleic acid  |
| SDS             | sodium dodecyl sulphate   |
| SEM             | standard error of the mean  |
| TEVC            | two-electrode voltage-clamp   |
| TGN             | Trans Golgi Network   |
| W NDP           | Wilson Disease Protein  |
| YFP             | Yellow Fluorescent Protein  |
| WB              | Western blot  |

**Symbols of amino acids**

|   |     |                |
|---|-----|----------------|
| A | Ala | Alanine        |
| C | Cys | Cysteine       |
| D | Asp | Asparagic acid |
| E | Glu | Glutamic acid  |
| F | Phe | Phenylalanine  |
| G | Gly | Glycine        |
| H | His | Histidine      |
| I | Ile | Isoleucine     |
| K | Lys | Lysine         |
| L | Leu | Leucine        |
| M | Met | Methionine     |
| N | Asn | Asparagine     |
| P | Pro | Proline        |
| Q | Gln | Glutamine      |
| R | Arg | Arginine       |
| S | Ser | Serine         |
| T | Thr | Threonine      |
| V | Val | Valine         |
| Y | Tyr | Tyrosine       |

## Curriculum Vitae



### Personal Information

Name Éva Lőrinczi  
 Birthdate and –place 05.10.1976, Bucharest, Romania

### Education

**July 1994** Graduation of the ‘Endre Ady’ High-school, Bucharest (RO)  
**August 1998** **Bachelor Degree in Biology from the University of Bucharest**  
 (RO), Faculty of Biology  
 Thesis title: “*Social behaviour of half-captive equids*”  
 supervised by Lect. Dr. Carmen Strungaru.  
**March 2000** **MSc in Neurobiology from the University of Bucharest (RO),**  
 Faculty of Biology, Dept of Animal Physiology and Biophysics  
 Thesis title: “*Inactivation of delayed rectifier potassium currents*  
*in the axonal membrane of Rana sp.*”  
 supervised by Prof. Dr. Gordon Reid  
**August 2000 –** PhD student at the Max Planck Institute of Biophysics,  
**February 2006** Frankfurt am Main, Germany.

### Publications

- **Lőrinczi, É.**, Friedrich, T. and Ernst Bamberg (2006) Voltage- and pH-dependent changes in vectoriality of photocurrents mediated by wild-type and mutant proteorhodopsins (*in preparation*)
- **Lőrinczi, É.**, Tsivkovskii, R., Haase, W., Bamberg, E., Lutsenko, S. and Friedrich, T.(2006) Effect of sequence variations on plasma membrane localization of Wilson Disease Protein expressed in *Xenopus* oocytes, J.Gen.Physiol 126 (1), *Abstract. (Paper submitted)*
- Babes A, **Lőrinczi É**, Ristoiu V, Flonta ML, Reid G. (2001) Slowed inactivation at positive potentials in a rat axonal K<sup>+</sup> channel is not due to preferential closed-state inactivation. *Physiol. Res.* 50(6):557-65.